The Transportation and Transformation of Energy Through Reversible Hydrogenation

By

Andrew James Carrier

A thesis submitted to the Graduate Program in Chemistry

in conformity with the requirements for the

Degree of Doctor of Philosophy

Queen's University

Kingston, Ontario, Canada

August, 2011

Abstract

Cycles of reversible hydrogenation reactions are important for at least two different energy-related applications: reversible chemical hydrogen storage and thermally regenerative fuel cells. Hydrogen fuel is a green alternative to conventional hydrocarbon fuels for transportation applications. This is because the combustion product of hydrogen is simply water, which is non-toxic and ubiquitous. Hydrogen is also an attractive fuel because of its high energy content; however, because it is a gas it has poor volumetric energy density. In Chapter 2, ionic liquids consisting of both cations and anions that can undergo reversible dehydrogenative aromatization were used to chemically store hydrogen. Cations investigated included pyridinium ions, which were easily hydrogenated but could not be regenerated through the dehydrogenation of piperidinium ions; and carbazole containing ammonium (whose synthesis failed) and imidazolium (which failed to hydrogenate) cations. The anions studied were heterocyclic carboxylates and sulfonates, these ions were observed to undergo both hydrogenation and dehydrogenation to various degrees when reacted in solution. However, as components of ionic liquids, they fail to react at a significant rate. The viscosity of the fluids was suspected to be hindering the diffusion of either hydrogen or the ions to or from the catalyst surface.

In addition to using hydrogen as the primary source of energy in a vehicle, reversible hydrogenation can form the basis of a thermally regenerative fuel cell: a device that converts low grade vehicle waste heat, from a conventional engine, into electricity

for the vehicles auxiliary power units. In Chapter 3, secondary benzylic alcohols, in particular 1-phenyl-1-propanol, were determined to be able to undergo dehydrogenation to the corresponding ketone rapidly and with extremely high selectivity over a palladium on silica catalyst. The dehydrogenation gave an initial rate of hydrogen evolution of 4.6 l of hydrogen per gram of palladium per minute and the enthalpy and entropy of the dehydrogenation is +56 kJ mol^{-1} and +117 J mol^{-1} K^{-1}. This adsorbed energy can then be released as electricity in a fuel cell and be used to power auxiliary units in a vehicle without decreasing fuel economy.

Acknowledgements

I would like to thank my family who have over the years provided with me with a near endless supply of support, both financial and psychological, and who have made this thesis possible. I would also like to thank my supervisors: Dr. Philip Jessop, who has hosted me in his laboratory for many years and with whom I've had many helpful discussions academic or otherwise; and Dr. Boyd Davis, who has always provided the unique perspective and resources of both an engineer and a businessman and who knew exactly what needed to be done. I thank Donal Macartney, Philip Jessop, and Cathleen Crudden for providing research opportunities throughout my undergraduate career; and all the faculty, administrative, and support staff of the Department of Chemistry who have supported me throughout my stay at the university.

I would like to acknowledge all of the graduate students who have provided a wonderful working environment, both in the Jessop group as well as those in the Crudden and Snieckus groups. In particular I thank Dr. David Heldebrant and Dr. Dominik Wechsler for their academic support and encouragement, as well as Vanessa Renée Little who has been my partner in hydrogen storage and thermally regenerative fuel cell research and has hosted me in Kingston during a portion of the time I have been writing this thesis.

I would like to acknowledge the financial support of the Natural Science and Engineering Research Council of Canada during my undergraduate research; and the William Neish and Milton Hershey Fellowships, and the Ontario Graduate Scholarship

programs for personal financial support during my graduate research. The research presented in this thesis was financially supported by the Natural Science and Engineering Research Council of Canada and the Ontario Centres of Excellence; the latter of which also provided many opportunities for professional development.

Statement of Originality

I hereby certify that I am the sole author of this thesis.

I certify that, to the best of my knowledge, my thesis does not infringe upon anyone's copyright nor violate any proprietary rights and that any ideas, techniques, quotations, or any other material from the work of other people included in my thesis, published or otherwise, are fully acknowledged in accordance with the standard referencing practices.

All contributions from collaborators are clearly noted in the text, and in particular the data presented in the Appendix (X-ray Diffraction Data) were recorded and reported by Dr. Ruiyao Wang.

I declare that this thesis has not been submitted for a higher degree to any other University or Institution.

Table of Contents

List of Tables

List of Figures

List of Schemes

List of Abbreviations

Ar	aryl
BDE	bond dissociation energy
Bu	butyl
Cb	9H-carbazol-9-yl
DOE	United States Department of Energy
DFT	density functional theory
DSC	differential scanning calorimetry
e	elementary charge
e^-	electron
ESI	electrospray ionization
Et	ethyl
F	Faraday constant
FID	flame ionization detector
FC	fuel cell
G	Gibbs free energy
GC	gas chromatography
h	hour(s)
H	enthalpy
Hex	hexyl
HRMS	high resolution mass spectrometry
I	electric current
IL	ionic liquid

IR	infrared
K	equilibrium constant, kelvin
M	metal
Me	methyl
MEA	membrane electrode assembly
Min	minute(s)
MOF	metal-organic framework
mp	melting point
MS	mass spectrometry
NMR	nuclear magnetic resonance
$^{-}NTf_2$	bis(trifluoromethylsulfonyl)amide
^{-}OTf	trifluoromethylsulfonate
^{-}OTs	p-toluenesulfonate
P	power, pressure
PEI	polyethylenimine
PEM	polymer electrolyte membrane, proton exchange membrane
Ph	phenyl
Pr	propyl
Py	pyridine
q	heat
Q	reaction quotient
ρ	density
s	second(s)
S	entropy
T	temperature

TBP^+	tetrabutylphosphonium
TGA	thermogravimetric analysis
V	electric potential, volume
VOC	volatile organic compound
w	work
x	mole fraction
X	unsaturated fluid
X^-	halide
XH_2	saturated fluid

Chapter 1

Introduction

1.1 Hydrogen as an Energy Carrier

Energy is required to perform any process on Earth, from biological processes occurring in cells, to geological processes carving mountains. In physics, energy is understood as the ability to do work. It exists in many different forms. Some familiar forms include the gravitational potential energy that causes objects to fall to the ground and planets to orbit stars; the kinetic energy that moves a train along its tracks; electromagnetic radiation from the sun that heats our planet and drives photosynthesis in plants; and thermal energy that heats our homes in winter. All types of energy are equivalent and one form may be transformed into another, though rarely with perfect efficiency. This is one of the laws of nature, the conservation of energy; though energy may change its form, the total energy will remain constant. After Albert Einstein (1879-1955) developed his theory of special relativity,[1] this law was expanded to include the conversion of mass to energy through his familiar equation $E=mc^2$ and was restated as the conservation of mass-energy.

1.1.1 Energy and the Environment

The discussion of energy is not merely limited to scientific discourse. Energy, which sustains us biologically, is actively traded economically. Energy allows us to manufacture goods, transport goods and passengers, light and control the climate of buildings, and run the electrical equipment that improves our productivity and entertains us. The most commonly traded forms of energy are electrical potential energy (supplied through municipal electrical grids) and chemical potential energy (supplied as fuel, food and batteries).

Energy can be obtained in many different ways but there are only two primary sources of energy on Earth, solar energy and nuclear energy. The most important source of energy is the Sun. The Sun is responsible for the energy required for photosynthesis in autotrophs, the foundation of the food chain (except in deep sea hydrothermal vents).[2] Fossil fuels, which consist of coal, peat and petroleum, are derived from biological matter and ultimately contain energy obtained from the Sun. Wind turbines and wave power generators[3, 4] are powered by wind that is generated by differential heating of the Earth by the Sun. Hydroelectric turbines are powered by the gravitational potential energy of water, but that energy was obtained by evaporation processes powered by the Sun. Solar cells are able to convert solar energy directly into electricity.[5, 6] Nuclear power generators use radioactive material directly to power steam turbines and geothermal energy[7] uses heat from the Earth (a small amount left over from planetary accretion and mostly from internal radioactivity). The outlier is tidal power generation,[8] which uses the gravitational

potential energy between the Earth and the Moon (and to a lesser extent the Earth and the Sun) to generate electricity.

There are advantages and disadvantages to using any of these particular technologies to generate electricity. Wind, wave and solar cells require high capital investment to construct and are unreliable in their generation of electricity. Additionally these facilities require a large footprint to yield a given amount of power and are not aesthetically pleasing. Concern exists regarding the effect of the immediate environment surrounding such facilities (particularly noise pollution with wind and wave generation) and the impact on productive fisheries in the case of wave farms. Hydroelectric power can only be generated where a river exists and requires the construction of a dam that changes the local environment. However the technology, which has been used since antiquity to grind grain, is relatively clean. Retrofitting existing dams would mitigate the damage caused by the construction of new dams. Nuclear power generation does not emit greenhouse gases, but the operation of a nuclear power plant does generate radioactive waste which remains dangerously radioactive for thousands of years. There also exists the possibility of accidental releases of radioactive material[9] and the generation of nuclear weapons. Fossil fuels are convenient and inexpensive sources of energy but their combustion releases carbon dioxide (a greenhouse gas) into the atmosphere and the extraction of fossil fuels from the ground causes significant damage to the local environment and leaks or spills during harvesting and transportation[10] can lead to environmental disasters. There is also a limited amount of fossil fuels that are

economically obtainable and exportation and utilization of less favourable sources is becoming more important.

The harvesting and combustion of petroleum and other fossil fuels has been identified as a major anthropogenic source of pollutants that affect the global environment.[11] Harvesting and transporting fossil fuels through various means can affect the environment directly as is the case with open pit and strip mining of coal or by accidental release such as marine oil spills. Petroleum, however, drives the global economy. A great deal of energy generation involves the combustion of fossil fuels. Its low cost to implement and produce electricity competes favourably with nuclear power generation as well as renewable energy sources.

Apart from energy sources, energy carriers must be used to transmit energy from place to place, unless energy is used directly where it is generated. Municipal electrical grids consist of wires that carry energy to buildings. Batteries are convenient carriers of electrical energy off the municipal grid. In the transportation industry, petroleum products dominate the energy carrier market due to the low cost and high energy density of these materials.

The convenience and low cost of petroleum compared to other energy sources are likely to allow it to remain an economical choice as an energy source but political and environmental reasons are encouraging the development of alternatives to petroleum in the role as an energy carrier. Hydrogen would appear to be an ideal energy carrier as it has a high molar enthalpy of combustion (ΔH_{comb} = -286 kJ mol^{-1}),[12] however, it is not particularly useful because it is a gas and is difficult to contain a large amount in a

portable application. Molecular hydrogen has a low molecular mass so the energy density per unit mass is very large (ΔH_{comb} = -143 MJ kg^{-1}).[12] Hydrogen cannot be used as an energy source because elemental hydrogen is rare on earth but it can be produced using energy from a primary source to form an effective energy carrier. An economy where hydrogen is the preferred energy carrier has been called a hydrogen economy and one where hydrogen is produced without the use of any fossil fuels would be a pure hydrogen economy.[13-24] There are many challenges involved in establishing and developing a hydrogen economy. Two of the most pressing are the efficient generation of hydrogen and the transportation and storage of hydrogen where it is needed.

1.1.2 The Hydrogen Economy

There are many reasons why a hydrogen based economy would be attractive compared to the current hydrocarbon economy. Some of the most prominent are based on environmental benefits. Hydrogen fuel combusts cleanly; the combustion product is water. Because water is ubiquitous and benign, and water is normally consumed in the production of hydrogen, there are no problems associated with emitting water into the environment. Hydrogen could be burned in an internal combustion engine[25] just as petroleum is, but hydrogen has the advantage that it can be combusted with much more efficient transfer of energy through the use of a fuel cell. In contrast, the combustion of petroleum has several drawbacks. It is the major contributor of anthropogenic greenhouse gas emissions.[26] Beyond releasing carbon dioxide into the atmosphere, hydrocarbons that

escape combustion are emitted as volatile organic compounds (VOCs). The high temperature of the engine and exhaust streams can cause the formation of nitrogen oxides.[27] Both VOCs and nitrogen oxides contribute to the formation of ground level ozone,[28, 29] a common pollutant in urban areas. Particulate matter,[30-32] which are fine particles of solids or liquids, are released from the burning of fossil fuels in vehicles and power plants and lower the breathing air quality in cities.

Politics is also an important motivation to the adoption of a hydrogen economy. The American economy is dependent on fossil fuels[33] and a great deal of these are derived from foreign sources. The combustion of fossil fuels remains the primary method of electricity generation in the United States of America. The transportation of goods and materials relies heavily on trucks that are powered by internal combustion engines. Consumers and workers transport themselves to and from employers and businesses primarily using fossil fuel powered personal vehicles or public transportation. The largest deposits of high quality crude oil are in the Middle East[33] and such dependence on foreign oil is undesirable as is purchasing from a cartel of sovereign states (Organization of the Petroleum Exporting Countries, OPEC) who can fix prices. There are even larger oil deposits in Canada[3433, 34, 34, 34] and Venezuela[35] (which is a member of OPEC) but they are more difficult to access and are generally of lower quality.

Petroleum acts as both a carrier and a source of energy. Petroleum products are simply pumped from underground deposits, but these oil wells are non-renewable resources. The chemical energy stored in petroleum is solar energy stored by photosynthesis by plants many millions of years ago. Hydrogen can be a carrier of

energy, but is not a source of energy (unless used in a fusion reactor). This is because hydrogen gas only occurs naturally on Earth in small quantities and must therefore be generated artificially.

As a carrier of energy for mobile applications, hydrogen is more desirable than petroleum products. For one, the problems associated with the distributed production of carbon monoxide and ground level ozone[28, 29] are immediately alleviated. Moreover, if the energy required to generate hydrogen comes from the combustion of fossil fuels then the carbon dioxide generated may be scrubbed[36-40] from the effluent of a stationary system and disposed of in an alternate manner than releasing it into the atmosphere. Using fossil fuel combustion as the energy source for hydrogen generation does not remove the economic dependence on petroleum products from foreign sources.

1.1.2.1 Properties of Hydrogen

Hydrogen is the lightest and most abundant of all the elements in the Universe, where it composes about 75% of the elemental mass and 90% of the number of atoms.[12] It is commonly found in the plasma state in stars (wherein it undergoes nuclear fusion to release energy and generate heavier elements); in nebulae, and in gas giant planets in molecular form. However, hydrogen is seldom seen naturally occurring as the pure element on Earth. Under standard conditions of temperature and pressure hydrogen occurs as a colorless, odorless, and highly flammable (when mixed with air or another oxidant) diatomic gas. However, hydrogen forms compounds with most other elements,

both through covalent bonds and as protons (H^+) and as hydride (H^-) ions. Hydrogen is most commonly encountered on Earth as water and hydrocarbons, both of which can be used as feedstocks in the industrial production of hydrogen gas. Hydrogen gas, like helium gas, does not accumulate to an appreciable extent in the Earth's atmosphere because it is light enough to occasionally escape the planet's gravitational field. The atmospheric concentrations of hydrogen and helium are about 0.5 ppm and 5.2 ppm respectively.[12]

By far the most common isotope of hydrogen is protium (^1H) with a nucleus consisting of one proton and no neutrons; deuterium (^2H) is another stable isotope with a natural abundance of 0.015% and consists of one proton and one neutron. Tritium (^3H) is an unstable isotope of hydrogen that undergoes beta decay to form ^3He with a half-life of approximately 12.32 years. It only occurs in trace concentrations naturally and must be produced artificially[41] in nuclear reactions for isotopic labeling experiments and other uses.

Hydrogen gas is extremely flammable when mixed in air and will burn or form explosive mixtures in a wide range of concentrations.[42] Hydrogen flames emit primarily ultraviolet light, which makes them nearly invisible to human eyes. Leaking hydrogen cylinders are therefore very dangerous and must be approached with caution as the gas stream may be burning. Fortunately, hydrogen is much less dense than air and the escaping hydrogen stream (and any flames) tend to burn straight upward rather than spreading outward.

Hydrogen presents a unique metallurgical challenge for storage and transport due to its ability to dissolve in many metals and alloys. It does so by dissociating on the surface of the metal (through a chemisorption process) into hydrogen atoms. These atoms are small enough to pass into the crystal lattice of the metal through its interstitial sites. In this way hydrogen can slowly leak out of containers but more importantly the containers can be damaged by hydrogen embrittlement.[43] Hydrogen embrittlement is the process by which the hydrogen atoms dissolved in the crystal lattice migrate to minuscule internal defects where they recombine to form molecular hydrogen gas that exerts pressure on the inside of the crystal lattice. This can eventually lead to material failures and explosions.

1.1.2.2 Production of Hydrogen

Hydrogen gas can be produced by the reaction of strong acid with metals (this was how hydrogen was first produced by Paracelsus (1493-1541)).[44] However, this is not the route used to produce hydrogen on an industrial scale. The most commonly used method for generating hydrogen is through steam reforming, usually from methane but also from other hydrocarbons.[45, 46] Other methods of obtaining hydrogen from fossil fuels include coal gasification,[47, 48] partial oxidation[49, 50] and plasma reforming.[51-55] Hydrogen can also be produced from water, either by electrolysis[56, 57] where electricity is inexpensive or through a sulfur–iodine cycle at high temperature.[58-60]

Steam reforming is the method of hydrogen production used for making bulk hydrogen for industrial use, the production of ammonia (through the Haber-Bosch

process) and the hydrocracking of petroleum. In this process, the hydrocarbon fuel is heated with steam at high temperature (700-1100 ºC) over a metal catalyst. The endothermic and reversible reaction generates carbon monoxide and hydrogen.

$$CH_4 + H_2O \rightleftharpoons CO + 3H_2 \quad \Delta H = +206 \text{ kJ mol}^{-1} \qquad (1)$$

This mixture of carbon monoxide and hydrogen is known as syngas and it can be used in hydroformylation reactions as well as a feedstock for Fischer-Tropsch chemistry. Additional hydrogen can be obtained from syngas by reacting with additional steam at a lower temperature (over a different catalyst) in an exothermic reaction forming carbon dioxide and water.[61, 62] This reaction is known as the water-gas shift reaction.

$$CO + H_2O \rightleftharpoons CO_2 + H_2 \quad \Delta H = -41.2 \text{ kJ mol}^{-1} \qquad (2)$$

Coal gasification is a process wherein coal is treated with hot steam and oxygen to yield a mixture of carbon monoxide, carbon dioxide, hydrogen as well as other products. The desired product is usually syngas as in the steam reformation of methane. Coal gasification reactors can be heated externally or they may be heated by the combustion of some of the coal feedstock. This process is frequently used where ample coal but few petroleum sources are available. Additional products of coal gasification consist of coke for heating, coal tar that can be processed to many different products, sulfur, and

ammonia. Coal gasification can also be performed *in situ* underground by injecting the oxygen and steam into a coal seam and collecting the coal gas from a well.[63] In this way, the energy contained in the coal can be mined with little impact on the surface where a regular coal mine would be.

The Kværner process is a method for generating hydrogen and activated carbon directly from hydrocarbons in a plasma burner. This process occurs at about 1600 ºC and the only products are carbon and hydrogen. The reaction is energy efficient and most of the energy used to produce the activated carbon and hydrogen is stored in the new chemical bonds.

1.1.2.3 Fuel Cells

A fuel cell is an electrochemical energy conversion device that is designed to transform the combustion energy stored in the chemical bonds of the fuel into electrical energy in a manner that is theoretically far more efficient than an internal combustion engine. A fuel cell is similar to a battery, but whereas a battery stores its chemical fuel supply internally, where it is eventually consumed and the battery becomes exhausted, a fuel cell generates electrical energy catalytically as the fuel is supplied externally. A fuel cell will continue to operate so long as a constant supply of fuel and oxidant is supplied to the anode and cathode respectively.

1.1.2.3.1 Polymer Electrolyte Fuel Cells

The most commonly studied fuel cell for use in an automotive application is the proton exchange membrane fuel cell (PEMFC). This may alternately be described as a polymer electrolyte membrane fuel cell. A PEMFC consists of an anode, a cathode, a proton exchange membrane (PEM), and a catalyst. The advantage of using a PEMFC over other types of fuel cells is its relatively low operating temperature, typically between 60 °C and 80 °C though they can be operated above 100°C under certain conditions.[64-66]

The anode is made of a porous material that is designed to allow the fuel, in this case hydrogen, to permeate the entire surface effectively. The anode collects the electrons generated by the anode half reaction:

$$H_2 \rightarrow 2H^+ + 2e^- \quad (3)$$

and passes them through an external circuit where they become the electrical current that can be used to do useful work. The protons generated travel separately from the electrons through a proton exchange membrane.

The cathode is also made of porous material. It is designed to allow the oxidant, which is oxygen, to permeate its surface where the electrons returning from the external circuit, the protons from the PEM and oxygen react in the cathode half reaction, which generates waste heat and water.

$$O_2 + 4H^+ + 4e^- \rightarrow 2H_2O \quad (4)$$

The proton exchange membrane[64-66] is sandwiched between the anode and the cathode and may only be micrometers thick. It consists of a cation exchange membrane which allows protons to pass through the membrane from the anode to the cathode, but which excludes the passage of electrons and forces them through the external circuit. If this were not the case, the electrons passing through the PEM would cause a short circuit and no current would flow through the external circuit, the energy being lost instead as waste heat. The standard material currently used in PEMs is Nafion® which is a fluorous sulfonic acid polymer developed by DuPont™.

The catalyst material is normally composed of platinum nanoparticles, which maximizes the catalyst surface area. The catalyst is the site of the redox chemistry that occurs in the fuel cell. The anode and cathode half reactions both occur on catalyst surfaces. Platinum nanoparticles are embedded in both the anode and cathode on the surfaces that face the PEM.[67-69] This is because the anode half reaction gives off protons, which must pass through the PEM, and the cathode uses protons obtained from the PEM. Water balance is an important issue in PEMFCs.[70, 71] The PEM requires adequate hydration in order to transport protons; if the PEM runs dry, the circuit cannot be completed. In contrast, if the catalyst layer becomes flooded with water, the redox chemistry will become impeded, as there would not be adequate interaction with either the fuel or the oxidant. The catalyst must have contact with water so the protons have

mobility from the anode to the cathode, but they must also have contact with hydrogen on the anode side, and oxygen on the cathode side in order to function. This is one of the major challenges associated with the development of PEMFC technology.

The catalyst used in PEM fuel cells is very expensive; therefore research is being performed to determine what other cost effective catalysts may be used in PEMFCs.[72-74] The catalyst can also be very sensitive to impurities in the fuel stream used to power the fuel cell.[75] Clean sources of hydrogen are therefore required. This is a major challenge to the development of fuel cells as power generators for small portable applications. However, the main challenge is that hydrogen itself has a very low volumetric density of only 0.0899 g/l at standard temperature and pressure. Various methods of portable hydrogen storage, both physical and chemical, are being developed.

1.1.3 Hydrogen Storage

Hydrogen has a high molar (and specific) enthalpy of combustion so it is attractive as a fuel for portable applications where a high power to mass ratio is desirable. However, hydrogen under standard conditions behaves as an ideal gas. One kilogram of hydrogen, which releases 143 MJ of energy when combusted, has a volume of about 12 200 litres. Operating a vehicle or handheld device while carrying around a large balloon of hydrogen is not feasible. One of the main challenges in using hydrogen as a portable energy carrier is making the hydrogen itself portable. There are many proposed methods for doing so, each with advantages and disadvantages. Targets for the

specification of hydrogen storage systems have been set by the United States Department of Energy[76] to make such systems able to carry a similar amount of energy as a petroleum fuel tank, so that a vehicle fuelled with hydrogen will have a similar driving range as a conventional vehicle before refuelling is required.

1.1.3.1 DOE Guidelines

The United States Department of Energy through its Office of Energy Efficiency and Renewable Energy has set targets for the performance of hydrogen storage technologies. Hydrogen storage is an important challenge that must be overcome if hydrogen powered vehicles are ever to become a viable alternative to those powered by petroleum. The target driving range of a hydrogen powered vehicle is 300 miles (~500 km), which is similar to the range of a petroleum powered car. For this driving range, 5–13 kg of hydrogen must be stored on board a fuel cell operated car.

Targets set by the DOE were chosen in such a manner as to deliver a vehicle whose operating costs and performance characteristics would be similar to conventional vehicles.[76] In 2003, initial targets for hydrogen storage systems were set with increasingly stringent goals occurring every five years starting in 2005. In 2009, the targets were modified based on additional information acquired over the six year period. Automotive manufacturers had developed many hydrogen fuel cell and hydrogen internal combustion engine vehicles and “real life” operation of these new vehicles generated more accurate data regarding fuel economy of these vehicles. Information about fuel economy as well as

the changing internal structure of hydrogen powered vehicles allowed for the relaxation of some of the hydrogen storage targets.

The updated hydrogen storage targets set by the DOE for 2015 are a capacity of 1.8 kWh/kg (5.5 wt.% hydrogen) and 1.3 kWh/l (40 g hydrogen/l) and the long term goals are 2.5 kWh/kg (7.5 wt.% hydrogen) and 2.3 kWh/l (70 g hydrogen/l) for the entire system. This includes the tank material, insulation, valves, tubing, and any additional components. Therefore the hydrogen storage material alone must exceed these targets. In addition to hydrogen storage on board the vehicle, depending on the hydrogen distribution system required to refuel vehicles, reasonable stationary storage methods may be required where hydrogen is produced or at refueling stations. There are additional targets set by the DOE for cycle life, delivery pressure, refueling time, and hydrogen purity.

Gravimetric storage density is the most challenging target to meet. This is because hydrogen is much less massive than other atoms. In most cases the goal is to store as many hydrogen atoms as possible for every heavy atom in the storage material. Even when hydrogen is compressed and liquefied and the gravimetric density of the material is 100% hydrogen, the mass of the materials used to contain it will drop the gravimetric capacity dramatically. For instance, the mass of special low–weight and high pressure cylinders for compressed hydrogen storage yield an overall gravimetric density of about 6 wt% hydrogen.

The cycle life of a hydrogen storage system is important because the fuel tank should last the life of the vehicle. Cycle life will depend heavily on the hydrogen storage

system. In cases where hydrogen is simply stored in a compressed form, the cycle life of the system is almost indefinite. In contrast, in systems where hydrogen is stored chemically, limits on the selectivity of the reaction involved will limit the cycle life. The delivery pressure can be easily controlled using a regulator as long as the system is capable of generating an equilibrium hydrogen pressure at or above the minimum required pressure. In reversible chemical storage systems, this is limited by thermodynamics. Refuelling time is only of concern in systems where hydrogen is recharged on board the vehicle. In this case it would be a function of the delivery rate of compressed or liquefied hydrogen to the storage system and, in those systems where adsorption or absorption occurs, the rate of these processes. Hydrogen purity is especially important in the operation of a fuel cell where the fuel cell catalysts are easily poisoned. Chemical storage systems are more likely to contaminate the hydrogen stream either because the storage system components are at least somewhat volatile, or they become entrained in hydrogen as it evolves.

Current hydrogen storage technologies comprise two broad categories: "reversible" storage mechanisms by which hydrogen is stored physically by compression, liquefaction, adsorption, or absorption processes where hydrogen can be refueled on board;[77, 78] and "irreversible" systems where hydrogen is stored chemically and released on demand, these systems require offboard regeneration of the storage material.

1.1.3.2 Compressed Hydrogen

Hydrogen stored in a typical compressed gas cylinder for laboratory use has an overall gravimetric density of approximately 1 wt% hydrogen. This is mostly due to the mass of the steel cylinder and the relatively low storage pressure of the gas (~160 bar). Materials technology is being used to develop special gas cylinders that store hydrogen at pressures of about 700 bar and that are made of lightweight materials. Gas cylinders for prototype hydrogen powered vehicles are typically composed of a pressure–bearing carbon fiber shell lined with a high molecular weight polymer to prevent gas permeation. Hydrogen cylinders of this type typically store hydrogen at a gravimetric density of about 6 wt%. This appears to be a simple solution to the hydrogen storage problem but there are drawbacks to using compressed hydrogen gas.[79-87] The carbon fiber used to make the high pressure cylinder is expensive and there is a great deal of energy required to compress hydrogen to these very high pressures. The cost of compressing hydrogen to 700 bar is actually higher than the cost of liquefying hydrogen, an alternative hydrogen storage technique. There are also safety concerns regarding the use of such high pressure gas cylinders by lay people. This technology is the closest to meeting the DOE goals for hydrogen storage; however, the gravimetric hydrogen storage density is unlikely to be improved substantially beyond this. Increasing gravimetric hydrogen storage density would require increasing the storage pressure. This would require stronger cylinders that would become more massive, negating any benefit of increased storage pressure. Higher

pressures would only exacerbate the costs of pressurizing the gas as well as the safety concerns associated with the refueling process.

1.1.3.3 Liquefied Hydrogen

Though it may seem an attractive option, there are several disadvantages to the use of liquefied hydrogen as an energy carrier.[88] The critical temperature is the highest temperature at which a compound can exist in the liquid state. The critical temperature of hydrogen is very low (33 K) and even at this temperature hydrogen is only a liquid under pressure, at ambient pressure hydrogen liquefies at its boiling point (20.3 K). Hydrogen is only a liquid over a very small range of temperatures. The density of liquid hydrogen at its melting point is only 70 g/l. There are more hydrogen atoms in a litre of petroleum than there are in a litre of pure liquid hydrogen.

To liquefy hydrogen, a large energy investment is required. Hydrogen (along with helium and neon) is one of the few gases which increase in temperature upon expansion at constant enthalpy at ambient temperature due to the Joule-Thomson effect.[89] To liquefy hydrogen, it must be cooled to a temperature below its inversion temperature (~193 K). This can be accomplished by pre-cooling the gas using liquid nitrogen. Hydrogen also exists as a mixture of two spin states. Orthohydrogen is the state where the two protons have parallel nuclear spins and parahydrogen is the state where the two protons have antiparallel nuclear spins.[90] At ambient temperature, orthohydrogen is thermodynamically favoured in a ratio of about 3:1 to parahydrogen. However, at temperatures where

hydrogen is a liquid, parahydrogen is thermodynamically favoured at a ratio of 99.79:0.21. Thus, liquid hydrogen is in a metastable state and slowly converts to parahydrogen in an exothermic process. The enthalpy of conversion is higher than the enthalpy of vaporization so even perfectly insulated liquid hydrogen will completely vaporize over time. To overcome this during liquefaction, hydrogen is placed in contact with a catalyst that rapidly converts orthohydrogen to parahydrogen while it is still being cooled.[91] Even when converted to parahydrogen imperfect insulation results in boil off losses of about 1% per day.

1.1.3.4 Physisorbed Hydrogen

Physisorption is the process by which a molecule is adsorbed to a surface only through weak van der Waals interactions. Such interactions are not specific to the chemical nature of the adsorbant or the adsorbate so any molecule is capable of being adsorbed to some extent on any surface. Physisorption of hydrogen onto high surface area materials is of interest for hydrogen storage applications because it greatly increases the volumetric density of hydrogen compared to the gaseous state.[92-103] Such materials could be reused many times. However, because the primary attractive force between hydrogen and the surface is only a weak van der Waals interaction, the heat of adsorption is very small and hydrogen is only weakly bound. This is advantageous during the desorption process when hydrogen must be delivered to the fuel cell. It is disadvantageous, however, because weak binding requires that very low temperatures and/or high pressures be used

for any significant binding to occur. Chemisorption processes, where the hydrogen molecule is chemically bound to a surface (typically by breaking into hydrogen atoms), proceed with a much higher heat of adsorption and can therefore be carried out at higher temperatures and lower pressures. However, chemisorption is not as easily reversible and heat would need to be used to deliver the bound hydrogen to a fuel cell.

Monolayer coverage of hydrogen is described by the Langmuir adsorption isotherm.[104] This is a simple model where it is assumed that the surface is perfectly flat with no defects with many equivalent binding sites each capable of holding one molecule of adsorbate. Adsorbed molecules are assumed to be immobile on the surface and to have no effect on further binding. Of course all of these assumptions are incorrect, but the Langmuir model provides a general picture for surface coverage at a given temperature and pressure.

Multilayer adsorption processes, where further layers of molecules are adsorbed onto the first monolayer, are described by the BET (Brunauer, Emmet, and Teller) adsorption isotherm.[105] In BET theory, as in the Langmuir model, the first monolayer of coverage is mediated by the adsorption enthalpy between the adsorbate and the surface. Further adsorbed layers are dictated by the liquefaction of the adsorbate onto previous monolayers. This stipulation prevents the formation of multilayers of hydrogen above its critical temperature (32.97 K) under pressure, or above its boiling point (20.28 K) at ambient pressure. Therefore, even if cooled in liquid nitrogen, such hydrogen storing materials would only be able to achieve monolayer coverage.

Because only monolayer coverage would be observed, the hydrogen storage density would be proportional to the accessible surface area of the material (the accessible surface area for hydrogen would be larger than that measured for nitrogen adsorption due to its smaller size). Because the primary forces involved in physisorption are van der Waals forces, similar amounts of hydrogen should be stored regardless of the nature of the surface. It has been determined that for simple physisorption, the potential gravimetric hydrogen storage density is only 2.6 wt% per 1000 m^2/g of surface area when cooled to 77 K, roughly independent of the surface material.[106] This gravimetric storage density drops rapidly if the surface is held at ambient temperature.

Current research into hydrogen storage through physisorption is largely related to the development of materials that have high accessible surface area and/or higher heats of adsorption. Increasing the heat of adsorption allows for more hydrogen to remain bound to the surface at higher temperatures. Metal-organic frameworks (MOFs) are currently being investigated for these purposes.

1.1.3.4.1 Metal-Organic Frameworks

Metal-organic frameworks are crystalline supramolecular materials formed by the self-assembly of metal–containing vertices with multi-functional ligand bridges. Such frameworks can be three-dimensional and are usually porous. MOFs are similar to zeolites (aluminosilicates with regular porous structure). MOFs are being investigated for

use in gas purification, separation, and storage[107-115] as well as uses in catalysis and as chemical sensors.

MOFs are grown through solvothermal processes where metal ions and ligands are mixed in a hot solvent and allowed to crystallize slowly. This slow and reversible crystallization process allowed for defects in the crystal structure to be self-corrected and allows for the formation of a large regular porous structure. In order to be used for gas storage, the MOF must have its pores desolvated. Sometimes, the internal structure of a MOF will collapse during desolvation due to the exposure of free metal binding sites and rearrangement of the material. However, the exposure of free metal binding sites[116] would be advantageous for a hydrogen–storing MOF as these sites allow for much higher heats of adsorption and therefore higher hydrogen storage temperatures.

The current best hydrogen–storing MOF is MOF-177 which is Zn_4O(1,3,5-benzenetribenzoate)$_2$. This MOF has a surface area of 4526 m^2/g and can store up to 1.23 wt% hydrogen at 1 bar of pressure and 77 K. This value increases to 7.1 wt% and 11.4 wt% hydrogen at 40 bar and 78 bar respectively.[117]

1.1.3.5 Metallic Hydrides

Various metals and alloys are capable of adsorbing hydrogen into their lattice reversibly at interstitial sites. The most familiar is palladium which is well known for adsorbing a large amount of hydrogen relative to its size. At ambient temperature and pressure, palladium metal will absorb hydrogen to a stoichiometry of $PdH_{0.7}$.[118] Although

this means that palladium can hold nine hundred times its volume of gaseous hydrogen, the high relative mass of palladium means that the fully saturated metal only contains 0.65 wt% hydrogen. Palladium is also a prohibitively expensive metal to use for such an application.

Other interstitial alloys exist[119-122] and generally consist of intermetallic alloys, usually in an AB_5 stoichiometry. Metal A is either an alkaline earth metal or a rare earth element and metal B is a transition metal element. These intermetallic compounds are capable of reversibly binding hydrogen at ambient temperature. An example of this is lanthanum nickel hydride ($LaNi_5$),[106] which reversibly binds six hydrogen atoms (to form $LaNi_5H_6$). This material can operate as a rechargeable metal hydride battery, though it is only stable for a few cycles.

In general, the volumetric hydrogen storage densities of these materials can be very high, as is the case with palladium. However, the large mass difference between hydrogen and transition metals yields very low gravimetric storage densities. These compounds may not be useful as hydrogen storage materials for this reason but they do find use as rechargeable batteries where they have largely replaced the use of nickel-cadmium batteries.[106]

1.1.3.6 Complex Hydrides

Complex hydrides are materials based on the lighter elements in groups 1, 2, and 13 of the periodic table.[123, 124] Perhaps the most popular are borohydrides and amine-

boranes.[125-146] These materials do not contain transition metal atoms and therefore have much higher gravimetric storage densities. This has made these materials very popular for study as potential hydrogen storage materials. Unlike in metallic hydrides, hydrogen atoms are not stored in interstitial lattice sites but are instead stored in covalent bonds. Hydrogen is generally released from these materials in one of two ways: through hydrolysis or thermolysis.

Hydrolysis reactions of complex hydrides are generally spontaneous and exothermic in nature. The rate of hydrogen evolution can be controlled by the rate of addition of water to the complex hydride, or by the addition of a catalyst to a solution of complex hydride in water which is otherwise kinetically stable. Such a storage technique would require the vehicle to carry a tank of water, which is heavy. However, part of the water contributes to the hydrogen storage density of the material and water can be recycled from its production at the cathode of the PEM fuel cell being operated by the complex hydride storage system.

Thermolysis is another option for releasing hydrogen from complex hydrides. This requires heating the complex hydride to evolve hydrogen directly; such processes may be endothermic or exothermic. In either case, catalysts are required to lower the temperature for dehydrogenation of these materials (for instance, magnesium hydride dehydrogenates at 300 ºC and lithium hydride must be heated well above 700 ºC to dehydrogenate). Not all of the hydrogen contained in these materials is always released, however in some cases that is desirable. If all the hydrogen contained in ammonia-borane

were evolved, the resulting product would be boron nitride, a rather intractable compound that is not readily recyclable.

When complex hydrides are handled in the solid state, repeated cycles of hydrogenation and dehydrogenation can change the morphological structure of the material. In order to ascertain the long-term stability of these materials, such changes in morphological structure must be investigated. Exothermic dehydrogenations are convenient on board a vehicle because they can be self-sustaining and the energy contained in the hydrogen does not need to be diverted to the release of more hydrogen. However complex hydrides are not easily regenerated, particularly when they have undergone hydrolysis and strong metal-oxygen bonds must be cleaved.

Complex hydrides may be useful materials for hydrogen storage applications. In order for this to be true, the rates and activation temperatures of thermal dehydrogenation must be improved. The cycle life of complex hydrides must also be determined. Inexpensive methods of regenerating exhausted material must be developed, particularly by a direct reaction with hydrogen gas. If these conditions are met, complex hydrides may become an economically viable hydrogen storage medium.

1.1.3.7 Organic Hydrides

Organic hydrides, or rather simple organic molecules which can release hydrogen in a dehydrogenation reaction, have been largely overlooked by the mainstream hydrogen storage research community as hydrogen storing materials. This is largely because of the

relatively low gravimetric hydrogen storage density of these materials when compared to complex hydrides. Organic hydrides also undergo endothermic dehydrogenation and as such they require the input of heat to release hydrogen (this heat coming from the combustion enthalpy of hydrogen) so only a portion of the stored hydrogen could be put to use doing productive work.

There are advantages to using organic hydrides as hydrogen storing materials. These include increased consumer safety, compatibility with existing infrastructure, and facile offboard reversibility. Instead of handling cryogenic or compressed hydrogen, consumers would fill their fuel tanks with an organic liquid similar to petroleum. Existing fuel distribution systems could be used to transport this fluid hydrogen storing material to and from the consumer. Early studies on hydrogen storage in organic hydrides were centered on the dehydrogenative aromatization of cyclohexane to benzene as well as similar systems.[147] Dehydrogenative aromatization is attractive as this is one of the most gravimetrically dense hydrogen storage systems, e.g., cyclohexane consists of 7.1% removable hydrogen.

Previous research has shown that substituting a heteroatom such as oxygen, or especially nitrogen on a ring system greatly lowers the enthalpy of dehydrogenation of the ring.[148-151] This is beneficial as it reduces the amount of energy siphoned from the combustion of hydrogen required to release stored hydrogen. The lowered enthalpy of dehydrogenation also tends to improve the kinetics of dehydrogenation. The reaction enthalpy lowering effect was predicted through theoretical calculations using density functional theory (DFT). These calculations showed that the inclusion of a heteroatom in

the ring lowered the enthalpy of dehydrogenation. The calculated change in reaction enthalpy for the replacement of a single CH_2/CH to an NH/N was -5.78 kcal/mol (-24.2 kJ/mol). The addition of subsequent nitrogens on the ring system depends on their placement relative to other ring nitrogen atoms. Placing a nitrogen atom adjacent to the existing nitrogen atom actually increases the dehydrogenation enthalpy, however placing an additional nitrogen in a 1,3 or 1,4 relationship to the original ring nitrogen further decreases the enthalpy of dehydrogenation. The effect of nitrogen on the enthalpy of dehydrogenation has been postulated to be related to the weakening of C-H bonds adjacent to nitrogen atoms in the ring.

Further contributions to this data were made by Clot et al. regarding the effect of structure on the enthalpy of dehydrogenation of several heterocycles using theoretical calculations.[152] All of the heterocycles studied were shown to dehydrogenate endothermically, none was predicted to dehydrogenate exothermically. It was also shown that the entropy of dehydrogenation of each of the heterocycles was approximately equal to that of the evolution of the equivalent amounts of hydrogen released. The change of the entropy of the substrate was far outweighed by the change in entropy associated with the formation of new gaseous molecules.

A dehydrogenation temperature, defined as the temperature for which the calculated Gibbs free energy of dehydrogenation was zero, was calculated for each substrate. This dehydrogenation temperature is a measure of the aptitude for each substrate to hydrogenate and dehydrogenate. Substrates with especially low dehydrogenation temperatures should be easily dehydrogenated on board the vehicle.

While the resulting molecules would be difficult to hydrogenate, this is a minor problem as the hydrogenation would be taking place off board where high pressures and temperatures could be used. High temperatures and pressures improve the kinetics of hydrogenation, and though high temperature disfavours hydrogenation thermodynamically, the high pressure of hydrogen used would force the reaction to completion through Le Chatelier's principle. Substrates with a high dehydrogenation temperature are difficult to dehydrogenate (a much more pressing concern).

Factors that favour dehydrogenation are those that would stabilize the unsaturated product, those that destabilize the saturated starting material, or both. Factors that stabilize the unsaturated product are the strength of the π-bonds formed and the aromatic character of the product molecule. Factors that destabilize the saturated starting material are those that weaken either the C-H or the N-H bonds in the molecule. Ring size was also determined to influence the dehydrogenation temperature of the substrates. Those with five-membered rings have a lower dehydrogenation temperature than those with six-membered rings. This can be explained by the number of molecules of hydrogen that must be evolved (and the number of C-H and N-H bonds that must be broken) before aromatic stabilization is achieved. The exception to this was the formation of cyclopentadiene, which as a neutral molecule is not aromatic (and is in fact not stable, it readily dimerizes in a Diels–Alder reaction). Calculations on the simple substrates benzene, pyridine, and aniline showed that the aniline had a lower dehydrogenation temperature than pyridine. This appears to show that substituent nitrogen atoms may have a stronger effect on dehydrogenation enthalpy than ring heteroatoms.

This knowledge stimulated the investigation of the combined dehydrogenation enthalpy lowering effects of both substituent groups and ring heteroatoms.[141, 142, 153, 154] Using DFT calculations, which were calibrated with experimental data, Cui was able to generate a set of three Hammett relationships that showed the connection between substituent and heteroatom effects on dehydrogenation enthalpy.

The experimental and calculated enthalpies of reaction for the dehydrogenation of a series of substituted cyclohexanes to their corresponding benzenes show a linear relationship with the Hammett parameter σ. In this relationship, it was shown that electron-donating groups lowered the enthalpy of dehydrogenation. Another linear relationship was discovered when graphing the calculated enthalpies of dehydrogenation of substituted piperidines to their corresponding benzenes. This plot showed a similar trend, although the Hammett ρ value was much larger and the electron-donating groups have a much larger effect than in the case of the carbocycles. Moreover, the dehydrogenation enthalpies were all lower in the piperidines than in the cyclohexanes. A third trend was observed for piperidines bearing conjugated substituents. This trend line showed that conjugated substituents have a stronger dehydrogenation enthalpy–lowering effect than substituents that are not conjugated, so much so that even mildly electron-withdrawing substituents remain beneficial for lowering dehydrogenation temperature.

A problem associated with the use of organic hydrides as hydrogen storage media is the fairly high volatility of the organic hydrides at the temperatures required to dehydrogenate them. As such, media consisting of non-volatile forms of organic hydrides would be desirable. Two options for organic materials that have negligible vapour

pressure are ionic liquids and liquid polymers. In this work ionic liquids whose cations and anions are both potentially capable of releasing hydrogen are investigated for the purpose of hydrogen storage in a hydrogen powered vehicle.

1.2 Energy Conversion and Waste Heat

Energy is conveniently stored in fuel but needs to be converted into another form in order to do useful work. Energy is usually released from fuel through combustion, generating thermal energy from chemical potential energy, which can then be converted into mechanical energy or electrical energy. Whenever thermal energy is converted into mechanical or electrical energy through a heat engine, some of the energy absorbed at the hot source is lost at a lower temperature cold sink, without having been used to do work. When no practical use can be found for this energy it is typically released to the environment and is known as waste heat. Waste heat is a source of thermal pollution, but more importantly it represents a waste of energy that could be put to better use. Major sources of waste heat are found in the processes involved in electrical power generation, oil refining, steelmaking, and vehicle engine operation. In point sources of waste heat, such as industrial processes, waste heat is normally disposed of in a nearby lake or stream. Where there is no convenient source of cold water, a cooling tower must be constructed to vent the waste heat into the atmosphere. Vehicle traffic, which is not a point source, is always discharging waste heat into the atmosphere through radiators and exhaust systems.

Whenever it is economically and technologically feasible, potential waste heat is put to good use. This waste heat that would otherwise be discharged into the environment is essentially free and would otherwise be considered garbage. Using waste heat productively reduces the need for the construction of equipment required to discharge it into the environment, e.g., a cooling tower. An example of a situation where waste heat is put to use is in cogeneration facilities. These are electrical power generators that discharge their relatively cool (though still very hot) steam output into residential and industrial heating applications.[155] This is considered an efficient use of fuel as most of the chemical energy of the fuel is put to practical use. Unfortunately, cogeneration facilities are only conducive to use in decentralized power generation in urban areas, where steam can be easily distributed for local heating. Some facilities can use trigeneration to also offer cooling in addition to heat and electricity through the use of absorption refrigeration.[156] This is useful in areas where the demand for heat varies seasonally.

There are other methods of recovering waste heat and putting it to practical use. These depend on the source of the waste heat and the desired end use. Heat exchangers are commonly used to transfer the heat contained in the output flow into the input flow in industrial processes. This lowers the need for heating the input flow by using waste heat from the output. Heat exchangers for these processes are typically arranged in counter current flow to maximize heat transfer. Power can also be obtained by using waste heat as the hot source powering an organic Rankine cycle.[157, 158] This is essentially a steam turbine but differs in the use of a low boiling organic compound in place of water so it may operate at a lower temperature.

1.2.1 Heat Engines

A heat engine is a device that converts thermal energy into mechanical energy, which may be converted into electricity. It operates through the driving force of the temperature difference between a hot source and a cold sink. No heat engine can convert heat into work with perfect efficiency; it must always vent some of the energy into the cold sink. In a heat engine, heat is absorbed from the hot source into a working fluid, which may be a liquid or a gas (or both), that is able to do some mechanical work before discharging energy into the cold sink.[159]

Heat engines can be described by thermodynamic cycles. Thermodynamic cycles consist of a series of thermodynamic processes where heat or work are exchanged between the system and the surroundings by varying one or more of the state functions of the system, for instance pressure, volume, or temperature. A thermodynamic process is completed when the series of thermodynamic processes returns the system to its initial state. The overall state of the system from beginning to the end of the thermodynamic cycle is unchanged but because heat and work are not state functions and their values are dependent on the path the thermodynamic system takes in completing its cycle, the change in heat and work of the thermodynamic system is non-zero.

From the first law of thermodynamics it can be seen that the overall heat input to the thermodynamic system must be balanced by work output because the overall change in internal energy is zero ($\Delta U = 0$).[159]

$$\Delta U = q + w \tag{5}$$

In a heat engine, a thermodynamic cycle takes in heat and outputs mechanical work. However, the thermodynamic cycle can also be operated in reverse wherein the input of mechanical work is used to transfer heat from a cold reservoir to a hot reservoir, this is referred to as a heat pump and is the process used in refrigeration and air conditioning.

If the path of a thermodynamic cycle is plotted on a P-V diagram it will form a closed loop because pressure and volume are both state functions and they must both return to their initial quantities upon completion of the cycle. The work output of a thermodynamic cycle can be determined easily from this plot because

$$w = \oint P\,dV \tag{6}$$

Therefore the work output of the thermodynamic cycle is equal to the area enclosed by the cycle in a P-V diagram.

Though there are many thermodynamic cycles, only the Carnot cycle (which is the ideally efficient cycle), the Rankine cycle (which is used to generate most of the electricity in the world), and the Otto and Diesel cycles (used in gasoline and diesel engines respectively) will be discussed.

1.2.1.1 The Carnot Cycle

The Carnot cycle was first devised by Nicolas Léonard Sadi Carnot in 1824.[160] He had devised the cycle as a theoretical model for steam engines at the time so the principles of their operation could be analyzed without relying on the less than ideal steam engines available. The model did not rely on the actual physical design of any particular steam engine. From this, he was able to devise the most efficient heat engine possible; one whose efficiency only depended upon the temperature differences between the hot source and the heat sink. The most important part of the Carnot cycle is the lack of exchange of heat between areas at different temperatures. The Carnot cycle only exists theoretically and a heat engine built upon this cycle, a Carnot heat engine, cannot be physically built.

The cycle consists of a reversible isothermal expansion of the working fluid at the hot source (in this part of the cycle a piston can perform work on the surroundings). The working fluid then continues to reversibly expand in an adiabatic process where no heat is exchanged between the system and the surroundings, this continues to perform work on the surroundings by way of the piston, but also cools the working fluid to the temperature of the cold sink. The working fluid is then compressed in a reversible isothermal process, work is done on the fluid by the piston and heat is vented to the surroundings. A reversible adiabatic compression then takes place where work is done on the fluid by the piston and the fluid increases in temperature to that of the hot source. The process then

continues in a cycle, continuously absorbing heat from the hot source and converting a portion of it to work while expelling the rest as heat into the cold sink.

In the P-V diagram of the Carnot cycle the isotherms and adiabats appear as a set of curves (**Figure 1.1**), although in a temperature–entropy (T-S) diagram (**Figure 1.2**) they form a rectangular loop.[160] The heat transferred in a thermodynamic process is

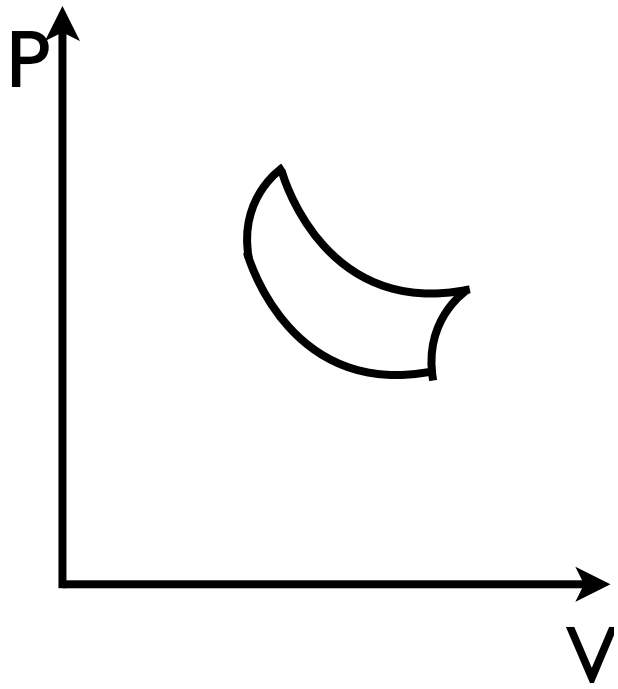

Figure 1.1. P–V Diagram of a Carnot Cycle

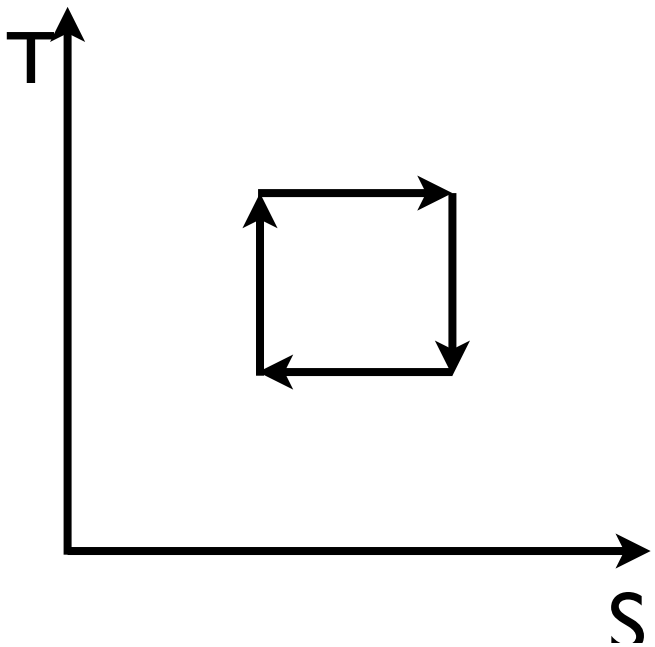

Figure 1.2. T–S Diagram of a Carnot Cycle

$$q = \int T\, dS \tag{7}$$

Thus, when moving to higher entropy, heat is being taken up by the system. The total heat absorbed by the system is the area under the upper curve of the T-S diagram. However, when moving toward lower entropy, heat is being expelled by the system to the surroundings. The heat discharged by the system is equal to the area under the lower curve of the T-S diagram. Because the internal energy of the system does not change over the course of a complete thermodynamic cycle, the difference between the heat input and heat output (the area enclosed in the loop) must be equivalent to the work output of the system. Because the T-S diagram has a rectangular loop it makes it easy to calculate the total work performed by the Carnot cycle.[160]

$$w = (T_h - T_c)(S_2 - S_1) \tag{8}$$

Where T_h and T_c are the temperatures of the hot source and cold sink respectively and S_1 and S_2 are the entropies of compressed and expanded working fluids respectively. The total heat absorbed from the surroundings at the hot source is:[159]

$$q_h = T_h(S_2 - S_1) \tag{9}$$

and the heat expelled from the system to the surroundings at the cold sink is:[159]

$$q_c = T_c(S_2 - S_1) \tag{10}$$

The efficiency of the Carnot cycle is the fraction of heat absorbed from the hot source that is transformed into mechanical work. Therefore the efficiency is[159]

$$\eta = \frac{w}{q_h} \tag{11}$$

$$\eta = \frac{(T_h - T_c)(S_2 - S_1)}{T_h(S_2 - S_1)} \tag{12}$$

$$\eta = 1 - \frac{T_c}{T_h} \tag{13}$$

And the efficiency of the cycle is only dependent on the absolute temperatures of the hot source and the heat sink. Carnot's theorem was that no heat engine can be more efficient than a Carnot heat engine given the same operating temperatures. However, realistically it is impossible to construct a Carnot heat engine because it relies on perfectly reversible thermodynamic processes. Even though it can never be realized, the Carnot cycle does yield a ceiling value on the efficiency of a heat engine operating at a given set of temperatures.

1.2.1.2 The Rankine Cycle

The Rankine cycle is a familiar cycle upon which external combustion steam engines are modeled. Steam turbines are used to generate about 80% of the Earth's electricity supply through fossil fuel burning and nuclear power plants. It is therefore a very important thermodynamic cycle. A difference between the Rankine cycle and the Carnot cycle is that the fluid (typically water) undergoes phase changes between liquid and gas during the cycle.

The Rankine cycle proceeds as follows. The working fluid (which at this stage is a liquid) undergoes adiabatic compression to high pressure. The fluid is then heated in an

isobaric process (changing to the gas phase). The hot gas then does work on a steam turbine which lowers both the temperature and pressure of the fluid in another adiabatic process. The fluid is then cooled in an isobaric process (which results in condensation) and the process is then repeated.

When examined on a T–S diagram, the Rankine cycle appears similar to the Carnot cycle. The Rankine cycle is isobaric where the Carnot cycle is isothermal, and the adiabatic processes are not perfectly isentropic (at the pump and the turbine). Additionally, during the phase changes the heat required for vaporization of the fluid in the boiler is lost directly to the condenser and is not used to perform work at all. A steam engine is generally limited in its efficiency by the physical properties of its working fluid and construction. This limits the upper and lower temperature limits (and therefore the theoretical Carnot efficiencies) that are achievable in the real system.

1.2.1.3 Internal Combustion Engines

An internal combustion engine is one where the heat source is the combustion of fuel within a combustion chamber containing a piston, rather than supplied from outside as in a Rankine cycle (an external combustion engine.) In these engines, mechanical energy is generated by the force applied to the piston through the temperature and pressure generated from the combusting fuel. There are many varieties of internal combustion engines, though this discussion will be limited to those operating in a four–stroke cycle as these are by far the most common in personal and commercial vehicles.

All four-stroke engines operate in a cycle of four steps. These steps differ in their details but in general consist of the intake of a mixture of fuel and an oxidant (typically air); compression of the combustible mixture by the piston in a compression stroke; combustion of the fuel mixture generating heat and pressure in the cylinder; then the exhausting of combustion products and waste heat. Most vehicle engines consist of multiple pistons which undergo the steps of this cycle in a staggered arrangement so each piston is able to exert force on a common crankshaft at a different time.

There are two commonly encountered types of four–stroke cycle engines. These are Otto engines which are most commonly fueled by gasoline (petrol) and Diesel engines which are fueled by Diesel fuel. These engines not only operate on different fuels but they also have different ignition processes and operate on different thermodynamic cycles. These differences in details lead to different thermal efficiencies and these engines are suited to different uses.

1.2.1.3.1 The Otto Cycle

An Otto, or gasoline engine, is one which usually uses gasoline (petrol) as its fuel and is operated in what closely approximates an ideal Otto cycle.[161] The ignition process in an Otto engine is triggered by a high voltage spark plug, which is timed to occur when the fuel–air mixture has reached the peak of its compression. The spark induced ignition results in rapid combustion of the fuel–air mixture which is complete before the piston has an opportunity to move very far, thus the heat input in the engine is approximated to

be an isochoric process. The Otto cycle is a thermodynamic cycle where the compression of the fuel–air mixture occurs adiabatically; the addition of heat occurs at constant volume; an adiabatic expansion occurs during the power stroke; and waste heat is rejected at constant volume.

A real four–stroke Otto engine can only approximate this process. There are no real adiabatic processes and thermal energy is continuously lost to the environment. The addition of heat at constant volume is also an approximation because the piston will move a small distance over the course of the combustion of the fuel mixture because that process, though rapid, is not instantaneous. In addition, a real internal combustion engine must intake fuel and air, and exhaust combustion products. These are normally represented by an isobaric compression (when venting the exhaust gas and waste heat) and isobaric expansion (during the intake of cool air). These two steps, though essential in the operation of a real engine, are usually ignored in a simplified thermodynamic analysis of these systems and they do not contribute significantly to the heat intake or work output of the engine.

1.2.1.3.2 The Diesel Cycle

A Diesel engine operates by the combustion of Diesel fuel and operates in a thermodynamic cycle which is approximated by an ideal Diesel cycle.[162] Diesel fuel consists of a mixture of hydrocarbons with a relatively low autoignition temperature; because of this, Diesel engines do not need an ignition source to combust fuel, the high

temperature and pressure in the cylinder is sufficient and the fuel is injected into the cylinder at the end of the compression. In colder climates, glow plugs may be required to preheat the cylinder as the cold engine block may cool the compressed air to below the autoignition temperature of the fuel. The glow plugs may be left on for a time after the engine is started until it reaches an optimum temperature in order to minimize vehicle emissions, but they generally do not need to be left on once the engine is running.

In a Diesel cycle, air undergoes an adiabatic compression; fuel is injected and a relatively slow combustion takes place (relative to an Otto cycle) so heat addition occurs at constant pressure and not constant volume; an adiabatic expansion occurs during the power stroke; and heat is exhausted at constant volume. The same isobaric intake of cool air and exhaust of combustion products and waste heat occurs in a real Diesel engine, but is usually ignored in the simplified thermodynamic treatment for the same reasons as in the Otto cycle.

Diesel engines are much more thermally efficient than Otto engines. This is because they are able to reach very high compression ratios[162] (the ratio of the volume of the cylinder at the end of the compression stroke to the volume of the cylinder at the end of the power stroke.) Gasoline powered engines cannot achieve these high compression ratios due to the incidence of engine knocking, or premature detonation of the fuel–air mixture. Although gasoline consists mainly of components with high autoignition temperatures to ensure appropriately timed combustion from the spark source, it does have some components that have a lower autoignition temperature. Diesel engines also experience knocking; however, because Diesel fuel is only injected at the end of the

compression stroke the knocking is associated with incomplete mixing of the fuel with air before combustion.

1.2.1.3.3 The Efficiency of Four–Stroke Engines

The thermal efficiency of an ideal Otto engine is given as[163]

$$\eta = 1 - \frac{1}{r^{\gamma-1}} \tag{14}$$

Where r is the engine compression ratio and γ is the specific heat capacity ratio of the working fluid.

$$\gamma = \frac{C_P}{C_V} \tag{15}$$

Where C_P is the specific heat capacity at constant pressure and C_V is the heat capacity at constant volume. Although the heat capacity ratio depends somewhat on the fuel mixture used it is usually assumed to be the same as dry air where the value is 1.4 over the normal temperature ranges in engines.[162] It can be seen that the engine efficiency depends on the compression ratio; the higher the ratio, the more efficient the engine. However, gasoline

engines can only be operated at a limited range of compression ratios before premature detonation of the fuel–air mixture causes engine knocking.

In an ideal Diesel engine the thermal efficiency is given as[163]

$$\eta = 1 - \frac{r^{1-\gamma}(r_c^{\gamma} - 1)}{\gamma(r_c - 1)} \tag{16}$$

This expression is more complicated than seen in the Otto engine due to the isobaric heating process. It also contains the r_c term, which is the cutoff ratio, the ratio of the cylinder volume from the beginning of the combustion process until it is complete. Given the same compression ratio, an Otto engine would be more efficient than a Diesel engine. However, Diesel engines can operate at much higher compression ratios and are therefore much more efficient.

These expressions are derived from ideal thermodynamic cycles and the efficiencies of real engines are actually much lower. Inefficiencies come from multiple sources present in the real world. Notably, there is heat loss through the engine block, friction of the moving parts inside the engine, incomplete combustion of the fuel, and the fact that the working fluid in the cylinder is not an ideal gas. Engines are also engineered to perform in such a way that may make them less thermally efficient. These may be related to vehicle performance or aesthetics, or in order to meet regulatory requirements in terms of emission standards. All these inefficiencies result in the generation of waste

heat. This waste heat may be put to practical use rather than being vented directly to the environment.

1.2.2 Direct Thermal to Electric Energy Converters

It would be advantageous to convert thermal energy directly into electrical energy without the intervention of mechanical energy. These devices could be used to transform waste heat from internal combustion engines into useful electrical energy.

1.2.2.1 Thermoelectric Devices

Thermoelectric devices are generators that convert heat directly into electricity across a temperature gradient; much like a heat engine generates mechanical energy.[164, 165] These are solid state devices; they usually have no moving parts and they operate on the principle of the Seebeck effect. The Seebeck effect is the conversion of a temperature gradient into an electric potential difference, though like heat engines the Seebeck effect also works in reverse and the application of an electrical potential difference results in the formation of a temperature gradient across the device (the Peltier effect). These so called thermoelectric effects have wide applications. They can be used to generate electricity, but also to measure temperatures using a thermocouple, or in heating or cooling applications.

The Seebeck effect was originally discovered in bimetallic devices, but can also be observed in semiconductor materials. The effect of the temperature gradient on electric potential difference across the material comes from two sources: charge carrier diffusion and phonon drag. The basic principle is that when there is a temperature gradient across a material with mobile charge carriers, either mobile electrons or electron holes, the electrons will diffuse from the hot side of the material toward the cold side and the electron holes will move in the opposite direction. This movement of charge carriers results in an electric current. However, if left to reach thermodynamic equilibrium, the material would eventually reach a uniform temperature and charge density and the electric current would cease to flow. Additionally for net charge to diffuse from one end of the material to the other, the electrons and electron holes must diffuse at different rates. Using p-type and n-type semiconductor materials is advantageous when compared to using a bimetallic couple, especially in power generation applications, because in semiconductor materials either the movement of the electrons or electron holes dominates whereas in metallic couples the two effects mostly cancel each other out. In this way, doped semiconductor materials yield much larger electric potential differences per temperature difference (**Figure 1.3**).

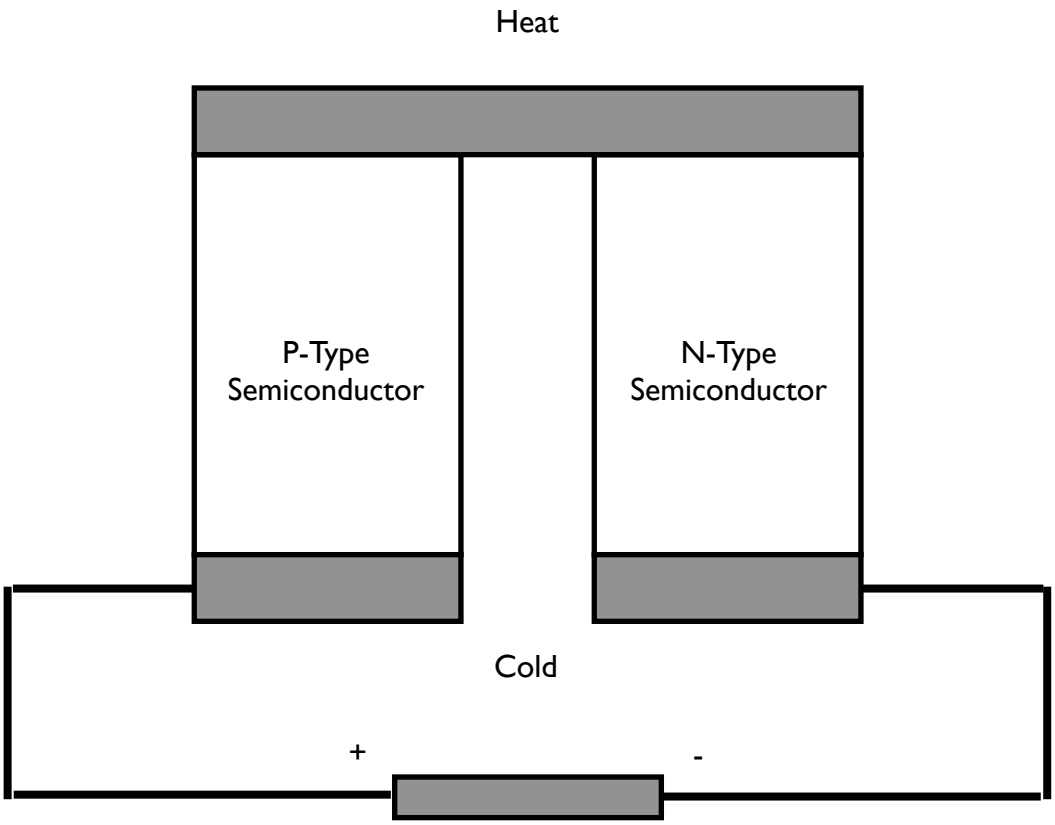

Figure 1.3. Diagram of a Thermoelectric Generator

Crystal lattices also experience vibrational modes known as phonons. When a phonon (a locally occurring vibrational mode of the lattice) encounters a free electron or electron hole it experiences a phenomenon known as phonon drag. The charge on the electron or electron hole is capable of distorting the local crystal structure. This distortion causes the charge carriers to slow down, however the propagating phonons tend to push electrons in the same direction as found in the thermoelectric field so these interactions can increase the gradient of electrons.

The electric potential difference observed in a thermoelectric device is dependent on the nature of the materials of which it is composed, any impurities or defects, and the temperatures at either end. The electric potential difference is given as[166]

$$V = \int_{T_c}^{T_h} (S_B(T) - S_A(T))\, dT \tag{17}$$

where S_A and S_B are the Seebeck coefficient (or thermopower) of either of the materials respectively. The Seebeck coefficient is temperature dependent. T_c and T_h are the temperature of the cold and hot sides of the material. When comparing one thermoelectric device to another a figure of merit, Z, is used.[166]

$$Z = \frac{\sigma S^2}{\kappa} \tag{18}$$

In this equation σ is the electrical conductivity (high electrical conductivity is desirable), S is the overall Seebeck coefficient for the device, the difference between the Seebeck coefficients of the materials (high thermopower is good as more electrical potential difference is generated per temperature difference), and κ is the thermal conductivity (low thermal conductivity maintains the temperature difference across the device). The figure of merit is typically multiplied by the average temperature across the

device to make the measure unitless. Higher values of ZT indicate higher device efficiencies. In general, thermoelectric devices are not very efficient.

1.2.2.2 Thermionic Converters

A thermionic converter is a solid state device that can be used to generate electricity directly from applied heat.[167] An electrode is heated until it contains enough thermal energy to overcome the electron binding potential (work function) of the electrode material and begins to emit electrons (although the charge carriers can be other ions). These electrons can then be captured by a cold electrode and complete an electrical circuit, thereby generating electricity (**Figure 1.4**).

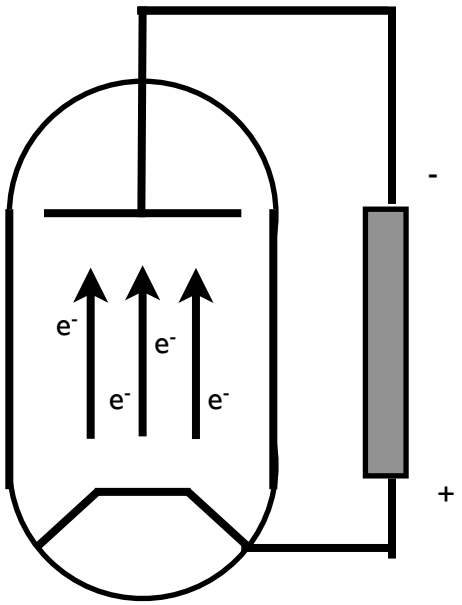

Figure 1.4. Diagram of a Thermionic Converter

A thermionic converter is a device that operates a thermodynamic cycle using mobile electrons as the working fluid. The current generated by these devices depends on the nature of the electrode and the working temperature. Increasing the temperature of the hot electrode increases the current generated by the device by raising the number of electrons that have sufficient energy to overcome the work function of the electrode material. Conversely, the electrode material can be engineered to have a lower work function, which would allow for acceptable currents to be generated from more modest operating temperatures. The thermal efficiency of these devices is also determined by the operating temperature which may be on the order of 1500–2000 ºC. Currently, all practical thermionic converters use cesium vapor to generate the plasma between the electrodes. This is because cesium is the most easily ionized of all the elements. The cesium vapor is also deposited onto the electrode surfaces where it affects the work function of the surfaces.[168]

Through most of the history of the development of thermionic converters the high temperature required for a reasonably efficient system relegated their use to the cores of nuclear reactors. A key application was in space faring technologies where radiant heat must be absorbed anyways. More recent developments in the technology have improved efficiencies at lower temperatures for use in industrial or commercial power generation.

1.2.2.3 Thermophotovoltaic Cells

A thermophotovoltaic device converts thermal energy into electricity through the intermediate generation of photons.[169] The device consists of two components: a thermal emitter, which emits photons upon heating; and a photovoltaic diode, which converts photons into electrical energy (**Figure 1.5**). These devices are suited for remote applications due to their lack of moving parts and low maintenance requirements. However, the high operating temperatures and low efficiency of thermophotovoltaic generators preclude their widespread use.

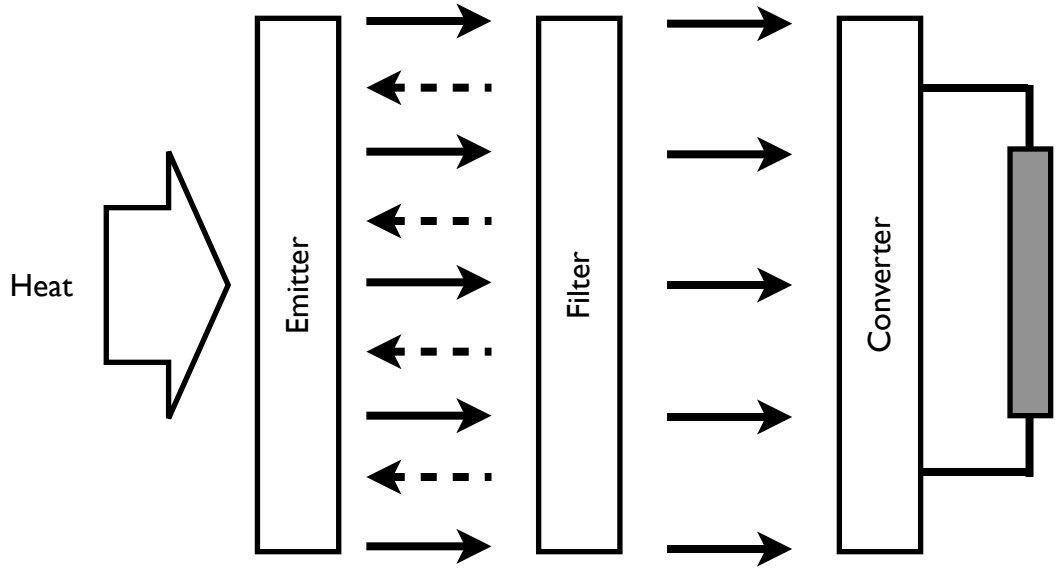

Figure 1.5. Diagram of a Thermophotovoltaic Cell

In order to be efficient, a thermophotovoltaic device must match the properties of the thermal emitter to the photovoltaic diode. Inefficient conversion of photons into

electricity is a major source of efficiency losses. To accomplish this, either optical filters or selective thermal emitters[170] are used to reduce the bandwidth of radiation the photovoltaic diode is exposed to. For instance, photons that do not have sufficient energy to generate a electron–hole pair in the photodiode will not be able to do so and will lose their energy thermally; however photons with excess energy can generate electron–hole pairs but their excess energy is lost as waste heat in the photodiode. This waste heat is undesirable, not only because of the loss of efficiency, but for the excess heating of the photodiode. A selective emitter only generates photons in a narrow wavelength range which can be efficiently converted by the photodiode. Using an optical filter allows photons with energies that are too high or too low to be recycled by being reflected back to the emitter material where they can be reabsorbed and emitted at a different wavelength.

The practical upper limit for the efficiency of a thermophotovoltaic converter is the Carnot efficiency. However, many characteristics of real systems prevent the Carnot efficiency from being reached. The Carnot efficiency would assume that all thermal energy is converted to photons and all photons are then converted to electricity with no losses; in addition the entropy change during the process would need to be zero, which is only possible when the emitter and the photodiode are at the same temperature (under which no energy transfer can take place). The emitter would have to behave as a perfect blackbody and any filters used would need to reflect photons perfectly without any scattering or absorbing any of the radiation. In the photodiode, thermalization of incident radiation as well as ohmic losses reduce the efficiency of energy conversion. The

geometry of such a system is also important. The emitter will emit light in all directions; therefore efficiency is maximized by completely surrounding the emitter with photodiodes. This is not practical economically or technologically. Photodiodes are costly and the thermal emitter would need to be heated externally which precludes completely surrounding the emitter. Photodiode costs can be reduced by using reflectors to redirect incident radiation onto the photodiode, though reflectors are not perfectly efficient either.

1.2.2.4 Thermally Regenerative Fuel Cell

A fuel cell differs from a battery in that it is supplied with fuel externally rather than containing a given amount internally. A thermally regenerative fuel cell is a system wherein the exhaust from the fuel cell is regenerated into fuel through the application of heat. In this way, thermal energy in the form of heat is being converted into electricity. The most popular type of fuel cell for automotive applications is the polymer electrolyte fuel cell (PEMFC). This device uses hydrogen as its fuel and oxygen or air as its oxidant and emits water as waste. It would be difficult to use hydrogen and oxygen in a thermally regenerative fuel cell as the application of heat generally does not result in thermal decomposition of water into hydrogen and oxygen gasses. The combustion process is, from a practical standpoint, irreversible in a vehicle. There are, however, other oxidants that can be used in place of the oxygen or air[171] whose reaction products can be thermally regenerated back into its starting materials at reasonable temperatures (**Figure 1.6**).

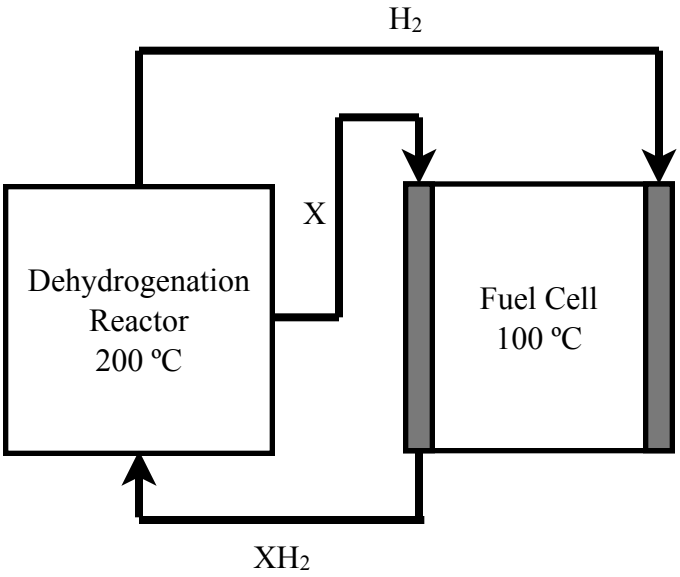

Figure 1.6. Diagram of a Thermally Regenerative Fuel Cell

The general process occurring in a PEM fuel cell is hydrogenation (or reduction) of an oxidant material to yield a product that is more thermodynamically stable than its starting materials (and thus electrical energy is evolved in the fuel cell). This hydrogenation process must therefore be exothermic. This means that heat may be applied to the product in a separate reactor in order to endothermically dehydrogenate it to regenerate the starting materials. The overall process is to convert thermal energy into electrical energy using chemical potential energy as an intermediate.

The driving force for the transfer of energy from the hot source to the cold sink (fuel cell) is the change in equilibrium constant. For instance, if a material XH_2 is capable of being dehydrogenated to yield one equivalent of hydrogen and one equivalent of X, then the law of mass action is

$$K = \frac{[X]P_{H_2}}{[XH_2]} \tag{19}$$

According to the van't Hoff equation

$$\ln\left(\frac{K_2}{K_1}\right) = \frac{\Delta H^\circ}{R}\left(\frac{1}{T_1} - \frac{1}{T_2}\right) \tag{20}$$

X is favoured at high temperature whereas XH_2 is favoured at low temperature if and only if the dehydrogenation reaction is endothermic. Moreover, the reaction must be localized in the hot sources and the fuel cell, otherwise a simple gradient of chemical compositions will occur throughout the temperature gradient between the hot source and the fuel cell and most of the energy transferred to the working fluid would be lost as heat before it reached the fuel cell.

Chapter 2

Hydrogen Storing Ionic Liquids

The catalyst and membrane of PEMFCs are sensitive to contamination with non-fuel material.[75] Therefore, the hydrogen storage material must not be allowed to vaporize over the operating temperature range of the fuel storage system. A few methods can be used to accomplish this. The simplest is to use a fluid that has a very high boiling point; however, neutral organic compounds can have small liquid ranges and such compounds would likely be solid under ambient temperatures (particularly in winter). The more elegant solution is to use materials that have no measurable vapour pressure such as ionic liquids[172] and polymers.

Ionic liquids (ILs) are salts that have a relatively low melting point, arbitrarily defined as below 100 ºC. There are ionic liquids whose melting points are below ambient temperature; these are commonly referred to as room temperature ionic liquids (RTILs). Ionic liquids typically consist of an organic cation and an organic or inorganic anion. Typical cations in ionic liquids are the alkylimidazolium, alkylpyridinium, phosphonium and ammonium ions, though others are known (Scheme 2.1). Ionic liquids have special properties that make them appealing for chemical hydrogen storage for fuel cell applications. These include:

1. a large liquid temperature range;
2. negligible vapour pressure;
3. potentially high density;
4. and high thermal stability.[172]

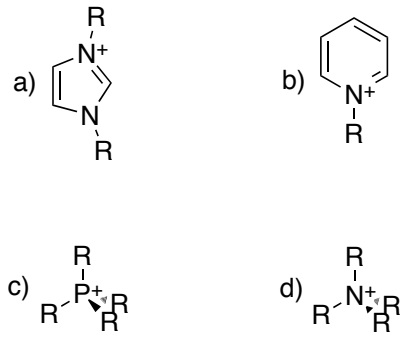

Scheme 2.1. Common cations used as components of ionic liquids: a) imidazolium, b) pyridinium, c) phosphonium, and d) ammonium

Ionic liquids have been used in hydrogen storage applications before, both as a solvent for conventional hydrogen storing compounds and, once, as a hydrogen storing material. Dupont's group[173] previously published the reversible hydrogenation of phenyl groups appended to an imidazolium ionic liquid with inert counterions. The goal of this research is to generate ionic liquids where both the cation and anion are capable of reversibly storing hydrogen without significant decomposition.

2.1 Ionic Liquids

Ionic liquids are salts with large, normally diffuse ions. As such, they form weak ion pairs and as a result cannot easily enter the gas phase. Ionic liquids are therefore normally thought to have no vapour pressure; they will decompose before boiling.[172] An ionic liquid may still be able to contaminate the hydrogen gas stream because microscopic droplets may become entrained in the hydrogen gas stream evolving from an ionic liquid hydrogen storage system.

Ionic liquids also have a distinct advantage in terms of melting point range. Because the liquid never boils and some ionic liquids have cryogenic melting points, it should be possible to design a hydrogen-storing ionic liquid which would be liquid even at winter temperatures and yet be non-volatile even in the heat of summer or at the operational temperature of the H_2-storage system. The effects of structural changes on the melting points of ionic liquids are normally described using Coulomb's Law because the primary attractive intermolecular force is the electrostatic force between ions.

$$E = \frac{q^+ q^-}{4\pi\varepsilon_0 \varepsilon r} \tag{21}$$

From Coulomb's Law it can be seen that the interaction energy is minimized when the charge on each ion has a magnitude of one. The interaction energy is also lowered by maximizing the distance between ions (by having large ionic radii) and by

maximizing the dielectric constant of the material. It is simple to ensure that the ions used only have a net charge of ±1. The most control over melting point beyond that is in the nature and size of the ions being used. Charge diffusion favours a low melting point as does having a large ionic radius. Increasing the ionic radius only lowers the melting point to a certain degree, as eventually van der Waals forces become significant and melting point begins increasing on increasing chain length. Therefore, in a series of homologous ionic liquids, there normally exists a minimum melting point species. Straight alkyl chains typically give lower melting points than branched chains due to increased rotational freedom and less efficient crystal packing. Since the gravimetric hydrogen storage density of any hydrogen storage material is of paramount importance and this capacity drops on increasing alkyl chain lengths the optimized structure will not necessarily be the minimum melting point homolog.

High thermal stability is a feature of many ionic liquids and the decomposition mechanism of most ionic liquids is the reverse mechanism by which they are formed. In general the anion acts as a nucleophile and attacks the cation to form neutral species. These are normally formed above the boiling points of the products and they quickly evaporate and are lost to the gas phase. Delaying the onset of thermal degradation can be achieved by choosing anions with poor nucleophilicity. Some commonly used anions are tetrafluoroborate, hexafluorophosphate, trifluoromethylsulfonate, and bis (trifluoromethane)sulfonimide (**Scheme 2.2**).

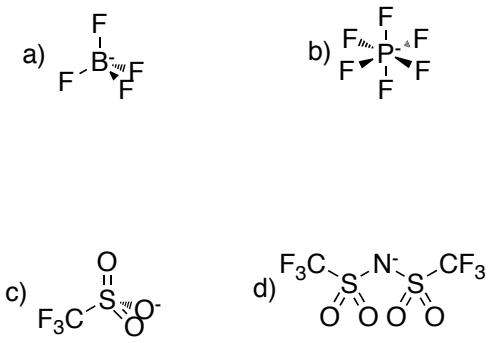

Scheme 2.2. Common anions used as components of ionic liquids: a) tetrafluoroborate, b) hexafluorophosphate, c) trifluoromethanesulfonate, and d) bis(trifluoromethane) sulfonimide

A set of ionic liquids with the capacity to store hydrogen has been previously reported. These imidazolium ionic liquids featured tethered phenyl rings, inert anions, high melting points, and very low gravimetric hydrogen storage densities (the highest being 3.2 wt%).[173] These ionic liquids were able to store hydrogen through reversible hydrogenation of the phenyl rings. However, imidazolium ions should also be susceptible to hydrogenation, which would generate protonated aminals (**Scheme 2.3**). These compounds would undergo rapid hydrolysis (**Figure 2.1**); water is a ubiquitous contaminant in ionic liquids. These problems must be resolved in order for this technology to become useful. Ionic liquid media should be developed in such a way as to avoid the aminal decomposition pathway, as well as have improved gravimetric hydrogen storage density by making both ions capable of hydrogen storage.

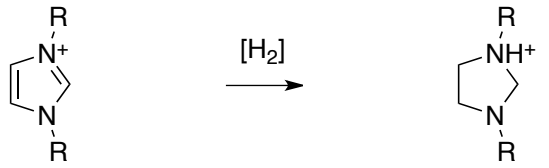

Scheme 2.3. Reduction of an imidazolium salt to a protonated aminal

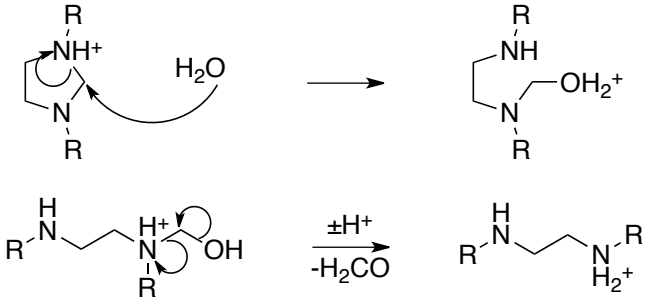

Figure 2.1. Hydrolysis of a protonated aminal to a protonated diamine and aldehyde

2.2 Preliminary Studies

The DOE targets for a hydrogen-fuelled vehicle are challenging to meet.[76] The development of hydrogen-storing ionic liquids that meet the gravimetric hydrogen storage density requirements while simultaneously retaining low melting points as well as high thermal stability is difficult. It is unlikely that all the goals of the DOE will be met early in research and the initial goal of the study was to develop a system that simply functions. As such, the thermal stability and reversibility with respect to hydrogenation have become the most important factors in developing the system. The physical characteristics and gravimetric storage densities can be manipulated afterward.

2.2.1 N-Alkylpyridinium Nicotinate

A good initial candidate for a hydrogen storing ionic liquid would be an N-alkylpyridinium salt. From previous research it is known that N-heterocycles have favourable thermodynamics for hydrogen storage[148, 152, 174] and N-alkylpyridinium is a familiar cation already used in ionic liquids.[172] N-Alkylpyridinium ions are also easy to prepare by alkylation of pyridine, an inexpensive and readily available starting material. A convenient anion partner would be the nicotinate ion; its acid, nicotinic acid (pyridine-3-carboxylic acid), is also inexpensive and readily available and is familiar as vitamin B_3. By pairing N-alkylpyridinium cations with nicotinate anions, it is possible to form a family of ionic liquids which could potentially be used as chemical hydrogen storing materials.

2.2.1.1 Synthetic Strategies

Both the cation and the anion of a hydrogen storing ionic liquid must be able to undergo reversible hydrogenation reactions to be useful as a hydrogen storage medium. Because of this, any hydrogen storing ionic liquid can be synthesized in the form of any combination of saturated or unsaturated ions as they will be interconverted later during use. In this way, bulk synthesis of a hydrogen-storing ionic liquid can be carried out using the combination of ions that is the least expensive and/or the most convenient. However,

in the laboratory it is useful to have samples of the ionic liquid in all of its accessible forms as pure compounds for characterization and physical property measurements.

In the case of the N-alkylpyridinium nicotinate series of ionic liquids, the forms accessible by reversible hydrogenation include the endpoints, the fully unsaturated N-alkylpyridinium nicotinate and the fully saturated N-alkylpiperidinium nipecotate, and as will be discussed, N-alkylpiperidinium nicotinate as an intermediate between the two. Though N-alkylpyridinium nipecotate can be prepared it is unlikely to ever be observed as the N-alkylpyridinium ion hydrogenates faster, and the N-alkylpiperidinium ion dehydrogenates slower than the nicotinate and nipecotate ions respectively (**Scheme 2.4**). N-Alkylpyridinium nicotinate is the most difficult to prepare. The starting materials include N-alkylpyridinium halides (produced through a simple S_N2 reaction between pyridine and an alkyl halide, (**Figure 2.2**) and nicotinic acid or its salts.

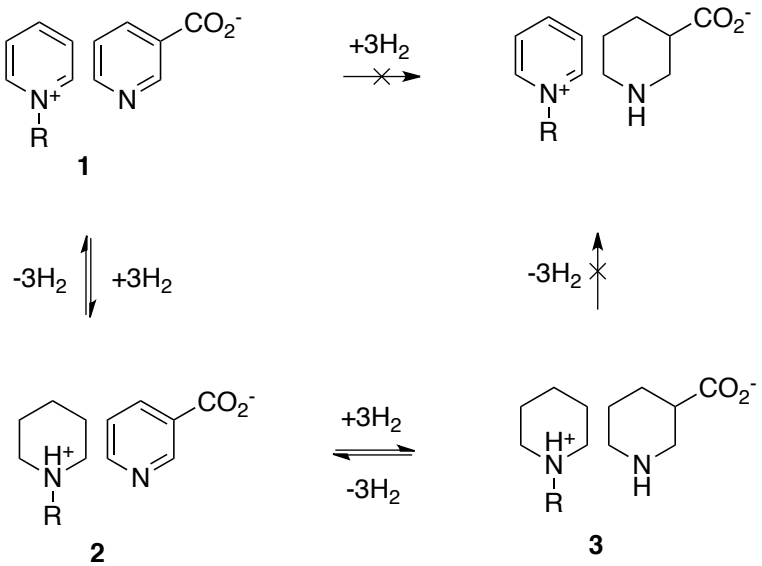

Scheme 2.4. Reversible hydrogenation of N-alkylpyridinium nicotinate to N-alkylpiperidinium nipecotate

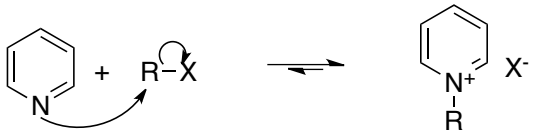

Figure 2.2. Alkylation of pyridine by an alkyl halide to form an N-alkylpyridinium halide

N-Alkylpyridinium nicotinate could not be extracted from mixtures of N-alkylpyridinium halide and either nicotinic acid or sodium nicotinate (**Scheme 2.5**). Successful preparation required the use of *in situ* deprotonation of nicotinic acid in the presence of N-alkylpyridinium halide using excess silver carbonate in refluxing methanol (**Scheme 2.6**). It is not clear whether halide ions exchange with the carbonate ion first resulting in the initial formation of N-alkylpyridinium carbonate followed by successive deprotonation of the nicotinic acid and decarboxylation; or whether nicotinic acid is deprotonated on the surface of the silver carbonate forming silver nicotinate followed by precipitation of the silver halide. In any case, filtration of the silver salts and concentration of the solution yields N-alkylpyridinium nicotinate, which appears pure by ^{1}H NMR spectroscopy though it is always stained very dark (this is not unusual in the formation of ionic liquids) and it continues to precipitate silver salts and metallic silver over a long period of time.

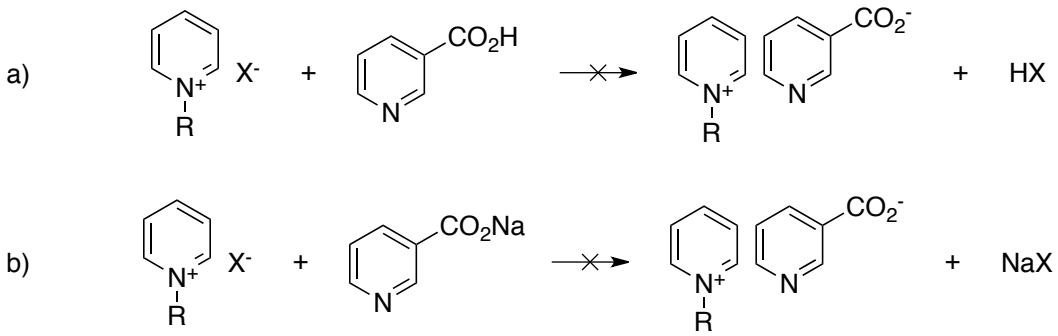

Scheme 2.5. Unsuccessful ion exchange of a halide ion using a) nicotinic acid or b) sodium nicotinate

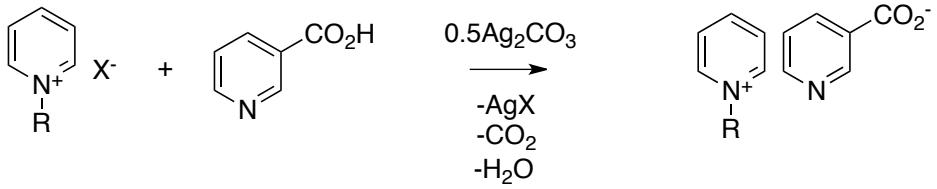

Scheme 2.6. Silver ion exchange of a halide ion using nicotinic acid and silver (I) carbonate

The two successively more saturated ionic liquids are much more easily synthesized by proton exchange. Heating nicotinic acid or nipecotic acid with N-alkylpiperidine yields the corresponding N-alkylpiperidinium nicotinate or N-alkylpiperidinium nipecotate respectively (**Scheme 2.7**). N-alkylpiperidines that are not readily available commercially can be prepared in several ways.[175] The simplest method is through reductive amination of piperidine with an aldehyde using palladium on carbon and hydrogen as the reducing agent (**Scheme 2.8**). Alternatives are the reduction of the amide formed between a linear acyl chloride and piperidine with lithium aluminium hydride or borane (**Scheme 2.9**), or the catalytic hydrogenation of an N-alkylpyridinium halide followed by deprotonation with a refluxing aqueous solution of sodium carbonate

(**Scheme 2.10**). The commercially viable option for bulk synthesis of this ionic liquid system is based on the formation of N-alkylpiperidinium nicotinate because the reaction is facile and the starting materials are both inexpensive and readily commercially available or are easily synthesized from inexpensive materials.

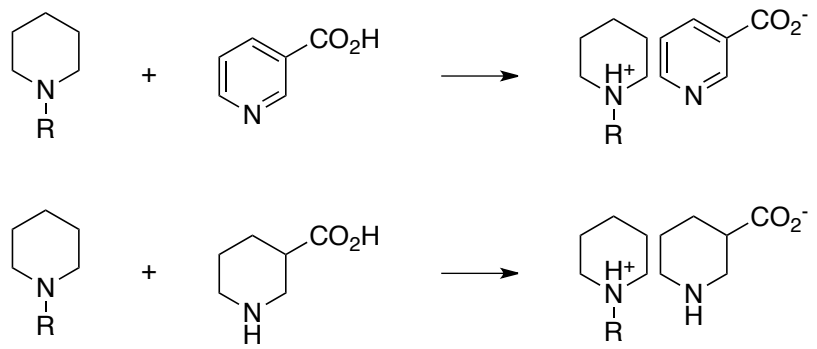

Scheme 2.7. Ionic liquid synthesis by proton transfer from a heterocyclic acid to a piperidine base

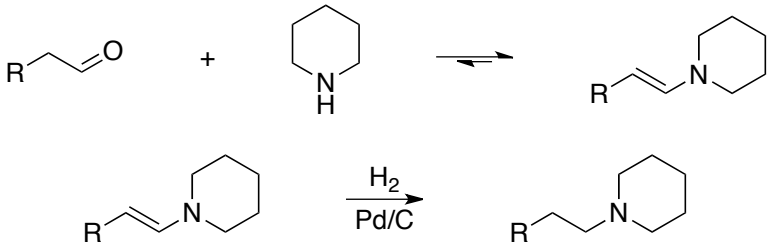

Scheme 2.8. Synthesis of N-alkylpiperidine via reductive amination of piperidine with an aldehyde using hydrogen gas and a heterogeneous palladium catalyst

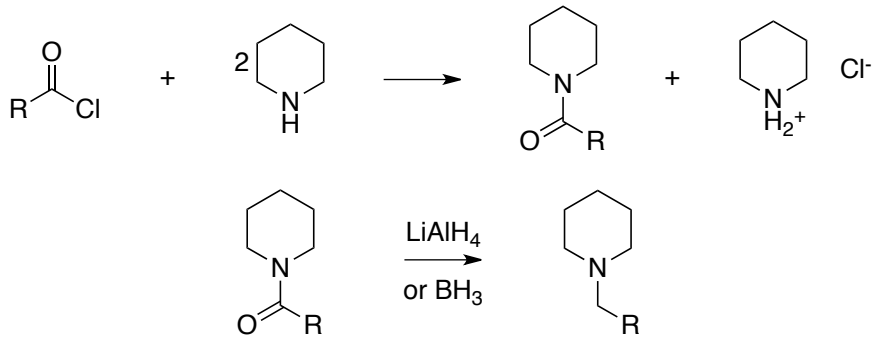

Scheme 2.9. Synthesis of an N-alkylpiperidine via reduction of an amide (prepared from the reaction of piperidine with an acyl chloride) using either lithium aluminium hydride or borane

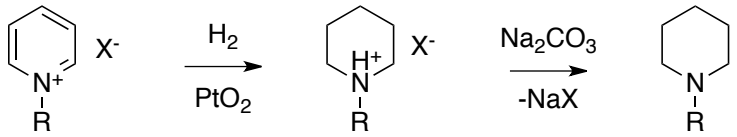

Scheme 2.10. N-Alkylpiperidine via catalytic hydrogenation of an N-alkylpyridinium salt followed by deprotonation

2.2.1.2 Physical Properties

The physical properties of N-alkylpyridinium nicotinate salts are unusual and unexpected. For instance, N-methylpyridinium nicotinate (**1a**) was observed to be a liquid of fairly low viscosity. The viscosity of ionic liquids is typically much higher than that of ordinary liquids.[172] More unusual in this case was the low melting point or glass transition temperature of the fluid. Even when submerged in a cryogenic bath of dry ice in acetone (-78 ºC) **1a** remained a free flowing liquid. It was not clear whether the liquid was kinetically trapped in a metastable state that would eventually solidify. It would

normally be expected that **1a** should be a solid at room temperature because it is a salt of electron rich and electron poor aromatic ring systems. Beyond the simple coulombic interactions of the salt there also exists the tendency to form strong π-stacking interactions.[176] All the atoms in each of the ring systems (apart from the hydrogen atoms on the methyl group) are coplanar, so stacking would be expected to be efficient.

Unfortunately, upon increasing saturation of the ring systems the melting points of the ionic liquids rapidly increased, even though π-stacking interactions were no longer possible. A homologous series of N-alkylpyridinium nicotinate ionic liquids was prepared in increasing states of saturation and the melting points of each were measured (**Table 2.1**). The hexyl homolog appears to retain enough rotational degrees of freedom to ensure that each form of the ionic liquid is liquid at ambient temperature.

Table 2.1. Melting points of N-alkylpyridinium nicotinates **1**, and N-alkylpiperidinium nicotinates **2** and nipecotates **3**

R=	**1**	**2**	**3**
CH_3 **a**	l	>200 ºC	>200 ºC
C_2H_5 **b**	l	>200 ºC	>200 ºC
C_4H_9 **c**	l	76–77 ºC	>200 ºC
C_6H_{13} **d**	l	l	l

l = liquid at ambient temperature

2.2.1.3 Hydrogenation

N-Alkylpyridinium nicotinate undergoes hydrogenation in a stepwise process. It can be hydrogenated at high temperature and pressure in an autoclave over a transition metal catalyst. In this process, it is beneficial to dilute the ionic liquid with a solvent, typically a low molecular weight alcohol such as methanol, ethanol or isopropyl alcohol. The solvent not only improves the solubility of hydrogen in the ionic liquid, but it also lowers the viscosity of the solution. Lowering the viscosity improves the rate of mass transfer of hydrogen into the solution, makes stirring more efficient, and improves the rate of mass transfer of the ionic liquid and hydrogen on and off the catalyst surface. All of these effects increase the rate of hydrogenation over that observed when no solvent is used, even though the effective concentration of the ionic liquid is lower.

Under these conditions, the pyridinium ion is hydrogenated much more rapidly than the nicotinate ion. The reaction can be stopped halfway through and N-alkylpiperidinium nicotinate can be isolated (**Scheme 2.11**). The pyridinium ion can actually be hydrogenated at ambient pressure, unlike the nicotinate ion. This is another method for isolating N-alkylpiperidinium nicotinate. Hydrogenation of the nicotinate ion requires high pressure (~100 bar), high temperature (~100 ºC), and long reaction times. However, this reaction does proceed to completion with both very high yield and high selectivity.

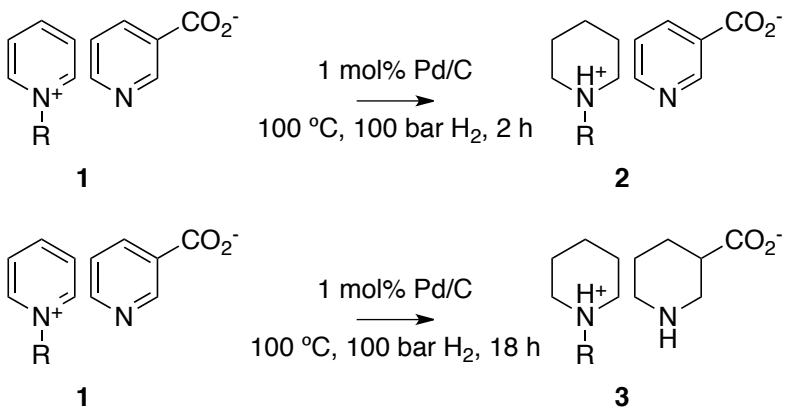

Scheme 2.11. Stepwise hydrogenation of N-alkylpyridinium nicotinate to N-alkylpiperidinium nipecotate via N-alkylpiperidinium nicotinate

2.2.1.4 Dehydrogenation

Dehydrogenation of these ionic liquids is an endothermic process. Therefore dehydrogenation is favoured at high temperature with removal of the evolving hydrogen (this is not practical in an automobile). However, there is a limit to how high a temperature the dehydrogenation reaction can be carried out before thermal degradation of the ionic liquid takes place. The upper temperature limit will depend on the thermal stability of any given ionic liquid. Preliminary reactions of N-hexylpiperidinium nipecotate (**3d**) were performed at 200 ºC. When the reaction mixture was analyzed by ^{1}H NMR spectroscopy, extensive decomposition was observed along with the formation of aromatic compounds. The complexity of the ^{1}H NMR spectrum precluded the assignment of any of the peaks because the product mixture consisted of many similar compounds.

An attempt was made to solve both the decomposition problem and the complexity of the ^{1}H NMR spectrum at the same time. To do so, the substrate ionic liquid used was **3a**, which has a much simpler ^{1}H NMR spectrum, and the temperature of the dehydrogenation reaction was lowered to 150 ºC to prevent thermal decomposition of the salt. Because the optimal dehydrogenation catalyst was unknown, several heterogeneous catalysts were tested in parallel reactions. **3a** is a solid at 150 ºC so a solvent was required to perform the reaction. Ethylene glycol was chosen as a solvent due to its high boiling point and its ability to dissolve the salt. After the reactions were complete, the catalysts were removed by filtration and the ethylene glycol was removed by distillation *in vacuo*. The resulting product mixtures were analyzed by ^{1}H NMR spectroscopy. Exact speciation was not performed; only the relative conversion of aliphatic to aromatic peaks was considered. This is because the starting material, **3a** has a complicated ^{1}H NMR spectrum consisting of many multiplets and overlapping peaks. The relative conversion of the reactions was determined algebraically by using the ^{1}H NMR spectra of the product mixtures. The starting material consists of 22 non-exchangeable aliphatic protons and zero aromatic protons, the desired product **1a** consists of three aliphatic protons and nine aromatic protons. By integrating the aromatic and aliphatic regions of the product spectra a system of two equations and two unknowns is formed and the relative conversion can be determined. The product spectra only showed aromatic peaks consistent with the formation of the nicotinate ion and not the N-methylpyridinium ion. The relative reactivities of the catalysts were determined from this data where the

conversion shown is amount of aromatic peaks formed. A conversion of 50% would be consistent with complete conversion to N-methylpiperidinium nicotinate (**2a**) (**Table 2.2**).

Table 2.2. Relative reactivity of heterogeneous catalysts in dehydrogenation of N-methylpiperidinium nipecotate to N-methylpiperidinium nicotinate

Catalyst	Loading (%)	Conversion (%)	Relative Reactivity
Pt/C	1.2	0.5	1
Rh/C	1.3	0.9	1.6
RuO_2	1.9	1.4	1.8
Pd/C	1.1	2.7	5.7
Ru/C	1.0	3.2	7.5

N-Methylpiperidinium nipecotate (100 mg) in 2 ml of ethylene glycol and catalyst were stirred at 600 rpm with a magnetic stir bar and heated to 150 ºC for 3 h in air. Samples were diluted with 5 ml of methanol, filtered through diatomaceous earth and the solvents were removed under high vacuum. The remaining solid was dissolved in D_2O and analyzed by ^1H NMR spectroscopy for conversion to aromatic products.

Conversions for the dehydrogenation reaction were low but the reaction kinetics were hindered by both the low catalyst loading as well as the low concentration of the reactants in the ethylene glycol. The low conversions made speciation of the product material almost impossible, however it was observed that the less costly precious metals ruthenium and palladium were more active than the more costly rhodium and platinum. The reaction was repeated without solvent by using N-hexylpiperidinium nicotinate (**2d**) as the substrate. This salt is a liquid at 150 ºC and does not require a solvent to ensure mass transfer to the catalyst surface. As a result, the rate of dehydrogenation of this

material should be higher. Because this salt is only partly saturated, only the piperidinium ion would be expected to undergo hydrogenation. After reacting this ionic liquid at the same catalyst loading and temperature as the previous reaction, no conversion of the N-hexylpiperidinium ion to the N-hexylpyridinium ion was observed. This means that the material that was dehydrogenating in the previous experiment was the nipecotate ion to the nicotinate ion. Piperidinium ions do not appear to be readily dehydrogenateable, at least at this fairly low temperature. This result is similar to that seen in the literature when another Lewis acid (a borane, in contrast to the proton in our system) is occupying the lone pair of a piperidine ring.[141, 142]

2.2.1.5 Thermal Stability

Thus far two major problems have been encountered regarding the use of N-alkylpyridinium nicotinate ionic liquids as hydrogen carriers: the low intrinsic reactivity of the piperidinium ion to dehydrogenation and the low thermal stability of the ionic liquids themselves. To determine the thermal stability of the ionic liquids, thermogravimetric analysis (TGA) experiments were performed. In these experiments, a small amount of the analyte (in this case the ionic liquid) is placed on a very sensitive microbalance. The material is then slowly heated either in a normal or inert atmosphere while the mass of the sample is continuously monitored. As the material starts to decompose into volatile material, the mass of the sample decreases and the fraction of the

mass remaining is recorded as a function of the temperature of the material. In this way the temperature of the onset of rapid decomposition can be determined.

In another mode, the TGA apparatus can be operated at a constant high temperature and the mass loss of the analyte can be recorded as a function of time. Most materials will decompose slowly at a temperature much lower than the temperature of the onset of rapid decomposition determined by a regular TGA experiment. This type of long term stability experiment is one that would be invested in when a good candidate fluid is found. The particular TGA apparatus we are using also features differential scanning calorimetry (DSC) where the relative heat flow to or from the analyte is measure (against a reference material). This allows for the observation of any phase transitions (with their accompanying enthalpy change) as well as confirming the mass loss is due to evaporation (a highly endothermic process) and not due to an artifact or operator error during the experiment.

A TGA apparatus could also be used in optimizing the reaction temperature for the dehydrogenation reaction of a material. When a material dehydrogenates, it loses a certain predictable percentage of its mass (for cyclohexane, its mass would drop by ~7% in converting to benzene). If a prospective material was thoroughly mixed with an appropriate amount of catalyst and then heated in the TGA apparatus, the onset of rapid loss of this predictable percentage of the mass of the material would indicate the optimal dehydrogenation temperature. In reality this experiment is not as simple. The ionic liquids being studied have a gravimetric density of hydrogen of less than 7% and when mixed with catalyst (even 1 mol% of catalyst contributes greatly to the total mass of the

system) the amount of mass loss being detected would be tiny and may be lost in the background noise of the apparatus.

Thermogravimetric analyses were performed to determine the thermal stabilities of the N-alkylpyridinium nicotinate series of ionic liquids (for example N-methylpiperidinium nipecotate (**3a**) (**Figure 2.3**)). In general, rapid decomposition of the ionic liquids was observed in the range of 200–250 ºC, depending upon the alkyl chain length and the degree of saturation of the ionic liquid. The decomposition of the ionic liquids occurs both in the presence and absence of any catalyst and is occurring at a lower temperature than observed for many other ionic liquids (for instance, 1-ethyl-3-methylimidazolium hexafluorophosphate has been reported as thermally stable up to 375 ºC,[177] though the decomposition temperatures reported are highly dependent on the conditions under which they are measured, and are generally not indicative of long term stability).[178] The low temperature of onset of rapid decomposition indicates that slow decomposition is likely occurring at even lower temperatures.

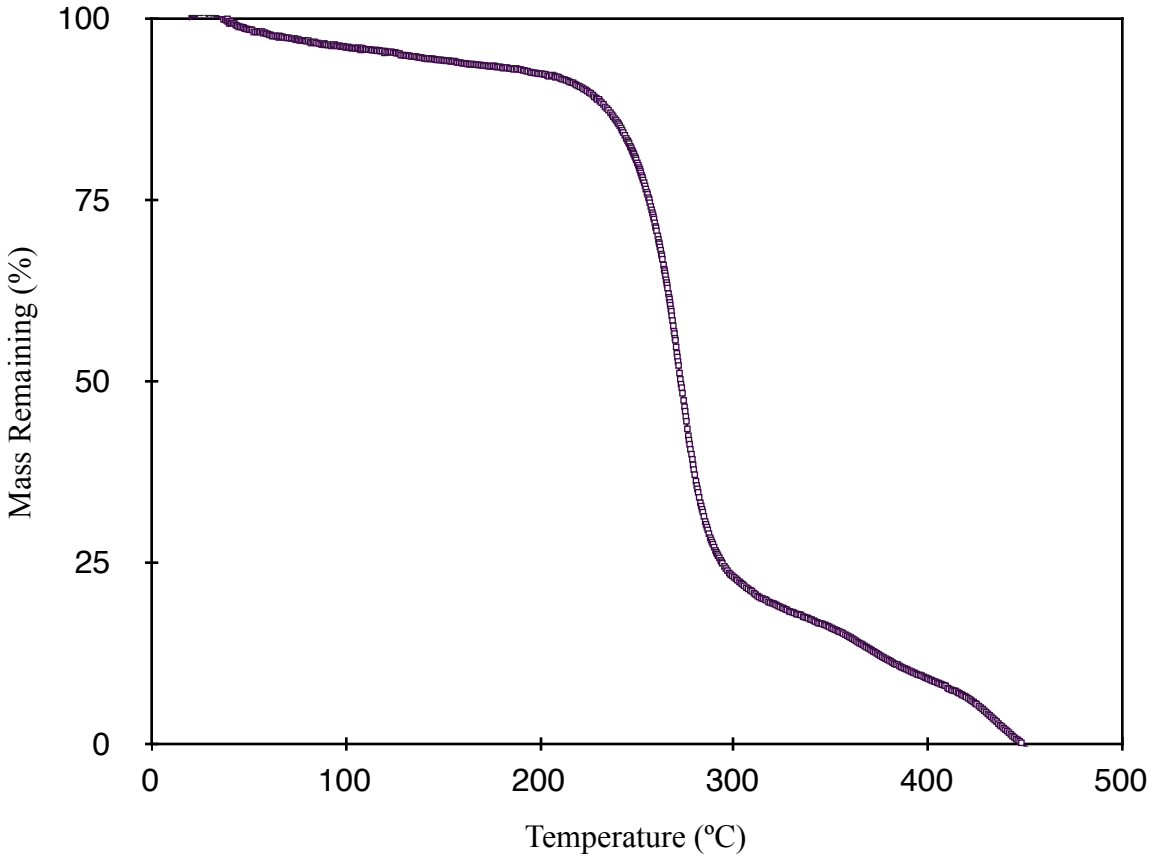

Figure 2.3. Thermogravimetric analysis of N-methylpiperidinium nipecotate (**3a**)

In order to determine the pathway by which these ionic liquids were decomposing, and hopefully to determine the steps required to prevent this thermal decomposition, a simple experiment was performed to determine the speciation of the decomposed material. The fully saturated material was heated to 200 ºC in a small round bottom flask equipped with a condenser. After an hour, a small amount of liquid was observed clinging to the lower section of the condenser tube. Because the reaction mixture was not splashing, this material must have evaporated from the reaction. Because ionic liquids do not evaporate, this must contain some neutral decomposition products. The condenser was carefully removed from the cooled reaction mixture, after which the

condensate was carefully rinsed from the glass using deuterated chloroform and analyzed by ^{1}H NMR spectroscopy. The condensate was found to consist of piperidine contaminated with a small amount of entrained ionic liquid. No other large peaks were observed, though small amounts of other decomposition products may have been masked by the ionic liquid peaks.

Decomposition mechanisms in which piperidine would be a product include the E1 or E2 elimination mechanisms where carboxylate acts as a base and deprotonates the position β to the nitrogen atom with concurrent (E2, **Figure 2.4**), or consecutive ($E1_{cb}$, **Figure 2.5**) elimination of piperidine (neutral amines are reasonable leaving groups). The E1 mechanism is unlikely because it would involve spontaneous leaving on the part of piperidine and the generation of a carbocation. The $E1_{cb}$ mechanism also seems unlikely because there is no particular stabilization of the carbanion that would be formed, neither nicotinate nor nipecotate ions are sufficiently basic to promote this reaction. If elimination were occurring, it would likely occur through the E2 mechanism. However, thermal decomposition of N-methylpiperidinium salts is known (longer alkyl chain analogues have similar onsets of thermal degradation) and these cannot eliminate to form piperidine (it lacks an appropriate β proton). Additionally, a much more acidic proton (the ammonium proton) is readily accessible and proton transfer from cation to anion was not observed (no N-alkylpiperidine was found in the decomposition products). If carboxylate is not basic enough to remove this proton then it is unlikely to be able to remove a less basic β proton.

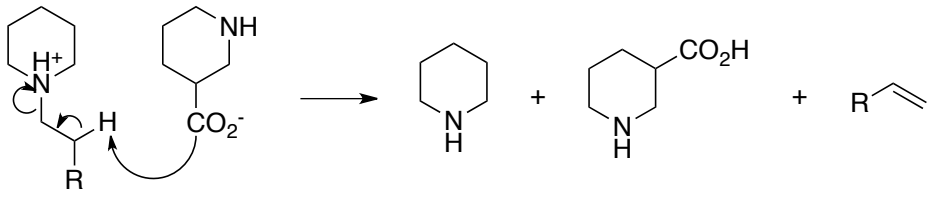

Figure 2.4. Decomposition via elimination of piperidine through an E2 mechanism

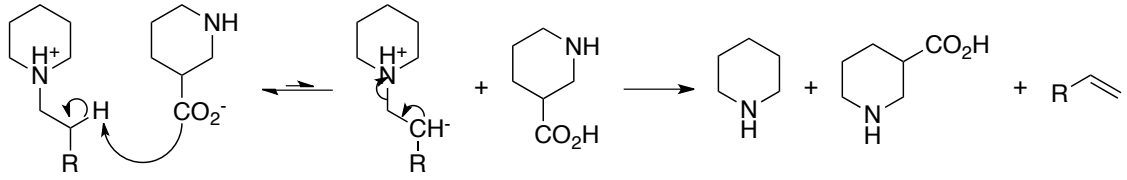

Figure 2.5. Decomposition via elimination of piperidine through an $E1_{cb}$ mechanism

An alternative mechanism is nucleophilic substitution. This could theoretically include both the S_N1 and S_N2 mechanisms but the S_N1 mechanism, which would require the formation of a very unstable primary carbocation, is unlikely. In the nucleophilic substitution reaction, the carboxylate ion would be acting as a nucleophile and removing the methyl group to form the methyl ester of the anion (**Figure 2.6**). It is also possible for the carboxylate ion to attack either of the α ring carbon atoms, though in this case ring opening would occur resulting in a large molecular weight amino ester (which would have a large boiling point and not necessarily show up in the condenser tube, **Figure 2.7**). The important result from this experiment is that no N-alkylpiperidine was observed.

Piperidine and N-methylpiperidine have the same boiling point (106 ºC) so if N-methylpiperidine was formed it would be expected to be similarly volatile and would also be observed in the condensate. Not only does this show that the proton did not migrate from the tertiary amine to the carboxylate, but also that it did not migrate to the secondary amine (of the anion, forming a zwitterion and free tertiary amine). If that were to occur, it would prevent the use of nitrogen heterocycles as both the anionic and cationic components of a hydrogen storing ionic liquid and any enthalpy lowering effects would need to come from substituent groups or from oxygen heterocycles.

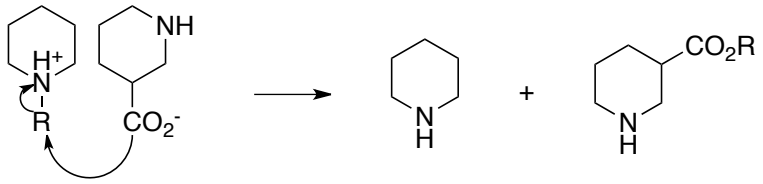

Figure 2.6. Decomposition of N-alkylpiperidinium nipecotate by alkyl transfer via an S_N2 reaction

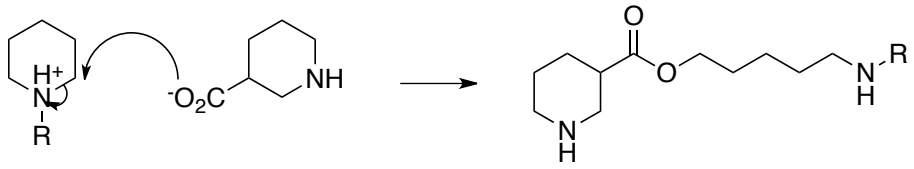

Figure 2.7. Ring opening decomposition of N-alkylpiperidinium nipecotate via an S_N2 reaction

2.2.1.6 Conclusions

N-Alkylpyridinium nicotinate and its saturated counterparts are inexpensive and have acceptable hydrogenation kinetics. Their melting points are tuneable and hydrogen storage capacities are good. They are susceptible to thermal decomposition at high temperatures such as those typically used during dehydrogenation reactions. The evidence suggests that this decomposition takes place by an S_N2 mechanism. Carboxylate is determined to be unacceptably nucleophilic as an anion in this pair.

2.2.2 N-Alkylpiperidinium 3-Pyridinesulfonates

The nucleophilic character of the nicotinate anion appears to be the source of the thermal instability of the N-alkylpyridinium nicotinate system. Thermal degradation of this system occurs rapidly at temperatures of approximately 200°C. To meet the cycle life requirements of the DOE, this system would require operation at temperatures much lower than that. Resolving the stability issue at high temperature would be beneficial in both increasing the cycle life of the material as well as allowing the dehydrogenation to occur at a higher temperature where the endothermic dehydrogenation is more favourable, both kinetically and thermodynamically. Changing the carboxylate anion into a much less nucleophilic sulfonate anion is a logical strategy for suppressing the S_N2 reaction that decomposes the ionic liquid. This change does come with consequences in terms of its effect on ease of dehydrogenation of the ring. The sulfonate group is a much

more powerful electron-withdrawing group than carboxylate, and though it is conjugated to the ring, it will likely raise the enthalpy of dehydrogenation.

2.2.2.1 Synthetic Strategy

N-Alkylpyridinium pyridinesulfonates cannot be prepared in the same way as N-alkylpyridinium benzenesulfonates (through the reaction of pyridine with an alkyl benzenesulfonate)[179] because pyridinesulfonyl chlorides would be self-reactive. To access this series, the commercially available 3-pyridinesulfonic acid was reacted with an N-alkylpiperidine. Equimolar amounts of the appropriate N-alkylpiperidine and 3-pyridinesulfonic acid were mixed in a sealed glass pressure tube with a magnetic stirrer and heated to 150°C. The reaction was complete and quantitative when the mixture stopped boiling. Only the methyl homolog was prepared (**Scheme 2.12**).

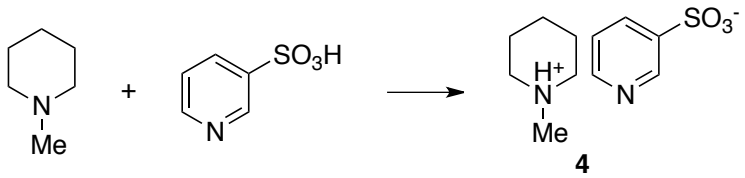

4

Scheme 2.12. Synthesis of N-methylpiperidinium 3-pyridinesulfonate (**4**) via proton transfer from 3-pyridinesulfonic acid to N-methylpiperidine

2.2.2.2 Hydrogenation

N-Methylpiperidinium 3-pyridinesulfonate (**4**) was prepared in a state of partial saturation; only the anion required hydrogenation to form the fully saturated material. The hydrogenation of alkylpyridinium cations has already been successfully demonstrated (**Section 2.2.1.3**) but the hydrogenation of 3-pyridinesulfonate anions is unknown. When hydrogenation was performed at either 100°C or 200°C, the product mixtures show only partial conversion of the anion (**Scheme 2.13**). The ^{1}H NMR spectrum of the saturated anion would be expected to be complicated because its structure is similar to the nipecotate ion, where each proton has a different resonance and is split by several other unique protons. Because there was no isolated sample of piperidine-3-sulfonate available commercially or through a simple synthesis[180] and the peaks associated with this product were so small (and partially obscured by the proton signals associate with the methylpiperidinium ion) the products of the hydrogenation could not be determined. Though it is likely that conversion to the desired product occurred, there could have been decomposition or hydrogenolysis of the anion. Regardless, not enough saturated material was formed for a study of the dehydrogenation of the material to be meaningful.

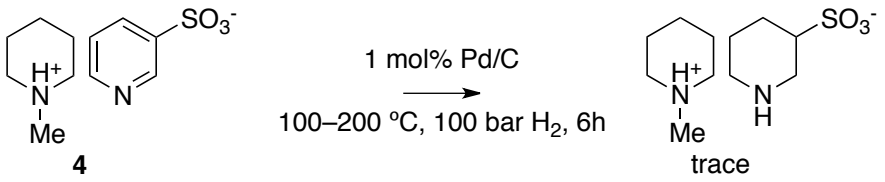

Scheme 2.13. Catalytic hydrogenation of N-methylpiperidinium 3-pyridinesulfonate

2.2.2.3 Conclusions

Although a nitrogen heteroatom lowers the enthalpy of dehydrogenation of a saturated ring, the presence of a sulfonate group, which is strongly electron withdrawing, would be expected to increase this reaction enthalpy. However, it has also been shown that conjugating substituents on the ring system can lower the enthalpy of dehydrogenation. When subjected to hydrogenation conditions, 3-pyridinesulfonate ions undergo limited conversion. It is unclear whether this is because of a problem with reaction kinetics or thermodynamics. The sulfonate group does have some advantages: it provides an ionic liquid with higher thermal stability and the sulfonate group has not been shown to be reduced through catalytic hydrogenation in the literature.

2.2.3 N-Alkylpiperidinium 2-(4'-Pyridyl)ethanesulfonates

The sulfonate anion provides the ionic liquid with thermal stability at the expense of limited reactivity in terms of hydrogenation, and the inclusion of a nitrogen heteroatom

in the ring is not sufficient to overcome this drawback. The hydrogenation of the 3-pyridinesulfonate ion appears to proceed, but it is either a very slow reaction or it is limited by thermodynamics. In order to benefit from the enhanced thermal stability of the sulfonate anion while retaining adequate reactivity of the heterocycle with respect to hydrogenation and dehydrogenation, the sulfonate group can be tethered to the ring through a short aliphatic chain. In this way, the strong electron withdrawing effect of the sulfonate group cannot affect the electronics of the ring. The heterocycle should undergo hydrogenation and dehydrogenation with activity similar to that seen in neutral molecules like alkylpyridines. The anion 2-(4-pyridyl)ethanesulfonate is a good candidate. It retains the stability of the sulfonate anion, but as the sulfonate group is tethered to the ring through an ethylene linkage, it loses the electron withdrawing effect that limits its reactivity. This is at the expense of increased mass and therefore decreased gravimetric hydrogen storage density.

2.2.3.1 Synthetic Strategy

N-Methylpiperidinium 2-(4'-pyridyl)ethanesulfonate (**5**) must be prepared in a way similar to the 3-pyridinesulfonate salt for the same reason; the sulfonyl chloride required to make the sulfonate ester would be self-reactive. 2-(4'-Pyridyl)ethanesulfonate salts can be prepared from the appropriate piperidine and 2-(4-pyridyl)ethanesulfonic acid. Equimolar amounts of N-alkylpiperidine and 2-(4-pyridyl)ethanesulfonic acid were mixed in a sealed glass pressure tube which contains a magnetic stirrer. The mixture was

heated to 150 °C and the reaction was complete and quantitative when the solution no longer boiled (**Scheme 2.14**). The 2-(4'-pyridyl)ethanesulfonic acid, which in solution exists as the zwitterion, is commercially available but can be prepared in the laboratory through the conjugate addition of sodium sulfite to 4-vinylpyridine (the 2 isomer can be prepared from 2-vinylpyridine, **Figure 2.8**).[180, 181]

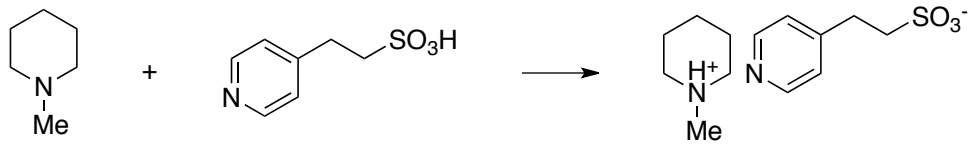

5

Scheme 2.14. Synthesis of N-methylpiperidinium 2-(4'-pyridyl)ethanesulfonate (**5**) via proton transfer from 2-(4'-pyridyl)ethanesulfonic acid to N-methylpiperidine

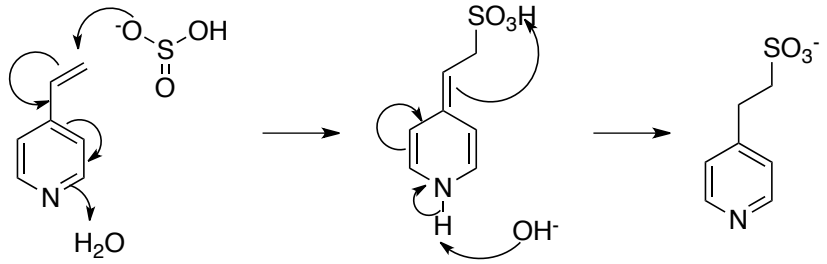

Figure 2.8. Preparation of 2-(4'-pyridyl)ethanesulfonate via conjugate addition of hydrogensulfite to 4-vinylpyridine

2.2.3.2 Hydrogenation

5 is prepared in the semi-saturated state and only the anion requires hydrogenation to form the fully saturated ionic liquid. In the fully unsaturated form, the cation is

predicted to hydrogenate rapidly as is the case in the previously studied systems. For the hydrogenation experiment, the ionic liquid was not prepared and isolated; rather it was generated *in situ* during the hydrogenation reaction. N-Alkylpiperidine was dissolved in isopropanol and 2-(4-pyridyl)ethanesulfonic acid was added with the solution to the autoclave. The sulfonic acid has low solubility in the alcohol so proton transfer to form the ionic liquid is slow. However, the heat (200 ºC), stirring, and reaction time (6 h) required for the hydrogenation would be sufficient to produce the ionic liquid by the end of the hydrogenation. After working up the reaction and isolating the product mixture, the anion appeared to be 46% hydrogenated and the remainder is unhydrogenated N-methylpiperidinium 2-(4'-pyridyl)ethanesulfonate (**Figure 2.9**).

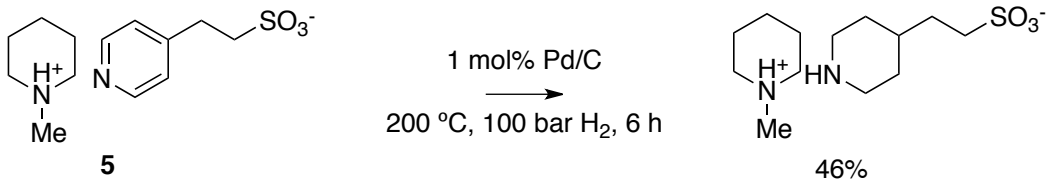

Figure 2.9. Catalytic hydrogenation of N-methylpiperidinium 2-(4'-pyridyl) ethanesulfonate

2.2.3.3 Conclusions

The initial hydrogenation reaction of the N-alkylpyridinium 2-(4-pyridyl)ethanesulfonate did not proceed to completion, but it did undergo significant conversion, and the reaction

has not been optimized. The solid precipitate of the sulfonic acid may have blocked the catalyst surface for a large portion of the reaction time, which would decrease yield of the saturated product. The fact that the hydrogenation did not produce any side products makes this choice of anion very promising and it should be investigated further as an anion partner in other ionic liquids.

2.2.4 Conclusions

The thermal stability of these ionic liquids is largely determined by the nucleophilicity of the anion. The leaving group ability of the pyridinium-piperidinium system cannot easily be adjusted as the leaving group forms the core of the cation. Maximum thermal stability with respect to the S_N2 is achieved by choosing an anion that is the conjugate base of a strong acid. Sulfonate is a good choice for a weakly nucleophilic anion but it is also strongly electron withdrawing and therefore increases the enthalpy of dehydrogenation of the piperidine ring to which it is attached. Tethering the anionic center away from the ring system will likely resolve the enthalpy problem but does so at the expense of hydrogen storage density. Moreover, the piperidinium cation appears to be resistant to dehydrogenation. Examination of the dehydrogenation chemistry of the cation must also be studied.

2.3 Hydrogenation and Dehydrogenation of Simple Heterocyclic Salts

Ionic liquids consist of cations and anions that are usually capable of reacting with each other, particularly at high temperature, in such a way as to reverse the reaction that formed them. Because the dehydrogenation of these ionic liquids would need to be carried out at fairly high temperatures, it is possible that the thermal decomposition of the fluids may compete with the hydrogenation and dehydrogenation reactions that are being studied. By isolating the hydrogen storing cations and anions and pairing them with an inert counterion, the hydrogenation and dehydrogenation of the individual ions can be studied and optimized without the concern of thermal decomposition taking place. After the reactivity of these ions is understood, thermally compatible ions can be paired to form useful hydrogen storing ionic liquids with high gravimetric hydrogen storage capacities.

Ions cannot be isolated apart from a counterion; they must therefore be prepared with a suitable counterion which would not be expected to be reactive with either the ion under study, or any catalysts or solvents used. Anionic heterocycles can be paired with the sodium cation, because it is unreactive and inexpensive. These salts can be prepared by simple deprotonation of the appropriate acid with an appropriate base such as sodium hydroxide, sodium methoxide or sodium hydride. An appropriate counterion for cationic heterocycles is the trifluoromethanesulfonate anion. It is a very poor nucleophile and these salts can be produced by protonation of a base with trifluoromethanesulfonic acid, or by alkylation using methyl trifluoromethanesulfonate.

Because these simple salts are not likely to be ionic liquids, there are physical constraints that need to be addressed. The salts will usually have fairly high melting points. If the materials are not liquid at the desired reaction temperature, a solvent is required to facilitate mass transfer of the material over the catalyst surface and the solvation of the hydrogen gas. The melting points of both the saturated and unsaturated forms of the salts must be considered. Although mixtures of compounds tend to have depressed melting points, it is possible that a high melting product salt could precipitate onto a catalyst surface, poisoning it. The materials being studied are all salts, so polar solvents will be required to solubilize them. Because dehydrogenation reactions require high temperatures, approximately 200 ºC, the boiling points of the solvents used must be high. Prospective solvents include ethylene glycol and formamide. However, the use of high boiling solvents presents a problem during the analysis of product mixtures. ^{1}H NMR spectroscopy is the analytical tool of choice for these reactions, but solvents with high boiling points are difficult to remove and may easily obscure the desired signals in the ^{1}H NMR spectrum. Evaporation under high vacuum conditions is probably the best method for removing the solvent, particularly because the product mixtures should be thermally stable and survive this treatment.

The overall goal is to measure the hydrogenation and dehydrogenation of various heterocyclic ions without the confounding influence of a reactive counterion. Frequently, the ^{1}H NMR spectra of the saturated salts are complex and signals may overlap in the aliphatic region. Limiting each salt to only one hydrogen-storing ion makes it much easier to distinguish which ions are reacting under which conditions. The resistance to

thermal decomposition also prevents the formation of most unwanted side products that would also appear in the ^{1}H NMR spectrum. Because the ions under study are all heterocycles, they would most likely exhibit the same lowered enthalpy of dehydrogenation when compared to the analogous carbocycle as has been determined for neutral compounds.

Although the use of an inert counterion prevents the main thermal decomposition mechanism, it is entirely possible that individual ions are not intrinsically thermally stable. Performing these reactions with inert counterions should make it clear whether any of the hydrogen-storing ions are intramolecularly or intermolecularly self-reactive. Hydrogen-storing ions that are intrinsically unreactive will also be readily identified so they can be excluded from further study.

2.3.1 Synthetic Strategy

The anions studied were the sodium salts of both saturated and unsaturated heterocyclic carboxylic acids. The heterocyclic carboxylic acids were obtained from commercial sources and dissolved in methanol and treated with one equivalent of sodium methoxide (Scheme 2.15). These reagents were chosen because sodium methoxide solution is readily available and the evaporation of methanol from sodium methoxide is much easier than the evaporation of water from sodium hydroxide. The product salts were concentrated to dryness *in vacuo* and then recrystallized from isopropanol or methanol. Sodium isonicotinate (6a), sodium nicotinate (7a), sodium 2-furoate (8a),

sodium isonipecotate (6b), sodium nipecotate (7b) and sodium 2-tetrahydrofuroate (8b) were obtained in this way (Scheme 2.16).

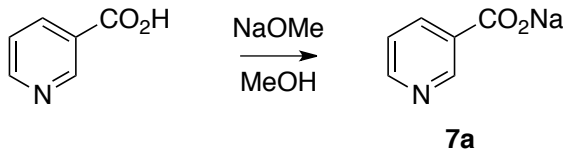

Scheme 2.15. Preparation of sodium salts of heterocyclic acids by deprotonation using sodium methoxide

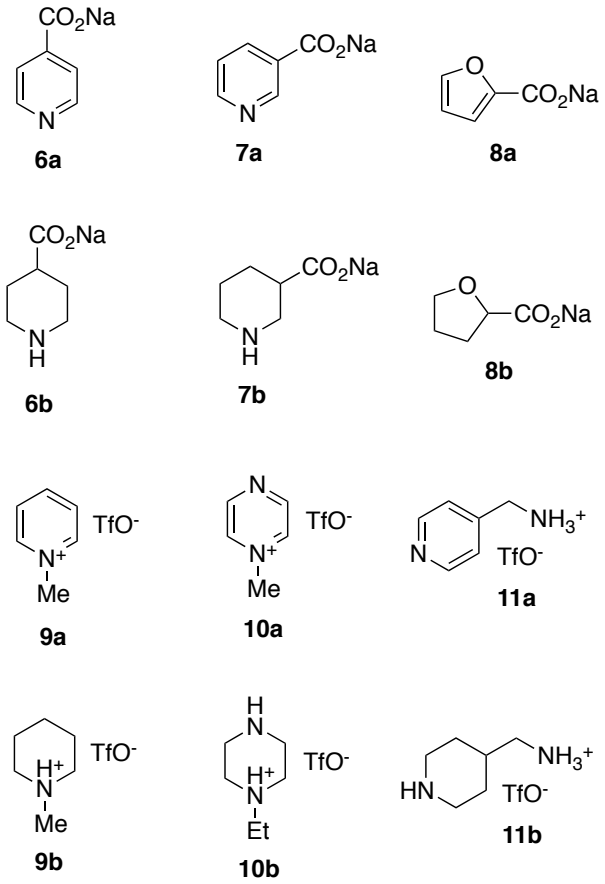

Scheme 2.16. Heterocyclic salts with only one hydrogen storing ion

The cations studied were the trifluoromethanesulfonate salts of nitrogen heterocycles. The saturated heterocycles were protonated with trifluoromethanesulfonic acid (using hexanes as an unreactive diluent to absorb some of the heat of proton transfer, Scheme 2.17). N-methylpiperidinium trifluoromethanesulfonate (9b), N-ethylpiperazinium trifluoromethanesulfonate (10b), 4-(ammoniummethyl)piperidine trifluoromethanesulfonate (11b), and 4-picolylammonium trifluoromethanesulfonate (11a) were prepared by this method. Unsaturated heterocycles were made by alkylation of pyridine nitrogens using methyl trifluoromethanesulfonate (methylene chloride was used as a diluent, Scheme 2.18). N-Methylpyridinium trifluoromethanesulfonate (9a) was prepared by alkylation of pyridine and N-methylpyrazinium trifluoromethanesulfonate (10a) was prepared by alkylation of pyrazine.

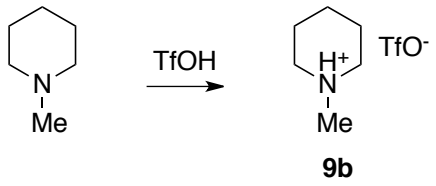

9b

Scheme 2.17. Protonation of amines with trifluoromethanesulfonic acid

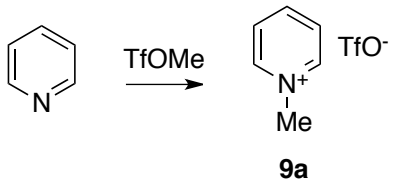

9a

Scheme 2.18. Alkylation of heterocycles using methyl trifluoromethanesulfonate

2.3.2 Hydrogenation

Hydrogenations were performed individually in a 160 ml stainless steel autoclave. The catalyst, solvent and salt were mixed in the autoclave along with a magnetic stir bar and air was excluded by flushing the autoclave three times with approximately 10 bar of hydrogen. After the reactor was heated to the prescribed temperature, it was pressurized and left to react. Reactions were quenched by rapidly cooling the autoclave in an ice water bath followed by venting the hydrogen gas. Reaction mixtures were isolated from the catalyst by filtration through diatomaceous earth. The solvent was removed *in vacuo* and the products were determined by ^{1}H NMR spectroscopy in methanol-d_4.

The unsaturated salts 6a, 7a and 8a were initially hydrogenated at 100 ºC under 100 bar of hydrogen pressure over 1 mol% of palladium on carbon (10 wt%) over the course of 18 h using ethanol as a solvent. Based on the results under these conditions (with respect to conversion and selectivity) the anions were hydrogenated again at a lower temperature if full conversion was reached or the selectivity was < 99%. The reaction temperature was increased if the conversion was less than complete but the selectivity was excellent. This was done in an attempt to optimize reaction conditions in such a way as to maximize both conversion and selectivity simultaneously (Table 2.3).

Table 2.3. Yields for the catalytic hydrogenation of the sodium salts of unsaturated heterocyclic carboxylates

T (ºC)	**6a**	**7a**	**8a**
		Yield (%)	
80	66	-	-
100	100	69	17
125	-	72	-
200	-	30[a]	100

Substrates, 20 mM in ethanol (10 ml) were hydrogenated over 10 mol% equivalent Pd (10 wt% Pd/C) at 100 bar of hydrogen in a 160 ml glass lined stainless steel autoclave for 18 h. The catalyst was removed by filtration and the solvent removed in vacuo. Yields of saturated products were determined by ^{1}H-NMR spectroscopy. [a]Reaction proceeded with degradation of starting material. All other reactions had ≥99% selectivity.

Among the salt, 6a is the most readily hydrogenated and 8a is the least. Both of these ions appear to be amenable to hydrogenation as they show excellent selectivity. Though 7a could be hydrogenated it did so more slowly than 6a. Increasing the reaction temperature to 200 ºC increased the conversion of both 7a and 8a, but 7a underwent extensive decomposition at this temperature. The hydrogenation of 7a appears to have good selectivity at lower temperatures so this salt could still be hydrogenated if given a longer reaction time, or more likely a larger catalyst loading. For these reactions an internal standard was not used, though decomposition was only observed when sodium nicotinate (7a) was hydrogenated at high temperature. However, decomposition resulting in volatile products would not be detected. Though the hydrogenation reactions were carried out in a closed vessel, volatile products may be lost during the work up steps and then they would not be detected in the product mixture.

Hydrogenation of the salts 9a and 10a was initially performed under similar conditions to that used to hydrogenate the anions, but using water as the solvent. Decomposition of the N-methylpyridinium cation was observed under these conditions, so the experiment was repeated with milder conditions. Further hydrogenation reactions were performed at 50 °C and 50 bar of hydrogen pressure using two different reaction times: 1 h and 21 h. Reaction mixtures were analyzed using ^{1}H NMR spectroscopy in deuterium oxide using 1,4-dioxane as an internal standard (Table 2.4).

Table 2.4. Conversions and selectivities of the catalytic hydrogenation of the trifluoromethanesulfonate salts of alkylated unsaturated N-heterocycles in water

	9a		**10a**	
t (h)	Conversion (%)	Selectivity (%)	Conversion (%)	Selectivity (%)
1	84	82	100	19
21	100	79	100	18

Substrates, 0.5 M in water (2 ml) were hydrogenated over 10 mol% equivalent Pd (10 wt% Pd/C) at 50 ºC and 50 bar of hydrogen in a 160 ml glass lined stainless steel autoclave. Conversions and selectivities were determined by ^{1}H-NMR spectroscopy.

The N-methylpyridinium and N-methylpyrazinium ions were both active towards hydrogenation. This was expected from the previous work on the N-alkylpyridinium nicotinate salts (Section 2.2.1.3). 10a also appeared to react more quickly than 9a. Neither reaction occurred with excellent selectivity, producing numerous unidentified products. 10a hydrogenated with a selectivity of less than 20%. These reactions were performed in

water and it is entirely possible that hydrolysis occurred. The pK_a of protonated pyridine in water is 5.21, whereas the first pK_a of protonated pyrazine is 1.1. Pyrazine is a much better leaving group than pyridine is, which may explain why the N-methylpyrazinium ion is less stable than the N-methylpyridinium ion. In either case, hydrolysis by way of the S_N2 mechanism yields methanol and pyrazinium (Figure 2.10) or pyridinium trifluoromethanesulfonate respectively. These dealkylated substrates are fully capable of being hydrogenated under the reaction conditions.

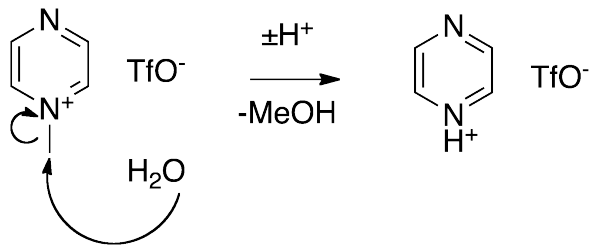

Figure 2.10. Hydrolysis of N-methylpyrazinium trifluoromethanesulfonate

2.3.3 Dehydrogenation

The saturated salts 6b and 7b were dehydrogenated by stirring in a test tube, which was open to the atmosphere at 200 ˚C, using 1 mol% Pd/C over 3 h. Sodium isonipecotate (6b) (mp 182-185 ˚C) could be dehydrogenated without the use of a solvent. Sodium nipecotate (7b) and sodium 2-tetrahydrofuroate (8b), which have melting

points greater than 260 ˚C, were dehydrogenated in ethylene glycol solution at reflux (195 °C).

In the case of 6b, the product solution was dissolved in methanol before each was filtered through a plug of diatomaceous earth to remove the catalyst. Solvent was removed *in vacuo* (in the case of ethylene glycol by distillation under high vacuum) and the resulting mixture was analyzed by ^{1}H NMR spectroscopy in deuterium oxide using 1,4-dioxane as an internal standard. Extensive decomposition was observed in the samples which were dehydrogenated in ethylene glycol but not in the sample which was dehydrogenated without solvent. Another solvent was required to successfully dehydrogenate the heterocycles with high melting points. Formamide was used as an alternative as it is able to dissolve the salts and is not nucleophilic. Dehydrogenation reactions were performed again using formamide as solvent for each salt at 150 °C and 200 °C (Table 2.5).

Table 2.5. Disappearance of starting materials and yields of products for the catalytic dehydrogenation of the sodium salts of saturated N-heterocyclic carboxylic acids in formamide

	6b		**7b**	
T (ºC)	Missing (%)	Yield (%)	Missing (%)	Yield (%)
150	29	0	59	0
200	34	21	58	27

Substrates were prepared as 0.5 M solutions in formamide (2 ml) were heated in test tubes over 10 mol% equivalent Pd (10 wt% Pd/C) for 3 h. Missing materials and yields were determined by ^{1}H NMR spectroscopy calibrated using dioxane as an internal standard.

Although the dehydrogenation of anions in ethylene glycol at high temperature resulted in extensive decomposition, in formamide only minor decomposition was observed. Ethylene glycol is a protic, nucleophilic solvent with two alcohol functional groups. For an unknown reason, the ethylene glycol appears to facilitate the decomposition of the carboxylate salts, either through reacting with them or by facilitating oxidation by air. Formamide was effective in minimizing decomposition because it is not nucleophilic. However, formamide is inconvenient because its signals appear at a similar region of the ^{1}H NMR spectrum as the products of the reaction whereas ethylene glycol has one signal in the ^{1}H NMR spectrum.

The products of the dehydrogenation of the saturated anions were measured using ^{1}H NMR spectroscopy using dioxane as an internal standard. In both cases there was considerable amount of starting material missing, a larger amount in the case of 7b. However, at 150 ºC no products of any kind were detected in the reaction mixture. Similar amounts of starting materials were missing when the reaction was run at a higher temperature, but in this case a significant amount of the desired unsaturated anions were detected, with no unwanted side products. It is unclear what has happened to the missing starting material. It could have been transformed into unwanted products, which were not detected because they were volatile, adsorbed to the catalyst surface, or otherwise lost during the reaction work up. It may be just as likely that the starting material itself was lost to adsorption or during the work up. All that can be said is that the yield of the product was less than the missing starting material and that no side products were detected, which gives the reaction an apparent 100% selectivity. However, the fact that

conversion was observed, and the detected products were free of other contaminants demonstrates that these ions do in fact undergo dehydrogenation under these conditions.

The catalyst support was activated carbon, which is known to adsorb charged species, especially aromatic ones. In all of the dehydrogenation reactions, the starting materials are charged and aromatic, while the product is charged but not aromatic. This means that adsorption on the activated carbon surface should be more selective for the starting material than for the product. If this were the mechanism by which the missing starting material was lost it would appear that the calculated conversions were higher and the yields were lower than the true value, which would account for the missing material.

The saturated cationic heterocycles N-methylpiperidinium, N-ethylpiperazinium and 4-(ammoniummethyl)piperidine (in N-heterocycles with two basic sites either site can be protonated and the relative basicity would depend on the solvent) form trifluoromethanesulfonate salts with low melting points and can be dehydrogenated without solvent. They were dehydrogenated by stirring in a test tube open to the atmosphere at either 150 ˚C or 200 ˚C, with 10 mol% Pd/C for 3 h. An additional experiment was performed at 100 °C for 10b. After the reaction, the samples were dissolved in methanol, filtered through a plug of diatomaceous earth to remove the heterogeneous catalyst and then concentrated *in vacuo*. The resulting mixtures were analyzed by ^{1}H NMR spectroscopy in deuterium oxide using 1,4-dioxane as an internal standard (Table 2.6).

Table 2.6. Disappearance of starting material and yields of the catalytic dehydrogenation of the trifluoromethanesulfonate salts of saturated N-heterocycles under solvent free conditions

	9b		**10b**		**11b**	
T (ºC)	Missing (%)	Yield (%)	Missing (%)	Yield (%)	Missing (%)	Yield (%)
100	-	-	74	0	-	-
150	64	<1	100	0	74	<1
200	18	3	78	0	42	0

Substrates were dehydrogenated over 10 mol% equivalent Pd (10 wt% Pd/C) in test tubes for 3 h under solvent free conditions. Missing materials and yields were determined by ^{1}H NMR spectroscopy calibrated using dioxane as an internal standard.

Dehydrogenations of all cations featured poor selectivities when calculated using the dioxane internal standard method, though this can be explained at least in part by the adsorption of material to the catalyst support, although the formation of many unidentified side products was apparent in some cases. The ^{1}H NMR spectra of the products from 10b and 11b show additional extraneous peaks indicative of decomposed material, but that of 9b does not. 9b has no obvious intrinsic decomposition pathways (that is to say, the molecules should not be self-reactive), so it may either undergo pyrolysis or reaction with water (or may be bound to the surface). In this case, it would appear that the selectivity of the hydrogenation of the N-methylpyridinium ion is 100% selective, though the yield is less than the conversion. In 10b and 11b, the nucleophilic nitrogen can cause intermolecular substitution or elimination reactions to occur, which would lower the intrinsic thermal stability (Figure 2.11). This was evident in the ^{1}H NMR spectra of 10b as pyrazine peaks were observed. The boiling point of pyrazine is 115 ˚C,

which would explain why selectivity for pyrazine in the 150 ˚C reaction is only 5% as opposed to 39% in 100 ˚C; at higher temperature more of the decomposed material has evaporated.

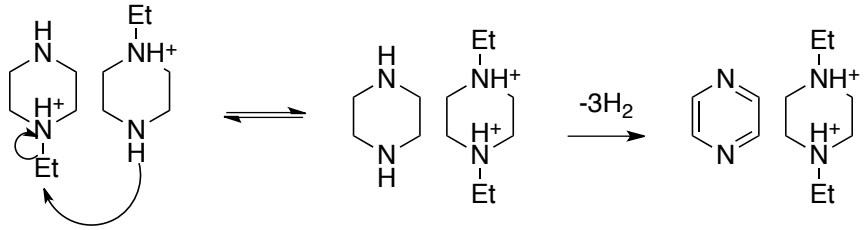

Figure 2.11. Dealkylation and dehydrogenation of N-ethylpiperazinium trifluoromethanesulfonate

2.3.4 Conclusion

Based on the results obtained by ^{1}H NMR spectroscopy, the hydrogenation of unsaturated anions was achieved with good conversion and selectivity. The dehydrogenation of the saturated cations proceeded with fair conversion (considering the use of solvent) and the apparent selectivity of the reactions was 100%, however, there was a significant amount of missing material and it is unclear whether the missing mass consisted of decomposed material, or was merely desired product lost during the work up or on the catalyst surface. Difficulties were encountered in the hydrogenation and dehydrogenation of cations, as poor selectivities were obtained. Choice of solvents in

these reactions is important. Use of a protic, nucleophilic solvent results in decomposition, and should be avoided. Fortunately, a hydrogen-storing ionic liquid would need no solvent. The work up procedure should be designed to minimize loss of starting material. Moreover, it is necessary to use an internal standard in all NMR samples. As was seen for dehydrogenation of anions and 9b, NMR spectra, without the use of an internal standard, can give misleading conversions when there is a loss of starting material or product. This is also complicated by selective adsorption by activated carbon of charged and aromatic species where these factors resulted in the inability to accurately determine conversion and selectivity.

For those reactions that do not proceed to high conversions or reacted with poor selectivities, a number of modifications can be considered. As mentioned before, a different solvent can be used, and performing the reactions under an inert atmosphere could only improve the selectivities measured. A hydrogen atmosphere would be the most appropriate as it would show the thermodynamic limits of these reactions as well as show which ions are susceptible to hydrogenolysis. Anions tend to favour dehydrogenation at higher temperatures without observing decomposed material and would benefit from the increased conversion, however the cations studied appeared to be much more sensitive to high temperature and decomposed easily.

Additional work would aim to diversify the ions studied. Other than the limited number of carboxylate ions studied, there are additional carboxylate and sulfonate ions that could be considered. Other cations, such as phosphonium ions, or furans with external cationic groups could be tested as well. Furthermore, work up methods need to

be explored because loss of material is a concern. Improvement on analytical methods will give more accurate results. In particular, selectivities and quantities of adsorption of different compounds on carbon should be quantified.

True ionic liquids can be formed by pairing an anion and cation that perform well in hydrogenation and dehydrogenation when investigated separately. Optimization of reactions can then be performed. Different types of catalyst should be tested as they are substrate specific, and catalyst loading can be adjusted. Temperature and reaction time cannot be as flexibly adjusted because it is targeted towards usage in fuel cells. For it to be practical, rapid hydrogen evolution at reasonably low temperature must be achieved. Eliminating the use of solvent would simplify the work up procedures and give a more reasonable approximation as to the behaviour of these ions in a real ionic liquid medium.

2.4 Tetrabutylphosphonium Ionic Liquids

Using ionic liquids with inert counterions, at least in research, greatly simplifies the study of the reactions of hydrogen storing ionic liquids in the following ways: thermal degradation of the liquids at high temperature is suppressed through the use of an unreactive counterion, the analysis of reaction products is simplified (and the inert counterion can potentially be used as an internal standard), and they have lower melting points than the alkali metal salts studied earlier. The use of inert cations, ones which would not be expected to react with the anion under study at the temperature chosen,

vastly improves the observed selectivity of any reactions studied and eliminated mass loss due to decomposition and volatilization of the ionic liquid.

There are many relatively inert counterions that can be used to generate ionic liquids of high thermal stability. The mechanism through which ionic liquids decompose is most typically the opposite of the one through which they were formed. Many ionic liquids are prepared through nucleophilic substitution reactions, therefore if the anion in an ionic liquid is a very poor nucleophile or the cation is a poor electrophile, then the ionic liquid will be more thermally stable. Of the common cations used in forming ionic liquids, pyridinium and imidazolium ions usually decompose through S_N2 displacement of their alkyl groups (**Figure 2.12**). Ammonium ions can undergo the same reaction, though in the presence of a reasonably strong base, ammonium ions with β-hydrogens can undergo elimination reactions (**Figure 2.13**). Phosphonium ions are similar to ammonium ions, though instead of undergoing β-elimination they tend to be deprotonated at the α position to form phosphonium ylids (**Figure 2.14**). Overall phosphonium salts tend to be more thermally stable than the other cations. It is important to note, however, that the ionic liquids are composed of organic materials that will eventually undergo pyrolysis through homolytic and heterolytic bond cleavage. As such, these materials would be unlikely to be stable for very long at temperatures exceeding 300 ºC.[182]

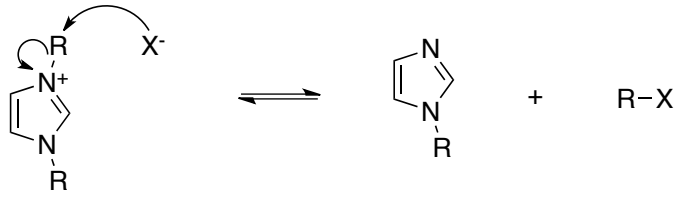

Figure 2.12. Mechanism of dealkylation of an imidazolium salt via an S_N2 mechanism

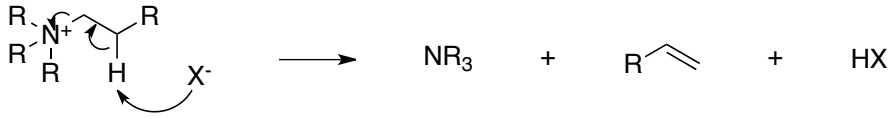

Figure 2.13. Mechanism of E2 elimination of an ammonium salt

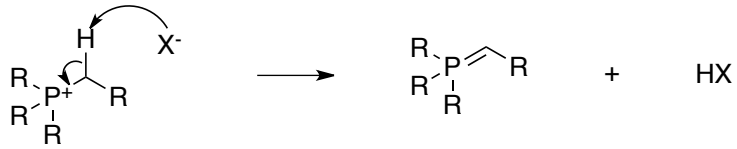

Figure 2.14. Mechanism of ylide formation from a phosphonium salt via α elimination

An inert counterion would merely be a spectator ion; even though it would not participate in any reactions it can be of use in analysis of the product mixtures. Over the course of hydrogenation and dehydrogenation some mass loss will inevitably be encountered, either due to the entrainment of droplets of ionic liquid in any gas streams leaving the reaction mixture, or through spattering of a vigorously stirred mixture on the sides of the glassware. This can be corrected for, to some degree, by using the inert counterion as an internal standard. This is especially convenient when using ^{1}H NMR spectroscopy as the analysis method because any protons that are assigned to the inert

counterion will not change over the course of the reaction. The relative proportions of signals from starting materials and products (compared to this internal standard before and after the reaction) can be used to determine the conversion and selectivity of the reaction with good accuracy.

The low melting points of the ionic liquids when compared to alkali metal salts allows them to be studied under solvent-free conditions. Solvents will affect the results of the reactions by changing the concentration of the ions, the polarity of the reaction medium, the solubility of gases, and the mass transport characteristics of the reaction mixture. The use of a solvent immediately decreases the concentration of the ions in the reaction mixture which would be expected to cause a linear decrease in reaction rate (or worse) though this would depend on the kinetics of the specific process. This also results in a very poor gravimetric hydrogen storage density; although this is not an issue during the offboard hydrogenation step, the use of a solvent on-board a vehicle would result in such a low hydrogen storage density that the material would be useless as a portable hydrogen storage material. The polarity of the reaction mixture is increased through the use of high polarity solvents (which are required to dissolve alkali metal salts, and have high enough boiling points to remain liquid at dehydrogenation temperatures). In reality, ionic liquids themselves do not necessarily have exceptionally high polarity and the polarity of the ionic liquids is highly dependent on the nature of the constituent ions.[183] Reactions run in high polarity solvents will have polar transition states stabilized by the solvent more than they would if the reaction was performed in the ionic liquid medium itself (ionic liquids can have diverse polarities depending on their nature; changes in

either ion, the length of any aliphatic chains and the presence of any functional groups can drastically change the polarity measured by solvatochromatic methods).[183] It is not clear what the nature of the transition state during hydrogenation or dehydrogenation is, though it likely consists of the dissociation of an N-H or C-H bond on the catalyst surface. If this step results in a polarised transition state then a polar solvent may artificially increase the reaction rate when comparing an ion in solvent to an ion as a component of an ionic liquid. Ionic liquids typically have high viscosities that are highly dependent on the nature of the ionic liquid as well as the amount of impurities in the material. Ionic liquids with high viscosities will have poor mass transfer rates. Not only does this affect the rate of transfer of hydrogen to and from the gas phase, but slow diffusion of ions through the medium also lowers the rate of transfer to and from the surface of the heterogeneous catalyst. Although a solvent is highly detrimental to the hydrogen storage density of the material even small amounts of solvent can greatly increase the rates of hydrogenation and dehydrogenation so long as these reactions are limited by the rate of mass transfer, and if the viscosity of the material is very high this may be the case. Even ionic liquids of sufficiently low melting points would benefit from the addition of a small amount of solvent during the offboard hydrogenation where the rate of reaction will be more important than the thermodynamics of the reaction (a great excess of hydrogen can be used).

Previously, the reversible hydrogenation of heterocyclic anions was studied using either alkylpyridinium, alkylpiperidinium or sodium counterions (**Sections 2.2.1 and 2.3**). Although these counterions were less than ideal (alkylpyridinium and

alkylpiperidinium salts decomposed, and sodium salts required a solvent) they did show at least some successful hydrogenation and dehydrogenation reactions of the anion. In order to get a better representation of the reactivity of heterocyclic anions as a component of a thermally stable ionic liquid, an unreactive cation is required even if it itself is not hydrogen storing. In this way, the best candidate anions can be determined as their reactivity in terms of reversible hydrogenation should be independent of the choice of the counterion. Inert cations, meaning those that do not store hydrogen, can always be substituted with a compatible hydrogen storing cation when formulating viable hydrogen storing ionic liquid materials. The tetrabutylphosphonium ion was chosen as a suitable inert cation because it has high thermal stability when paired with a variety of anions. Tetrabutylphosphonium bromide also has a melting point of approximately 100 ºC,[184] which is well below the temperature range suitable for dehydrogenations. The heterocyclic anions being studied tend to have lower melting points than the corresponding bromide salts so it is likely that the tetrabutylphosphonium salts being studied will have melting points below 100 ºC.

2.4.1 Synthetic Strategies

There are at least three different methods available to prepare tetrabutylphosphonium ionic liquids. The first is through nucleophilic substitution of a suitable electrophile with tributylphosphine.[185] Tetrabutylphosphonium bromide can undergo ion exchange through metathesis using an appropriate silver salt.[186]

Tetrabutylphosphonium hydroxide is also commercially available as an aqueous solution and can simply be mixed with an organic acid to yield the desired ionic liquid product. Each of these routes has potential advantages and disadvantages.

The reaction of tributylphosphine with an electrophile is a straightforward method of preparing quaternary phosphonium salts. This is the industrial route to the production of tetrabutylphosphonium halides.[185] Because tributylphosphine is an excellent nucleophile, quaternization is normally rapid. However, because halides are much better leaving groups than carboxylates, the reaction may fail when forming tetrabutylphosphonium carboxylates, although the reaction may proceed adequately when forming tetrabutylphosphonium sulfonates (**Figure 2.15**). Additionally, the butyl esters and sulfonates are not commercially available and would require synthesis. Tributylphosphine has a strong nauseating odor, is air sensitive and is potentially pyrophoric. Although this may be a commercially viable route for bulk production at an appropriate facility, these ionic liquids are not going to be economically viable for hydrogen storage applications (due to low gravimetric storage density) so the development of an economic synthesis through this route is entirely unnecessary.

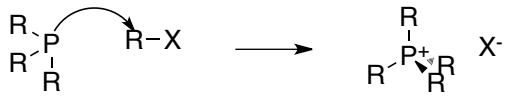

Figure 2.15. Mechanism for formation of a tetraalkylphosphonium salt via an S_N2 mechanism

Tetrabutylphosphonium bromide is a commercially available material that can undergo metathesis to form any number of ionic liquids. Much in the same way as the alkylpyridinium nicotinate salts were formed, it is possible to heat a solution of tetrabutylphosphonium bromide and an appropriate organic acid in methanol in the presence of excess silver carbonate to affect the ion exchange (**Scheme 2.19**). After filtration and removal of the solvent, the desired ionic liquid is obtained. However, the exchange (as determined by ^{1}H NMR spectroscopy) is never complete and in general never more than 90% of the anions are the desired carboxylate. Performing the exchange in a similar way using silver (I) oxide instead of silver carbonate gave similar results. Preforming silver carboxylates and sulfonates by deprotonation of the acid with one equivalent of sodium hydroxide solution followed by precipitation with a slight excess of silver nitrate solution yields solid precursors (though some of the silver sulfonates are actually soluble in water). Accurately weighing both the isolated silver carboxylate and tetrabutylphosphonium bromide and heating in methanol also results in incomplete exchange, some of the silver carboxylate remains in the precipitate. This method of preparation is costly and it would require a method of increasing the exchange of ions or a method of purifying the final material (simple aqueous washing is ineffective as all the materials are very soluble in water).

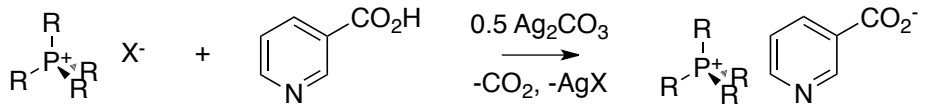

Scheme 2.19. Ion exchange of a tetraalkylammonium salt using silver (I) carbonate and nicotinic acid

Aqueous solutions of tetrabutylphosphonium hydroxide are commercially available. To prepare other tetrabutylphosphonium salts, the solution only needs to be mixed with the appropriate acid (**Scheme 2.20**). Even organic acids with limited solubility in water, such as benzoic acid, will eventually dissolve as they are deprotonated (though ultrasonication greatly increases the rate of mass transfer). The result is an aqueous solution of the ionic liquid product. On a small (100 mg) scale the water can be removed under high vacuum (approximately 8 h for the bulk and an additional 24 h of the more tightly bound water). Naturally, this is not viable on a large scale but because it does not rely on the exchange of ions it results in very pure ionic liquid. This was the method used to prepare ionic liquids for further study of their reactivity. If this method of preparation were to be used on scale a much more volatile solvent would be required. A solution of tetrabutylphosphonium methoxide in methanol would probably be an ideal starting material.

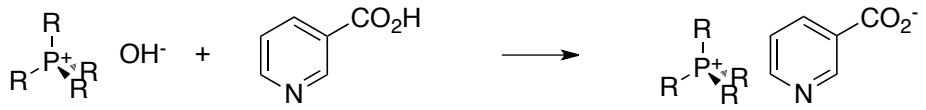

Scheme 2.20. Deprotonation of nicotinic acid using tetrabutylphosphonium hydroxide

2.4.2 Hydrogenations

Overall, the hydrogenations and dehydrogenations of the tetrabutylphosphonium salts of different anionic heterocycles were problematic (**Table 2.7**). Although hydrogenation was detected, in the majority of cases the reactions were slow. The highest conversion was observed for **12d**, which only experienced 7.4% conversion over a 20 h period. The hydrogenation reactions were performed in isopropanol in order to decrease the viscosity of the reaction medium and increase the rate of reaction. This is justifiable because hydrogenation would occur offboard the vehicle and would benefit from enhanced reaction rate in a re-hydrogenation facility, where the gravimetric density of the medium is unimportant. Naturally, the use of solvent would decrease the rate of reaction because of the lowered concentration of the ions in solution. Because the ionic liquids were only diluted with an equal volume of isopropanol the rate would normally be expected to be lowered by half (if the reaction is first order in anion) because the molarity of the solution is halved. The viscosity of the solution is much less than half the viscosity of the pure ionic liquid and this should be able to more than double the rate constant if the reaction is limited by the rate of mass transfer because of the increase in the mass transfer

of the anions from the bulk solution to and from the catalyst surface. Therefore the conversions reported would likely be higher than those reported if the hydrogenation were carried out without additional solvent.

The saturated substrates would be in very high demand in a commercial application. Therefore the rate of the hydrogenation would need to be reasonably rapid in order to meet the needs of consumers. A hydrogenation that only proceeds to less than 10% completion after 20 h clearly will not meet this demand. Changing the heterogenous catalyst may increase the rate of hydrogenation, though the optimal catalyst would likely vary with each specific substrate. For instance, the 2-(4'-pyridyl)ethanesulfonate ion was hydrogenated to 46% conversion at 100 ºC in ethanol over a Pd/C in a similar time frame (16 h) when it was paired with the N-methylpiperidinium ion (**Section 2.2.3.2**). Although, in this case it is unclear whether the difference in rate of hydrogenation is attributable to the increased temperature, slightly more polar solvent, the catalyst choice, or the weakly acidic counterion.

The rate of the reaction would be improved by running the reaction at a higher temperature. Although this is disfavoured thermodynamically, the vast excess of hydrogen present in the reactor would allow the hydrogenation to proceed to completion. Increasing the temperature may also lower the selectivity, which has thus far been very high. It could be argued that the ionic liquid must be able to be held at the dehydrogenation temperature for long periods of time without suffering thermal degradation and so raising the hydrogenation temperature should not be a problem. However, the dehydrogenation reaction would only be expected to occur at a low back

pressure of hydrogen gas. If the ionic liquids are held at high temperature and in the presence of a large partial pressure of hydrogen for an extended period of time in the presence of a catalyst then the probability of hydrogenolysis of the ionic liquid would be

Table 2.7. Conversions for the catalytic hydrogenation of the tetrabutylphosphonium salts of unsaturated heterocyclic carboxylates and sulfonates

Substrate		Conversion (%)
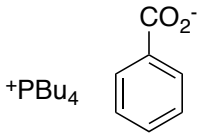	**12a**	N/D
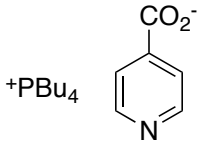	**12b**	6.9%
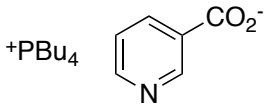	**12c**	1.7%
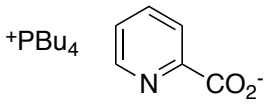	**12d**	7.4%
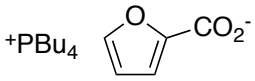	**12e**	2.3%
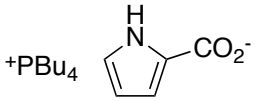	**12f**	N/D
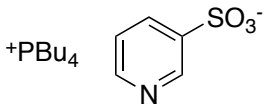	**12g**	5.3%
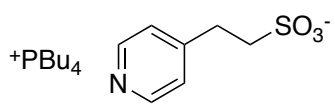	**12h**	N/D

Samples were heated to 75 ºC over 1 mol% equivalent Pd (5 wt% Pd/SiO_2) and pressurized with 70 bar of H_2 in a stainless steel autoclave for 20 h. Product mixtures were analyzed by ^1H NMR in D_2O. N/D indicates that no conversion was detected.

significant. Optimization of reaction temperature to maximize the rate of hydrogenation before hydrogenolysis is observed would require considerable amounts of all the substrates under study and many long experiments and would be very expensive. Naturally, optimization of hydrogenation reactions is only necessary for those substrates for which the reaction is readily reversible so not all substrates need to be screened so thoroughly.

2.4.3 Dehydrogenations

The dehydrogenation of the saturated anions was examined (**Table 2.8**), though the substrates tested were limited to the carboxylate anions because the required sulfonic acids were not commercially available nor was there any established method for their preparation. Of all the materials tested, only **13b** showed any dehydrogenation, and even it only proceeded to 0.7% completion in the course of an hour. This is less than the loading of palladium used (1 mol%) and is certainly not enough to meet the demands of a hydrogen fuel cell powered vehicle. All of the reactions were run without solvent at 170 ºC. None of the materials experienced any thermal decomposition and all except the isonipecotate ion remained unchanged from the start of the reaction.

There is a limit to the temperature that can be used to perform the dehydrogenation of the hydrogen storing ionic liquid, not only in terms of the thermal stability of the liquid or the selectivity of the dehydrogenation reactions, but also in terms of the efficiency of the system. The higher the temperature required to perform the

dehydrogenation (and the higher the enthalpy of dehydrogenation), the more hydrogen that must be consumed to sustain the dehydrogenation reaction.

Table 2.8. Conversions for the catalytic dehydrogenation of the tetrabutylphosphonium salts of saturated heterocyclic carboxylates and sulfonates

Substrate		Conversion (%)
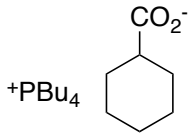	**13a**	N/D
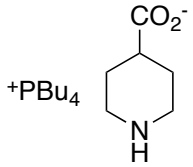	**13b**	0.7
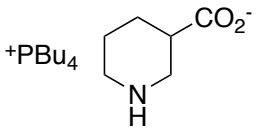	**13c**	N/D
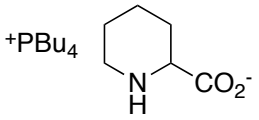	**13d**	N/D
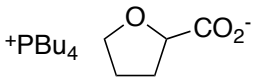	**13e**	N/D
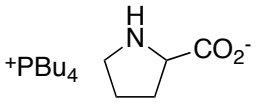	**13f**	N/D

Samples were heated to 170 ºC over 1 mol% equivalent Pd (5 wt% Pd/SiO_2) and sparged with Ar for 1 h. Product mixtures were analyzed by ^1H NMR in D_2O. N/D indicates that no conversion was detected.

The lack of observed dehydrogenation of these fluids may not be a lack of thermal energy, in either the thermodynamic or kinetic sense, but may be related to the lack of mass transfer between the substrate and the catalyst; this is suggested by the significant

conversions observed for the corresponding sodium salts when a solvent was used. The viscosity of these pure ionic liquids is high; even at high temperature they are thick liquids. If the substrate or product ions fail to diffuse to or from the catalyst surface, the reaction will fail. Hydrogen also has poor solubility in ionic liquids;[155] this could potentially prevent the hydrogen gas from diffusing away from the catalyst after it forms and would block the catalyst surface from further reactions. The low rate of dehydrogenation is comparable to that seen for **3a**, which was reacted in ethylene glycol, a solvent with fairly high viscosity.

2.4.4 Conclusions

Most of the anions showed at least some conversion when hydrogenated, so with optimization of the catalyst choice, catalyst loading, reaction temperature, and solvent choice, it is entirely possible at least some of them may be able to be fully hydrogenated in a reasonable time. The dehydrogenation reactions are much less promising; the main concern is the viscosity of the ionic liquids. The viscosity of fluids tends to lower as the temperature is increased. It may be possible to have a useful rate of dehydrogenation at higher temperatures due to the increased reaction rate as well as the lowered fluid viscosity. This is not necessarily the best solution because increasing the temperature of dehydrogenation will require more energy to be provided from the stored hydrogen and would therefore decrease the effective energy storage density of the ionic liquid. It may be possible to design an ionic liquid that has relatively low intrinsic viscosity, or a small

amount of a non-reactive high boiling additive may be added to lower the viscosity of the resulting mixture. It is unlikely that there is an intrinsic lack of reactivity of all of the anions studied because the sodium salts studied in solution showed considerable conversion. At this point it makes little sense to attempt to design an ionic liquid with both an inert counterion and low viscosity because the viscosity of an ionic liquid with both hydrogen storing cations and anions would not likely have the same viscosity. The viscosity of the fluid will clearly be an important property to consider when designing marketable hydrogen storing ionic liquids, both due to the kinetics of dehydrogenation as well as pumping and pipelining the material.

2.5 Carbazole Containing Ionic Liquids

The reasons for making ionic liquids where the cation is capable of storing hydrogen whereas the counterion is inert are largely the same as those for making ionic liquids where the cation is inert and the anion is hydrogen storing. There are many inert anions available and several of these have properties that are beneficial. Most of the anions used to form ionic liquids contain no hydrogen atoms and therefore would remain invisible in the ^{1}H NMR spectrum. Although these anions cannot be used as an internal standard, they greatly simplify the ^{1}H NMR spectrum and allow for the easy determination of changes in the starting material over the course of the reaction. Many poorly nucleophilic anions are available; these can be used to form ionic liquids with high thermal stability because they will not readily react with their cationic partner. However,

as in all ionic liquids, the individual bonds will begin to undergo cleavage at very high temperatures. The anion in an ionic liquid also has a strong effect on the melting point and the hydrophilicity of the material.

The choice of inert anion is important. For instance, halogen ions may be invisible in ^{1}H NMR, but they are fairly nucleophilic (particularly the highly polarizable iodide ion). Ionic liquids with halide ions tend to undergo thermal decomposition at lower temperatures than observed with salts with less nucleophilic anions. In addition, halogen ions can coordinate to metal centers so an ionic liquid with halogen counterions may poison the surface of the heterogeneous catalyst during hydrogenation or dehydrogenation. Larger anions, such as tetrafluoroborate or hexafluorophosphate, are much less nucleophilic than halides and yield ionic liquids with lower melting points (due to the larger more diffuse anions). These anions are usually non-coordinating (except with very potent electrophiles) and have high thermal stability. However, tetrafluoroborate and hexafluorophosphate can undergo hydrolysis or decompose with the release of hydrogen fluoride. Better than these are the anions trifluoromethylsulfonate (triflate) and bis(trifluoromethane)sulfonimide (bistriflimide). These anions are very poor nucleophiles, depress the melting points of the salts they are in, are non-coordinating, and have low hydrophilicity. The bistriflimide ion would be an ideal partner for any cation studied.

In earlier sections of this thesis only pyridinium ions had been examined as potential hydrogen storing cations. The pyridinium ion conveniently forms the cationic core of many existing ionic liquids. N-Alkylpyridinium ions are easily made through the

alkylation of pyridine. Although N-alkylpyridinium ionic liquids are easy to prepare, and they readily hydrogenate, it is very difficult to dehydrogenate the resulting piperidinium ion (**Section 2.2.1.4**). Therefore the N-alkylpyridinium ion is not a reversible hydrogen storing material.

In the work of Crabtree's group,[147, 151] it was postulated that the presence of nitrogen in a heterocycle lowered the dehydrogenation enthalpy by affecting the C-H bond acidity of the neighbouring methylene groups. Quaternizing the nitrogen atom seems to eliminate this benefit.[140, 141] The lone pair of electrons appears to be the key factor in the enthalpy-lowering effect because it is not universal to nitrogen; oxygen heterocycles also benefit somewhat. The reactivity of nitrogen heterocycles with respect to dehydrogenation is disrupted if the nitrogen lone pair of electrons is occupied by alkyl groups, protons and other Lewis acids. N-Alkylpyridinium ions will never be effective hydrogen storing cations.

Pyridine itself could still be used as a hydrogen storing heterocycle; however, it cannot be protonated or alkylated and still be able to reversibly hydrogenate so it cannot form the cationic portion of the cation. It could be appended to another cationic center and function as the hydrogen storing moiety of the ion. Alternatives to the pyridinium ion include ammonium ions, phosphonium ions and imidazolium ions. These ionic liquids are formed from amines, phosphines and imidazoles respectively through nucleophilic substitution of an electrophile.[154] This presents a synthetic challenge. In order to incorporate pyridine heterocycles into the cation, either the nucleophile or the electrophile would need to contain the pyridine ring. Pyridine nitrogens are good

nucleophiles and would easily compete with the other nucleophiles in the substitution reaction.[187] If pyridine was part of the nucleophile, it would be alkylated in the wrong place, and if it were part of the electrophile it would dimerize or polymerize (**Scheme 2.21**).

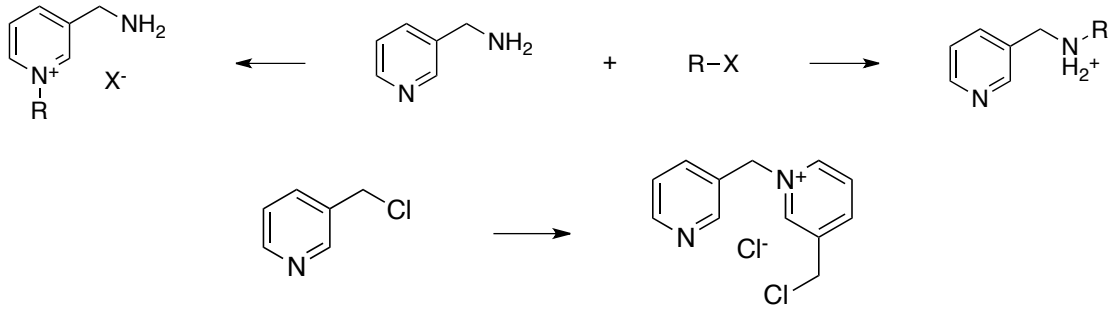

Scheme 2.21. Competitive nucleophilicity of the pyridine nitrogen

However, there are other nitrogen heterocycles which are not nucleophilic. Pyridine nitrogens are nucleophilic because the nitrogen's lone pair is not part of the aromatic system;[187] it points outward and is available for bonding. Pyrrole nitrogens, however, have nitrogen lone pairs which are part of the aromatic ring system.[187] Pyrroles are very poor bases and nucleophiles, and when they do react with strong acids or electrophiles they are attacked in the 2 or 5 position, not on the ring nitrogen.[187] Pyrroles are also slightly acidic and this can be used strategically during a synthesis by temporarily converting the non-nucleophilic neutral molecule into a nucleophilic anion.

Pyrroles, like pyridine, are good hydrogen storing heterocycles. In particular N-ethylcarbazole (which contains a pyrrole ring) has been shown by Pez,[174] and again by Crabtree's group,[148, 152] to be an effective hydrogen-storing heterocycle. It has both good

thermodynamics as well as a fairly high gravimetric density of stored hydrogen (in the dodecahydrocarbazole).[174] Any group appended to the carbazole ring system beyond an ethylene linker is unlikely to have any strong impact on the electronic properties of the ring, so a carbazolylethylammonium or a carbazolylethylimidazolium salt should have similar dehydrogenation enthalpies. However, these extra groups may have steric effects on the approach of the ring to a catalyst surface or may themselves change the binding behaviour on the catalyst.

2.5.1 Ammonium Ionic Liquids

There are other cationic centers that can be used other than pyridinium or imidazolium that would not be susceptible to reduction or π-stacking on the catalyst surface. A simple ammonium ion cannot be reduced, and it is much less massive than a pyridinium or imidazolium ion, though pendant carbazole rings would need to be appended to it through a tether. It is true that such a cation could still participate in π-cation stacking interactions, though if the ammonium center is sterically hindered it would be unlikely, and even if it did so a simple electrostatic interaction of the ammonium ion would not compete with the carbazole moiety for binding to the catalyst surface.

2.5.1.1 Synthetic Strategies

Ammonium ionic liquids containing carbazole rings could be prepared in at least two ways. They could be prepared by the more typical alkylation of an amine, or through appending carbazole rings to the peripheral aliphatic chains of a preexisting ammonium ion (**Scheme 2.22**). The first route has the advantage of allowing the purified neutral starting materials to react to form a single ionic product; any remaining starting materials can be removed through solvent washing or the application of high vacuum. Appending carbazole rings to the periphery of a preformed ammonium ion has the advantage of avoiding steric congestion around the ammonium center during the synthesis; however, it would generally form other salts at the same time as the ionic liquid and could potentially result in problems during the purification of the ionic liquid (unless the desired product is insoluble in water but the co-precipitated salts are not).

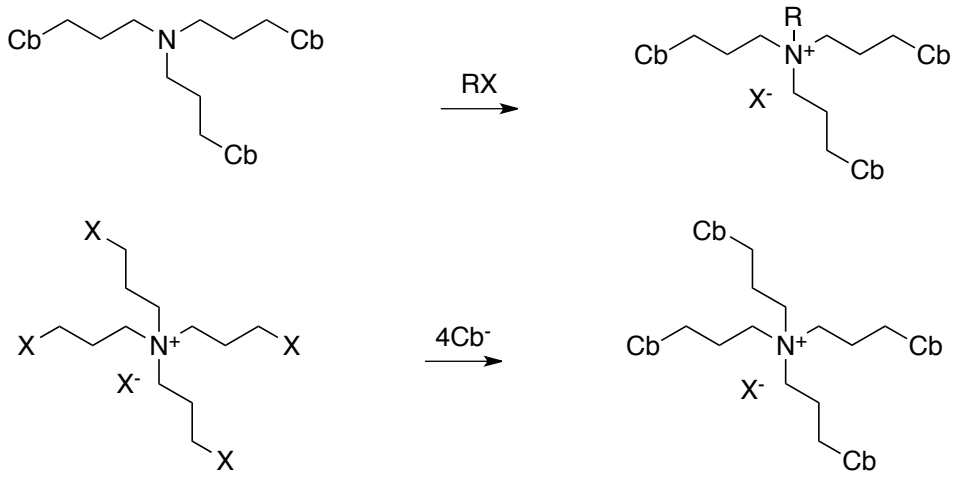

Scheme 2.22. Synthetic strategies for carbazole containing ammonium salts

Another issue is determining how many carbazole rings should be appended to each ammonium ion. Clearly, in terms of gravimetric hydrogen storage density, the more carbazole rings the better the ionic liquid. However, there are many reasons for not completely saturating the ammonium ions with carbazole rings, both synthetically, in terms of reactivity, and for the physical properties of the fluid. Highly symmetrical cations tend to have higher melting points than similar cations with lower symmetry,[172] this is due to the efficiency of packing the ions in the crystal structure. In addition, the large size of carbazole rings would greatly increase the molecular weight of the cation and van der Waals forces may become significant. The steric interactions between neighbouring carbazole rings may conformationally lock the molecule and limit the degrees of freedom of movement. Rigidity in the ion would also facilitate crystalline packing. Size disparity between the cation and anion may alleviate these crystal packing problems to some extent, but an ammonium ion with four carbazole rings would likely be an intractable insoluble solid and would likely be useless as a hydrogen storage material. The rigidity of many carbazole rings around the ammonium center, along with the additional steric hindrance, may prevent any of the carbazole rings from interacting with the catalyst surface and therefore prevent either hydrogenation or dehydrogenation from taking place.

Each additional carbazole moiety placed on the ion increases the steric crowding and the difficulty of the synthesis. When synthesizing these materials through a final alkylation of an amine (**Scheme 2.22**, top), the amine precursor should already be

composed of hydrogen-storing carbazole rings, in this case the electrophile could be a simple alkyl halide. However, the more carbazoles appended to the amine the more difficult it is for the amine nitrogen to attack the electrophile. When appending carbazole rings to a preformed ammonium ion, the carbazoles would continue to attack electrophilic centers until the ion became too crowded for further reactions to take place. In this case, however, the periphery of the preformed ion is less crowded than the case where the center of a bulky amine must be alkylated (**Scheme 2.22**, bottom).

2.5.1.2 Tri(carbazolylethyl)amine

The first method attempted was by initial formation of a tertiary amine with appended carbazole rings followed by alkylation. An inexpensive readily available starting material for this product is triethanolamine. Triethanolamine can be activated by treating it with thionyl chloride to form the hydrochloride salt of tri(2-chloroethyl)amine (**14**), a nitrogen mustard (**Scheme 2.23**). This material is safe to handle in its protonated form but the free base is an extremely toxic blistering agent used as a war chemical,[188] therefore its production and use on any scale would be severely restricted. However, these particular compounds have also seen use as chemotherapy agents.[189] This compound is prepared and stored as the hydrochloride salt, which is a solid, and is only deprotonated to react in the presence of nucleophiles that can quench it.

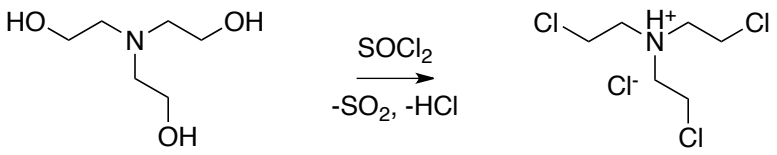

Scheme 2.23. Chlorination of triethanolamine using thionyl chloride

In an inert atmosphere glove box, **14** along with three equivalents of recrystallized carbazole was diluted with dry tetrahydrofuran with stirring in a glass pressure tube. To this mixture, four equivalents of sodium hydride were slowly added with the evolution of hydrogen gas. The sodium hydride was added in small aliquots and additional sodium hydride was only added after gas evolution had ceased to prevent material loss due to excessive foaming of the reaction mixture. After all the sodium hydride had been added and the hydrogen evolution had ceased, the pressure tube was sealed and removed from the glove box. The tube was then heated in an oil bath with stirring at 60 ºC for four days. The solution was then filtered to remove the precipitated sodium chloride and concentrated *in vacuo* to yield a solid material which was then washed with toluene to yield the desired amine, tri(2-carbazolylethyl)amine (**15**), in 77% yield (**Scheme 2.24**). The white solid was crystallized by slow evaporation from chloroform. The single crystal X-ray analysis is shown in Appendix B (**Figure 2.16**). There is very little room available about the central nucleophilic nitrogen for the approach of an electrophile.

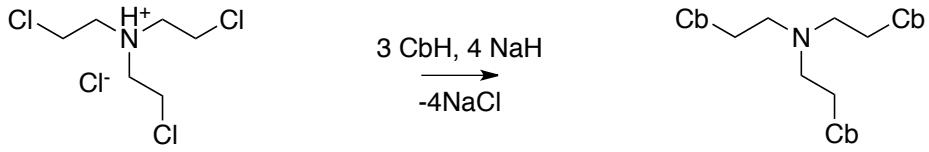

Scheme 2.24. Substitution of tri(2-chloroethyl)ammonium chloride with sodium carbazolide

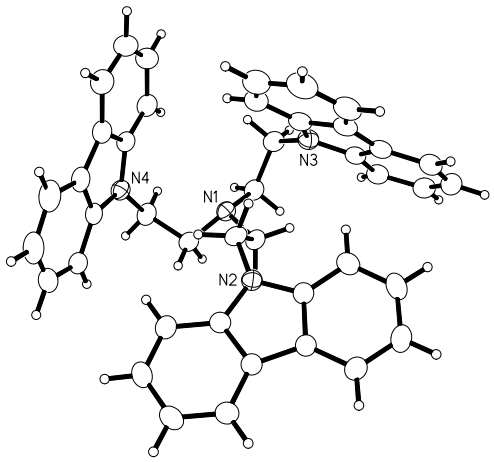

Figure 2.16. Molecular structure of tri(carbazolylethyl)amine (**15**)

2.5.1.3 Butyltri(carbazolylethyl)ammonium

Attempts were made to alkylate **15** with numerous electrophiles, 1-chlorobutane, 1-bromobutane, 1-iodobutane, and iodomethane. These reactions were performed without solvent, or with tetrahydrofuran, acetonitrile, dimethylsulfoxide, dimethylformamide or chloroform. In every case the reaction failed (**Scheme 2.25**). With each of these electrophiles, the leaving group, a halide, is also a nucleophile.[187] The reaction is

reversible and because the nucleophilic center is quite sterically crowded (as can be observed in the molecular structure, **Figure 2.16**), the dealkylation by the halide ion may be thermodynamically favoured due to the relief of steric congestion.

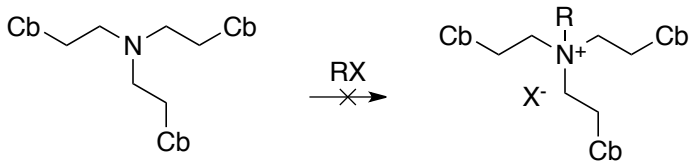

Scheme 2.25. Unsuccessful alkylation of tri(2-carbazolylethyl)amine

Alkyl tosylates have sulfonate leaving groups which are not nucleophilic; as such they alkylate the amine irreversibly. However, treating the amine with butyl tosylate in many different solvents resulted in no reaction. The tosylate leaving group is large and would limit the approach of the amine. To get around this obstacle, butyl tosylate could be used as an irreversible electrophile, but a small amount of iodide could be added as a catalyst. The iodide ion generates a small amount of butyl iodide, which performs the alkylation whereas the departure of the tosylate leaving group drives the reaction to completion (**Figure 2.17**). However, this strategy ultimately failed. It appears that the nitrogen atom is simply too hindered to react with any alkylating agent.

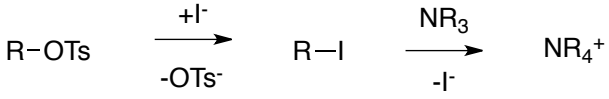

Figure 2.17. Iodide catalyzed alkylation of an amine

2.5.1.4 Butyldi(carbazolylethyl)amine

In order to relieve some of the steric hindrance about the nitrogen, an analogous amine with two carbazole rings and a butyl chain was prepared. Butyldiethanolamine is a fairly inexpensive starting material, and was chlorinated in the same way as triethanolamine to yield the hydrochloride salt of butyldi(2-chloroethyl)amine (**16**), another protonated nitrogen mustard (**Scheme 2.26**). Carbazole was appended via an S_N2 reaction under similar conditions as in the preparation of **15** using two equivalents of carbazole and three equivalents of sodium hydride. Butyldi(2-carbazolylethyl)amine (**17**) was isolated in good yield (**Scheme 2.27**) and single crystals were grown from the slow evaporation of chloroform for X-ray crystallography (tabulated in Appendix B, **Figure 2.18**). This amine, like the tri(carbazolylethyl)amine, did not react with any alkylating agents under any of the conditions tested.

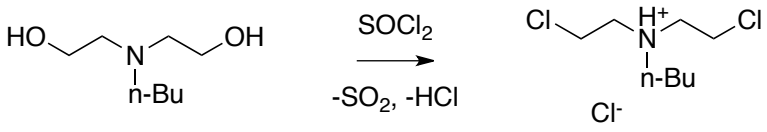

Scheme 2.26. Chlorination of butyldiethanolamine with thionyl chloride

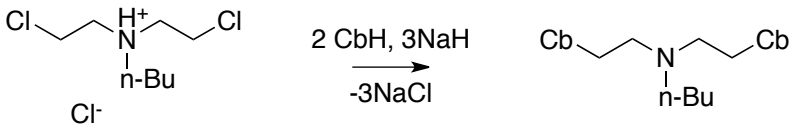

Scheme 2.27. Substitution of butyldi(2-chloroethyl)ammonium chloride with sodium carbazolide

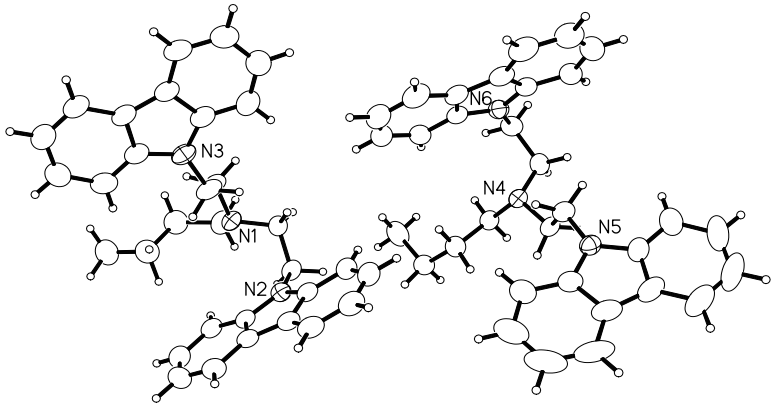

Figure 2.18. The molecular structure of butyldi(carbazolylethyl)amine

The substitution of carbazole for chlorine in the nitrogen mustards is a fairly easy reaction, even though as successive carbazole rings are added to the amine the steric bulk of the electrophile increases. This is due to the neighbouring group effect of the amine on the chloride leaving group.[190] This is also the effect that makes nitrogen and sulfur mustards powerful blistering agents. After the amine is deprotonated in the reaction mixture, it can behave as an internal nucleophile and displace the chloride leaving group. This reaction, which forms a highly reactive and strained three-membered aziridinium ion, is reversible, but because the nucleophile is always held in proximity to the leaving

group it occurs rapidly and frequently. During this time the chloride can reform the starting material by attacking either of the carbon atoms of the symmetric aziridinium ion, thus scrambling the carbon atoms (**Figure 2.19**). In this synthesis neither of the carbon atoms is distinguishable so the effect is not observable. The incoming nucleophile would be more likely to attack the reactive aziridinium ion than the open chain electrophile as it is more reactive, and even when two other carbazole moieties are already present the aziridinium ion points two equivalent electrophilic sites away from the bulk of the rest of the molecule. In this way it is possible to substitute up to three chlorine atoms with three carbazole rings in good yield, depending on the starting amine.

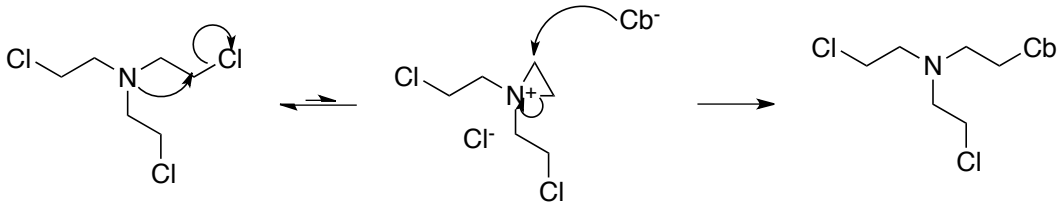

Figure 2.19. Neighbouring group assistance in carbazolide substitution

The alkylation of the resultant carbazole containing tertiary amine consistently failed. Although it may have succeeded if a substrate containing only one carbazole ring were prepared; such a cation would not have a high enough gravimetric hydrogen storage density to be worthwhile. When examining the X-ray molecular structure of the two different amines (**Figure 2.16** and **Figure 2.18**) in the solid state they appear to be quite sterically crowded about the amine nitrogen. If the bond angles about the amine nitrogen are examined they are not equivalent; however, the average bond angle for **17** is 111.7º

and that of **15** is 111.3º, both of these are comparable to that of trimethylamine (110.9º), so the nucleophilicity of the lone pair of electrons should be similar to that observed in simple tertiary amines. (Larger than tetrahedral bond angles imply greater s-character in the N-C sp^3 bonding orbitals and therefore greater p-character in the lone pair hybrid orbital, which lowers the electronegativity of the orbital and enhances the nucleophilicity of the lone pair).[191] It would seem that simple steric encumbrance is the only reason the final alkylations fail.

2.5.1.5 Tetra(carbazolylethyl)ammonium

An entirely different approach to forming carbazole-containing ammonium ionic liquids is to preform the ammonium core and then append the carbazole rings to the outside. This strategy results in the co-formation of the final ionic product with salts in the last step of the synthesis, which could complicate the purification of the material. However, this could be overcome through solvent washing, recrystallization, or perhaps chromatography if necessary. Less steric congestion is encountered by carbazolide nucleophiles approaching the outer periphery of the ammonium ion than would be experienced by an electrophile approaching a bulky amine. Another advantage of this method, at least when investigating the optimal number of carbazole rings to incorporate into the cation, is that it only requires one starting material. For instance, if tetra(2-chloroethyl)ammonium chloride (**19**) is treated with excess sodium carbazolide the carbazolide will react until the substrate becomes too sterically hindered for further

substitution. Subsequent materials could be constructed with aliphatic chains in place of those 2-chloroethyl moieties that did not react in order to manipulate the physical properties of the fluid.

Triethanolamine was readily alkylated with 2-chloroethanol to yield tetraethanolammonium chloride (**18**) in good yield (**Scheme 2.28**). Further reactions require activation of the alcohol moieties by conversion into leaving groups. This can be accomplished by conversion to a sulfonate or to a halide. The most straightforward approach to doing this is to dissolve the ammonium salt in thionyl chloride. The thionyl chloride behaves as both the solvent and reagent for this reaction, and in a way an indicator. Thionyl chloride reacts with alcohols through an internal nucleophilic substitution reaction generating the desired alkyl chloride along with acidic hydrogen chloride and sulfur dioxide gasses. After the ammonium salt is fully dissolved and further additions of thionyl chloride generate no more gas, the reaction is complete. At this point, the remaining thionyl chloride can be removed on a rotary evaporator to give the white solid product (**19**) in quantitative yield (**Scheme 2.29**).

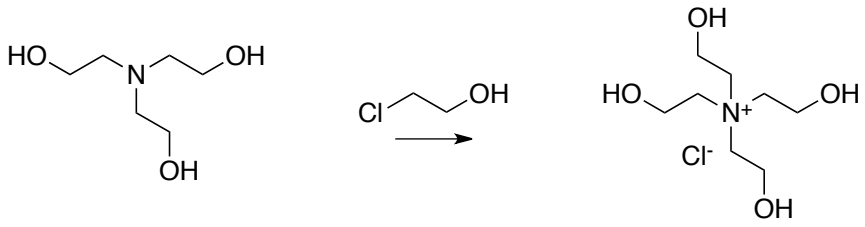

Scheme 2.28. Preparation of tetraethanolammonium chloride (**18**) via alkylation of triethanolamine with 2-chloroethanol

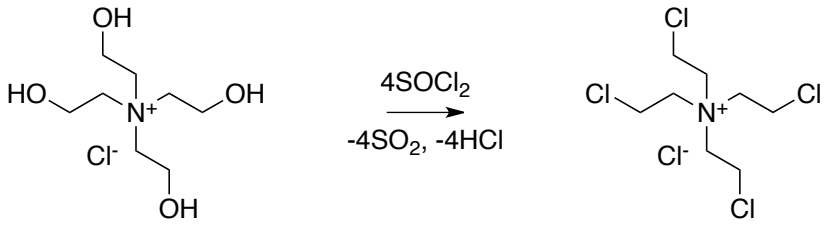

Scheme 2.29. Chlorination of tetraethanolammonium chloride (**18**) with thionyl chloride

19 should be a good precursor for the core of a carbazole-containing ammonium ionic liquid. The last step in the synthesis, apart from exchanging ions, is appending carbazole to the periphery. In earlier syntheses, carbazole was converted into a nucleophile by generating sodium carbazolide in tetrahydrofuran using sodium hydride as a base. However, **19** is not soluble in tetrahydrofuran. The only polar aprotic solvents that dissolve **19** are dimethylformamide and dimethylsulfoxide. Regardless, the reaction was also attempted in tetrahydrofuran and acetonitrile with the expectation that small amounts of carbazole substitution may increase the solubility of the precursor in the given solvent and allow for further reactions in the solution phase. In each case, carbazole was dissolved in the dried solvent and deprotonated with potassium tert-butoxide, a strong non-nucleophilic base. Deprotonation of carbazole forming potassium carbazolide was evident by the strong coloration of the resulting solution, in particular in dimethylsulfoxide where the solution is bright red. **19** was then added and the reaction tube sealed and then heated. Absolutely no change was observed in the reactions carried out in tetrahydrofuran or acetonitrile (where the ammonium salt is insoluble); as the reaction proceeds there should be a change in colour as the carbazolide ion is quenched.

The reactions using dimethylformamide or dimethylsulfoxide where heated to 150 ºC. The reaction in dimethylsulfoxide appeared to turn slightly brownish.

After several hours of heating, the reaction mixtures were cooled. An aliquot of each was taken and quenched with water in an effort to cause precipitation of the desired product, which would likely be insoluble in water. Both reaction mixtures formed a fine precipitate when quenched with water. The precipitate was washed several times with water to remove the reaction solvent completely and then dried. Both the dimethylformamide product and dimethylsulfoxide product were dissolved in dimethylsulfoxide-d_6 and analyzed by ^{1}H NMR spectroscopy. Only carbazole was recovered from either reaction mixture.

The remaining reaction mixtures of these reactions were slowly evaporated to dryness with gentle heating under high vacuum in case the water treatment resulted in the decomposition or dissolution of desired products. When fully dried the reaction mixtures were heterogeneous with white oolitic masses of carbazole interspersed with brownish-black material, which after ^{1}H NMR analysis also appeared to be carbazole. Interestingly no evidence of **19** was observed even though it was added in significant quantity (1/4 equivalent with respect to carbazole). The reaction failed to introduce even one carbazole ring to the ammonium ion so this method is unlikely to be fruitful in the construction of carbazole containing ammonium ionic liquids.

2.5.1.6 Tetra(carbazolylbutyl)ammonium via Olefin Metathesis

Another method for appending the carbazole moieties to the periphery of the ammonium salt without relying on nucleophilic attack would be through the use of olefin metathesis. If an ammonium ion were prepared with a periphery of terminal olefins and was cross metathesized with carbazole containing terminal olefins the evolution of ethylene gas should drive the reaction to completion. This strategy has an advantage over the use of carbazolide nucleophiles as the carbazole moieties are appended using much less reactive species (carbazolide can be quenched by proton sources) and the metathesis would occur away from both the bulky ammonium and carbazole units. Ammonium salts prepared in this way would contain an internal double bond, but this would likely be removed upon the first hydrogenation of the material.

To synthesize the same ammonium salt that would be generated by the other methods the starting materials required would be N-vinylcarbazole and tetravinylammonium chloride. N-vinylcarbazole is commercially available, though it is moderately expensive. It must be prepared in two steps, first by alkylation of carbazole with 1,2-dichloroethane followed by dehydrohalogenation (**Scheme 2.30**). N-allylcarbazole (**20**) is an alternate starting material that can be prepared by simple alkylation of carbazole with allyl chloride. Tetravinylammonium chloride would be more difficult to prepare. Trivinylamine is not commercially available (it is hydrolytically unstable) and it would require an alkylation with 1,2-dichloroethane followed by a dehydrohalogenation, which would compete with elimination of the tertiary amine.

Tetraallylammonium chloride (**21**) is a simpler choice because the starting materials triallylamine and allyl chloride are readily available. If **20** and **21** were used, the resulting ammonium salt would feature four carbon chains and would result in a lower gravimetric hydrogen storage density. However, the lower steric hindrance and greater flexibility of the salt would increase the chances of successfully appending the carbazole units.

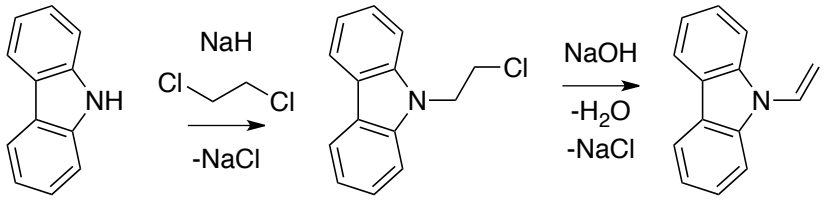

Scheme 2.30. Synthesis of N-vinylcarbazole via S_N2 substitution of 1,2-dichloroethane with sodium carbazolide followed by elimination of chloride under basic conditions

The catalyst chosen was related to the second generation Grubbs' catalyst. Tricyclohexylphosphine[1,3-bis(2,4,6-trimethylphenyl)-4,5-dihydroimidazol-2-ylidene] [(phenylthio)methylene]ruthenium(II) dichloride (**Scheme 2.31**) is stable in air and can be used in aqueous media. It is reported to be highly selective in ring opening and cross metathesis. Although **21** is soluble in water, **20** is not. Isopropanol was used as a compromise as both materials (and the catalyst) are soluble and the solvent is conveniently volatile. However, the metathesis reaction failed to generate any of the desired products. Though the initial reactions in the mixture probably consisted of ring-closing in **21** (**Scheme 2.32**), ring-opening in the presence of **20** with the evolution of ethylene should be favourable. Because the reaction is driven by thermodynamics, the

product mixture should have eliminated all possible ethylene when it is complete (an irreversible process that is entropically favoured). However, the thermodynamically favoured product is not necessarily the desired product and self-metathesis (**Scheme 2.33**) is a competing reaction.

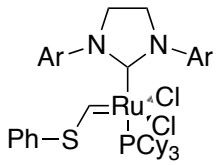

Scheme 2.31. Tricyclohexylphosphine[1,3-bis(2,4,6-trimethylphenyl)-4,5-dihydroimidazol-2-ylidene][(phenylthio)methylene]ruthenium(II) dichloride

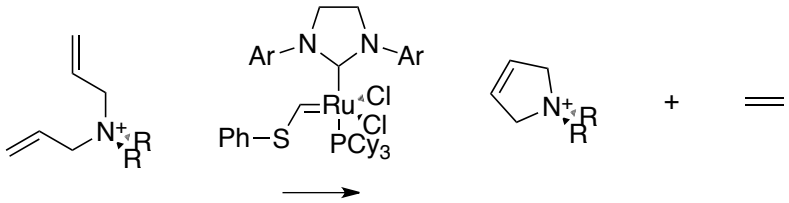

Scheme 2.32. Ring closing metathesis of tetraallylammonium chloride (**21**)

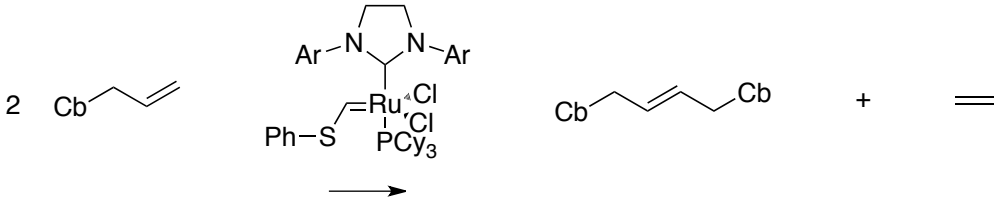

Scheme 2.33. Self metathesis of N-allylcarbazole (**20**)

2.5.2 Imidazolium Ionic Liquid

Earlier research was published by Dupont's group[173] on ionic liquids where the cation was hydrogen storing and the anion was inert. These ionic liquids were based on an imidazolium ion with appended phenyl groups. The phenyl groups were reported to undergo reversible hydrogenation without degradation of the imidazolium ring (**Scheme 2.34**). The hydrogen storage capacity of the reported materials was low because of the use of inert counterions. Cations of this type may have acceptable hydrogen storage capacities when paired with hydrogen storing anions. However, a major fault with these ionic liquids is the very long hydrogenation times required (up to 104 h when using 1 mol % Pd/C catalyst). The long reaction time is likely related to the low reactivity of ordinary benzene rings.

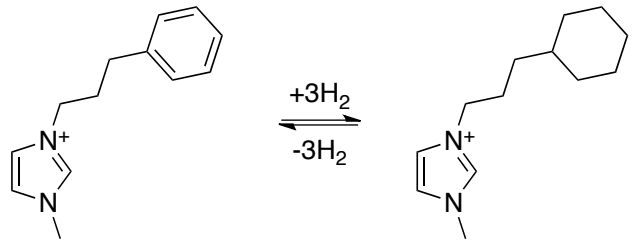

Scheme 2.34. Reversible hydrogenation of an aromatic imidazolium salt

The reported imidazolium ionic liquids were thermally stable at the reaction temperatures used, and the reactions were reported to be selective. This is unusual

considering the reactivity of imidazolium salts with reducing agents (for instance, sodium borohydride) which I observed to induce decomposition of the ionic liquid. However, this reactivity was not observed when using high pressures of hydrogen and palladium catalysts to reduce phenyl rings. Overall the imidazolium ionic liquids proposed by Dupont's group[173] appear to be functional hydrogen storing molecules, the only drawbacks being the low hydrogen storing density, which can be alleviated through the use of a hydrogen storing anion, and low reactivity, which can be alleviated through the use of activated heterocycles. Our strategy to increase the reactivity was to substitute the less reactive phenyl groups with the carbazole heterocycle previously described by Pez[174] and Crabtree[148, 152] as being an excellent hydrogen storing heterocycle (**Scheme 2.35**).

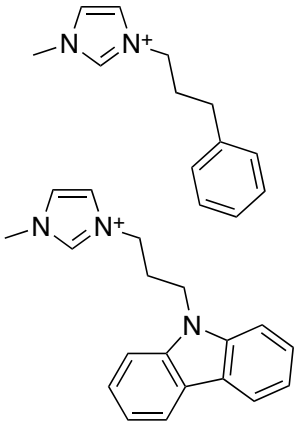

Scheme 2.35. Phenyl and carbazole containing imidazolium ions

2.5.2.1 Synthetic Strategy

The strategy for forming the carbazole-containing ionic liquid consisted of forming the halide salt and subsequently exchanging anions for the bistriflimide ion to improve the physical properties of the ionic liquid (low melting point, etc.) and more importantly prevent coordination of the halide anion to the catalyst surface, which would poison the catalyst and prevent any reaction. The imidazolium halide could be produced from the commercially available N-methylimidazole and haloalkylcarbazole, which would need to be prepared. Although a preparation of 9-(3'-chloropropyl)carbazole (**22**) exists in the literature, wherein carbazole is deprotonated with sodium hydride in dimethylformamide solution followed by quenching with 1-bromo-3-chloropropane, it is far from ideal. The use of the high boiling solvent requires a long work up procedure and sodium hydride and dimethylformamide mixtures can potentially explode with the formation of carbon monoxide and dimethylamine, even at ambient temperature.[192] The explosive decomposition can usually be prevented on lab scale reactions through the use of an ice water bath, though slow heat transfer from large reactions makes this hazardous, and low temperature greatly reduces the reaction rate.

An alternative method from the patent literature[193] involves deprotonating carbazole in tetrahydrofuran using potassium tert-butoxide, a strong, soluble, non-nucleophilic base; followed by quenching the resulting anion with 1-bromo-3-chloropropane (**Scheme 2.36**). This reaction mixture can safely be heated without worrying about explosive decomposition, and the work up procedure is greatly

simplified. In contrast to the high reported yields, the reaction in the laboratory consistently yielded 65% of the desired 9-(3'-chloropropyl)carbazole (**22**), with the remainder being ordinary carbazole. This is likely due to some elimination of the 1-bromo-3-chloropropane by potassium carbazolide to yield allyl chloride, carbazole and potassium bromide. The product can be separated from the starting material using column chromatography (hexanes on silica gel), but the low solubility of the product in hexanes requires the use of large amounts of solvent. However, the difference in retention factors between the starting material and product is sufficiently large that rinsing the mixture of products through a short silica plug with hexanes is satisfactory for the isolation of the desired product.

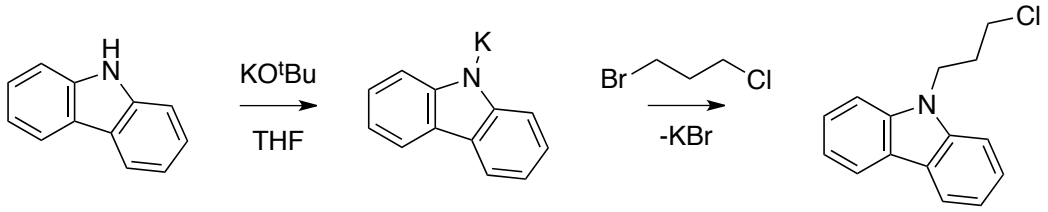

Scheme 2.36. Chloroalkylation of carbazole with 1-bromo-3-chloropropane under basic conditions

N-methylimidazole and **22** both have sufficiently high boiling points that they can be mixed and heated without the use of a reflux condenser; however, the standard procedure for preparing ionic liquids was to mix equimolar amounts of the two liquids with a magnetic stir bar in a sealed glass pressure tube and heating to 150 ºC for 30 min

(**Scheme 2.37**). The resulting 1-(9'-carbazolyl)propyl-3-methylimidazolium chloride was a viscous oil. The oil was mixed with a very slight excess of lithium bistriflimide in water, resulting in a milky suspension of ionic liquid in water. The ionic liquid failed to separate on its own, so dichloromethane was used to extract and isolate the final product, 1-(9'-carbazolyl)propyl-3-methylimidazolium bistriflimide (**23**), which was obtained as an oil after drying under high vacuum.

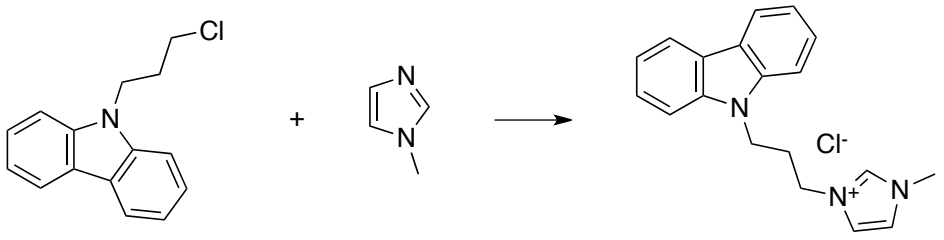

Scheme 2.37. Alkylation of N-methylimidazole with 3-chloropropylcarbazole

2.5.2.2 Hydrogenation

Dupont's group[173] hydrogenated their phenyl-containing ionic liquid under solvent free conditions using 1 mol% Pd/C catalyst and 50 bar of hydrogen at 70 ºC with vigorous stirring. Although the reaction took 104 h to complete, the isolated yield of saturated product was nearly quantitative (97%). The concern with this reaction is the long time required for full conversion. The carbazole heterocycle is far more activated to hydrogenation than phenyl groups, so a reaction occurring under the same conditions should reach full conversion in a shorter time. An aliquot of **23** was reacted under

conditions identical to the Dupont procedure also using solvent free conditions, however the reaction was stopped after 24 h, which should have been long enough to reach completion, or at least a measurable conversion. However, only the starting material was isolated after working up the reaction with no evidence of additional aliphatic signals in the ^{1}H NMR spectrum. Although the Dupont ionic liquid required 104 h to react to full conversion it would almost certainly have achieved some measurable conversion over the course of 24 h (barring some unusually long induction period).

The hydrogenation was repeated using another aliquot **23**, however, in order to reduce the viscosity of the fluid and improve mass transfer throughout the catalytic cycle it was diluted with an equal volume of solvent. The solvent used was dichloromethane because **23** was poorly soluble in alcohols and most other solvents. Other than the addition of solvent the reaction was repeated under the same conditions as used previously. The result again was a total lack of conversion of the carbazole ionic liquid.

2.5.2.3 Discussion

The difference in results obtained between **23** and the phenyl ionic liquid reported in the literature are unusual considering that the more active heterocycle is the one that is unreactive. This is not likely a thermodynamic problem as the carbazole heterocycle has already been demonstrated to undergo reversible hydrogenation, therefore the issue is likely a kinetic one. The only structural difference between the Dupont ionic liquid and the one under investigation is the hydrogen-storing aromatic ring. Both ionic liquids

feature the same methylimidazolium cationic center, the same anion, and the same tether length between the imidazolium ring and the hydrogen-storing moiety (propylene).

The differences are the electronic and steric properties of carbazole when compared to benzene. Although there was the potential for contamination of the ionic liquid with chloride ions the ion exchange using lithium bistriflimide is known to be very effective. In addition, previous hydrogenations carried out with N-alkylpyridinium halide ionic liquids failed to show a total loss of activity of the palladium catalyst due to poisoning of the catalyst surface. Carbazole is more electron-rich than benzene and can therefore donate more electron density to the catalyst surface during binding. The carbazole moiety also forms a very bulky tertiary amine after hydrogenation which may be able to poison the surface; but N-ethylcarbazole yields a similar amine and palladium catalysts are known to hydrogenate these molecules efficiently without being poisoned. The carbazole in **23** is tethered to an electron-poor imidazolium ring. It may be possible that while in the bulk solution, the ionic liquid folds in such a way as to increase the π-stacking opportunities in an intra- or intermolecular interaction. If the imidazolium ion binds to the catalyst surface, the carbazole rings may not be able to orient themselves on the catalyst surface, either because they are sterically large, or they are otherwise interacting with the imidazolium ions. Evidence for this interaction could come from an X-ray crystal structure of the imidazolium salt, though single crystals of **23** have never been grown (nor has it ever solidified).

Chapter 3

Thermally Regenerative Fuel Cells

In a vehicle, energy is stored in petroleum, which is consumed in an internal combustion engine to release its chemical potential energy and convert it into mechanical energy that moves the vehicle forward. However, heat engines like the internal combustion engine have very low efficiencies and much of the chemical potential energy is lost as waste heat to the surroundings. Of the heat lost to the surroundings, about half is lost through the engine block and half is lost through the exhaust gas. A method of reclaiming a portion of this waste heat would be beneficial because the fuel economy of the vehicle would increase and the cost of transportation would decrease.

Vehicles not only use mechanical energy to get around but also contain auxiliary components that require energy in the form of electricity. Electrical energy in a moving vehicle is much more expensive than in a stationary application because the electricity cannot be obtained from electrical lines. Electricity in a vehicle is stored in a battery or generated *in situ*. An alternator is used to generate electricity for the auxiliary components after the engine is started. It draws power from the motion of the internal combustion engine to generate electricity and is only 50–62% efficient.[194] Instead of drawing on the mechanical energy of the engine to generate electricity, a method of

harnessing the waste heat lost by the engine would generate electricity without reducing mileage.

A thermally regenerative fuel cell (TRFC) is a device that can be used to convert heat into electricity.[171] It consists, in part, of a fuel cell, that like a normal fuel cell is an electrochemical energy converter which transforms the chemical potential energy of a fuel (in the proposed system, hydrogen) with an oxidant (typically oxygen, but in the proposed system an unsaturated organic molecule) into electrical energy. In a fuel cell, the fuel and oxidant are supplied to the fuel cell externally and not stored internally like in an electrochemical cell. Therefore, a fuel cell will operate as long as it receives a continuous supply of fuel.

A thermally regenerative fuel cell operates on the principle wherein heat energy is absorbed to perform a chemical reaction and is stored in high energy chemical bonds. The reverse reaction is then carried out within the fuel cell in such a way as the chemical energy is released as electrical energy instead of as heat (**Figure 1.6**, see **Section 1.2.2.4**). Finding a suitable reversible reaction and the ideal conditions required for optimal operation to most efficiently transform heat into electricity is the primary goal for this research whereas specifics of the engineering of the system may be considered in the future. The objective is to find a reaction that absorbs heat rapidly through highly selective reactions.

The thermally regenerative fuel cell would be operated in a continuous closed loop so the parameters that make a good hydrogen storage system are not the same as the parameters that make a good thermally regenerative fuel cell. For instance, the

gravimetric capacity of the fluid is not important because the hydrogen evolved is continuously recycled; however the thermodynamics and kinetics of the reactions occurring must transfer a reasonable amount of power to the fuel cell to be worthwhile.

In order for the thermally regenerative fuel cell system to be commercially viable, and therefore actually used in the real world, it must meet the needs of the end users of the technology and deliver benefits that are worth the additional cost compared to a conventional cooling system. The thermally regenerative fuel cell system consists of four main components: the fuel cell, housing, catalysts, and working fluid. The fuel cell and housing must be constructed in such a way as to last the life of the vehicle. Ideally the catalyst should also last the life of the vehicle, however it is possible to install the catalysts in a cartridge-based manner where they can be replaced and recycled after many years of service. The working fluid would be expected to be replaced more frequently but should not require replacement so often as to be prohibitively expensive or tedious. Replacing the working fluid no more than once a month should be an acceptable target.

The scope of this research has been to determine ideal catalyst and working fluid pairs that would be appropriate for use in a thermally regenerative fuel cell system. These components cannot be considered separately because the characteristics of the reactions that would occur in the system are dependent on the precise interaction between the working fluid and the catalyst. The choice of working fluid will determine the thermodynamics, physical properties, phase behaviour, recurring costs, and will on its own determine part of the cycle life of the system. The catalyst-fluid pair will determine the kinetics, capital expense, and the bulk of the cycle life of the system.

3.1 Apparatus

The TRFC proposed herein consists of two different reactors, one where heat is absorbed at high temperature and the other where it is released as electricity at low temperature (**Figure 1.6**). In the high temperature reactor, which is heated by the engine block and replaces the standard cooling system, a flow reactor containing a heterogeneous catalyst and a saturated fluid (XH_2) capable of releasing hydrogen absorbs heat and releases hydrogen and an unsaturated fluid (X). In the low temperature reactor, which consists of a fuel cell, hydrogen is passed over the anode and the unsaturated fluid is passed over the cathode yielding electricity and the saturated fluid which is pumped to the high temperature reactor to complete the cycle. Neither of the reactions described is likely to proceed to completion and therefore the fluid entering and exiting both reactors is likely to contain a mixture of saturated and unsaturated fluid. Diluents and other components may also compose part of the fluid at any point in the system.

The overall structure of a thermally regenerative fuel cell consists of two main parts: the dehydrogenation reactor that sits in contact with the engine block (and would replace the radiator system), and the fuel cell. The system would be operated in a continuous flow manner with the saturated fluid (XH_2) entering the dehydrogenation reactor and then hydrogen and the unsaturated fluid (X) exiting the dehydrogenation chamber and being pumped to the anode and cathode of a PEM fuel cell where they recombine and are returned to the dehydrogenation chamber.

The dehydrogenation chamber serves the same function as the radiator system in a conventional vehicle. It absorbs the waste heat from the engine and discharges it into the atmosphere. However, the dehydrogenation chamber also converts some of this waste heat into chemical potential energy by carrying out a dehydrogenation reaction over a catalyst. The efficiency of conversion of waste heat into chemical potential energy is a function of the heat capacity of the working fluid, enthalpy of dehydrogenation, the amount of catalyst and the flow rate. The dehydrogenation chamber would replace the radiator system and would not take any additional room compared to a conventional vehicle.

The fuel cell would be a new component in the vehicle and would require additional space under the hood. Although it could in theory replace the alternator in its ability to recharge the vehicle's battery, keeping the alternator in place and allowing it to be switched on in the event of a TRFC malfunction alleviates the risk of vehicle failure. If this were to occur the vehicle could continue to operate as usual but would not benefit from the increased fuel efficiency of the thermally regenerative fuel cell system. The fuel cell should be of the PEM type and would consist of a stack large enough to give the required voltage.

The rest of the apparatus would consist of tubing connecting the fuel cell to the dehydrogenation chamber, a phase separator after the dehydrogenation chamber and a pump to circulate the working fluid. Heat exchangers may be used to increase the efficiency of the use of the waste heat. After its useful lifetime the working fluid could be combusted to recover its energy content.

3.2 Thermodynamics

The thermodynamics of the system are determined solely by the working fluid chosen. The free energy of hydrogenation in the fuel cell will determine the electrical potential (voltage) of the fuel cell. The free energy measured in a batch reaction in the lab under constant pressure conditions (open system) is the Gibbs free energy of hydrogenation (ΔG). However, the installed thermally regenerative fuel cell system will be a flow reactor in an open system operating at one atmosphere of pressure (obtained through the use of a pressure relief valve).

The driving force for converting vehicle waste heat into electricity is the difference in temperature between the dehydrogenation chamber and the fuel cell. The hydrogenation of the working fluid is reversible, but the equilibrium constants at the temperature of the dehydrogenation chamber (K_H) and the fuel cell (K_L) must be different. In the dehydrogenation chamber at high temperature the equilibrium constant should favour the formation of unsaturated fluid and hydrogen; in the fuel cell at lower temperature the formation of the saturated fluid should be favoured. The law of mass action for the dehydrogenation of a saturated fluid XH_2 to the unsaturated fluid X and hydrogen is[159]

$$K = \frac{[X]P_{H_2}}{[XH_2]} \tag{22}$$

where

$$K_L > K_H \tag{23}$$

From the van't Hoff equation[159]

$$\ln\left(\frac{K_H}{K_L}\right) = \frac{\Delta H^\circ}{R}\left(\frac{1}{T_L} - \frac{1}{T_H}\right) \tag{24}$$

The ΔH^o of the dehydrogenation reaction must be positive; therefore the dehydrogenation must be endothermic. This is what would be expected based on Le Châtelier's principle.[159]

The working fluid would enter the dehydrogenation chamber at some composition, Q_L, where Q_L is the reaction quotient and if the hydrogenation at the fuel cell approached equilibrium, would be similar to the equilibrium constant at the temperature of the fuel cell K_L. The fluid undergoes dehydrogenation because it is trying to approach a new equilibrium constant K_H and exits the dehydrogenation chamber at Q_H. The fluid's composition defined by the reaction quotient, Q, will always fall between K_L and K_H.

In the fuel cell, the fluid enters with a composition Q_H that is close to K_H. Because Q_H is not equal to K_L, the equilibrium constant at the fuel cell, the fuel cell is able to generate electric potential. This is defined by the Nernst equation[193]

$$E_{cell} = E^{\circ}_{cell} - \frac{RT_L}{nF} \ln Q_H \tag{25}$$

Where E_{cell} is the electric potential difference across the fuel cell, E^{o}_{cell} is the standard cell potential at the temperature T_L, n is the number of electrons transferred and F is the Faraday constant. The standard cell potential is a function of the equilibrium constant and can be easily determined. There is no electric potential difference when Q is equal to K_L. Therefore[159]

$$\ln K_L = \frac{nFE^{\circ}_{cell}}{RT_L} \tag{26}$$

So the electric potential difference across the cell is increased by increasing the difference between Q_H and K_L. The greatest difference comes when Q_H is equal to K_H because Q_H cannot pass this value. Therefore to maximize the potential of the fuel cell the fluid leaving the dehydrogenation chamber should have a composition close to the equilibrium composition K_H, and K_H and K_L should be as different as possible. To increase the difference in value between K_H and K_L, the enthalpy of dehydrogenation

should be maximized. This, however, is not always the best course of action as will be discussed when concerning kinetics.

There is more going on when running a thermally regenerative fuel cell than just the transfer of energy between the hot source and the fuel cell. The working fluid is also changing temperature between these two points. The thermally regenerative fuel cell would be expected to run at a constant pressure (though the system is more or less closed there would be a pressure release valve to maintain atmospheric pressure inside). So the energy required to heat the working fluid from the low temperature of the fuel cell to the high temperature of the dehydrogenation chamber is[159]

$$q = \int_{T_L}^{T_H} c_p(T)\,dT \tag{27}$$

This is potentially a significant amount of energy, though it is minimized when c_p is small. This heat would be wasted if it were merely disposed of to the atmosphere on the way to the fuel cell, which would result in a dramatic drop of the efficiency of heat recovery. One way to diminish this is to use a counter current heat exchanger. The return stream from the fuel cell can cool the hot fluid from the dehydrogenation chamber and in doing so it would become preheated before entering the hot source. The system would not be isolated from the environment and heat losses through conduction and radiation from the apparatus would occur, but the investment in a heat exchanger would reduce these losses considerably. It is not essential to completely eliminate these losses as cooling the engine block is one of the important functions of the TRFC; however, using a heat

exchanger would allow for more of the waste heat to be recovered as electricity rather than being vented to the environment.

3.3 Kinetics

The kinetics of the dehydrogenation and hydrogenation reactions will depend on the nature of the catalyst at either site, the composition of the fluid entering both sites and the temperature at each site. The reaction rate constant is described by the Eyring equation[195, 196]

$$k = \frac{k_b T}{h} e^{\frac{-\Delta G^{\ddagger}}{RT}} \tag{28}$$

and is related to the temperature and the transition state free energy of the reaction. However, because the reaction is occurring on a heterogeneous catalyst, the rate is also determined by the surface area of the catalyst, the proportion and nature of the sites available, the relative rates and affinities for binding of all the components of the working fluid as well as hydrogen and the proportion of empty sites as is generally described by the Langmuir adsorption isotherm.[159] The reaction kinetics in the fuel cell will determine the electric current in the cell.

It may appear that the best fluids are those that have the largest enthalpies of reaction. Certainly these compounds would have the largest difference in equilibrium

constant between the two temperature states[159] and as a result would generate a larger potential difference.[197] This would be beneficial but electric potential is not the only consideration required. Indeed the goal is the transmission of power from heat to electricity. It does not matter if a great potential can be generated if it is transferred very slowly.

3.4 Current and Voltage

The rate of transfer of energy, or the power of a fuel cell, is determined by both the electric potential (voltage) and electric current (amperage). This can be related to the chemical potential of the cell, μ, and the rate of electron transfer $\partial e/\partial t$. The chemical potential of the cell is a thermodynamic quantity determined by the nature of the working fluid and the operating conditions of the cell.[159] The rate of electron transfer is a kinetic property and determined by the nature of the fuel cell catalyst and membrane and other operating characteristics. It is difficult to predict but can be measured directly using an ammeter and is limited by the rate of dehydrogenation over the engine block and the rate of hydrogenation at the fuel cell. The rate of dehydrogenation is a quantity that can be measured fairly easily and determines the maximum value for the current through an attached fuel cell or fuel cell stack.

In an actual automotive application a fuel cell stack will be used instead of a single fuel cell. The reason for doing so is to increase the voltage obtained from the thermally regenerative fuel cell system. If the individual cells are assembled in a series

circuit the voltage of the fuel cell stack will be the sum of the individual cell voltages.[197] In this way a fuel cell stack which would generate a large current with a small electric potential difference can exchange its excess electric current to improve the cell voltage. A less likely scenario would be where a single cell could generate a very large potential difference but only yield a small current. In this case a fuel cell stack where the individual cells are connected in a parallel circuit can exchange some of the excess potential difference for a larger current.[197] Adjusting the current and voltage output of the TRFC is important as the auxiliary equipment being powered by the device would likely have narrow operating thresholds for current and voltage.

Regardless of the arrangement of individual cells in a stack, the total energy transferred from the engine block to the fuel cell per unit time, the power, is dependent on the kinetics and thermodynamics of the dehydrogenation reactor and on the efficiency of the fuel cell. In the fuel cell, the output power is defined as

$$P = IV \tag{29}$$

Whereas in the dehydrogenation reactor the input of power is defined as

$$P = \Delta G \frac{dH_2}{dt} \tag{30}$$

Because the fuel cell, and the system overall, is not perfectly efficient, the power output in the fuel cell is somewhat less than this depending on the efficiency of the cell. However, no arrangement of the fuel cell stack will change the total power output of the fuel cell. It can only change many lower energy electrons for few high energy electrons or vice versa.

3.5 Phase Behaviour

The physical properties and phase behaviour of the system are also determined by the working fluid. The working fluid would be expected to be composed of at least two compounds, the saturated and unsaturated forms of the fluid undergoing hydrogenation and dehydrogenation. It may also contain intermediate compounds if the hydrogenation reaction occurs over more than one step and potential decomposition products and diluents. The fluid composition will determine several important physical properties of the system. In particular, the melting point of the working fluid will determine if the fluid is solid (and therefore not pumpable) at a given temperature. Viscosity will also determine how difficult the material is to pump even if it is a fluid. Density of the fluid will control how many molecules of the fluid are in the dehydrogenation reactor or fuel cell in a given time and will affect the rates of both reactions. Certain mixtures may result in interesting phase behaviour where the components of the material may form more than one phase through separation. This may be a useful way of overcoming the expected thermodynamics and kinetics by taking advantage of Le Châtelier's principle.[159]

The phase behaviour of the working fluid used in the thermally regenerative fuel cell system will affect the detailed structure of the apparatus used, and will also have an impact on the thermodynamics and kinetics (and therefore the voltage and current obtained) from the hydrogenation reaction in the fuel cell.

The physical state of the working fluids in the system is important in determining both the structure of the apparatus as well as the thermodynamics and kinetics of the hydrogenation and dehydrogenation reactions. Although the hydrogen released by the dehydrogenation reaction and absorbed by the hydrogenation reaction may be expected to be the major component of gas phase, it is not necessarily the case that the saturated fluid, unsaturated fluid, or any mixture composed of the two is only a liquid. This will depend on the composition of the working fluid and the operating temperatures of both the dehydrogenation reactor and the fuel cell stack.

Herein, the fully unsaturated fluid (one where no further hydrogen can be removed) will be denoted X, whereas the fully saturated fluid will be referred to as XH_2, (although XH_2 refers to the fully saturated fluid, it would realistically contain a small amount of the unsaturated material because complete hydrogenation may not occur for thermodynamic or kinetic reasons). Naturally some potential working fluids are able to carry more than one equivalent of hydrogen in their structure. However, in most cases either the fully hydrogenated or fully dehydrogenated state is preferred (as happens in aromatization or dearomatization reactions where three equivalents of hydrogen is gained or lost rapidly with no significantly detectable intermediates). Instances where stepwise addition or removal of hydrogen take place will be discussed individually but the effects

on the phase behaviour of such systems will be similar to those discussed here. T_L refers to the lower temperature region in the fuel cell stack, T_H refers to the high temperature region in the dehydrogenation reactor.

Working fluids where X and XH_2 both have boiling points above T_H require the simplest apparatus to be used in the thermally regenerative fuel cell. Because both X and XH_2 are liquids, neither can be expected to be separated from the other, however both are easily isolated from the hydrogen gas evolving in the dehydrogenation reactor. This is accomplished by introducing a liquid-gas separator in the line exiting the dehydrogenation reactor before the fuel cell stack where the liquid stream is directed toward the cathode end of the fuel cell stack and the gas stream is directed toward the anode. A method for increasing the surface area of the liquid stream would increase the release of dissolved hydrogen into the gas phase and some mechanism to prevent entrained working fluid from entering the anode of the fuel cell stack would be required. This system is perfectly acceptable but it suffers from the disadvantage that the output stream of the dehydrogenation reactor is limited to that dictated by thermodynamics, the fluid exiting the reactor can only be enriched in X as far as the K_H value will allow. This limits the cell voltage (because the K_H composition is closer to that of K_L than pure X) as well as the current (pure X has a higher rate of hydrogenation than an X/XH_2 mixture). Similar arguments can be made regarding the rate of dehydrogenation in the dehydrogenation reactor whose input stream is limited to the composition dictated by K_L.

When the working fluid consists of XH_2 with a boiling point well above T_H and X with a boiling point between T_L and T_H, there exists two different situations that require

two different apparatus. If the difference in boiling point is large then a simple distillation is all that is required to effectively separate X and XH_2. After the dehydrogenation reactor, a simple liquid-gas separator would remove both X and hydrogen from XH_2 (which would be returned to the dehydrogenation reactor to continue to dehydrogenate). X must then be condensed and separated from the hydrogen so they can be sent to the cathode and anode respectively. In the situation where X and XH_2 have similar boiling points, a fractional distillation would be required to separate the two. The excess waste heat from the heat exchanger can be used to facilitate the distillation and the return stream from the fuel cell stack could be used to cool the condenser (which also preheats the fluid entering the dehydrogenation reactor). In both of these cases the XH_2 is left in the dehydrogenation reactor and if the fuel cell stack is physically above the dehydrogenation reactor no pumping would be required as the freshly hydrogenated XH_2 formed in the fuel cell could be returned to the reactor by gravity. This reactive distillation presents thermodynamic and kinetic advantages over the non-distillative system. X is constantly removed from the dehydrogenator and therefore the concentration of XH_2 will remain high and relatively constant, this keeps the rate of dehydrogenation close to the initial rate observed when there is XH_2 alone. Additionally the rate of hydrogenation reaction (and current) in the fuel cell stack will be higher since it should also be close to the initial rate observed when pure X and hydrogen are fed into the fuel cell. The cell voltage should also be higher when pure X is fed into the fuel cell compared to the composition dictated by K_H.

In the situation where XH_2 has a boiling point higher than T_H but X has a boiling point below T_L the separation of X and XH_2 is easy but the separation of X and hydrogen is not. This would require a membrane that allowed for selective transportation of either X or hydrogen from the gas stream. Membranes that selectively allow for the transfer of hydrogen do exist but this technology is in its infancy.[198-201] Moreover, such membranes are usually delicate thin films of palladium metal. Such thin films are not ideal for robust application and palladium even as a thin film is likely to be an efficient catalyst for the hydrogenation of X to XH_2, defeating the purpose of the system. The heat generated during this reaction may be enough to destroy the delicate membrane. With the current technology, the formation of very low boiling X cannot be tolerated as such systems preclude the separation of the oxidant and reductant required for the thermally regenerative fuel cell.

Systems where X has a boiling point above T_H but XH_2 has a boiling point below T_H present a unique challenge. Separation of X and XH_2 is similar to that encountered in the opposite situation, however in this case the material requiring dehydrogenation is the one that does not want to remain in the reactor. The dehydrogenation reactor must therefore be loaded from the top, the XH_2 can reflux in the reactor and exit from the bottom as X whereas the hydrogen can pass through the condensing area and pass to the anode of the fuel cell. The same thermodynamic and kinetic benefits applied to any of the systems featuring separation of X and XH_2 would be observed here.

In systems where X and XH_2 both have boiling points below T_H the dehydrogenation will occur in the gas phase. If both components condense above T_L then

separation of the two components after the reactor will be impossible, the rate of the gas phase reaction will also need to be very much greater than the rate of condensation for significant dehydrogenation to take place. If either component does not condense above T_L then the same difficultly separating the organic components from the hydrogen stream will exist.

Ideally both X and XH_2 will have melting points well below -40 ºC. This would allow the thermally regenerative fuel cell to operate when the engine block reaches the appropriate temperature even in areas with very cold winters. However, this is not essential as the thermally regenerative fuel cell does not need to function until the engine is warm to operate. So long as the material is fluid at T_L the system should work as it will reach a temperature above this point rapidly due to the heat provided by the engine block. Additionally, even if the pure components melt above T_L their mixtures should have depressed melting points and, so long as all the compositions met within the system are liquid, the material will still be able to flow.

The phase behaviour of a chosen working fluid can dictate whether or not that compound can be used in the thermally regenerative fuel cell system. Many types of phase behaviour are acceptable and various apparatuses are required to accommodate each type. Some systems also benefit from enrichment caused by phase separation and can exhibit better thermodynamic and kinetic properties than would be seen were this not the case.

3.6 Working Fluids

The nature of the working fluid (and whether it is consists of a single compound or a mixture) will determine the rate of energy transfer from the engine block to the fuel cell. It will also determine the physical properties of the system. The working fluid must be thermally stable and not undergo degradation at an appreciable rate at the highest temperature encountered in the system. It should also be inexpensive and be available commercially in bulk, or be simple to scale to bulk manufacturing. Ideally the toxicity of the fluid should be no higher than that of ethylene glycol currently used as engine coolant (which it would replace). In contrast with materials designed for hydrogen storage, the gravimetric density of hydrogen is unimportant. Hydrogen simply cycles back and forth in a closed loop and there is no net production or consumption of hydrogen (outside unwanted side reactions). Because increasing hydrogen pressure would disfavour dehydrogenation as much as it would favour hydrogenation, there is no benefit to operating the system outside of ambient pressures. Operating at ambient pressure decreases the safety risk to the end user.

Initial experiments to find suitable working fluids were initially performed by an undergraduate summer student, Stephen Murphy, under the guidance of a postdoctoral researcher, Dr. Dominik Wechsler. The initial goal was to find materials that contained functional groups capable of undergoing reversible hydrogenation that were also thermally stable. As a result, several substances, in particular aromatic substances, were subjected to very high temperatures in sealed autoclaves (to simulate longer times spent

at 200 ºC) and were dehydrogenated at high temperature and hydrogenated under high pressure in autoclaves. Neither the results of the hydrogenations nor the dehydrogenations of any of the materials were particularly promising in terms of either conversion or selectivity.

Beginning from this point, I reordered the priorities for what the characteristics of the working fluid should be. The thermal stability of a fluid is unimportant if the material cannot undergo hydrogenation or dehydrogenation. In addition, because the working system would be closed and therefore at a uniform pressure, I eliminated aromatic rings (for the most part) as functional groups which can undergo hydrogenation at ambient pressure and focussed on materials that only had one reactive chemical bond. Starting from tables of typical bond dissociation energies[202] for core organic elements, I was able to tabulate likely candidates (**Table 3.1)**. These molecules were those where the enthalpy of dehydrogenation was not too high.

Table 3.1. Enthalpy of dehydrogenation calculated via BDEs

Reaction	ΔH_{rxn} (kJ mol^{-1})
$H_3C\text{-}CH_3 \rightarrow H_2C{=}CH_2 + H_2$	+134
$H_3C\text{-}OH \rightarrow H_2C{=}O + H_2$	-3
$H_3C\text{-}NH_2 \rightarrow H_2C{=}NH + H_2$	+55

Bond dissociation energies obtained from reference 202. Reaction enthalpies calculated using Hess' Law.

Typical bond dissociation energies do not take into account the structural characteristics of molecules. For instance, if dehydrogenation results in a conjugated double bond or aromatization it would be expected that that dehydrogenation enthalpy would be lower than expected based on a typical bond dissociation energy alone.

3.7 Selectivity and Cycle Life

No chemical reaction proceeds with perfect selectivity, that is to say that only one product is obtained. This limits the useful life of any compound undergoing reversible reactions as part of a chemical cycle. To maximize the life of the thermally regenerative fuel cell system and minimize the frequency of fluid changes, the reactions occurring in both the high temperature reactor and the fuel cell must be exceptionally selective. Ideally, the cycle life will expand to a period of at least a month before the fluid would have degraded to the point of significant loss of efficiency. A complete cycle of the material requires both a dehydrogenation and hydrogenation step. An acceptable threshold level of decomposition before a fluid change would be required and the number of cycles that can occur before this would occur determines the required selectivity of the reactions. The number of cycles per hour of operation would depend on rate of pumping and the residence time of the fluid on each of the catalyst beds. The amount of degradation that can be tolerated before the fluid must be changed would depend on the required power output of the fuel cell. **Table 3.2** shows the amount of intact material left after a given number of cycles at different selectivities. Assuming the fluid undergoes ten

cycles of hydrogenation and dehydrogenation per hour over a forty hour work week (assuming implementation for long haul transportation) then 3000 cycles would represent almost two months of operation. If a drop to only 70% purity of active fluid would be acceptable after two months then a selectivity of 99.99% or higher would be adequate.

Table 3.2. Remaining working fluid at a given selectivity after a given amount of cycles

Selectivity (%)	Cycles	
	3000	30 000
99.99	74%	5%
99.995	86%	22%
99.999	97%	74%

There is little guidance in the chemical literature regarding reactions with very high selectivities. This is largely due to the lack of interest in accurately measuring selectivity. In an organic synthesis, a reaction with 99% selectivity would be considered very successful and there is no incentive to determine just how much higher the selectivity actually is. There is also the problem of detecting such small quantities of an impurity. A simple ^{1}H NMR spectrum is insufficient to accurately determine quantities less than 1%. The use of analytical equipment with lower detection limits is then required. Typically such high selectivities are usually reported as “>99%”. To the best of our knowledge, there has been no report of a dehydrogenation reaction with a measured selectivity of greater than 99%.

3.8 Catalysis

The choice of catalyst at the engine block and in the fuel cell will affect the rate and selectivity of the reactions at either end of the thermally regenerative fuel cell. It will not affect the thermodynamics of either reaction. It is important to note that neither the dehydrogenation in the high temperature reactor or the hydrogenation in the fuel cell will proceed in the absence of a catalyst. Heterogeneous catalysts would be used because they are generally more stable than homogeneous catalysts and more practically because they are easier to sequester to the high temperature and low temperature reactors and to keep out of intermediate temperature zones in between. The catalyst in the high temperature reactor does not necessarily need to be the same as the catalyst in the fuel cell. Catalyst selection is crucial; not only does the catalyst determine the rate of the hydrogenation and dehydrogenation reactions, but it also determines the bulk of the selectivity of those reactions. Ideally, only those reactive sites on the working fluid that undergo reversible hydrogenation will react and the fluid can cycle between the two forms indefinitely. This is generally not the case. The working fluid may react in a different way to yield unwanted side products which may be either inert (and act as a diluent) or change the selectivity or activity of the catalyst. In particular, at high temperature in the presence of hydrogen, hydrogenolysis reactions may compete with dehydrogenation.

The activity and selectivity of a heterogeneous catalyst will depend on the metal or metals it is composed of, the materials supporting the catalyst and the shape of the catalyst particles including the types and numbers of different active sites. The metal choice will determine the crystal structure and therefore the different available surface morphologies along with the relative size and spacing of individual metal atoms as well as the electron richness of the metal atoms. Materials used to disperse the metal particles to increase the surface area of the catalytic metal are capable of being acid or base catalysts themselves (such as zeolites in hydrocracking of fuels)[203] and also have electronic effects on nearby metal atoms. Small catalyst particles would have higher activities than larger catalyst particles due to increased surface area. Surface features such as terraces, adatoms, edges and kinks will all have different activities and selectivities for particular reactions. For instance, the (111) surface of a metal with a face–centered cubic unit cell, such as palladium or platinum is particularly suited to the hydrogenation of benzene because the triangular arrangement of surface atoms overlaps with the π-orbitals of the aromatic system.[204]

3.9 Reactions

The proposed thermally regenerative fuel cell system is a closed system held under a constant pressure, only varying the temperature in different sections to favour either hydrogenation or dehydrogenation (and catalysts required to perform these reactions are sequestered in different portions of the TRFC). Although high pressures of

hydrogen favour hydrogenation it is not favourable to operate under those conditions because the dehydrogenation would be similarly impeded. Safety and practicality dictate an ambient pressure system. Screening of substrates that may undergo hydrogenation at ambient pressure under hydrogen gas was necessary.

3.9.1 Hydrogenation at Ambient Pressure

Two aromatic substrates, N-methylindole and benzofuran, and an aromatic ketone, propiophenone, were chosen as initial substrates. Both benzofuran and propiophenone were able to selectively hydrogenate an individual double bond and were passed for further scrutiny. The N-methylindole was poorly reactive and the material that was converted did so with poor selectivity for N-methylindoline (**Table 3.3.**)

However, it is unusual that benzofuran was so readily hydrogenated when the indole was not. The product of hydrogenation of N-methylindole would be a tertiary aniline. These compounds are basic and may bind to the catalyst, thereby poisoning it. The product of benzofuran hydrogenation is an ether, which would not bind to the metal surface as strongly because this is only weakly basic. There are likely electronic reasons for the difference in reactivity of these two heterocycles. Though they are both more electron rich than benzene, furan is “less aromatic” than pyrrole[205] and can undergo electrophilic addition in competition with electrophilic substitution.[187]

Table 3.3. Conversions and selectivities for the catalytic hydrogenation of potential hydrogen carriers at ambient pressure

Compound	Product	Conversion (%)	Selectivity (%)
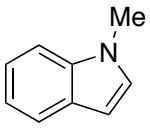	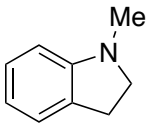	N/D	N/D
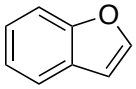	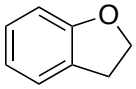	100	≥99
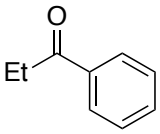	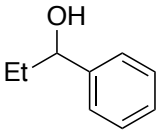	79	≥99

Reactions were performed by mixing an organic substrate with 0.1 mol% equivalent of Pd in the form of palladium on activated carbon, 10 wt%, reduced. The mixtures were flushed with hydrogen gas at a rate of 10 ml/min and were heated with stirring in an oil bath held at 100 ºC for a period of 6 h. The samples were diluted in chloroform-d and filtered through a tissue plug in a Pasteur pipette and analyzed by ^{1}H NMR spectroscopy. The conversion and selectivity of the hydrogenation reaction of N-methylindole were both poor and not quantifiable.

Selective reduction of the aryl ketone to the secondary alcohol without total reduction to the alkane is not necessarily unusual under the fairly mild conditions of temperature and pressure. Catalytic reduction of benzylic alcohols is a well known method of functional group removal.[206] This reaction is routinely used for the deprotection of benzyl protected alcohols or acids, though the usual catalyst in this process is nickel metal.

3.9.2 Dehydrogenation Under Argon

The hydrogenation reactions of the substrates must be reversible at a higher operating temperature. In order to minimize the chance of hydrogenolysis, the reactions

were sparged with argon. Upon heating to 200 ºC in the presence of palladium on carbon, both 2,3-dihydrobenzofuran and 1-phenyl-1-propanol underwent dehydrogenation. 1-Phenyl-1-propanol gave excellent selectivity for propiophenone whereas 2,3-dihydrobenzofuran gave both benzofuran and 2-ethylphenol (**Table 3.4.**)

Table 3.4. Conversions and selectivities for the catalytic dehydrogenation of potential carriers under argon

Compound	Product	Conversion (%)	Selectivity (%)
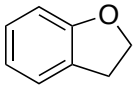	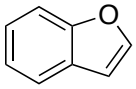	82	59
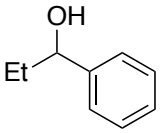	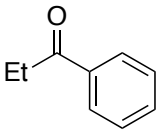	100	≥99

Reactions were performed by mixing an organic substrate with 0.1 mol% equivalent of Pd in the form of palladium on activated carbon, 10 wt%, reduced. The mixtures were flushed with argon gas at a rate of 10 ml/min and were heated with stirring in an oil bath held at 200 ºC for a period of 6 h. The samples were diluted in chloroform-d and filtered through a tissue plug in a Pasteur pipette and analyzed by ^{1}H NMR spectroscopy.

Although some amount of hydrogenolysis may be expected, even while sparging with an inert gas, the amount of hydrogenolysis observed under these conditions is astonishing. The only source of hydrogen in the reaction was from the dehydrogenation of the 2,3-dihydrobenzofuran to form benzofuran. About 65% of the hydrogen released from 2,3-dihydrobenzofuran was able to hydrogenolyze other 2,3-dihydrobenzofuran molecules before being desorbed from the catalyst surface and swept away by the argon. The hydrogenolysis reaction must therefore be very fast, faster than the desorption of

hydrogen from the catalyst surface. If the reaction were performed under an atmosphere of hydrogen instead, total hydrogenolysis to 2-ethylphenol would be anticipated. Although the choice of catalyst can make an enormous difference in the observed selectivity of a reaction, the fact that hydrogenolysis occurs so rapidly when the partial pressure of hydrogen in the system is essentially zero makes it unlikely that a catalyst will be found that can selectively dehydrogenate this material under a hydrogen atmosphere. Although benzofuran undergoes hydrogenation both rapidly and selectively at 100 ºC, it is unsuitable as a working fluid because of the selectivity issue at 200 ºC.

3.9.3 Kinetics of Dehydrogenation of 1-Phenyl-1-Propanol over Pd/C

A kinetics experiment was performed to ascertain both the rate of the reaction, as well as the equilibrium constant of the dehydrogenation reaction. In the real system, the overall reaction rate will be affected by the rate of the reverse (hydrogenation) reaction. Useful kinetic data requires that the reaction is performed under an atmosphere of hydrogen gas, this also allows for the establishment of the equilibrium constant. The observed rate of conversion was very high, even when only using a 0.1 mol% loading of palladium (**Figure 3.1)**. Unfortunately, significant hydrogenolysis was observed. The reaction proceeded with 65% selectivity for dehydrogenation and the remaining 35% for hydrogenolysis to form propylbenzene. Unusually, both the formation of propiophenone and propylbenzene appears to slowly approach an equilibrium value.

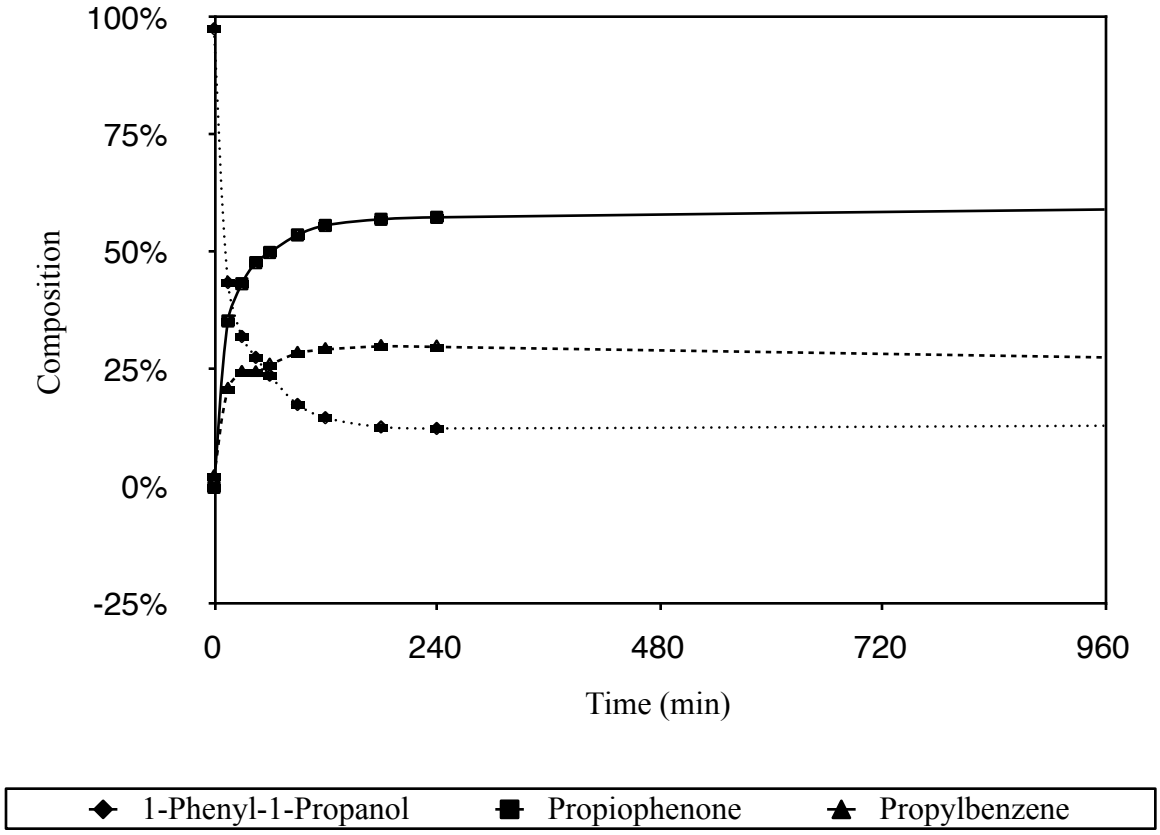

Figure 3.1. Dehydrogenation of 1-phenyl-1-propanol at 200°C over 0.1 mol% Pd/C under hydrogen at ambient pressure

Though the dehydrogenation of 1-phenyl-1-propanol should be reversible the hydrogenolysis should not be, especially under a hydrogen atmosphere. The only source of oxygen atoms in the system would be from the water liberated during the hydrogenolysis. Water is a generally a poor oxidant and should have evaporated rapidly over the course of the reaction (which occurs at 200 ºC). However, propylbenzene is approaching an equilibrium value over the course of the reaction, and the propiophenone concentration does not decrease over time to form more propylbenzene so the formation

of propylbenzene appears to be reversible. Because the only source of oxygen atoms would be from water it would have to be acting as an oxidant. However, this is both theoretically unlikely and mixtures of water and propylbenzene treated under these conditions do not yield either the alcohol or the ketone. A much more plausible explanation for the decrease in the rate of the formation of propylbenzene is the deactivation of the sites on the catalyst surface which promote hydrogenolysis.

3.9.4 Dehydrogenation of 1-Phenyl-1-Propanol under Hydrogen

In an attempt to improve the selectivity of the dehydrogenation of 1-phenyl-1-propanol, the reaction was attempted using different catalyst supports. However, to save time the kinetics of the reaction were not measured. Because palladium metal demonstrated very high activity at low catalyst loading, palladium on different catalyst supports was examined first (**Table 3.5**). Using palladium supported on alumina improved the selectivity of the reaction while slightly decreasing the catalytic activity. Switching to palladium supported on silica improved the selectivity to the point where propylbenzene was not observable in the ^{1}H NMR spectrum of the product mixture. Though the activity of the palladium on silica catalyst was not as high as the activity of the palladium on carbon catalyst, the selectivity was excellent.

Table 3.5. Conversions and selectivities for the catalytic dehydrogenation of 1-phenyl-1-propanol under hydrogen using different heterogeneous palladium catalysts

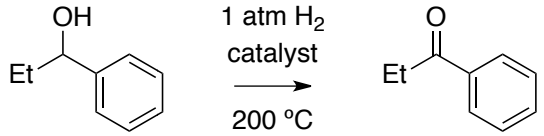

Catalyst	Conversion (%)	Selectivity (%)
Pd/C (10 wt%)	87	66
Pd/Al_2O_3 (5 wt%)	81	85
Pd/SiO_2 (5 wt%)	69	≥99

Reactions were performed by mixing 1-phenyl-1-propanol with 0.1 mol% equivalent of Pd. The mixtures were flushed with hydrogen gas at a rate of 10 ml/min and were heated with stirring in an oil bath held at 200 ºC for a period of 4 h. The samples were diluted in chloroform-d and filtered through a tissue plug in a Pasteur pipette and analyzed by ^{1}H NMR spectroscopy.

3.9.5 Kinetics of Dehydrogenation of 1-Phenyl-1-Propanol over Pd/SiO_2

The kinetics of the dehydrogenation of 1-phenyl-1-propanol over 0.1 mol% palladium on silica catalyst and under an atmosphere of hydrogen were recorded. Only trace amounts of propylbenzene were observed in the product mixture after several hours of being heated to 200 ºC over the catalyst under a hydrogen atmosphere (**Figure 3.2.**) The initial rate of dehydrogenation was high. The composition of the product mixture as determined by the ^{1}H NMR analysis of small aliquots removed from the reaction mixture was first recorded after ten minutes, and the reaction conversion at this point was 22%. A smooth curve drawn through all of the data points in the experiment is nearly linear over the period between the start of the reaction and the acquisition of the first data point so

the initial reaction rate is likely similar to the average reaction rate over this time. The average turnover frequency at the beginning of the reaction is 22 mol of hydrogen per mole of palladium per minute, or more practically 0.414 g of hydrogen per gram of palladium per minute. At standard temperature and pressure, this is equivalent to 4.63 litres of hydrogen per gram of palladium per minute. This is a significant amount of hydrogen for a fuel cell to process. If the fuel cell could react all the hydrogen delivered at this rate with perfect efficiency this would be equivalent to 665 A of current per gram of palladium in the dehydrogenation reactor. Of course, no fuel cell would operate with this high current output, and no fuel cell operates with perfect efficiency either, but this rate of hydrogen evolution easily allows for the use of several individual cells in a stack connected in series if the output voltage of each individual cell is small. This kinetic data was obtained from a batch reaction; a practical working system would be a flow reactor, the kinetics of which would depend on the flow rate and residence time of the working fluid, and on the catalyst loading.

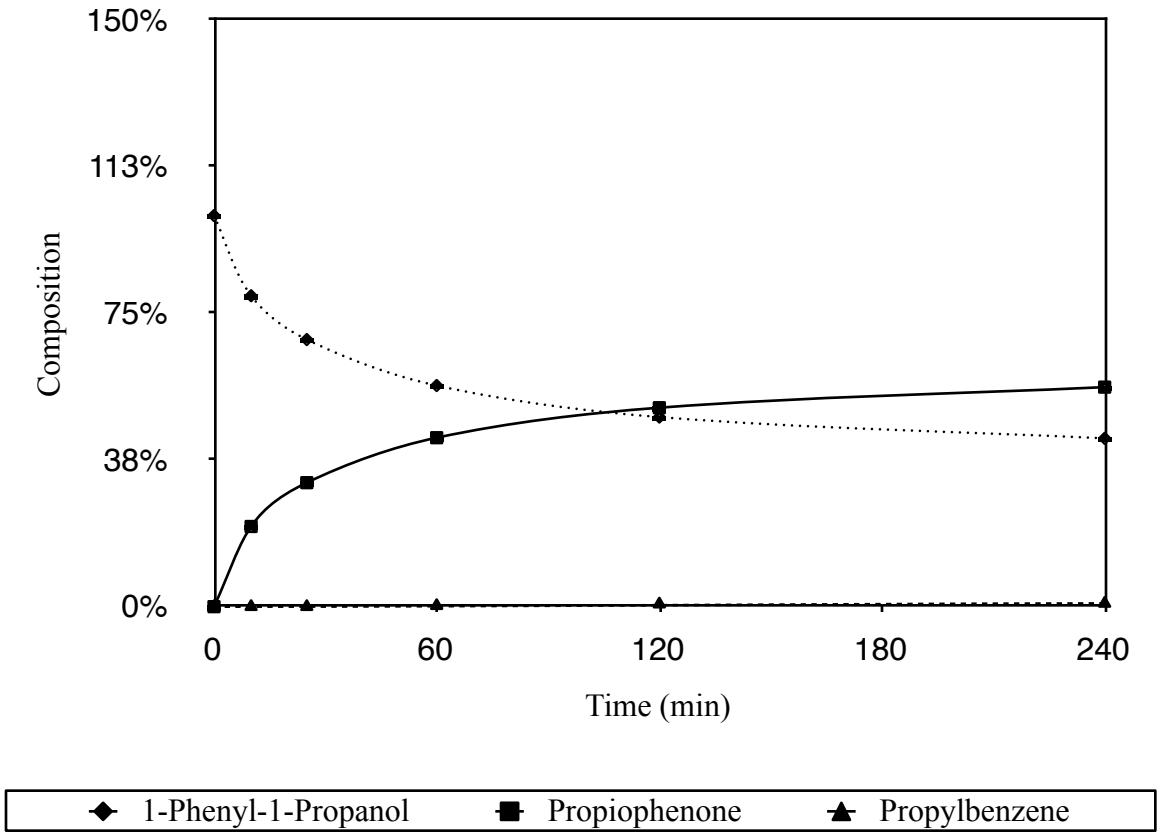

Figure 3.2. Dehydrogenation of 1-phenyl-1-propanol at 200°C over 0.1 mol% Pd/SiO_2 under hydrogen at ambient pressure

3.9.5.1 Kinetics of Equilibrium Reactions

In a reversible reaction that is proceeding to equilibrium the rate of the reaction is dependent both on the concentrations of the reactants and products. For a reversible unimolecular reaction

$$A \rightleftharpoons B \tag{31}$$

the rate law can be written as[159]

$$\frac{dB}{dt} = k_1 C_A - k_{-1} C_B \tag{32}$$

$$\frac{dB}{dt} = k_1 C_A - k_{-1}(C_{A0} - C_A) \tag{33}$$

$$\frac{dB}{dt} = (k_1 + k_{-1}) C_A - k_{-1} C_{A0} \tag{34}$$

Where C_{A0} is the initial concentration of the reactant. From the definition of the equilibrium constant the following

$$k_1 + k_{-1} = k_{-1} \frac{C_{A0}}{C_{Ae}} \tag{35}$$

where C_{Ae} is the concentration of the reactant at equilibrium. This gives the rate law

$$\frac{dB}{dt} = \frac{k_{-1} C_{A0}}{C_{Ae}} (C_{Ae} - C_A) \tag{36}$$

This can be integrated to give the integrated rate law[159]

$$\ln\left(\frac{C_{A0}-C_{Ae}}{C_A-C_{Ae}}\right)=(k_1+k_{-1})t \tag{37}$$

From the integrated rate law and the equilibrium constant both k_1 and k_{-1} can be solved. Using this model the observed rate constants for the dehydrogenation and hydrogenation reactions can be calculated under the conditions the reaction was run under; notably, a constant partial pressure of 1 atm of hydrogen, 0.1 mol% catalyst loading, and 200 ºC. The assumption that the volume and polarity of the solvent (which is composed of the reactants) is also made.

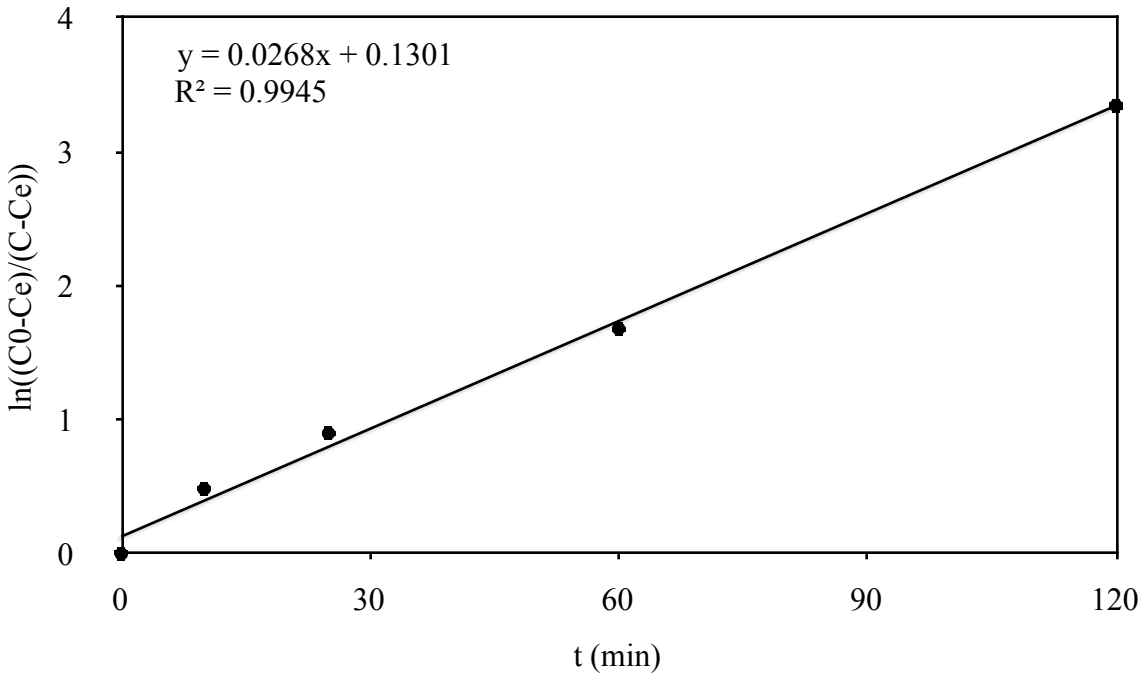

Figure 3.3. Determination of the rate constants of the reversible first order dehydrogenation of 1-phenyl-1-propanol

Linear regression of the kinetic data fits the model of a first order reaction under equilibrium conditions fairly well, deviations may be explained by the likelihood of the changing nature of the solvent. From the linear regression a value for $k_{1obs}+k_{-1obs}$ of 0.0268 min^{-1} was found. Converting to customary units yields $4.47x10^{-4}$ s^{-1}. Because the equilibrium constant is known $K = k_{1obs}/k_{-1obs} = 1.15$ the rate constants can be solved. The observed rate constant for the dehydrogenation is $k_{1obs} = 2.39x10^{-4}$ s^{-1} and the observed rate constant for the hydrogenation is $k_{-1obs} = 2.08x10^{-4}$ s^{-1}.

3.9.6 Kinetics of Dehydrogenation of Benzylic Alcohols over Pd/SiO_2

When candidate fluids were initially considered, 1-phenyl-1-propanol was chosen based on its boiling point, which is well above the proposed temperature of the dehydrogenation reactor. However, the smaller benzylic alcohols are likely also capable of dehydrogenation and may do so even more rapidly than 1-phenyl-1-propanol. 1-Phenyl-1-ethanol and acetophenone have boiling points above the temperature of the proposed dehydrogenation chamber as well, though they are very close. The vapour pressure of these compounds would be much higher than 1-phenyl-1-propanol but this may not be an issue in the actual system if the pressure relief valve is in a cool location in the apparatus where all the organic compounds would have already condensed. Benzyl alcohol has a boiling point above 200 ºC, but its dehydrogenation product, benzaldehyde, boils at 178 ºC. If benzyl alcohol could dehydrogenate selectively, it could be used in a system where the product is distilled from the starting material. This would have both thermodynamic and kinetic advantages.

The kinetics of dehydrogenation of 1-phenyl-1-propanol, 1-phenyl-1-ethanol and benzyl alcohol were compared (**Figure 3.4)**. Though 1-phenyl-1-ethanol dehydrogenates faster than 1-phenyl-1-propanol, this is not apparent at the beginning of the reaction, where they appear to dehydrogenate at the same rate. Benzyl alcohol appears to be almost entirely unreactive under these conditions and only a small amount of benzaldehyde was observed at the end of the reaction.

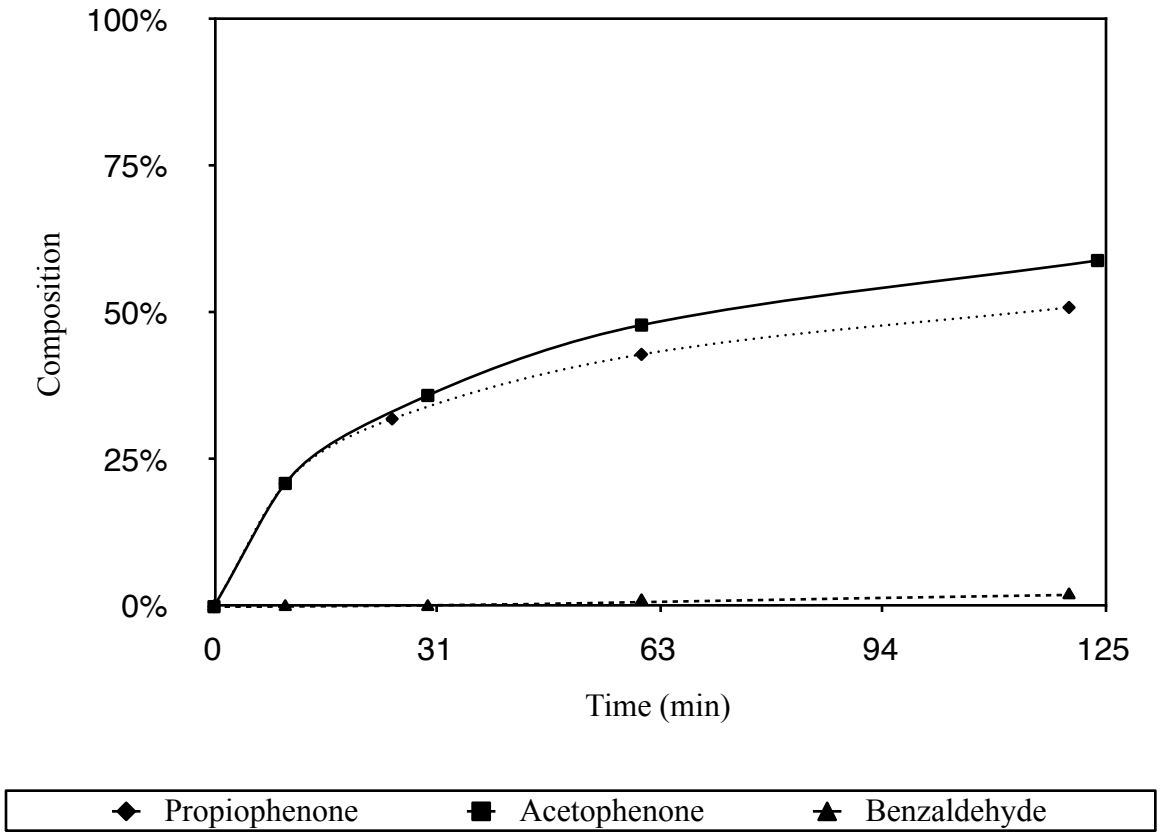

Figure 3.4. Dehydrogenation benzylic alcohols at 200 ºC over 0.1 mol% Pd/SiO_2 under hydrogen at ambient pressure

It is not unusual that the smaller secondary benzylic alcohol (with a methyl group) was dehydrogenated slightly faster than the larger one (with an ethyl group). This can be explained entirely by a steric effect. Electronic effects between methyl and ethyl groups would be small. The smaller methyl group on 1-phenyl-1-ethanol makes it easier for 1-phenyl-1-ethanol to approach the catalyst surface at the right orientation to react. The effect is small because an ethyl group has its terminal methyl group pointed away from the reactive site most of the time, and there is only a small rotational barrier to do so. If

larger branched benzylic alcohols were examined, there would likely be a large decrease of rate observed when looking at the isopropyl compound and a further reduction of rate with the tert-butyl compound. There is no reason to examine either of these compounds because they would be predicted to have a lower rate of reaction with no thermodynamic advantage, and they would be more expensive to produce than the linear compounds.

The case of benzyl alcohol is different than when considering the difference between the secondary alcohols. Benzyl alcohol would be predicted to have a higher rate of reaction than either of the other compounds; a hydrogen atom is very much smaller than even a methyl group. Electronic effects dominate here because a hydrogen atom is electronically different from an alkyl group. In the case of secondary alcohols the product is a ketone; with benzyl alcohol the product is an aldehyde. This reaction is less thermodynamically favourable, and though thermodynamics cannot correlate directly to kinetic observations it is not a stretch to imagine the transition state forming an aldehyde may be less stable than one forming a ketone where the alkyl group is able to donate electron density. Although this reaction would be able to absorb more heat per mole of fluid, and be able to operate in a reactive distillation setup, it is not useful because the dehydrogenation does not occur at a reasonable rate.

3.9.7 Determining Selectivity through Gas Chromatography

When palladium supported on silica is used as the dehydrogenation catalyst no propylbenzene is detected in the ^{1}H NMR of the product mixture. This would be

sufficient evidence of excellent selectivity in a synthetic reaction. However, because the material in a thermally regenerative fuel cell is continuously cycled, even small amounts of propylbenzene forming will degrade the working fluid over time. To establish exactly how selective the dehydrogenation reaction is, an analytical method with a much lower limit of detection than NMR spectroscopy is required. Gas chromatography (GC) is a convenient method for detecting small amounts of impurities in samples.

A method was developed for the determination of 1-phenyl-1-propanol, propiophenone, and propylbenzene in a sample using hexadecane as an internal standard. Calibration curves were constructed for each of the three analytes comparing the response factors in relation to hexadecane, which would be added as a standard in a known amount after each reaction. Reactions were carried out with different catalysts using a known amount of 1-phenyl-1-propanol. After they were complete, a known amount of hexadecane was added to the reaction mixture and the sample was diluted with methanol and injected into the gas chromatograph. The amounts of each component were calculated using the calibration curves and because the total number of moles of products should be equal to the amount of 1-phenyl-1-propanol at the beginning of the reaction the amount of material lost as volatiles, to adsorption on the catalyst, to the sides of the glassware, or to decomposition could also be determined. The results of these experiments are in **Table 3.6.**

The results of the GC experiment when palladium on silica was used as a catalyst showed 0.07% propylbenzene formed over the course of the reaction. The propylbenzene peak in this GC trace was very small and broad. When the same sample was reinjected

into the GC apparatus, the second injection of the same product mixture showed no detectable peak at this location. It is entirely possible that the detected propylbenzene was an artifact in the GC trace which occurred coincidentally at the retention time where propylbenzene would be expected to be observed.

When platinum was used as a catalytic metal a very large new peak was observed in the GC trace. This peak co-eluted with the propiophenone peak. Because of this neither the quantity of propiophenone nor the amount of volatile losses could be determined from this experiment. The new peak does not correspond to any of the expected products. This product is likely a product of hydrogenation of the aromatic ring in the molecule; however this reaction normally requires higher pressures to occur. GC–MS and the retention time indicate that the product is likely 1-cyclohexyl-1-propanol. Perhaps the relatively high temperature of the reaction allows this ring reduction to occur at ambient pressure.

One weakness of this experiment is the amount of material lost over the course of the reaction, though it is not particularly high, it is high compared to the concentration of the propylbenzene side product. This is particularly troubling when considering that the main analyte, propylbenzene, which we are trying make undetectable has a lower boiling point than the other components of the mixture. The catalysis experiments that were analysed by gas chromatography were performed in 16x150 mm test tubes which allow for a certain amount of reflux space, but the test tubes were only air cooled. The evolving

Table 3.6. Product compositions for the catalytic dehydrogenation of 1-phenyl-1-propanol over different catalysts as determined by gas chromatography

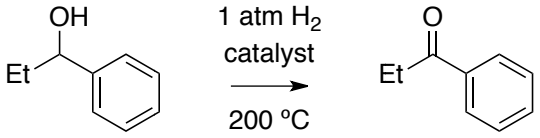

Catalyst	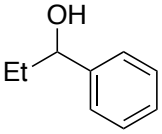	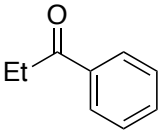	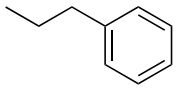	Losses
Ni/SiO_2	49.8±0.2%	27.6±0.2%	18.8±0.1%	3.8±0.1%
Pd/C	22.6±0.1%	62.0±0.5%	11.9±0.1%	3.6±0.1%
Pd/Al_2O_3	33.7±0.2%	59.0±0.5%	2.1±0.1%	5.2±0.1%
Pd/SiO_2	48.8±0.2%	47.9±0.4%	0.07%[a]	3.2±.01%
Pt/C	52.9±0.3%	N/D[b]	15.4±0.1%	N/D[b]

Reactions were performed by mixing 1-phenyl-1-propanol with 0.1 mol% equivalent of catalytic metal. The mixtures were flushed with hydrogen gas at a rate of 10 ml/min and were heated with stirring in an oil bath held at 200 ºC for a period of 4 h. The samples were spiked with a known amount of a hexadecane internal standard, diluted in acetone and filtered through a tissue plug in a Pasteur pipette and analyzed by gas chromatography. Pt/C generated a large side product peak which co-eluted with the expected product. Ni/kieselguhr was run at 1 mol% catalyst loading. [a]A small broad peak was detected in the GC trace at the same retention time as for propylbenzene. This peak was not detected on subsequent injections and may have been an artifact. [b]A new product peak overlapped with that of propiophenone and the amount of propiophenone in the sample as well as the amount lost as volatiles could not be determined.

hydrogen gas in the reaction is also capable of entraining material and carrying it away. However, the amount of material detected as volatile losses in each of the experiments is fairly consistent. If propylbenzene were being preferentially vaporised, then the catalysts which are known to generate copious amounts of propylbenzene would be expected to lose more material as volatiles. However, propylbenzene is also abundant in each of the samples analysed other than the palladium on silica catalysed reaction. Finally, the previous experiments where NMR analysis was used were performed on a larger scale in pear shaped flasks topped with an efficient Dimroth condenser; in these experiments

propylbenzene was detected at a comparable level to those performed in test tubes. Although the composition of the lost material is unknown, it is probable that if propylbenzene were formed in an appreciable amount it would have been detectible in the gas chromatogram.

3.9.8 Catalyst Screening for Dehydrogenation of 1-Phenyl-1-Propanol

Working with Vanessa Little, who had started working on this project, an assortment of commercially available catalysts were purchased. The objective was to determine if there were any catalysts that were better than palladium on silica either in cost or activity. The reactions were performed in a similar manner to the ones performed for GC analysis but these samples were analyzed by NMR spectroscopy. In some cases unidentified products were formed. It is suspected that these compounds are likely products of dearomatization of the ring as postulated earlier. The results of the experiments are in **Table 3.7.**

Table 3.7. Product compositions for the dehydrogenation of 1-Phenyl-1-propanol over different catalysts as determined by ^{1}H NMR

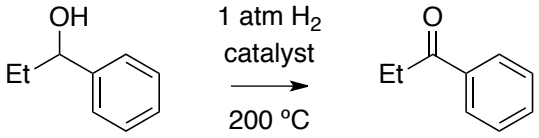

Catalyst	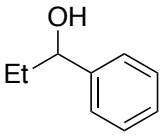	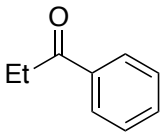	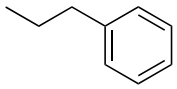	Unidentified
$Pd/CaCO_3$	52±0.2%	44.6±0.1%	3.4±0.1%	-
$Pd/CaCO_3$•Pb	73±2%	27±0.03%	-	-
$Pd/BaSO_4$	29±0.9%	54.7±0.7%	16.3±0.7%	-
$Pd/BaCO_3$	73±7%	27±0.03%	-	-
$Pd/BaCO_3$ (H_2O)	69±4%	30.1±0.2%	1±0.2%	-
Pd/Al_2O_3	49±0.9%	49.7±0.1%	0.6±0.1%	0.7±0.1%
$Pd/PEI/SiO_2$ (1 wt%)	62±2%	38±0.04%	-	-
$Pd/PEI/SiO_2$ (3 wt%)	51±13%	45.1±0.5%	3.9±0.5%	-
Pd/SiO_2	51±0.9%	49±0.05%	-	-
Pt/Al_2O_3 (10 wt%)[a]	50%	47.6%	1.7%	0.8%
$Pt/CaCO_3$	19±6%	64.4±0.7%	2.2±0.8%	14.4±0.6%
Pt/SiO_2	87±3%	13±0.01%	-	-
Pt/C (10 wt%)	33±2%	56.3±0.7%	2.3±0.4%	8.6±0.4%
Pt/Ir mesh (10 wt% each)	97.9±0.2%	N/D[b]	N/D[b]	N/D[b]
Rh/Al_2O_3 (0.5 wt%)	35±0.6%	54.6±1%	9.8±1.3%	0.7±0.1%

Table 3.7. Product compositions for the dehydrogenation of 1-Phenyl-1-propanol over different catalysts as determined by ^{1}H NMR

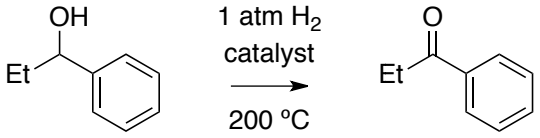

Catalyst	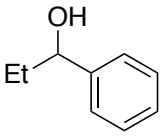	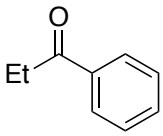	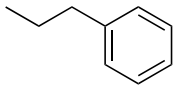	Unidentified
Rh/C	39±2%	56±0.6%	3.4±0.2%	1.6±0.4%
Rh/Al_2O_3	25±0.7%	64.4±0.2%	9.5±0.1%	1.1±0.1%
Ru/Al_2O_3	87±4%	10.5±1%	2.1±1.4%	0.4±0.5%
Ru/Al_2O_3 (0.5 wt%)	85±2%	12.6±0.3%	2.4±0.3%	-
Ru/C	64±1%	25.6±0.4%	10.4±0.4%	-

Reactions were performed in duplicate by mixing 1-phenyl-1-propanol with 0.1 mol% equivalent of catalytic metal. The headspace above the mixtures was flushed with hydrogen gas at a rate of 10 ml/min and the mixtures were heated with stirring in an oil bath held at 200 ºC for a period of four hours. The samples were diluted in chloroform-d and filtered through a tissue plug in a Pasteur pipette and analyzed by ^{1}H NMR spectroscopy. All catalysts are 5 wt% metal on support unless otherwise noted. [a]Only one experiment performed. [b]Selectivity at such low conversion could not be accurately determined.

There is some discrepancy between some of the data in **Table 3.7** and that presented in **Table 3.6**. The difference in reaction conditions is that the data presented in **Table 3.6** is for reactions that were sparged with hydrogen continuously and before heat was applied, whereas the data in **Table 3.7** is for reactions where only the headspace was flushed with hydrogen (though the evolution of hydrogen during the reaction saturates the liquid with hydrogen after a period of time).

Of all the catalysts examined only palladium on calcium carbonate poisoned with lead and palladium (1%) supported on polyethylenimine and silica have similar

selectivities to palladium on silica, but both of these catalysts are less active than palladium on silica. The palladium supported on polyethylenimine and silica at 3% palladium loading has much lower selectivity than the sample with less palladium. From this set of experiments it appears that palladium on silica is still the best catalyst to use.

Barium sulfate and barium carbonate supported palladium were investigated because these catalysts are supposed to bind substrates less strongly than other supported palladium catalysts.[207] If this were the case, then a more rapid turnover of the reaction would occur because product molecules would leave the surface faster, freeing up room for incoming reactants. However, the experimental results show that, except for palladium on barium sulfate, these types of catalysts are less active (show lower conversion in a given time) than palladium on silica. The palladium on barium sulfate did have a higher activity than palladium on silica, but the selectivity of this catalyst was very poor.

Rhodium and platinum catalysts were generally more active and less selective than palladium on silica. An exception was platinum on silica which was as selective as palladium on silica but less active (and more costly). Ruthenium catalysts appear to be both less active and less selective than palladium on silica. Platinum–iridium mesh had a low surface area compared to all the other catalysts studied and therefore had very low activity, to the point where the conversion was too low for the selectivity of the reaction to be accurately determined.

3.9.9 Dehydrogenation of Conjugated Carbon–Carbon Single Bonds

Additional working fluids were investigated to determine the scope of the dehydrogenation reaction and, more importantly, whether other selectively dehydrogenated liquids could be identified. Dehydrogenation of a carbon-carbon single bond to form a carbon-carbon double bond has a higher enthalpy of reaction and therefore the equilibrium constant difference at high and low temperature would be larger leading to a higher potential difference in the fuel cell. Carbon-carbon bonds are also much less susceptible to hydrogenolysis than a benzylic alcohol. This means that the dehydrogenation of a carbon-carbon single bond may occur at a higher temperature than that used in the 1-phenyl-1-propanol system. This also means that more active catalysts may be used because selectivity is less problematic.

A series of saturated compounds, where the dehydrogenation of a single carbon-carbon bond would result in either extended conjugation or aromatization of a π-system, were dehydrogenated over various catalysts. Palladium, platinum, rhodium and ruthenium on carbon, as well as nickel on kieselghur were used. The cyclic compounds succinic anhydride, succinimide, ethylene carbonate, and 2-imidazolidinone; and the linear compounds diethyl succinate, 2-methylsuccinic acid, and bibenzyl were all heated to 200 ºC in air with these catalysts (using 1 mol% loading for Pd, Pt, Rh, and Ru and 10 mol% loading for Ni). However, none of these materials underwent any dehydrogenation, or any reaction at all, at 200 ºC. Heating ethylene carbonate to reflux using a heating mantle also resulted in no reaction.

The dehydrogenation of these carbon-carbon bonds appears to suffer from the same problem as encountered with benzyl alcohol. The thermodynamic enthalpy of dehydrogenation is high and consequently the energy of the transition state leading to the dehydrogenated products is also high. Even at the reflux temperature of ethylene carbonate, which is fairly high (243 ºC at 740 mmHg), no reaction takes place. The use of these materials is therefore not practical for the envisioned application. It would likely take very high temperatures to effect a dehydrogenation, at which point it is likely that many other side reactions would also occur.

3.9.10 Phase Behaviour and the Dehydrogenation of Diols

Because there are thermodynamic and kinetic advantages associated with the distillation of the dehydrogenated product from the dehydrogenation reactor, working fluids that would drop significantly in boiling point after dehydrogenation were sought. In alcohols, dehydrogenation to a ketone changes the molecules from those that are both hydrogen bond donating and accepting to ones only capable of accepting hydrogen bonds. This results in a decrease in the boiling point of the fluid. This effect is most apparent with low molecular weight alcohols; e.g., methanol boils at 65 ºC, whereas formaldehyde boils at -21 ºC. In larger molecules, other intermolecular forces affect boiling point to an extent where there is a much smaller difference, e.g., 1-phenyl-1-propanol boils at 227 ºC, whereas propiophenone boils at 218 ºC. In the thermally regenerative fuel cell system, the saturated compound should have a boiling point higher

than 200 ºC. This would require a high molecular weight alcohol and therefore lower the boiling point difference.

In order to have a relatively low molecular weight alcohol with a high boiling point, it is necessary to have two or more functional groups in the molecule. Changing two alcohols into two carbonyls has a dramatic effect on boiling point. Ethylene glycol boils at 197 ºC, but glyoxal boils at 51 ºC; 2,4-pentanediol boils at 201 ºC, but acetylacetone boils at 140 ºC. A series of small diols with either a 1,2 or 1,3 relationship were subjected to dehydrogenation conditions over either palladium on silica or ruthenium on alumina (ruthenium on various supports has been reported to dehydrogenate simple alcohols).[208, 209] The results for palladium on silica are outlined in **Table 3.8.** and the results for ruthenium on alumina are outlined in **Table 3.9.**

Table 3.8. Product compositions for the catalytic dehydrogenation of diols over Pd/ SiO_2

Compound	Starting Material	SM -$1H_2$	SM -$2H_2$
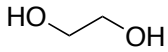	100%	0%	0%
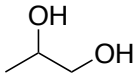	99%	1%	0%
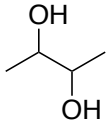	97%	3%	0%
	N/D	N/D	0%
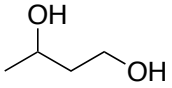	100%	0%	0%
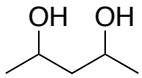	N/D	N/D	0%

Reactions were performed by mixing an organic substrate with 0.1 mol% equivalent of Pd in the form of palladium, 5% on silica powder, reduced, dry (Escat™ 1351). The mixtures were flushed with hydrogen gas at a rate of 10 ml/min and were heated with stirring in a Carousel 12 Place Reaction Station™ at 200 ºC for a period of one hour. The samples were diluted in chloroform-d and filtered through a tissue plug in a Pasteur pipette or were diluted in deuterium oxide and allowed to settle in a glass sample vial before decanting as noted. Samples were analyzed by ^1H NMR spectroscopy. Data points labelled N/D were experiments which showed some change in the proton NMR spectrum but the small product signals could not be assigned to any particular product.

Table 3.9. Product compositions for the catalytic dehydrogenation of diols over Ru/ Al_2O_3

Compound	Starting Material	SM -$1H_2$	SM -$2H_2$
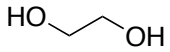	N/D	N/D	N/D
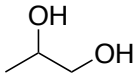	99%	1%	0%
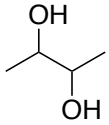	96%	4%	0%
	N/D	N/D	N/D
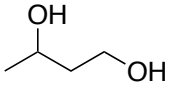	N/D	N/D	N/D
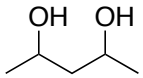	N/D	N/D	N/D

Reactions were performed by mixing an organic substrate with 0.1 mol% equivalent of Ru in the form of ruthenium, 5% on alumina powder (Degussa type H213). The mixtures were flushed with hydrogen gas at a rate of 10 ml/min and were heated with stirring in a Carousel 12 Place Reaction Station™ at 200 ºC for a period of one hour. The samples were diluted in chloroform-d and filtered through a tissue plug in a Pasteur pipette or were diluted in deuterium oxide and allowed to settle in a glass sample vial before decanting as noted. Samples were analyzed by ^1H NMR spectroscopy. Data points labelled N/D were experiments which showed some change in the proton NMR spectrum but the small product signals could not be assigned to any particular product.

The product mixtures were analyzed by NMR spectroscopy in deuterium oxide. The nature of the substrates can lead to complicated NMR spectra. Each of the diols would be expected to undergo sequential dehydrogenation, this yields three potential products for symmetrical diols and four products for unsymmetrical diols. In addition, any aldehydes formed could easily form hydrates in deuterium oxide solution. Of course, side reactions may also occur. Although hydrogenolysis of a simple alcohol is unlikely, at 200 ºC dehydration reactions may occur and if they occur would likely be followed by

hydrogenation of the resulting alkenes. All of these potential products would have signals in the aliphatic region of the proton NMR spectrum, only unhydrated aldehydes would have clearly distinguishable signals.

In many cases the composition of the product mixture could not be accurately determined due to the presence of a large number of small product peaks. However, in these cases as in the ones where the products were known, the total conversion of starting material was very small. In the mixtures where the composition was known, there was no detected doubly dehydrogenated product. One exceptional case was the dehydrogenation of ethylene glycol over ruthenium on alumina. The product mixture consisted of the starting material and another single broad peak which did not correlate to either glycolaldehyde or glyoxal, the expected products.

The products of the reactions were expected to have much lower boiling points than the starting material and this may explain the lack of detection in the NMR spectra. However, a lack of observed volumetric loss over the course of the reaction casts doubt on the formation of desired product followed by their loss as volatiles. There were no promising fluids identified in this screening experiment and the likelihood of either dehydrations or polymerization of these molecules at high temperature makes these compounds unattractive for further study.

3.9.11 Dehydrogenation of Benzylic Amines

The dehydrogenation of carbon-oxygen and carbon-carbon single bonds has been examined. Dehydrogenation of amines to imines may also be possible, though there are problems associated with using an amine as a hydrogen carrier. The product of dehydrogenation, an imine, is susceptible to hydrolysis, particularly under acid catalyzed conditions, i.e., over a fuel cell membrane. This can be avoided by running the system under scrupulously dry conditions; though how this could be implemented in the hands of the public is not known. Both amines and imines are basic, and they might poison catalyst surfaces.

Amines do have interesting properties that blend some of the advantages of carbon-oxygen and carbon-carbon compounds. For instance, to be able to dehydrogenate a carbon-oxygen compound must be an alcohol and not an ether. Alcohol O–H bonds cannot be used to bridge conjugation (though they can be cross conjugated). This extension of conjugation is possible in carbon-carbon compounds, for instance in bibenzyl. However, the C–H acidity in carbon-carbon compounds is not nearly as high as the N–H acidity in carbon nitrogen compounds. Thus N-benzylaniline, the nitrogen containing analog of bibenzyl, might be expected to undergo dehydrogenation more readily than the alkane. Primary and secondary benzylic amines and anilines were reacted over palladium on silica and ruthenium on alumina and compared to the analogous alcohols. The results are summarized in **Table 3.10** and **Table 3.11.** The alcohols show the same dehydrogenation trends previously observed. Benzyl alcohol has low reactivity

and 1-phenyl-1-ethanol has low selectivity when dehydrogenated over the ruthenium catalyst. Benzyl amine and N-benzylaniline show low reactivity over both catalysts, and α-methylbenzylaniline was completely unreactive. α-Methylbenzylamine showed no reaction over ruthenium but when reacted over palladium formed many different products, some of which were the product of disproportionation of the amine with formation of ammonia.

The only amine that showed any promise was α-methylbenzylamine. Although this was reactive, it was very unselective. Disproportionation of primary amines under a reducing atmosphere (such as hydrogen) is known in the literature.[153] This compound is not an improvement over 1-phenyl-ethanol, and would suffer problems with hydrolysis even if the selectivity issue could be resolved with a careful choice of catalyst.

Table 3.10. Product compositions for the catalytic dehydrogenation of benzylic alcohols and amines over Pd/SiO_2

Compound	Starting Material	Dehydrogenation	Hydrogenolysis
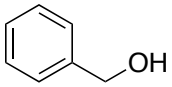	97%	3%	0%
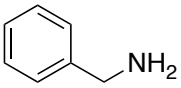	N/D	N/D	N/D
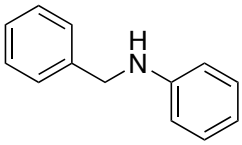	99%	1%	0%
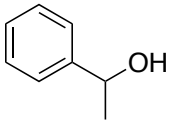	51%	49%	0%
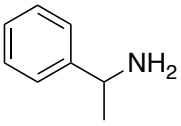	N/D	N/D	N/D
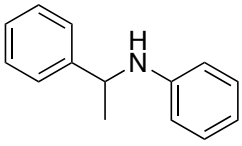	100%	0%	0%

Reactions were performed by mixing an organic substrate with 0.1 mol% equivalent of Pd in the form of palladium, 5% on silica powder, reduced, dry (Escat™ 1351). The mixtures were flushed with hydrogen gas at a rate of 10 ml/min and were heated with stirring in a Carousel 12 Place Reaction Station™ at 200 ºC for a period of one hour. The samples were diluted in chloroform-d and filtered through a tissue plug in a Pasteur pipette or were diluted in deuterium oxide and allowed to settle in a glass sample vial before decanting as noted. Samples were analyzed by ^1H NMR spectroscopy. Data points labelled N/D were experiments which showed some change in the proton NMR spectrum but the small product signals could not be assigned to any particular product. α-Methylbenzyl amine generated many different products.

Table 3.11. Product compositions for the catalytic dehydrogenation of benzylic alcohols and amines over Ru/Al_2O_3

Compound	Starting Material	Dehydrogenation	Hydrogenolysis
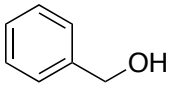	N/A	N/A	N/A
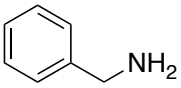	N/D	N/D	N/D
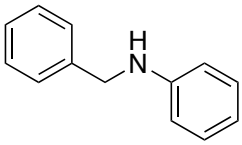	N/D	N/D	N/D
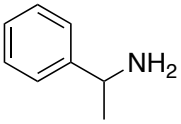	86%	10%	4%
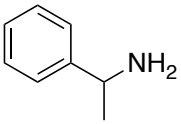	100%	0%	0%
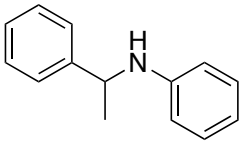	100%	0%	0%

Reactions were performed by mixing an organic substrate with 0.1 mol% equivalent of Ru in the form of ruthenium, 5% on alumina powder (Degussa type H213). The mixtures were flushed with hydrogen gas at a rate of 10 ml/min and were heated with stirring in a Carousel 12 Place Reaction Station™ at 200 ºC for a period of one hour. The samples were diluted in chloroform-d and filtered through a tissue plug in a Pasteur pipette or were diluted in deuterium oxide and allowed to settle in a glass sample vial before decanting as noted. Samples were analyzed by ^1H NMR spectroscopy. Data points labelled N/D were experiments which showed some change in the proton NMR spectrum but the small product signals could not be assigned to any particular product. α-Methylbenzyl amine generated many different products.

3.9.12 Determination of Equilibrium Constant

From all of the previous work, it would appear that secondary benzylic alcohols are the best (and realistically the only) candidates as working fluids in a thermally regenerative fuel cell. The best catalyst for this process appears to be palladium supported on a matrix of amorphous silica. The kinetics of this reaction appear to be able to provide more than adequate current to a fuel cell stack, however, the thermodynamics of this process have not yet been determined. A simple way to determine this is to perform bomb calorimetry on the starting material and the product, determine their enthalpies of combustion and then calculate the enthalpy of reaction. However, even with a well calibrated calorimeter this results in the subtraction of two large numbers. Though the relative error of each enthalpy of combustion may be small, the relative error of the difference can be very large.

There is another approach that can be used to determine the enthalpy of reaction. The van't Hoff equation relates the enthalpy of reaction to the equilibrium constants of the reaction at two different temperatures. A van't Hoff plot can be constructed in such a way as to determine both the standard enthalpy and standard entropy of the reaction. Linear regression of a plot of the natural logarithm of the equilibrium constant versus the reciprocal of the temperature will yield the enthalpy of the reaction in the slope and the entropy of reaction in the intercept.

However, the reactions being studied are far from instantaneous; even at 200 ºC they require several hours to reach completion. To be sure that the reaction has reached

equilibrium, and that the values measured are accurate, the equilibrium composition should be approached from both directions. If a reaction that starts with 100% 1-phenyl-1-propanol and a reaction that starts with 100% propiophenone are both held at the same temperature under the same partial pressure and both show the same product composition then both reactions have reached equilibrium. An example of this experiment can be seen in **Figure 3.5.** At lower temperatures, the reaction can become very slow. Because increasing the catalyst loading does not affect the thermodynamics of the reaction, it can be used to mitigate the slowness of the reaction.

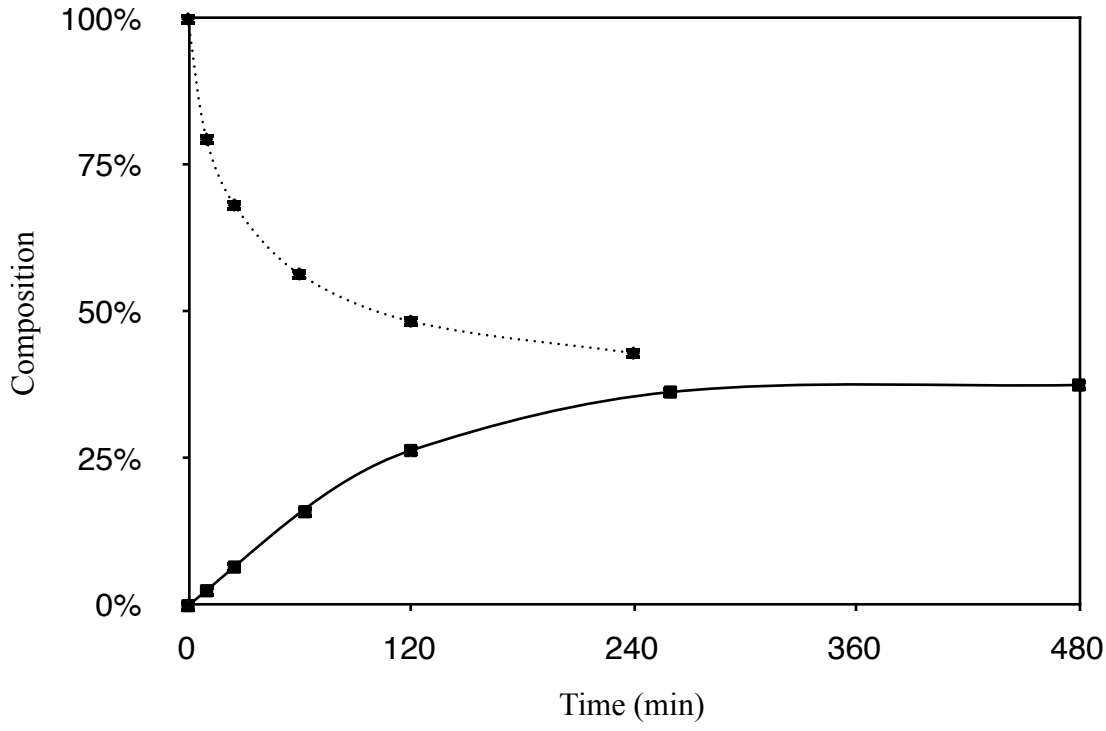

Figure 3.5. Dehydrogenation of 1-phenyl-1-propanol approaching equilibrium at 200°C under hydrogen at ambient pressure

Equilibrium constants for reactions occurring below 200 ºC were measured in this way by a summer student, John Vandersleen. His data was replotted in a van't Hoff plot (**Figure 3.6**) and the enthalpy of dehydrogenation was determined to be +55.7 ± 2.3 kJ mol^{-1}. The entropy of the dehydrogenation was found to be about +117.3 ± 5.4 J mol^{-1} K^{-1}. From this thermodynamic data, and the kinetic data measured earlier it is possible to determine the amount of power being absorbed in the dehydrogenation reactor, at least under batch reaction conditions.

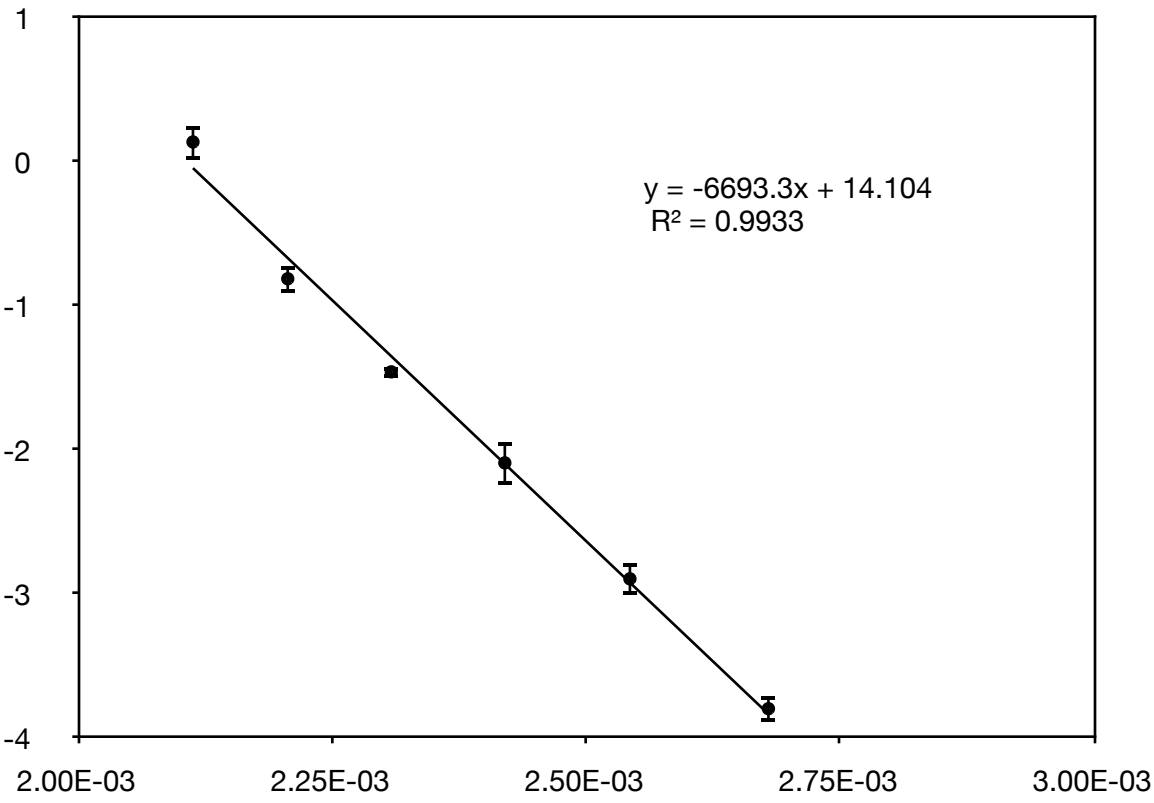

Figure 3.6. Van't Hoff plot of the dehydrogenation of 1-phenyl-1-propanol

The amount of power absorbed or released is given by

$$P = \Delta G \frac{dH_2}{dt} \tag{38}$$

At 100 ºC, the free energy of reaction would be ~12 kJ mol^{-1}. The initial rate of hydrogen evolution is about 3.45 mmol s^{-1} g-Pd^{-1}. This yields a power of about 41 W g-Pd^{-1} if all of the hydrogen were reacted in the fuel cell. In order to increase the power absorbed from the engine block, one must use either a working fluid with a higher free energy of dehydrogenation or a catalyst with faster kinetics. These are not generally mutually exclusive; reactions with high free energies tend to have slower kinetics, though it is not impossible to find an excellent catalyst able to minimize the transition state energy.

3.10 Prototypes

A prototype of the system was constructed as a proof of principle of its operation. A diagram illustrating its basic structure is shown as **Figure 3.7.** The construction of the prototype thermally regenerative fuel cell revealed difficulties in the engineering that were not obvious from the theoretical design. However, some of these issues were easily addressed whereas others will require further study to resolve. Fuel cell hardware, a flow metering pump, and membrane electrode assemblies (MEAs) were purchased. Most

adjustments to the prototype TRFC system were made in the dehydrogenation chamber, which was either constructed from a Parr autoclave or from a large glass multi-necked reactor.

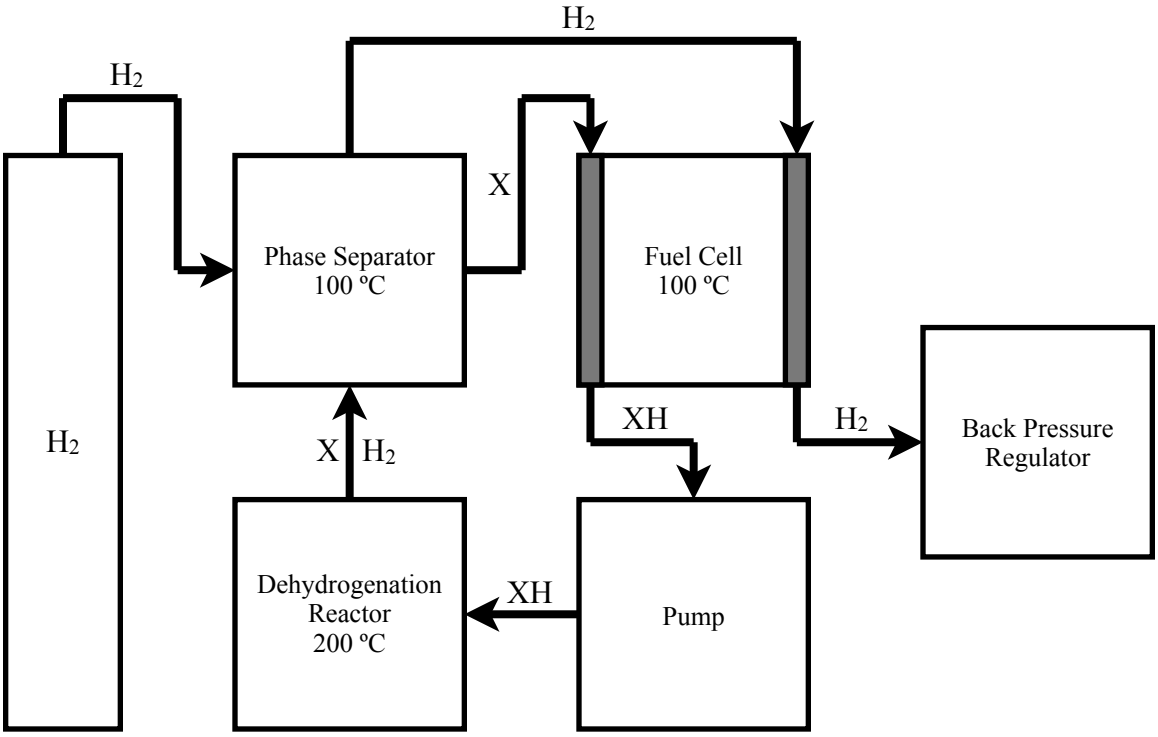

Figure 3.7. Diagram of a TRFC prototype

The first prototype construction was made using a large glass reactor stirred with a motor driven impeller. This initial apparatus used PTFE tubing to connect the reactor to the fuel cell and a peristaltic pump to circulate the fluid (the tubing in and immediately around the pump was made of polyethylene to facilitate the pump's action). The reactor was heated externally using a heating mantle equipped with a temperature controller. It was immediately observed that stirring using an impeller was entirely unnecessary due to

the mixing generated by the rapid evolution of hydrogen gas in the reactor. However, the small particle size of the commercially available palladium on silica catalyst allowed the catalyst particles to migrate into the tubing where it continued to generate hydrogen. The hydrogen displaced the fluid and the pump no longer operated properly.

Attempts were made to prevent the catalyst from leaving the dehydrogenation reactor. The initial solution was to place a small filter over the outlet from the dehydrogenation reactor leading toward the pump. This filter almost immediately became clogged with the small catalyst particles. Furthermore, the evolution of hydrogen from the catalyst particles stuck in the filter filled the tubing with gas. A J-shaped outlet, where the evolved gasses would travel in the opposite direction of the intended fluid flow was installed but the catalyst particles clogged the filter to the point where the pump became ineffective. Some of the smaller particles were also able to pass through the filter material and enter the tubing.

Attempts were made to immobilize the catalyst in a porous material, much like a tea bag. Palladium on silica was tied in several layers of fine cotton cloth and immersed in the hot working fluid. The effect of the dehydrogenation was to allow the cotton to balloon with hydrogen and float to the top of the reactor where the dehydrogenation ceased because the catalyst had been separated from the reactor. The cotton also proved to be an ineffective filter because small catalyst particles began to leak into the fluid. A similar result was observed using dialysis tubing to contain the catalyst; however the dialysis tubing contained the catalyst particles more satisfactorily than the cotton.

Because the main problem with catalyst migration was the small particle size, attempts were made to make the catalyst particles large and therefore less apt to enter the tubing. Simply sintering the powdered catalyst into a pellet was ineffective because the sintered silica removed most of the accessible surface area of the catalyst and made it almost inert. Embedding the catalyst in a puck of Bakelite resin had the same result; in addition some of the resin leached into the organic fluid. Making large porous catalyst particles was required. Enlisting the help of a colleague, Jennifer Du, who is skilled in the construction of mesoporous silica monoliths, a monolith whose outer surface was covered with palladium metal was made and tested. This monolith was active in the dehydrogenation of the fluid, though it was less active than the finely powdered catalyst and very much less selective (**Figure 3.8.**) Endcapping any exposed silanol functional groups with chlorotrimethylsilane did not increase the selectivity of this catalyst. A simple heterogeneous catalyst was made by impregnating pellets of amorphous silica (obtained from Saint-Gobain NorPro) with palladium (II) acetate in methanol, followed by reducing the material in a hydrogen atmosphere. This impregnation catalyst was effective in catalysing the dehydrogenation reaction with the same selectivity (99.9+% as determined by ^{1}H NMR) as the commercially available powdered catalyst.

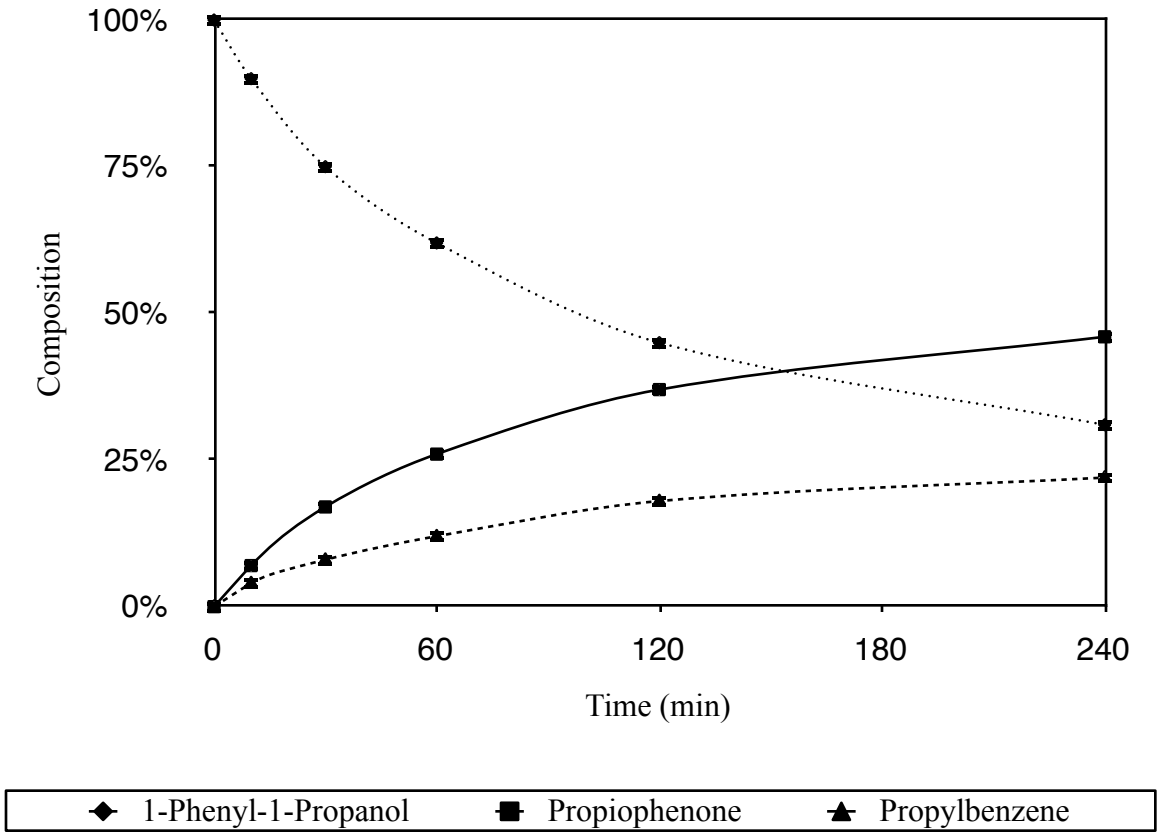

Figure 3.8. Dehydrogenation of 1-phenyl-1-propanol over Pd/SiO_2 (mesoporous) under hydrogen at ambient pressure

Resolving the catalyst migration issue did not result in the successful long term function of the prototype thermally regenerative fuel cell. Both the saturated and unsaturated fluids were discovered to damage the Nafion® membrane in the MEA. This eventually resulted in the rupture of the membrane and fluid being pumped into the anode side of the fuel cell. The MEAs removed from the fuel cell appeared dried, cracked and discoloured (orange, brown or even black) with the electrodes either peeled off from the membrane or visibly cracked. Desiccation of the Nafion® had occurred and it is

unfortunate that the only fluid identified that could undergo reversible hydrogenation with high selectivity was incompatible with the most widely available and most well studied fuel cell membrane. This issue has not been resolved yet but it is being actively studied by other researchers in our group. Because the Nafion® membrane is not chemically compatible with the only fluid identified that undergoes dehydrogenation and hydrogenation selectively the best course of action would be to investigate other, less widely available, membrane materials. Another option would be to investigate other secondary benzylic alcohols with minor structural changes (such as longer aliphatic chains) to see if these may be more compatible with Nafion® while retaining their selective reactivity and low cost.

Chapter 4

Conclusions and Future Work

4.1 Conclusions for the Hydrogen Storing Ionic Liquid Project

The hydrogen storage method investigated in this thesis is a chemical method using an organic hydride. To have an acceptable gravimetric storage density of hydrogen, organic molecules must consist of a large percentage of bonds that can be dehydrogenated. The organic molecules that have the most available hydrogen are those that form aromatic rings upon dehydrogenation. For instance, cyclohexane consists of 7.1% available hydrogen. These dehydrogenations have been widely studied and most research is concerned with reducing the enthalpy of this endothermic reaction to improve the net energy storage of organic hydrides. The research presented in this thesis was concerned with making other improvements to organic hydrides in terms of beneficial physical properties. The benefits of using an ionic liquid as a hydrogen storing material are the potential for large liquid ranges, negligible vapour pressures, high densities, and high thermal stabilities. All of these benefits may or may not be present with any particular ionic liquid. It is also important that any ionic liquid used as a hydrogen storage material features both anions and cations that store hydrogen to have a reasonable hydrogen storage density.

In this thesis I have demonstrated that it is possible to synthesize hydrogen storing ionic liquids in a single step from inexpensive starting materials. However, this only appears to be possible for those ionic liquids that can be manufactured by a proton transfer process. The piperidinium ionic liquids prepared by this method were not effective hydrogen storage materials due to the inability of the piperidinium ion to dehydrogenate. Other ionic liquids that could be prepared by proton transfer would include ammonium and phosphonium ionic liquids of the NR_3H^+ and PR_3H^+ variety (though phosphines are generally less basic than amines). Synthesis of amines and phosphines containing hydrogen storing rings would be a multistep process using stoichiometric quantities of costly starting materials making the manufacture of ionic liquids based on these prohibitively expensive. Another option is to use a two-step process where the cation is formed as a halide salt where the halide is exchanged in a subsequent step through an ion exchange process. Although a silver exchange process, as demonstrated within, could be used, it is not economically viable on a large scale. An alternative would be to use a selective extraction from aqueous solution, though that may not be possible depending on the ions used. This ion exchange method can be used with more diverse cations such as tetraalkylammonium, tetraalkylphosphonium, sulfonium and imidazolium salts. There is a nearly endless number of combinations of cations and anions that can be combined to form ionic liquids so it is difficult to determine which combinations, if any, could form an effective and economical hydrogen storing fluid.

Of the ionic liquids studied, none underwent a complete cycle of hydrogenation and dehydrogenation. In fact, dehydrogenation was only observed to a significant extent

in simple sodium salts of nipecotic and isonipecotic acid when they were dissolved in formamide. Even then the selectivites of these reactions was unknown due to the large amount of missing starting material when compared to the observed yield of desired product. Only a small amount of conversion was observed for the isonipecotate ion when paired with the tetrabutylphosphonium ion without the addition of extraneous solvent. It appears that the viscosity of the ionic liquid is preventing dehydrogenation of the heterocycles, either by preventing diffusion of the ionic liquid to and from the catalyst surface, or by preventing the diffusion of the evolved hydrogen from the catalyst surface through the ionic liquid. This assumes that the ions have a tendency to dehydrogenate at all; the N-alkylpiperidinium ion was never observed to dehydrogenate regardless of the presence of a solvent.

Although ionic liquids could be constructed that had both anions and cations that could potentially store hydrogen, no effective hydrogen storing ionic liquids were discovered during this research. Except for the simple case of proton transfer from a heterocyclic acid to an N-alkylpiperidine, these materials are not simple to make. Although ion exchange using silver salts is facile on very small scales, this method of preparing ionic liquids is not economically viable for producing what should be a low cost material on a multi-ton scale. More difficult are elaborate cations which must be synthesized in multiple steps. Only one of these, a carbazole-containing imidazolium ion, was successfully constructed, and it failed to undergo catalytic hydrogenation. In conclusion, all but the most simple ionic liquids will not be feasible to use on such a large scale.

There are also general problems with the concept of using a hydrogen storing ionic liquid, especially when compared to the other options for portable hydrogen storage. Storing hydrogen for portable applications is a complex problem. There are many approaches to storing hydrogen and each has advantages and disadvantages.

Ionic liquids are considerably more expensive to manufacture than petroleum products. However, because the ionic liquid, at least theoretically, can be recycled whereas the combustion of a hydrocarbon is a one-time use, it may be economically viable to use the ionic liquid hydrogen storage media as long as the initial manufacturing cost and regeneration costs are competitive with the cost of the equivalent amount of gasoline in terms of energy storage over the lifetime of the material. This would require that the ionic liquids be manufactured at relatively low cost, be very thermally stable and that the hydrogenation and dehydrogenation reactions be very selective to prolong the useful life of the material.

The longevity (resistance to degradation) of the ionic liquid once in use is also very important. The ionic liquid must be cycled many times to compete with the lower cost of gasoline, however the number of times the ionic liquid can be cycled will depend on the thermal stability of the ionic liquid as well as the selectivities of the hydrogenation and dehydrogenation reactions. In this thesis it was determined that the ionic liquids synthesized were considerably less thermally stable than ionic liquids that had non-coordinating anions such as bistriflimide or hexafluorophosphate. The carboxylate ionic liquids were particularly unstable due to the nucleophility of the carboxylate ion. Using sulfonate ionic liquids resulted in fluids with improved thermal stability, but the electron

withdrawing effect of the sulfonate group necessitated the use of a tether between the hydrogen storing ring and the anionic center. This increases the mass of the ion without increasing its hydrogen storage capacity and results in a lowered gravimetric hydrogen storage capacity.

Any clear advantage to using an ionic liquid in place of a neutral organic hydride as a hydrogen storage material, such as low volatility and large liquid range, is not sufficient to compensate for the cost and lack of reactivity of these materials. Neutral fluids usually have low viscosities, which would result in similar pumping costs to gasoline both onboard the vehicle and during distribution. These fluids also have reasonable reaction kinetics and, so long as they do not have too many peripheral groups, a reasonably high gravimetric density of hydrogen. Most neutral liquids do not have obvious decomposition mechanisms so they should be reasonably stable until pyrolysis occurs. Neutral liquids will likely suffer the same selectivity problems during hydrogenation and dehydrogenation as ionic liquids would, but it may be easier to separate the decomposed material from the bulk during regeneration. Organic hydrides, unless of high complexity, are less expensive to manufacture than ionic liquids. The only major disadvantages of using a neutral liquid are their typically low boiling points and high vapour pressures. However, this may be less of a problem with neutral fluids that have many hydrogen bonding interactions. If this is not the case, then the boiling point can be increased by forming oligomers of the hydrogen storing ring. If this increases the melting point to the point that the material is solid at ambient temperature a eutectic mixture could be used to ensure that the mixture remains fluid at low temperature.

In conclusion, it appears from the experimental results and these more general considerations that ionic liquids will not likely be economically viable as hydrogen storage media. One reason is the relative cost of manufacturing ionic liquids compared to the cost of gasoline, or even to other fine chemicals and other hydrogen storage media. The thermal decomposition and less than perfect selectivity of the hydrogenation and dehydrogenation reactions will result in significant loss of material over time and if there is no simple method of removing the decomposed material from the bulk, then the recycled ionic liquid will become increasingly contaminated. The high cost ionic liquid would then have a limited cycle life and limited recyclability. Most ionic liquids have fairly high viscosities. This may limit the reaction kinetics as the ions will need to diffuse through the bulk to the catalyst surface. High viscosities also increase the energy required to pump the fluid, both onboard the vehicle and during manufacturing and distribution and this can lead to significant parasitic energy losses.

4.2 Future Work for the Hydrogen Storing Ionic Liquid Project

I cannot recommend that more time and resources should be spent trying to find an effective hydrogen storing ionic liquid because it is not likely to be a fruitful endeavour. However, the use of organic hydrides as a hydrogen storage medium is still a feasible alternative to simple physical methods. The benefits ascribed to the use of an ionic liquid would primarily be the large liquid range and low vapour pressures these materials tend to exhibit. This is also true of some polymers, which depending on the

method of synthesis, may be simpler to prepare; though they will likely be even more difficult to analyze. Alternatives to liquid polymers, at least in the characteristic of having a depressed melting point would be mixtures of simple neutral compounds. Perhaps bi or terpyridines, though these materials are much more expensive than bulk compounds. Small oligomers of polyvinylpyridine may be another acceptable candidate.

4.3 Conclusions for the Thermally Regenerative Fuel Cell Project

A family of compounds, secondary benzylic alcohols, was found to be able to reversibly hydrogenate with very high selectivities over a commercially available heterogeneous catalyst, palladium supported on amorphous silica. Such compounds could be used as working fluids in a thermally regenerative fuel cell. Studying this reversible hydrogenation at different temperatures and over time allowed for the determination of the reaction thermodynamics and the kinetics of the bulk reaction. Other potential working fluids were examined and few showed any dehydrogenation under the conditions used to dehydrogenate the secondary benzylic alcohols. Those that showed any signs of dehydrogenation did so with far from adequate selectivity for the purpose of a thermally regenerative fuel cell.

When 1-phenyl-1-propanol or propiophenone was passed across the cathode of a fuel cell that contained a Nafion™ membrane (with hydrogen passed across the anode) no electrochemical reduction of the fluid was observed, though a potential difference was measured across the fuel cell. This was followed by crossover of the working fluid to the

anode side of the fuel cell due to the rupture of the membrane. When disassembled, the membrane electrode assembly was desiccated and discolored with visible cracks in the membrane. Additionally, the electrode layers were frequently disconnected from the membrane material. The Nafion™ membrane is not compatible with the only organic fluids that have been determined to be amenable to use in a thermally regenerative fuel cell. This will require the development of a new membrane type for the fuel cell.

The electrochemical reduction of propiophenone could not be studied because Nafion™ membranes are decomposed by the organic fluid. The kinetics and selectivity of the reduction on the cathode are not known, and because the mechanism of the reduction is not likely to be the same as bulk hydrogenation on a palladium surface neither the rate nor selectivity of the reaction in the electrochemical cell may be the same as measured during bulk hydrogenation. However, the Ando paper[171] provides some information for the reduction of acetone in water, which though not exactly relevant does give some idea of the fuel cell potential as the reaction enthalpies for acetone and propiophenone are almost the same. The hydrogenation of a mixture of 10% v/v of acetone and 10% v/v of isopropanol in aqueous solution yields an open circuit voltage of approximately 125 mV and a short circuit current of approximately 35 mA at 298 K. Increasing the temperature to 333 K lowered the open circuit voltage to approximately 90 mV and increased the short circuit current to about 50 mA. These reactions were performed in aqueous solution so the increased concentration of reactants in the proposed thermally regenerative fuel cell should increase the output potential and current, though solvation of the ketone will change in the absence of water and will likely have a significant effect.

A real thermally regenerative fuel cell is also a flow system. The membrane degradation prevented the prototype from completing its cycle. However, the data from the batch reaction is still applicable to the flow system as rate data is available for the dehydrogenation throughout the relevant fluid composition range. The steady state compositions entering and leaving the dehydrogenation reactor and fuel cell respectively are unknown. However, reaction times can be adjusted with fluid flow rate to maximize the hydrogen extracted during hydrogenation and the saturation of the fluid exiting the fuel cell stack.

It appears that the proposed thermally regenerative fuel cell is likely to be economically viable as the benefits of increased fuel economy would likely outweigh the cost of operating the system in the long term, though this will depend in part on the longevity of the materials used. The secondary benzylic alcohols identified and the ketones they are prepared from are inexpensive materials that are readily available and can be easily manufactured on a very large scale from common starting materials. The cost of fluid, which must be changed periodically, should be low. The amount of palladium required in the dehydrogenation reactor to yield sufficient hydrogen gas is also relatively low, and would not be prohibitively costly to the implementation of the thermally regenerative fuel cell system. However, the longevity of the catalyst, in terms of retaining selectivity and activity over time due to morphological changes of the catalyst surface or due to catalyst poisoning, is unknown. Therefore, it is not known whether the catalyst would last the life of the system, or if it too would require periodic replacement. A lack of knowledge of the fuel cell reaction prevents an economic

assessment on the number of fuel cells required in the stack, as well as the nature and amount of catalyst on each electrode and the nature of the membranes required. However, it would appear that the fuel cell will likely be the most costly component of the thermally regenerative fuel cell system.

4.4 Future Work for the Thermally Regenerative Fuel Cell Project

An effort was made to investigate the dehydrogenation of diols as these working fluids would change phase after dehydrogenation (the diketones or aldehydes generated would have a much lower boiling point that the starting diols). The unsaturated product could be easily separated from the saturated starting materials before being passed to the fuel cell. This would allow for enhanced kinetics and thermodynamics of the reactions in the dehydrogenation reactor because the product material is continuously removed (the reaction would not incur product inhibition) and the fuel cell (which is supplied an enriched hydrogen acceptor). However, there was no successful dehydrogenation observed. Only a limited number of heterogeneous catalysts were investigated and the reactions were not performed at particularly high temperatures. In reality, heat can be absorbed from a diesel engine at temperatures more than 200 ºC, so if higher temperatures are required to dehydrogenate diols they may still be viable working fluids. Operating the dehydrogenation reactor at higher temperature would actually benefit the thermally regenerative fuel cell by enhancing the temperature difference between the dehydrogenation reactor and the fuel cell, if diols were able to dehydrogenate at a higher

temperature than benzylic alcohols without undergoing unwanted reactions (such as dehydrations and hydrogenolysis) they may be superior working fluids. Low molecular weight diols are inexpensive and, with appropriate equipment, combinatorial chemistry could easily be used along with gas chromatography to perform dehydrogenation reactions over many different heterogeneous catalysts at different temperatures with complete knowledge of the conversions and selectivities of each. If any promising dehydrogenation reactions were discovered they could be analyzed in greater detail by conventional methods.

The main problem with the development of the thermally regenerative fuel cell is the incompatibility of Nafion™ membranes with the benzylic alcohol or ketone. These compounds appear to desiccate the membrane and destroy its activity. An alternative membrane material would be polybenzimidazole. This membrane does not use water channels to conduct protons and is chemically compatible with aromatic solvents and alcohols.[210]

Polybenzimidazole membranes are usually operated at a higher temperature than Nafion™ membranes.[65, 211, 212] As a result, there would be less of a difference between the equilibrium constants at the operating temperatures of the dehydrogenation reactor and the fuel cell. This would reduce the voltage of TRFC, and the hydrogenation rate would likely be lower because the reactants entering the fuel cell will be closer to their equilibrium composition than they would otherwise. However, operating at a higher temperature allows the fuel cell to operate with higher efficiency and at higher power densities,[64-66] which may more than make up for the difference in expected cell potential.

Of course, polybenzimidazole membranes are not the only other option and other membranes will need to be investigated.

Once the membrane issue is resolved, real study can begin on the reduction on the cathode of the fuel cell. During the experiments in which the equilibrium constant was determined, it was apparent that the simple hydrogenation of the ketone with hydrogen gas is very slow at 100 ºC. However, the reduction in the fuel cell may proceed through a different mechanism, such as through a series of single electron reductions and protonations. Acetone was successfully reduced in aqueous solution in Ando's paper.[171] This substrate does not have the additional stabilization of the aromatic ring so it seems entirely feasible that the reduction of the aryl ketone to the benzylic alcohol may take place with similar or better reaction kinetics if a benzylic radical, or charge is built up in the benzylic carbon in the transition state of the hydrogenation. This would be due to the stabilization of charges (and radicals) by the neighbouring aromatic ring, as well as the increase in reactant concentration if no diluent is used. Acetone and propiophenone have very similar enthalpies of hydrogenation so the cell potential obtained in a TRFC should be similar if they are operated under the same conditions. However, the proposed TRFC would be run at a higher temperature (which should decrease the cell potential and increase the cell current) and at a higher concentration (which would increase the cell potential and the cell current).

After the system is characterized in the laboratory and the kinetics and thermodynamics are fully understood, then the information acquired can be used to model a flow system and eventually be used to make a fully functional prototype. A

thermally regenerative fuel cell attached to a functional diesel engine would be a good demonstration of the technology and would increase the value of the TRFC for potential investors who may be interested in commercialization. Construction of a functional prototype system would also allow not only for optimization of the operating parameters (flow rates, catalyst loadings, temperatures, etc.), it would also allow a more detailed economic analysis as the amount and cost of the catalysts and membranes become known. Commercialization is the key to getting the technology used in the real world where it can have an actual impact on the way the transportation industry uses fuel.

A thermally regenerative fuel cell system has applicability outside of the intended use as a device to increase fuel efficiency in transportation. It could be used anywhere electricity is particularly valuable and where waste heat generation is not desireable. One example would be for portable military applications. Additionally it would be valuable in isolated areas where the cost of delivering fuel is high as fewer fuel shipments would be required. This could be isolated areas such as research stations, northern communities, or indigenous communities.

References

(1) Einstein, A. The electrodynamic moving body. *Annalen Der Physik* **1905***, 17*, 891-921.

(2) Karl, D. M.; Wirsen, C. O.; Jannasch, H. W. Deep-Sea Primary Production at the Galapagos Hydrothermal Vents. *Science* **1980***, 207*, 1345-1347.

(3) Dunnett, D.; Wallace, J. S. Electricity generation from wave power in Canada. *Renewable Energy* **2009***, 34*, 179-195.

(4) Valerio, D.; Beirao, P.; da Costa, J. S. Optimisation of wave energy extraction with the Archimedes Wave Swing. *Ocean Eng.* **2007***, 34*, 2330-2344.

(5) Hoffert, M. I.; Caldeira, K.; Benford, G.; Criswell, D. R.; Green, C.; Herzog, H.; Jain, A. K.; Kheshgi, H. S.; Lackner, K. S.; Lewis, J. S.; Lightfoot, H. D.; Manheimer, W.; Mankins, J. C.; Mauel, M. E.; Perkins, L. J.; Schlesinger, M. E.; Volk, T.; Wigley, T. M. L. Advanced technology paths to global climate stability: Energy for a greenhouse planet. *Science* **2002***, 298*, 981-987.

(6) Kalogirou, S. A. Solar thermal collectors and applications. *Progress in Energy and Combustion Science* **2004***, 30*, 231-295.

(7) Axtmann, R. C. Environmental-Impact of a Geothermal Power-Plant. *Science* **1975***, 187*, 795-803.

(8) Baker, C. Tidal Power. *Energy Policy* **1991***, 19*, 792-797.

(9) Devell, L.; Tovedal, H.; Bergstrom, U.; Appelgren, A.; Chyssler, J.; Andersson, L. Initial Observations of Fallout from the Reactor Accident at Chernobyl. *Nature* **1986**, *321*, 192-193.

(10) Peterson, C. H.; Rice, S. D.; Short, J. W.; Esler, D.; Bodkin, J. L.; Ballachey, B. E.; Irons, D. B. Long-term ecosystem response to the Exxon Valdez oil spill. *Science* **2003**, *302*, 2082-2086.

(11) Shindell, D. T.; Miller, R. L.; Schmidt, G. A.; Pandolfo, L. Simulation of recent northern winter climate trends by greenhouse-gas forcing. *Nature* **1999**, *399*, 452-455.

(12) Weast, R. C. Handbook of chemistry and physics : a ready-reference book of chemical and physical data. 90th Edition, CRC Press, Boca Raton, FL **2009**

(13) Balat, M. Potential importance of hydrogen as a future solution to environmental and transportation problems. *Int J Hydrogen Energy* **2008**, *33*, 4013-4029.

(14) Barreto, L.; Makihira, A.; Riahi, K. The hydrogen economy in the 21st century: a sustainable development scenario. *Int J Hydrogen Energy* **2003**, *28*, 267-284.

(15) Bockris, J. O. M. Hydrogen economy in the future. *Int J Hydrogen Energy* **1999**, *24*, 1-15.

(16) Conte, M.; Iacobazzi, A.; Ronchetti, M.; Vellone, R. Hydrogen economy for a sustainable development: state-of-the-art and technological perspectives. *J. Power Sources* **2001**, *100*, 171-187.

(17) Crabtree, G. W.; Dresselhaus, M. S.; Buchanan, M. V. The hydrogen economy. *Phys Today* **2004**, *57*, 39-44.

(18) Dunn, S. Hydrogen futures: toward a sustainable energy system. *Int J Hydrogen Energy* **2002***, 27*, 235-264.

(19) Elam, C. C.; Padro, C. E. G.; Sandrock, G.; Luzzi, A.; Lindblad, P.; Hagen, E. F. Realizing the hydrogen future: the International Energy Agency's efforts to advance hydrogen energy technologies. *Int J Hydrogen Energy* **2003***, 28*, 601-607.

(20) Gregory, D. P. Hydrogen Economy. *Sci. Am.* **1973***, 228*, 13-21.

(21) Marban, G.; Vales-Solis, T. Towards the hydrogen economy? *Int J Hydrogen Energy* **2007***, 32*, 1625-1637.

(22) Muradov, N. Z.; Veziroglu, T. N. From hydrocarbon to hydrogen-carbon to hydrogen economy. *Int J Hydrogen Energy* **2005***, 30*, 225-237.

(23) Muradov, N. Z.; Veziroglu, T. N. "Green" path from fossil-based to hydrogen economy: An overview of carbon-neutral technologies. *Int J Hydrogen Energy* **2008***, 33*, 6804-6839.

(24) Schultz, M. G.; Diehl, T.; Brasseur, G. P.; Zittel, W. Air pollution and climate-forcing impacts of a global hydrogen economy. *Science* **2003***, 302*, 624-627.

(25) White, C. M.; Steeper, R. R.; Lutz, A. E. The hydrogen-fueled internal combustion engine: a technical review. *Int J Hydrogen Energy* **2006***, 31*, 1292-1305.

(26) Mitchell, J. F. B.; Johns, T. C.; Gregory, J. M.; Tett, S. F. B. Climate Response to Increasing Levels of Greenhouse Gases and Sulfate Aerosols. *Nature* **1995***, 376*, 501-504.

(27) Atkinson, R. Atmospheric chemistry of VOCs and NOx. *Atmos. Environ.* **2000***, 34*, 2063-2101.

(28) Baldasano, J. M.; Valera, E.; Jimenez, P. Air quality data from large cities. *Sci. Total Environ.* **2003***, 307*, 141-165.

(29) Dickerson, R. R.; Kondragunta, S.; Stenchikov, G.; Civerolo, K. L.; Doddridge, B. G.; Holben, B. N. The impact of aerosols on solar ultraviolet radiation and photochemical smog. *Science* **1997***, 278*, 827-830.

(30) Brunekreef, B.; Holgate, S. T. Air pollution and health. *Lancet* **2002***, 360*, 1233-1242.

(31) Rogge, W. F.; Hildemann, L. M.; Mazurek, M. A.; Cass, G. R.; Simoneit, B. R. T. Sources of Fine Organic Aerosol .2. Noncatalyst and Catalyst-Equipped Automobiles and Heavy-Duty Diesel Trucks. *Environ. Sci. Technol.* **1993***, 27*, 636-651.

(32) Schauer, J. J.; Rogge, W. F.; Hildemann, L. M.; Mazurek, M. A.; Cass, G. R. Source apportionment of airborne particulate matter using organic compounds as tracers. *Atmos. Environ.* **1996***, 30*, 3837-3855.

(33) Lugar, R. G.; Woolsey, R. J. The new petroleum. *Foreign Affairs* **1999***, 78*, 88-+.

(34) Soderbergh, B.; Robelius, F.; Aleklett, K. A crash programme scenario for the Canadian oil sands industry. *Energy Policy* **2007***, 35*, 1931-1947.

(35) James, K. H. The Venezuelan hydrocarbon habitat, part 2: Hydrocarbon occurrences and generated-accumulated volumes. *J. Pet. Geol.* **2000***, 23*, 133-164.

(36) Klara, S. M.; Srivastava, R. D. US DOE integrated collaborative technology development program for CO2 separation and capture. *Environ. Prog.* **2002***, 21*, 247-253.

(37) Liang, Y.; Harrison, D. P.; Gupta, R. P.; Green, D. A.; McMichael, W. J. Carbon dioxide capture using dry sodium-based sorbents. *Energy Fuels* **2004***, 18*, 569-575.

(38) Pennline, H. W.; Luebke, D. R.; Jones, K. L.; Myers, C. R.; Morsi, B. I.; Heintz, Y. J.; Ilconich, J. B. Progress in carbon dioxide capture and separation research for gasification-based power generation point sources. *Fuel Process Technol* **2008**, *89*, 897-907.

(39) Rau, G. H. CO2 Mitigation via Capture and Chemical Conversion in Seawater. *Environ. Sci. Technol.* **2011**, *45*, 1088-1092.

(40) White, C. M.; Strazisar, B. R.; Granite, E. J.; Hoffman, J. S.; Pennline, H. W. Separation and capture of CO2 from large stationary sources and sequestration in geological formations - Coalbeds and deep saline aquifers. *J. Air Waste Manage. Assoc.* **2003**, *53*, 645-715.

(41) Park, T. K.; Kim, S. K. Tritium: Its generation and pathways to the environment at CANDU 6 generating stations. *Nucl. Eng. Des.* **1996**, *163*, 405-411.

(42) Spiegel, C. S. Designing and Building Fuel Cells.

(43) Louthan, M. R.; Rawl, D. E.; Caskey, G. R.; Donovan, J. A. Hydrogen Embrittlement of Metals. *Materials Science and Engineering* **1972**, *10*, 357-&.

(44) Dobbin, L. Paracelsus and the discovery of hydrogen. *J. Chem. Educ.* **1932**, *9*, 1122-null.

(45) Ahmed, S.; Krumpelt, M. Hydrogen from hydrocarbon fuels for fuel cells. *Int J Hydrogen Energy* **2001**, *26*, 291-301.

(46) Cortright, R. D.; Davda, R. R.; Dumesic, J. A. Hydrogen from catalytic reforming of biomass-derived hydrocarbons in liquid water. *Nature* **2002**, *418*, 964-967.

(47) Chiesa, P.; Consonni, S.; Kreutz, T.; Williams, R. Co-production of hydrogen, electricity and CO2 from coal with commercially ready technology. PartA: Performance and emissions. *Int J Hydrogen Energy* **2005***, 30*, 747-767.

(48) Stuermer, D. H.; Ng, D. J.; Morris, C. J. Organic Contaminants in Groundwater Near an Underground Coal-Gasification Site in Northeastern Wyoming. *Environ. Sci. Technol.* **1982***, 16*, 582-587.

(49) Ashcroft, A. T.; Cheetham, A. K.; Green, M. L. H.; Vernon, P. D. F. Partial Oxidation of Methane to Synthesis Gas-using Carbon-Dioxide. *Nature* **1991***, 352*, 225-226.

(50) Dissanayake, D.; Rosynek, M. P.; Kharas, K. C. C.; Lunsford, J. H. Partial Oxidation of Methane to Carbon-Monoxide and Hydrogen Over a Ni/al2o3 Catalyst. *Journal of Catalysis* **1991***, 132*, 117-127.

(51) Bromberg, L.; Cohn, D. R.; Rabinovich, A.; O'Brien, C.; Hochgreb, S. Plasma reforming of methane. *Energy Fuels* **1998***, 12*, 11-18.

(52) Bromberg, L.; Cohn, D. R.; Rabinovich, A.; Alexeev, N. Plasma catalytic reforming of methane. *Int J Hydrogen Energy* **1999***, 24*, 1131-1137.

(53) Wang, Y. F.; You, Y. S.; Tsai, C. H.; Wang, L. C. Production of hydrogen by plasma-reforming of methanol. *Int J Hydrogen Energy* **2010***, 35*, 9637-9640.

(54) Yao, S. L.; Okumoto, M.; Nakayama, A.; Suzuki, E. Plasma reforming and coupling of methane with carbon dioxide. *Energy Fuels* **2001***, 15*, 1295-1299.

(55) Zhou, L. M.; Xue, B.; Kogelschatz, U.; Eliasson, B. Nonequilibrium plasma reforming of greenhouse gases to synthesis gas. *Energy Fuels* **1998***, 12*, 1191-1199.

(56) Holladay, J. D.; Hu, J.; King, D. L.; Wang, Y. An overview of hydrogen production technologies. *Catalysis Today* **2009***, 139*, 244-260.

(57) Khaselev, O.; Turner, J. A. A monolithic photovoltaic-photoelectrochemical device for hydrogen production via water splitting. *Science* **1998***, 280*, 425-427.

(58) Kodama, T.; Gokon, N. Thermochernical cycles for high-temperature solar hydrogen production. *Chem. Rev.* **2007***, 107*, 4048-4077.

(59) Okeefe, D.; Allen, C.; Besenbruch, G.; Brown, L.; Norman, J.; Sharp, R.; Mccorkle, K. Preliminary-Results from Bench-Scale Testing of a Sulfur-Iodine Thermochemical Water-Splitting Cycle. *Int J Hydrogen Energy* **1982***, 7*, 381-392.

(60) Perkins, C.; Weimer, A. W. Likely near-term solar-thermal water splitting technologies. *Int J Hydrogen Energy* **2004***, 29*, 1587-1599.

(61) Grenoble, D. C.; Estadt, M. M.; Ollis, D. F. The Chemistry and Catalysis of the Water Gas Shift Reaction .1. the Kinetics Over Supported Metal-Catalysts. *Journal of Catalysis* **1981***, 67*, 90-102.

(62) Rhodes, C.; Hutchings, G. J.; Ward, A. M. Water-Gas Shift Reaction - Finding the Mechanistic Boundary. *Catalysis Today* **1995***, 23*, 43-58.

(63) Campbell, J. H. Pyrolysis of Subbituminous Coal in Relation to Insitu Coal-Gasification. *Fuel* **1978***, 57*, 217-224.

(64) Costamagna, P.; Yang, C.; Bocarsly, A. B.; Srinivasan, S. Nafion (R) 115/zirconium phosphate composite membranes for operation of PEMFCs above 100 degrees C. *Electrochim. Acta* **2002***, 47*, 1023-1033.

(65) Li, Q. F.; He, R. H.; Jensen, J. O.; Bjerrum, N. J. Approaches and recent development of polymer electrolyte membranes for fuel cells operating above 100 degrees C. *Chemistry of Materials* **2003***, 15*, 4896-4915.

(66) Zhang, J. L.; Xie, Z.; Zhang, J. J.; Tanga, Y. H.; Song, C. J.; Navessin, T.; Shi, Z. Q.; Song, D. T.; Wang, H. J.; Wilkinson, D. P.; Liu, Z. S.; Holdcroft, S. High temperature PEM fuel cells. *J. Power Sources* **2006***, 160*, 872-891.

(67) Antoine, O.; Bultel, Y.; Durand, R. Oxygen reduction reaction kinetics and mechanism on platinum nanoparticles inside Nafion (R). *J Electroanal Chem* **2001***, 499*, 85-94.

(68) Ferreira, P. J.; la O', G. J.; Shao-Horn, Y.; Morgan, D.; Makharia, R.; Kocha, S.; Gasteiger, H. A. Instability of Pt/C electrocatalysts in proton exchange membrane fuel cells - A mechanistic investigation. *J. Electrochem. Soc.* **2005***, 152*, A2256-A2271.

(69) Litster, S.; McLean, G. PEM fuel cell electrodes. *J. Power Sources* **2004***, 130*, 61-76.

(70) Tuber, K.; Pocza, D.; Hebling, C. Visualization of water buildup in the cathode of a transparent PEM fuel cell. *J. Power Sources* **2003***, 124*, 403-414.

(71) Nam, J. H.; Kaviany, M. Effective diffusivity and water-saturation distribution in single- and two-layer PEMFC diffusion medium. *Int. J. Heat Mass Transfer* **2003***, 46*, 4595-4611.

(72) Fernandez, J. L.; Raghuveer, V.; Manthiram, A.; Bard, A. J. Pd-Ti and Pd-Co-Au electrocatalysts as a replacement for platinum for oxygen reduction in proton exchange membrane fuel cells. *J. Am. Chem. Soc.* **2005***, 127*, 13100-13101.

(73) Stamenkovic, V. R.; Fowler, B.; Mun, B. S.; Wang, G. F.; Ross, P. N.; Lucas, C. A.; Markovic, N. M. Improved oxygen reduction activity on Pt3Ni(111) via increased surface site availability. *Science* **2007***, 315*, 493-497.

(74) Wang, B. Recent development of non-platinum catalysts for oxygen reduction reaction. *J. Power Sources* **2005***, 152*, 1-15.

(75) Baschuk, J. J.; Li, X. G. Carbon monoxide poisoning of proton exchange membrane fuel cells. *Int. J. Energy Res.* **2001***, 25*, 695-713.

(76) United States Department of Energy

Targets for On-Board Hydrogen Storage Systems: Current R&D Focus is on 2010 Targets. *http://www1.eere.energy.gov/hydrogenandfuelcells/storage/pdfs/targets_onboard_hydro_storage.pdf* (accessed 02/13, 2008).

(77) Eberle, U.; Felderhoff, M.; Schuth, F. Chemical and Physical Solutions for Hydrogen Storage. *Angewandte Chemie-International Edition* **2009***, 48*, 6608-6630.

(78) Zuttel, A. Hydrogen storage methods. *Naturwissenschaften* **2004***, 91*, 157-172.

(79) Aceves, S. M.; Berry, G. D. Thermodynamics of insulated pressure vessels for vehicular hydrogen storage. *Journal of Energy Resources Technology-Transactions of the Asme* **1998***, 120*, 137-142.

(80) Aceves, S. M.; Berry, G. D.; Martinez-Frias, J.; Espinosa-Loza, F. Vehicular storage of hydrogen in insulated pressure vessels. *Int J Hydrogen Energy* **2006***, 31*, 2274-2283.

(81) Aceves, S. M.; Berry, G. D.; Rambach, G. D. Insulated pressure vessels for hydrogen storage on vehicles. *Int J Hydrogen Energy* **1998***, 23*, 583-591.

(82) Aceves, S. M.; Espinosa-Loza, F.; Ledesma-Orozco, E.; Ross, T. O.; Weisberg, A. H.; Brunner, T. C.; Kircher, O. High-density automotive hydrogen storage with cryogenic capable pressure vessels. *Int J Hydrogen Energy* **2010***, 35*, 1219-1226.

(83) Aceves, S. M.; Martinez-Frias, J.; Garcia-Villazana, O. Analytical and experimental evaluation of insulated pressure vessels for cryogenic hydrogen storage. *Int J Hydrogen Energy* **2000***, 25*, 1075-1085.

(84) Ahluwalia, R. K.; Peng, J. K. Dynamics of cryogenic hydrogen storage in insulated pressure vessels for automotive applications. *Int J Hydrogen Energy* **2008***, 33*, 4622-4633.

(85) Ananthachar, V.; Duffy, J. J. Efficiencies of hydrogen storage systems onboard fuel cell vehicles. *Solar Energy* **2005***, 78*, 687-694.

(86) Berry, G. D.; Aceves, S. M. Onboard storage alternatives for hydrogen vehicles. *Energy Fuels* **1998***, 12*, 49-55.

(87) Sarkar, A.; Banerjee, R. Net energy analysis of hydrogen storage options. *Int J Hydrogen Energy* **2005***, 30*, 867-877.

(88) Sherif, S. A.; Zeytinoglu, N.; Veziroglu, T. N. Liquid hydrogen: Potential, problems, and a proposed research program. *International Journal of Hydrogen Energy,* **1997***, 22*, 683-688.

(89) Maytal, B. Z.; Shavit, A. On the Joule-Thomson integral inversion curves of quantum gases. *Cryogenics* **1997***, 37*, 33-38.

(90) Bonhoeffer, K. F.; Harteck, P. Para- and ortho hydrogen. *Zeitschrift Fur Physikalische Chemie-Abteilung B-Chemie Der Elementarprozesse Aufbau Der Materie* **1929**, *4*, 113-141.

(91) Matsumoto, M.; Espenson, J. H. Kinetics of the interconversion of parahydrogen and orthohydrogen catalyzed by paramagnetic complex ions. *J. Am. Chem. Soc.* **2005**, *127*, 11447-11453.

(92) Chahine, R.; Bose, T. K. Low-Pressure Adsorption Storage of Hydrogen. *Int J Hydrogen Energy* **1994**, *19*, 161-164.

(93) Chambers, A.; Park, C.; Baker, R. T. K.; Rodriguez, N. M. Hydrogen storage in graphite nanofibers. *J Phys Chem B* **1998**, *102*, 4253-4256.

(94) Chen, P.; Wu, X.; Lin, J.; Tan, K. L. High H-2 uptake by alkali-doped carbon nanotubes under ambient pressure and moderate temperatures. *Science* **1999**, *285*, 91-93.

(95) Darkrim, F. L.; Malbrunot, P.; Tartaglia, G. P. Review of hydrogen storage by adsorption in carbon nanotubes. *Int J Hydrogen Energy* **2002**, *27*, 193-202.

(96) Dillon, A. C.; Jones, K. M.; Bekkedahl, T. A.; Kiang, C. H.; Bethune, D. S.; Heben, M. J. Storage of hydrogen in single-walled carbon nanotubes. *Nature* **1997**, *386*, 377-379.

(97) Dillon, A. C.; Heben, M. J. Hydrogen storage using carbon adsorbents: past, present and future. *Applied Physics A-Materials Science & Processing* **2001**, *72*, 133-142.

(98) Cheng, H. M.; Yang, Q. H.; Liu, C. Hydrogen storage in carbon nanotubes. *Carbon* **2001**, *39*, 1447-1454.

(99) Lee, S. M.; An, K. H.; Lee, Y. H.; Seifert, G.; Frauenheim, T. A hydrogen storage mechanism in single-walled carbon nanotubes. *J. Am. Chem. Soc.* **2001**, *123*, 5059-5063.

(100) Panella, B.; Hirscher, M.; Roth, S. Hydrogen adsorption in different carbon nanostructures. *Carbon* **2005**, *43*, 2209-2214.

(101) Amankwah, K. A. G.; Noh, J. S.; Schwarz, J. A. Hydrogen Storage on Superactivated Carbon at Refrigeration Temperatures. *Int J Hydrogen Energy* **1989**, *14*, 437-447.

(102) Anson, A.; Benham, M.; Jagiello, J.; Callejas, M. A.; Benito, A. M.; Maser, W. K.; Zuttel, A.; Sudan, P.; Martinez, M. T. Hydrogen adsorption on a single-walled carbon nanotube material: a comparative study of three different adsorption techniques. *Nanotechnology* **2004**, *15*, 1503-1508.

(103) Baughman, R. H.; Zakhidov, A. A.; de Heer, W. A. Carbon nanotubes - the route toward applications. *Science* **2002**, *297*, 787-792.

(104) Langmuir, I. The Adsorption of Gases on Plane Surfaces of Glass, Mica and Platinum. *J. Am. Chem. Soc.* **1918**, *40*, 1361-1403.

(105) Brunauer, S.; Emmett, P. H.; Teller, E. Adsorption of Gases in Multimolecular Layers. *J. Am. Chem. Soc.* **1938**, *60*, 309-319.

(106) Schlapbach, L.; Zuttel, A. Hydrogen-storage materials for mobile applications. *Nature* **2001**, *414*, 353-358.

(107) Dinca, M.; Long, J. R. Strong H-2 binding and selective gas adsorption within the microporous coordination solid Mg-3(O2C-C10H6-CO2)(3). *J. Am. Chem. Soc.* **2005**, *127*, 9376-9377.

(108) Dinca, M.; Yu, A. F.; Long, J. R. Microporous metal-organic frameworks incorporating 1,4-benzeneditetrazolate: Syntheses, structures, and hydrogen storage properties. *J. Am. Chem. Soc.* **2006***, 128*, 8904-8913.

(109) Chen, B. L.; Eddaoudi, M.; Hyde, S. T.; O'Keeffe, M.; Yaghi, O. M. Interwoven metal-organic framework on a periodic minimal surface with extra-large pores. *Science* **2001***, 291*, 1021-1023.

(110) Chen, B. L.; Ockwig, N. W.; Millward, A. R.; Contreras, D. S.; Yaghi, O. M. High H-2 adsorption in a microporous metal-organic framework with open metal sites. *Angewandte Chemie-International Edition* **2005***, 44*, 4745-4749.

(111) Kaye, S. S.; Dailly, A.; Yaghi, O. M.; Long, J. R. Impact of preparation and handling on the hydrogen storage properties of Zn4O(1,4-benzenedicarboxylate)(3) (MOF-5). *J. Am. Chem. Soc.* **2007***, 129*, 14176.

(112) Rosi, N. L.; Eckert, J.; Eddaoudi, M.; Vodak, D. T.; Kim, J.; O'Keeffe, M.; Yaghi, O. M. Hydrogen storage in microporous metal-organic frameworks. *Science* **2003***, 300*, 1127-1129.

(113) Sun, D. F.; Ma, S. Q.; Ke, Y. X.; Collins, D. J.; Zhou, H. C. An interweaving MOF with high hydrogen uptake. *J. Am. Chem. Soc.* **2006***, 128*, 3896-3897.

(114) Wong-Foy, A. G.; Matzger, A. J.; Yaghi, O. M. Exceptional H-2 saturation uptake in microporous metal-organic frameworks. *J. Am. Chem. Soc.* **2006***, 128*, 3494-3495.

(115) Dybtsev, D. N.; Chun, H.; Yoon, S. H.; Kim, D.; Kim, K. Microporous manganese formate: A simple metal-organic porous material with high framework stability and highly selective gas sorption properties. *J. Am. Chem. Soc.* **2004***, 126*, 32-33.

(116) Dinca, M.; Dailly, A.; Liu, Y.; Brown, C. M.; Neumann, D. A.; Long, J. R. Hydrogen storage in a microporous metal-organic framework with exposed Mn2+ coordination sites. *J. Am. Chem. Soc.* **2006***, 128*, 16876-16883.

(117) Rowsell, J. L. C.; Millward, A. R.; Park, K. S.; Yaghi, O. M. Hydrogen sorption in functionalized metal-organic frameworks. *J. Am. Chem. Soc.* **2004***, 126*, 5666-5667.

(118) Greenwood, N. N.; Earnshaw, A. Chemistry of the Elements (2nd Edition). **1998**.

(119) Anani, A.; Visintin, A.; Petrov, K.; Srinivasan, S.; Reilly, J. J.; Johnson, J. R.; Schwarz, R. B.; Desch, P. B. Alloys for Hydrogen Storage in Nickel-Hydrogen and Nickel Metal Hydride Batteries. *J. Power Sources* **1994***, 47*, 261-275.

(120) Berube, V.; Radtke, G.; Dresselhaus, M.; Chen, G. Size effects on the hydrogen storage properties of nanostructured metal hydrides: A review. *Int. J. Energy Res.* **2007***, 31*, 637-663.

(121) Bobet, J. L.; Akiba, E.; Nakamura, Y.; Darriet, B. Study of Mg-M (M = Co, Ni and Fe) mixture elaborated by reactive mechanical alloying - hydrogen sorption properties. *Int J Hydrogen Energy* **2000***, 25*, 987-996.

(122) Iwakura, C.; Oura, T.; Inoue, H.; Matsuoka, M. Effects of substitution with foreign metals on the crystallographic, thermodynamic and electrochemical properties of AB(5)-type hydrogen storage alloys. *Electrochim. Acta* **1996***, 41*, 117-121.

(123) Bogdanovic, B.; Brand, R. A.; Marjanovic, A.; Schwickardi, M.; Tolle, J. Metal-doped sodium aluminium hydrides as potential new hydrogen storage materials. *J. Alloys Compounds* **2000***, 302*, 36-58.

(124) Bogdanovic, B.; Schwickardi, M. Ti-doped alkali metal aluminium hydrides as potential novel reversible hydrogen storage materials. *J. Alloys Compounds* **1997***, 253*, 1-9.

(125) Amendola, S. C.; Sharp-Goldman, S. L.; Janjua, M. S.; Spencer, N. C.; Kelly, M. T.; Petillo, P. J.; Binder, M. A safe, portable, hydrogen gas generator using aqueous borohydride solution and Ru catalyst. *Int J Hydrogen Energy* **2000***, 25*, 969-975.

(126) Chandra, M.; Xu, Q. A high-performance hydrogen generation system: Transition metal-catalyzed dissociation and hydrolysis of ammonia-borane. *J. Power Sources* **2006***, 156*, 190-194.

(127) Fakioglu, E.; Yurum, Y.; Veziroglu, T. N. A review of hydrogen storage systems based on boron and its compounds. *Int J Hydrogen Energy* **2004***, 29*, 1371-1376.

(128) Hamilton, C. W.; Baker, R. T.; Staubitz, A.; Manners, I. B-N compounds for chemical hydrogen storage. *Chem. Soc. Rev.* **2009***, 38*, 279-293.

(129) Keaton, R. J.; Blacquiere, J. M.; Baker, R. T. Base metal catalyzed dehydrogenation of ammonia-borane for chemical hydrogen storage. *J. Am. Chem. Soc.* **2007***, 129*, 1844-+.

(130) Kim, J. H.; Lee, H.; Han, S. C.; Kim, H. S.; Song, M. S.; Lee, J. Y. Production of hydrogen from sodium borohydride in alkaline solution: development of catalyst with high performance. *Int J Hydrogen Energy* **2004***, 29*, 263-267.

(131) Kojima, Y.; Suzuki, K.; Fukumoto, K.; Sasaki, M.; Yamamoto, T.; Kawai, Y.; Hayashi, H. Hydrogen generation using sodium borohydride solution and metal catalyst coated on metal oxide. *Int J Hydrogen Energy* **2002***, 27*, 1029-1034.

(132) Kojima, Y.; Haga, T. Recycling process of sodium metaborate to sodium borohydride. *Int J Hydrogen Energy* **2003***, 28*, 989-993.

(133) Kong, V. C. Y.; Foulkes, F. R.; Kirk, D. W.; Hinatsu, J. T. Development of hydrogen storage for fuel cell generators. I: Hydrogen generation using hydrolysis hydrides. *Int J Hydrogen Energy* **1999***, 24*, 665-675.

(134) Krishnan, P.; Yang, T. H.; Lee, W. Y.; Kim, C. S. PtRu-LiCoO2 - an efficient catalyst for hydrogen generation from sodium borohydride solutions. *J. Power Sources* **2005***, 143*, 17-23.

(135) Nguyen, M. T.; Nguyen, V. S.; Matus, M. H.; Gopakumar, G.; Dixon, D. A. Molecular mechanism for H-2 release from BH3NH3, including the catalytic role of the lewis acid BH3. *Journal of Physical Chemistry a* **2007***, 111*, 679-690.

(136) Orimo, S.; Nakamori, Y.; Eliseo, J. R.; Zuettel, A.; Jensen, C. M. Complex hydrides for hydrogen storage. *Chem. Rev.* **2007***, 107*, 4111-4132.

(137) Pons, V.; Baker, R. T. Soluble Boron-Nitrogen High Polymers from Metal-Complex-Catalyzed Amine Borane Dehydrogenation. *Angewandte Chemie-International Edition* **2008***, 47*, 9600-9602.

(138) Stephens, F. H.; Baker, R. T.; Matus, M. H.; Grant, D. J.; Dixon, D. A. Acid initiation of ammonia-borane dehydrogenation for hydrogen storage. *Angewandte Chemie-International Edition* **2007***, 46*, 746-749.

(139) Stephens, F. H.; Pons, V.; Baker, R. T. Ammonia - borane: the hydrogen source par excellence? *Dalton Transactions* **2007**, 2613-2626.

(140) Vajo, J. J.; Skeith, S. L.; Mertens, F. Reversible storage of hydrogen in destabilized LiBH4. *J Phys Chem B* **2005***, 109*, 3719-3722.

(141) Wechsler, D.; Cui, Y.; Dean, D.; Davis, B.; Jessop, P. G. Production of H-2 from Combined Endothermic and Exothermic Hydrogen Carriers. *J. Am. Chem. Soc.* **2008***, 130*, 17195-17203.

(142) Wechsler, D.; Davis, B.; Jessop, P. G. The dehydrogenation of combined organic and inorganic hydrogen-storage carriers. *Canadian Journal of Chemistry-Revue Canadienne De Chimie* **2010***, 88*, 548-555.

(143) Zuttel, A.; Wenger, P.; Rentsch, S.; Sudan, P.; Mauron, P.; Emmenegger, C. LiBH4 a new hydrogen storage material. *J. Power Sources* **2003***, 118*, 1-7.

(144) Chen, P.; Xiong, Z. T.; Luo, J. Z.; Lin, J. Y.; Tan, K. L. Interaction of hydrogen with metal nitrides and imides. *Nature* **2002***, 420*, 302-304.

(145) Matsunaga, T.; Buchter, F.; Mauron, P.; Bielman, A.; Nakamori, Y.; Orimo, S.; Ohba, N.; Miwa, K.; Towata, S.; Zuttel, A. Hydrogen storage properties of Mg[BH4](2). *J. Alloys Compounds* **2008***, 459*, 583-588.

(146) Mauron, P.; Buchter, F.; Friedrichs, O.; Remhof, A.; Bielmann, M.; Zwicky, C. N.; Zuttel, A. Stability and reversibility of LiBH4. *J Phys Chem B* **2008***, 112*, 906-910.

(147) Sebastian, D.; Bordeje, E. G.; Calvillo, L.; Lazaro, M. J.; Moliner, R. Hydrogen storage by decalin dehydrogenation/naphthalene hydrogenation pair over platinum catalysts supported on activated carbon. *Int J Hydrogen Energy* **2008***, 33*, 1329-1334.

(148) Moores, A.; Poyatos, M.; Luo, Y.; Crabtree, R. H. Catalysed low temperature H-2 release from nitrogen heterocycles. *New Journal of Chemistry* **2006***, 30*, 1675-1678.

(149) Crabtree, R. H. Hydrogen storage in liquid organic heterocycles. *Energy & Environmental Science* **2008**, *1*, 134-138.

(150) Wang, Z. H.; Tonks, I.; Belli, J.; Jensen, C. M. Dehydrogenation of N-ethyl perhydrocarbazole catalyzed by PCP pincer iridium complexes: Evaluation of a homogenous hydrogen storage system. *Journal of Organometallic Chemistry* **2009**, *694*, 2854-2857.

(151) Sotoodeh, F.; Smith, K. J. Kinetics of Hydrogen Uptake and Release from Heteroaromatic Compounds for Hydrogen Storage. *Ind Eng Chem Res* **2010**, *49*, 1018-1026.

(152) Clot, E.; Eisenstein, O.; Crabtree, R. H. Computational structure-activity relationships in H-2 storage: how placement of N atoms affects release temperatures in organic liquid storage materials. *Chemical Communications* **2007**, 2231-2233.

(153) Cui, Y.; Kwok, S.; Bucholtz, A.; Davis, B.; Whitney, R. A.; Jessop, P. G. The effect of substitution on the utility of piperidines and octahydroindoles for reversible hydrogen storage. *New Journal of Chemistry* **2008**, *32*, 1027-1037.

(154) Dean, D.; Davis, B.; Jessop, P. G. The effect of temperature, catalyst and sterics on the rate of N-heterocycle dehydrogenation for hydrogen storage. *New Journal of Chemistry* **2011**, *35*, 417-422.

(155) Cardona, E.; Piacentino, A. A methodology for sizing a trigeneration plant in mediterranean areas. *Appl. Therm. Eng.* **2003**, *23*, 1665-1680.

(156) Srikhirin, P.; Aphornratana, S.; Chungpaibulpatana, S. A review of absorption refrigeration technologies. *Renewable & Sustainable Energy Reviews* **2001**, *5*, 343-372.

(157) Hung, T. C. Waste heat recovery of organic Rankine cycle using dry fluids. *Energy Conversion and Management* **2001***, 42*, 539-553.

(158) Saleh, B.; Koglbauer, G.; Wendland, M.; Fischer, J. Working fluids for low-temperature organic Rankine cycles. *Energy* **2007***, 32*, 1210-1221.

(159) Atkins, P.; de Paula, J. In *Physical Chemistry;* W. H. Freeman and Company: New York, 2002; , pp 1139.

(160) Carnot, S. In *Reflections on the Motive Power of Heat and on Machines Fitted to Develop That Power;* Thurston, R. H., Ed.; J. Wiley & Sons: New York, 1890; .

(161) Mozurkewich, M.; Berry, R. S. Optimal Paths for Thermodynamic Systems - the Ideal Otto Cycle. *J. Appl. Phys.* **1982***, 53*, 34-42.

(162) Bonnick, A. Automotive Science and Mathematics, Butterworth-Heinemann, **2008**.

(163) Stone, R.; Ball, J. K. In *Chapter 2: Thermodynamics of Prime Movers;* Automotive Engineering Fundamentals; Society of Automotive Engineers: 2004; pp 17.

(164) Rowe, D. M. Thermoelectrics, an environmentally-friendly source of electrical power. *Renewable Energy* **1999***, 16*, 1251-1256.

(165) Slack, G. A.; Hussain, M. A. The Maximum Possible Conversion Efficiency of Silicon-Germanium Thermoelectric Generators. *J. Appl. Phys.* **1991***, 70*, 2694-2718.

(166) Bhushan, B. In *4.3.2 Thermoelectric Applications;* Springer Handbook of Nanotechnology; Springer - Verlag: 2004; pp 133.

(167) Wilkins, D. R. A Unified Theoretical Description of Thermionic Converter Performance Characteristics. *J. Appl. Phys.* **1968***, 39*, 2452-&.

(168) Lundin, J.; Holmlid, L. Electron-Excitation Energy-Transfer from Highly Excited Cs Atoms Forming High Rydberg State Atoms and Molecules. *J. Phys. Chem.* **1991**, *95*, 1029-1034.

(169) Coutts, T. J. A review of progress in thermophotovoltaic generation of electricity. *Renewable & Sustainable Energy Reviews* **1999**, *3*, 77-184.

(170) Pralle, M. U.; Moelders, N.; McNeal, M. P.; Puscasu, I.; Greenwald, A. C.; Daly, J. T.; Johnson, E. A.; George, T.; Choi, D. S.; El-Kady, I.; Biswas, R. Photonic crystal enhanced narrow-band infrared emitters. *Appl. Phys. Lett.* **2002**, *81*, 4685-4687.

(171) Ando, Y.; Aoyama, Y.; Sasaki, T.; Saito, Y.; Hatori, H.; Tanaka, T. Effect of catalytic and electrochemical acetone hydrogenation on the I-V characteristics of an acetone. *Bull. Chem. Soc. Jpn.* **2004**, *77*, 1855-1859.

(172) Wasserscheid, P.; Welton, T. In *Ionic Liquids in Synthesis;* WILEY-VCH Verlag GmbH & Co. KGaA: Weinheim, 2003; , pp 364.

(173) Stracke, M. P.; Ebeling, G.; Cataluna, R.; Dupont, J. Hydrogen-storage materials based on imidazolium ionic liquids. *Energy Fuels* **2007**, *21*, 1695-1698.

(174) Pez, G. P.; Cooper, A. C.; Scott, A. R. Worldwide Patent WO/2009/005872, 2009.

(175) Buffat, M. G. P. Synthesis of piperidines. *Tetrahedron* **2004**, *60*, 1701-1729.

(176) Meyer, E. A.; Castellano, R. K.; Diederich, F. Interactions with aromatic rings in chemical and biological recognition. *Angewandte Chemie-International Edition* **2003**, *42*, 1210-1250.

(177) Ngo, H. L.; LeCompte, K.; Hargens, L.; McEwen, A. B. Thermal properties of imidazolium ionic liquids. *Thermochimica Acta* **2000**, *357*, 97-102.

(178) Kosmulski, M.; Gustafsson, J.; Rosenholm, J. B. Thermal stability of low temperature ionic liquids revisited. *Thermochimica Acta* **2004***, 412*, 47-53.

(179) Emling, B. L. Some Alkyl Benzenesulfonates. *J. Am. Chem. Soc.* **1952***, 74*, 4702-4703.

(180) Freifelder, M.; Wright, H. B. Hypocholesteremic agents. I. Hydrogenation of some pyridinesulfonic and pyridinealkanesulfonic acids. *J. Med. Chem.* **1964***, 7*, 664-5.

(181) Doering, W. E.; Weil, R. A. N. Electrophilic Reactions of 2-Vinylpyridines and 4-Vinylpyridines. *J. Am. Chem. Soc.* **1947***, 69*, 2461-2466.

(182) Buschow, K. H. J.; Cahn, R. W.; Flemings, M. C.; Ilschner, B.; Kramer, E. J.; Mahajan, S. Encyclopedia of Materials - Science and Technology, Volumes 1-11.

(183) Dzyuba, S. V.; Bartsch, R. A. Expanding the polarity range of ionic liquids. *Tetrahedron Lett.* **2002***, 43*, 4657-4659.

(184) Knifton, J. F. Ethylene-Glycol from Synthesis Gas Via Ruthenium Melt Catalysis. *J. Am. Chem. Soc.* **1981***, 103*, 3959-3961.

(185) Sun, J.; Wang, L.; Zhang, S.; Li, Z.; Zhang, X.; Dai, W.; Mori, R. ZnCl2/ phosphonium halide: An efficient Lewis acid/base catalyst for the synthesis of cyclic carbonate. *Journal of Molecular Catalysis A: Chemical* **2006***, 256*, 295-300.

(186) Yang, C.; Fu, Y.; Huang, Y.; Yi, J.; Guo, Q.; Liu, L. Room-Temperature Copper-Catalyzed Carbon-Nitrogen Coupling of Aryl Iodides and Bromides Promoted by Organic Ionic Bases. *Angew. Chem. , Int. Ed.* **2009***, 48*, 7398-7401, S7398/1-S7398/182.

(187) Clayden, J.; Greeves, N.; Warren, S.; Wothers, P. In *Organic Chemistry;* Oxford University Press: New York, 2001; , pp 1512.

(188) Munro, N. B.; Talmage, S. S.; Griffin, G. D.; Waters, L. C.; Watson, A. P.; King, J. F.; Hauschild, V. The sources, fate, and toxicity of chemical warfare agent degradation products. *Environ. Health Perspect.* **1999***, 107*, 933-974.

(189) Gilman, A. The Initial Clinical Trial of Nitrogen Mustard. *Am. J. Surg.* **1963***, 105*, 574-578.

(190) Capon, B. Neighbouring Group Participation. *Quarterly Reviews* **1964***, 18*, 45-111.

(191) Wiberg, K. B.; Bader, R. F. W.; Lau, C. D. H. Theoretical-Analysis of Hydrocarbon Properties .1. Bonds, Structures, Charge Concentrations, and Charge Relaxations. *J. Am. Chem. Soc.* **1987***, 109*, 985-1001.

(192) Hulshof, J. W.; Vischer, H. F.; Verheij, M. H. P.; Fratantoni, S. A.; Smit, M. J.; de Esch, I. J. P.; Leurs, R. Synthesis and pharmacological characterization of novel inverse agonists acting on the viral-encoded chemokine receptor US28. *Bioorg. Med. Chem.* **2006***, 14*, 7213-7230.

(193) Cuthbertson, T. J.; Ibanez, M.; Rijnbrand, C. A.; Jackson, A. J.; Mittapalli, G. K.; Zhao, F.; MacDonald, J. E.; Wong-Staal, F. , Hepatitis C Virus Entry Inhibitors, WO2008021745, 2008.

(194) van Basshuysen, R.; Schäfer, F. Internal Combustion Engine Handbook - Basics, Components, Systems, and Perspectives, SAE International, **2004**.

(195) Evans, M. G.; Polanyi, M. Application of the transition-state method to the calculation of reaction velocities, especially in solution. *Trans. Faraday Soc.* **1935***, 31*, 875-94.

(196) Eyring, H. Activated complex in chemical reactions. *J. Chem. Phys.* **1935***, 3*, 107-15.

(197) Giancoli, D. C. In *Physics for Scientists and Engineers with Modern Physics;* Prentice Hall: Upper Saddle River, New Jersey, 2000; , pp 1172.

(198) Ishikawa, K.; Seki, Y.; Kita, K.; Matsuda, M.; Nishida, M.; Aoki, K. Hydrogen permeation in rapidly quenched amorphous and crystallized Nb20Ti40Ni40 alloy ribbons. *Int J Hydrogen Energy* **2011***, 36*, 1784-1792.

(199) Kim, D.; Park, Y.; Kang, S.; An, H.; Park, J. Pd-Cu-Ni ternary alloy membrane with high temperature durability for hydrogen separation and purification. *Jpn. J. Appl. Phys.* **2010***, 49*, 100208/1-100208/3.

(200) Kwon, I. M.; Song, I.; Park, Y.; Lee, J.; Yun, H.; Kim, H. The synthesis and pore property of hydrogen membranes derived from polysilazane as inorganic polymer. *J. Korean Ceram. Soc.* **2009***, 46*, 462-466.

(201) Paglieri, S. N.; Wermer, J. R.; Buxbaum, R. E.; Ciocco, M. V.; Howard, B. H.; Morreale, B. D. Development of membranes for hydrogen separation: Pd coated V-10Pd. *Energy Mater.* **2008***, 3*, 169-176.

(202) Speight, J. G. Lange's Handbook of Chemistry (16th Edition), McGraw-Hill, **2005**.

(203) Martens, J. A.; Parton, R.; Uytterhoeven, L.; Jacobs, P. A.; Froment, G. F. Selective Conversion of Decane into Branched Isomers - a Comparison of Platinum/zsm-22, Platinum/zsm-5 and Platinum Usy Zeolite Catalysts. *Applied Catalysis* **1991***, 76*, 95-116.

(204) Toyoda, K.; Nakano, Y.; Hamada, I.; Lee, K.; Yanagisawa, S.; Morikawa, Y. First-principles study of benzene on noble metal surfaces: Adsorption states and vacuum level shifts. *Surf Sci* **2009***, 603*, 2912-2922.

(205) Cyranski, M. K.; Krygowski, T. M.; Katritzky, A. R.; Schleyer, P. V. To what extent can aromaticity be defined uniquely? *J. Org. Chem.* **2002***, 67*, 1333-1338.

(206) Hartung, W. H.; Simonoff, R. Hydrogenolysis of Benzyl Groups Attached to Oxygen, Nitrogen, Or Sulfur. *Organic Reactions* **1953***, 7*, 263-326.

(207) Burke, S. D.; Danheiser, R. L. Handbook of Reagents for Organic Synthesis - Oxidizing and Reducing Agents, Wiley, **1999**.

(208) Adair, G. R. A.; Williams, J. M. J. Oxidant-free oxidation: ruthenium catalysed dehydrogenation of alcohols. *Tetrahedron Lett.* **2005***, 46*, 8233-8235.

(209) Kim, W. H.; Park, I. S.; Park, J. Acceptor-free alcohol dehydrogenation by recyclable ruthenium catalyst. *Org. Lett.* **2006***, 8*, 2543-2545.

(210) Staff, P. D. L. Chemical Resistance of Plastics and Elastomers (3rd Electronic Edition), William Andrew Publishing, **2001**.

(211) Rikukawa, M.; Sanui, K. Proton-conducting polymer electrolyte membranes based on hydrocarbon polymers. *Progress in Polymer Science* **2000***, 25*, 1463-1502.

(212) Wainright, J. S.; Wang, J. T.; Weng, D.; Savinell, R. F.; Litt, M. Acid-Doped Polybenzimidazoles - a New Polymer Electrolyte. *J. Electrochem. Soc.* **1995***, 142*, L121-L123.

(213) Jun, D.; Paar, M.; Binder, J.; Marek, J.; Pohanka, M.; Stodulka, P.; Kuca, K. Preparation and In Vitro Evaluation of Monoquaternary Inhibitors of Brain Cholinesterases. *Letters in Organic Chemistry* **2009***, 6*, 500-503.

(214) Tong, B.; Liu, Q.; Tan, Z.; Welz-Biermann, U. Thermochemistry of Alkyl Pyridinium Bromide Ionic Liquids: Calorimetric Measurements and Calculations. *Journal of Physical Chemistry a* **2010***, 114*, 3782-3787.

(215) Koizumi, T.; Fuchigami, T.; Kandeel, Z. E.; Sato, N.; Nonaka, T. Reaction-Mechanism of Cathodic Crossed Coupling of Acetone with Unsaturated-Compounds in Acidic Solution. *Bull. Chem. Soc. Jpn.* **1986***, 59*, 757-762.

(216) Koch, V. R.; Miller, L. L.; Osteryoung, R. A. Electroinitiated Friedel-Crafts Transalkylations in a Room-Temperature Molten-Salt Medium. *J. Am. Chem. Soc.* **1976***, 98*, 5277-5284.

(217) Katritzky, A. R.; Degaszafran, Z. Proton and C-13 Nmr-Studies of 1-Substituted Pyridinium Salts. *Magn. Reson. Chem.* **1989***, 27*, 1090-1093.

(218) Voltrova, S.; Srogl, J. Reaction of thiolesters with nitrogen ylides. *European Journal of Organic Chemistry* **2008**, 1677-1679.

(219) Ahmed, M.; Bronger, R. P. J.; Jackstell, R.; Kamer, P. C. L.; van Leeuwen, P. W. N. M.; Beller, M. Highly selective hydroaminomethylation of internal alkenes to give linear amines. *Chemistry-a European Journal* **2006***, 12*, 8979-8988.

(220) Forsyth, C. M.; Dean, P. M.; MacFarlane, D. R. Sodium pyridine-3-carboxylate. *Acta Crystallographica Section C-Crystal Structure Communications* **2007***, 63*, M169-M170.

(221) Bortolini, O.; De Nino, A.; Garofalo, A.; Maiuolo, L.; Russo, B. Mild Oxidative Conversion of Nitroalkanes into Carbonyl Compounds in Ionic Liquids. *Synthetic Communications* **2010***, 40*, 2483-2487.

(222) Das, D.; Dasgupta, A.; Das, P. K. Improved activity of horseradish peroxidase (HRP) in 'specifically designed' ionic liquid. *Tetrahedron Lett.* **2007***, 48*, 5635-5639.

(223) Milen, M.; Gruen, A.; Balint, E.; Dancso, A.; Keglevich, G. Solid-Liquid Phase Alkylation of N-Heterocycles: Microwave-Assisted Synthesis as an Environmentally Friendly Alternative. *Synthetic Communications* **2010***, 40*, 2291-2301.

(224) Hsieh, B. R.; Litt, M. H. Poly(N-acylethylenimines) with pendant carbazole derivatives. 1. Synthesis. *Macromolecules* **1985***, 18*, 1388-94.

Appendix A

Experimental

Heterogeneous catalysts were obtained from Strem Chemicals, Inc. (Newburyport, MA, USA) with the exception of platinum (IV) oxide and ruthenium (IV) oxide, which were obtained from Sigma-Aldrich (Oakville, ON, Canada). Palladium (II) acetate was obtained from Pressure Chemical Company (Pittsburgh, PA, USA). All reagents were obtained from Sigma-Aldrich (Oakville, ON, Canada) with the exception of 1-phenyl-1-propanol which was obtained from Acros Organics (Geel, Belgium). Solvents were obtained from Fisher Scientific Company (Ottawa, ON, Canada) with the exception of anhydrous ethanol, which was obtained from Commercial Alcohols (Chatham, ON, Canada). A palladium covered mesoporous silica monolith was provided by Jennifer Du. Amorphous silica pellets were provided by Saint-Gobain NorPro (Akron, OH, USA).

NMR Spectra were acquired on a Bruker Avance 400 MHz NMR spectrometer equipped with an autosampler (Bruker Biospin Ltd. Milton, ON, Canada). IR spectra were acquired on a Nicolet Avatar IR spectrometer (Fisher Scientific Ltd., Nepean, ON, Canada). Melting points were obtained on a capillary melting point apparatus (Arthur H. Thomas Co., Philadelphia, PA, USA). High resolution mass spectra were acquired on a

QStar XL QqTOF mass spectrometer (Applied Biosystems Inc., Foster City, CA, USA). Gas chromatography was performed on a Shimadzu Scientific Instruments GC-17A chromatograph (Columbia, MD, USA) using a DB-5 column from Agilent Technologies Canada Inc. (Mississauga, ON, Canada). X-ray crystallography data were acquired using a Bruker SMART APEX II X-ray diffractometer with graphite-monochromated Mo K_α radiation (Bruker AXS Inc. Madison, WI, USA). Thermogravimetric analysis and differential scanning calorimetry were acquired using a Simultaneous Thermal Analyzer STA 1500 (Rheometric Scientific Inc., Piscataway, NJ, USA). High pressure hydrogenations were performed in either 31 ml or 160 ml Parr stainless steel autoclaves (Parr Instrument Co., Moline, IL, USA). Fuel Cell hardware and MEAs were obtained from Fuel Cell Store (Boulder, CO, USA). Quantitative yield indicates that ≥99% of the expected mass of the desired compound was obtained after the solvent was removed. All compounds appeared to be pure by ^{1}H NMR spectroscopy and without additional solvent or impurity peaks.

A.1 Preparation of Compounds

N-Methylpyridinium Iodide

Pyridine (5.10 ml, 4.99 g, 63.1 mmol) was dispensed into a heavy walled glass pressure tube containing a magnetic stir bar. The tube was then suspended above an oil bath preheated to 150 ºC on a hot plate equipped with a magnetic stirrer. Stirring was

initiated and iodomethane (3.97 ml, 9.06 g, 63.8 mmol) was added slowly to the pyridine. After the total amount of alkyl halide was added, the pressure tube was sealed and lowered into the hot oil bath until the solution ceased boiling. At this point the tube was removed from the hot oil bath and allowed to slowly cool. After reaching ambient temperature, the contents of the pressure tube were subjected to high vacuum to remove any traces of unreacted pyridine or alkyl halide. N-Methylpyridinium iodide was obtained as a yellowish solid (13.91 g, 63.0 mmol, >99%).

Melting point 115–116 ºC (lit. 117–118 ºC)[213]

The NMR spectra are consistent with that presented in the literature.[213]

^{1}H NMR (400 MHz, DMSO-d_6) δ 9.02 (d, *J* = 5.7 Hz, 2H), 8.60 (t, *J* = 7.8 Hz, 1H), 8.15 (dd, *J* = 5.7, 7.8 Hz, 2H), 4.38 (s, 3H) ppm.

^{13}C{^{1}H} NMR (101 MHz, DMSO-d_6) δ 145.47 (s), 145.08 (s), 127.66 (s), 48.10 (s) ppm.

IR (KBr disc, ν): 3118 m, 3072 m, 3037 m, 2988 m, 2845 w, 2796 w, 2703 w, 2570 w, 2047 w, 2007 w, 1974 w, 1932 w, 1891 w, 1848 w, 1817 w, 1632 s, 1581 w, 1486 s, 1443 w, 1286 m, 1207 m, 1188 s, 1133 m, 1053 m, 1024 w, 952 w, 866 w, 769 s, 676 s, 532 w, 443 s cm^{-1}.

HRMS(ESI): m/z calcd for $[C_6H_8N]^+$ 94.0657; m/z found 94.0661.

N-Ethylpyridinium Bromide

N-Ethylpyridinium bromide was synthesized by a similar method as N-methylpyridinium iodide and was obtained as a yellowish solid (11.79 g, 62.7 mmol, >99%).

Melting point 99–100 ºC (lit. 18.15 ºC,[214] 118–119 ºC,[215] 120-121 ºC)[216] The NMR spectra are consistent with that presented in the literature.[217]

^{1}H NMR (400 MHz, DMSO-d_6) δ 9.25 (d, *J* = 6.0 Hz, 2H), 8.63 (t, *J* = 7.8 Hz, 1H), 8.18 (dd, *J* = 6.0, 7.8 Hz, 2H), 4.71 (q, *J* = 7.3 Hz, 2H), 1.53 (t, *J* = 7.3 Hz, 3H) ppm.

^{13}C{^{1}H} NMR (101 MHz, DMSO-d_6) δ 145.41 (s), 144.56 (s), 128.03 (s), 56.17 (s), 16.39 (s) ppm.

IR (KBr disc, ν): 3132 m, 3055 m, 2977 m, 2939 m, 2051 w br, 1634 s, 1583 w, 1488 s, 1465 m, 1387 w, 1318 w, 1244 w, 1217 w, 1174 s, 1092 w, 1059 w, 1029 w, 973 w, 779 m, 683 s, 555 m br, 479 m cm^{-1}.

HRMS(ESI): m/z calcd for $[C_7H_{10}N]^+$ 108.0813; m/z found 108.0816.

N-Butylpyridinium Bromide

N-Butylpyridinium bromide was synthesized by a similar method as N-methylpyridinium iodide and was obtained as a beige solid (13.55 g, 62.9 mmol, >99%).

Melting point 95-96 ºC (lit. 95–97 ºC)[218]

The NMR spectra are consistent with that presented in the literature.[218]

^{1}H NMR (400 MHz, DMSO-d_6) δ 9.34 (d, *J* = 5.7 Hz, 2H), 8.66 (t, *J* = 7.8 Hz, 1H), 8.21 (dd, *J* = 5.7, 7.8 Hz, 2H), 4.74 (t, *J* = 7.4 Hz, 2H), 1.93 – 1.82 (m, 2H), 1.30 – 1.18 (m, 2H), 0.84 (t, *J* = 7.4 Hz, 3H) ppm.

^{13}C{^{1}H} NMR (101 MHz, DMSO-d_6) δ 145.53 (s), 144.78 (s), 128.03 (s), 60.15 (s), 32.72 (s), 18.63 (s), 13.31 (s) ppm.

IR (KBr disc, ν): 3431 m br, 3133 w, 3115 m, 3080 m, 3011 s, 2963 s, 2949 s, 2934 s, 2870 s, 2727 w, 2049 w, 2002 w, 1910 w, 1702 w, 1628 s, 1577 w, 1503 m, 1487 s, 1380 m, 1321 m, 1291 m, 1247 m, 1214 m, 1169 s, 1142 m, 1113 m, 1073 m, 1056 m, 1034 m, 1022 m, 985 m, 947 m, 889 w, 826 w, 800 s, 771 s, 733 m cm^{-1}.

HRMS(ESI): m/z calcd for $[C_9H_{14}N]^+$ 136.1126; m/z found 136.1131.

N-Hexylpyridinium Bromide

N-Hexylpyridinium bromide was synthesized by a similar method as N-methylpyridinium iodide and was obtained as a viscous yellowish liquid (15.31 g, 62.7 mmol, >99%).

^1H NMR (400 MHz, DMSO-d_6) δ 9.36 (d, *J* = 5.9 Hz, 2H), 8.66 (t, *J* = 7.8 Hz, 1H), 8.17 (dd, *J* = 7.8, 5.9 Hz, 2H), 4.76 (t, *J* = 7.3 Hz, 2H), 3.87 (s, 3H), 1.81 (dt, *J* = 14.9, 7.4 Hz, 2H), 1.25 – 0.78 (m, 6H), 0.53 (t, *J* = 7.1 Hz, 3H) ppm.

$^{13}C\{^1H\}$ NMR (101 MHz, DMSO-d_6) δ 145.57 (s), 144.55 (s), 128.04 (s), 60.43 (s), 30.77 (s), 30.36 (s), 24.78 (s), 21.64 (s), 13.53 (s) ppm.

IR (KBr disc, ν): 3051 m, 2957 s, 2931 s, 2859 m, 1633 s, 1582 w, 1488 s, 1467 m, 1380 w, 1321 w, 1218 w, 1172 m, 775 m, 686 m cm^{-1}.

HRMS(ESI): m/z calcd for $[C_{11}H_{18}N]^+$ 164.1439; m/z found 164.1437.

N-Butylpiperidine

N-Butylpyridinium bromide (5.00 g, 23.1 mmol) was dissolved in 5 ml of isopropanol and was dispensed into a 160 ml stainless steel autoclave. To this was added 1 mol% equivalent of platinum (IV) oxide powder (52.5 mg, 231 μmol) and a magnetic stir bar. The autoclave was sealed and placed in an electric heating apparatus above a magnetic stirrer. Stirring was initiated and the autoclave was pressurized to approximately 10 bar of hydrogen for one minute and then slowly depressurized. This pressurization/depressurization cycle was performed three times to flush the autoclave and gas lines of air and ensure an atmosphere of hydrogen. The flushed autoclave was resealed at ambient pressure and was heated to 100 ºC. The temperature inside the autoclave was allowed to equilibrate for 30 min. The autoclave was then pressurized with 100 bar of hydrogen and sealed and the contents were left to react for a period of 16 h. The autoclave was then removed from the electric heater and immersed in an ice water bath for 15 min to rapidly cool the apparatus. The gas pressure was then slowly vented in a fumehood. The autoclave was opened and the contents were filtered through diatomaceous earth to remove the precipitated particles of platinum black. The solution was concentrated *in vacuo* to remove the isopropanol. To the resultant solid material was added a concentrated aqueous solution of sodium carbonate (~100 ml). Vigorous mixing generated a milky white suspension that was dispensed into a separatory funnel and an additional ~10 ml of concentrated sodium carbonate solution was used to rinse any remaining residue from the original flask into the separatory funnel. The aqueous

suspension was extracted twice with ~50 ml of methylene chloride. The combined organic extracts were dried over anhydrous sodium sulfate, filtered and concentrated *in vacuo* to yield N-butylpiperidine as a colorless oil (3.01 g, 21.3 mmol, 92%). No further purification was necessary.

The NMR spectra are consistent with that presented in the literature.[218]

^{1}H NMR (400 MHz, $CDCl_3$) δ 2.31 (s, 3H), 2.26 – 2.14 (m, 2H), 1.61 – 1.49 (m, 4H), 1.48 – 1.32 (m, 4H), 1.26 (dq, J = 14.8, 7.3 Hz, 2H), 0.86 (t, J = 7.3 Hz, 3H) ppm.

^{13}C{^{1}H} NMR (101 MHz, $CDCl_3$) δ 59.36 (s), 54.64 (s), 29.15 (s), 26.00 (s), 24.50 (s), 20.91 (s), 14.03 (s) ppm.

IR (NaCl thin film, ν): 2955 m, 2933 s, 2857 m, 2800 m, 2762 m, 2692 w, 2614 w, 1468 m, 1454 m, 1442 m, 1376 m, 1350 m, 1326 w, 1309 m, 1291 w, 1272 m, 1261 m, 1239 w, 1209 w, 1156 m, 1132 m, 1101 w, 1056 m, 1039 w, 1006 w, 984 w, 969 w, 907 w, 861 w, 770 w, 738 w cm^{-1}.

HRMS(ESI): m/z calcd for $C_9H_{19}N$ 141.1517; m/z found 141.1521.

N-Hexylpiperidine

N-hexylpiperidine was synthesized by a similar method as N-butylpiperidine and was obtained as a colorless oil (3.05 g, 18.0 mmol, 88%).

The NMR spectra are consistent with that presented in the literature.[219]

^{1}H NMR (400 MHz, $CDCl_3$) δ 2.38 – 2.23 (m, 4H), 2.23 – 2.13 (m, 2H), 1.51 (dt, J = 11.3, 5.6 Hz, 4H), 1.46 – 1.30 (m, 4H), 1.29 – 1.12 (m, 6H), 0.81 (t, J = 6.8 Hz, 3H) ppm.

$^{13}C\{^{1}H\}$ NMR (101 MHz, $CDCl_3$) δ 59.65 (s), 54.60 (s), 31.77 (s), 27.39 (s), 26.91 (s), 25.96 (s), 24.47 (s), 22.53 (s), 13.93 (s) ppm.

IR (NaCl thin film, ν): 2932 s, 2855 m, 2800 m, 2762 m, 2692 w, 2668 w, 1468 m, 1454 m, 1442 m, 1377 m, 1350 m, 1326 w, 1307 m, 1269 m, 1258 m, 1156 m, 1132 m, 1102 m, 1060 w, 1040 m, 992 w, 963 w, 943 w, 891 w, 860 w, 780 w cm^{-1}.

HRMS(ESI): m/z calcd for $C_{11}H_{23}N$ 169.1830; m/z found 169.1836.

N-Methylpyridinium Nicotinate (1a)

Equimolar amounts N-methylpyridinium iodide (553 mg, 2.50 mmol) and nicotinic acid (308 mg, 2.50 mmol) were weighed into a 100 ml single–necked round bottom flask equipped with a magnetic stir bar. To this was added 0.55 mol equivalent of silver (I) carbonate powder (379 mg, 1.38 mmol). Approximately 50 ml of methanol was added to the solids and the flask was then equipped with a reflux condenser. The apparatus was clamped over an oil bath equipped with a magnetic stirrer and stirring was initiated to form a slurry. Cold water was passed through the condenser and the oil bath temperature was slowly increased to 75 ºC. After the slurry began to reflux, the reaction was allowed to continue for 30 min. The apparatus was then removed from the oil bath and allowed to cool to ambient temperature while continuing stirring. After ambient temperature was reached, the solution was filtered by gravity through cellulose filter paper to remove the bulk of the precipitated silver (I) iodide and remaining silver (I) carbonate. The filter cake was washed with an additional 10 ml of methanol. The filtrate

was then filtered through a small plug of diatomaceous earth to remove the remaining silver salts. Concentrating the solution *in vacuo* yields N-methylpyridinium nicotinate as a dark brown oil (538 mg, 2.49 mmol, >99%). The resultant ionic liquids are typically dark but appear to be of good purity via ^{1}H NMR analysis (the peaks associated with the N-methylpyridinium ion and the nicotinate ion integrate as they would in a 1:1 mixture), however a small amount of silver will precipitate over time and/or will plate the surface of the storage container.

^{1}H NMR (400 MHz, DMSO-d_6) δ 9.21 (d, J = 5.9 Hz, 2H), 9.00 (d, J = 1.3 Hz, 1H), 8.58 (t, J = 7.8 Hz, 1H), 8.47 (dd, J = 4.8, 1.7 Hz, 1H), 8.19 – 8.06 (m, 3H), 7.29 (dd, J = 7.7, 4.8 Hz, 1H), 4.46 (s, 3H) ppm.

^{13}C{^{1}H} NMR (101 MHz, DMSO-d_6) δ 167.80 (s), 150.38 (s), 149.29 (s), 145.73 (s), 144.87 (s), 136.13 (s), 135.16 (s), 127.59 (s), 122.62 (s), 47.69 (s) ppm.

IR (KBr disc, ν): 3044 s, 2940 s, 2818 s, 2579 w, 1635 s, 1581 s, 1548 s, 1495 s, 114 m, 1372 s, 1289 m, 1126 w, 1191 s, 1148 w, 1114 w, 1090 m, 1033 s, 834 m, 760 s, 706 m, 680 s, 449 m cm^{-1}.

HRMS(ESI): m/z calcd for $[C_6H_8N]^+$ 94.0657; m/z found 94.0661; m/z calcd for $[C_6H_4NO_2]^-$ 122.0242; m/z found 122.0242.

N-Ethylpyridinium Nicotinate (1b)

N-Ethylpyridinium nicotinate was synthesized by a similar method as N-methylpyridinium nicotinate and was obtained as a dark brown oil (574 mg, 2.49 mmol, >99%).

^{1}H NMR (400 MHz, DMSO-d_6) δ 9.36 (d, *J* = 5.7 Hz, 2H), 9.03 (d, *J* = 1.2 Hz, 1H), 8.62 (t, *J* = 7.8 Hz, 1H), 8.47 (dd, *J* = 4.8, 1.7 Hz, 1H), 8.26 – 8.08 (m, 3H), 7.29 (ddd, *J* = 7.7, 4.8, 0.5 Hz, 1H), 4.75 (q, *J* = 7.3 Hz, 2H), 1.52 (t, *J* = 7.3 Hz, 3H) ppm.

^{13}C{^{1}H} NMR (101 MHz, DMSO-d_6) δ 167.99 (s), 150.38 (s), 149.31 (s), 145.22 (s), 144.73 (s), 136.14 (s), 135.13 (s), 128.00 (s), 122.62 (s), 56.25 (s), 16.19 (s) ppm.

IR (KBr disc, ν): 3056 s, 2975 s, 2940 s, 2817 s, 2598 w, 2227 w, 2053 w, 1634 s, 1560 s, 1488 s, 1468 m, 1409 m, 1371 s, 1320 m, 1295 m, 1244 w, 1221 w, 1191 w, 1175 s, 1090 m, 1036 s, 973 w, 834 m, 782 m, 761 s, 687 s, 647 w, 621 w cm^{-1}.

HRMS(ESI): m/z calcd for $[C_7H_{10}N]^+$ 108.0813; m/z found 108.0817; m/z calcd for $[C_6H_4NO_2]^-$ 122.0242; m/z found 122.0243.

N-Butylpyridinium Nicotinate (1c)

N-Butylpyridinium nicotinate was synthesized by a similar method as N-methylpyridinium nicotinate and was obtained as a dark brown oil (645 mg, 2.50 mmol, >99%).

^{1}H NMR (400 MHz, DMSO-d_6) δ 9.41 (d, *J* = 6.1 Hz, 2H), 9.00 (s, 1H), 8.64 (t, *J* = 7.8 Hz, 1H), 8.44 (dd, *J* = 4.8, 1.6 Hz, 1H), 8.19 (t, *J* = 6.9 Hz, 2H), 8.13 (d, *J* = 7.7 Hz, 1H), 7.27 (dd, *J* = 7.7, 4.8 Hz, 1H), 4.72 (t, *J* = 7.4 Hz, 2H), 1.92 – 1.81 (m, 2H), 1.28 – 1.16 (m, 2H), 0.81 (t, *J* = 7.4 Hz, 3H) ppm.

^{13}C{^{1}H} NMR (101 MHz, DMSO-d_6) δ 167.18 (s), 150.51 (s), 148.99 (s), 145.35 (s), 145.11 (s), 136.05 (s), 135.78 (s), 128.04 (s), 122.48 (s), 60.35 (s), 32.78 (s), 18.70 (s), 13.19 (s) ppm.

FT-IR(KBr disc, ν): 3424 m br, 3128 w, 3043 m, 2960 m, 2936 m, 2872 m, 1633 m, 1594 s, 1549 s, 1542 w, 1501 w, 1487 m, 1466 w, 1406 m, 1386 m, 1170 m, 1088 w, 1022 w, 841 w, 771 w, 789 m cm^{-1}.

HRMS(ESI): m/z calcd for $[C_9H_{14}N]^+$ 136.1126; m/z found 136.1122; m/z calcd for $[C_6H_4NO_2]^-$ 122.0242; m/z found 122.0244.

N-Hexylpyridinium Nicotinate (1d)

N-Hexylpyridinium nicotinate was synthesized by a similar method as N-methylpyridinium nicotinate and was obtained as a dark brown oil (714 mg, 2.50 mmol, >99%).

^{1}H NMR (400 MHz, DMSO-d_6) δ 9.38 (t, *J* = 5.7 Hz, 2H), 9.02 (t, *J* = 2.0 Hz, 1H), 8.63 (t, *J* = 7.8 Hz, 1H), 8.46 (dd, *J* = 4.9, 1.6 Hz, 1H), 8.22 – 8.12 (m, 3H), 7.28 (dd, *J* = 7.8, 4.8 Hz, 1H), 4.70 (t, *J* = 7.6 Hz, 2H), 1.92 – 1.81 (m, 2H), 1.21 – 1.09 (m, 6H), 0.73 (t, *J* = 7.5 Hz, 3H) ppm.

$^{13}C\{^{1}H\}$ NMR (101 MHz, DMSO-d_6) δ 167.61 (s), 150.49 (s), 149.20 (s), 145.32 (s), 145.02 (s), 136.14 (s), 135.27 (s), 128.04 (s), 122.52 (s), 60.63 (s), 30.82 (s), 30.46 (s), 25.00 (s), 21.74 (s), 13.61 (s) ppm.

FT-IR(KBr disc, ν): 3425 s br, 3045 m, 2952 m, 2670 w, 2538 w, 1604 s, 1562 m, 1477 w, 1454 w, 1381 s, 1325 w, 1297 w, 1147 w, 1111 w, 1028 w, 949 w, 839 w, 811 w, 755 m, 699 m, 637 w cm^{-1}.

HRMS(ESI): m/z calcd for $[C_{11}H_{18}N]^+$ 164.1439; m/z found 164.1443; m/z calcd for $[C_6H_4NO_2]^-$ 122.0242; m/z found 122.0242.

N-Methylpiperidinium Nicotinate (2a)

Nicotinic acid (5.07 g, 41.1 mmol) was weighed and placed in a heavy walled glass pressure tube equipped with a magnetic stir bar (the smallest pressure tube that can contain the total amount of the reagents should be used to minimize the head space). An equimolar amount of N-methylpiperidine (5.00 ml, 4.08 g, 41.1 mmol) was added and the pressure tube was sealed and placed in an oil bath (equipped with a magnetic stirrer) that was preheated to 150 ºC that was placed behind a blast shield. The reaction is complete when the mixture ceases boiling and there is no visible reflux of the N-methylpiperidine in the pressure tube (approximately 15–30 min). The mixture was then allowed to cool to ambient pressure and the cap was removed from the pressure tube and replaced with a rubber septum. The pressure tube was then subjected to high vacuum to remove traces of

unreacted N-methylpiperidine. The product N-methylpiperidinium nicotinate (9.14 g, 41.1 mmol, >99%) was obtained as a yellowish solid.

Melting point ~170 ºC dec.

^{1}H NMR (400 MHz, DMSO-d_6) δ 9.03 (dd, *J* = 2.1, 0.9 Hz, 1H), 8.61 (dd, *J* = 4.8, 1.8 Hz, 1H), 8.19 (dt, *J* = 7.8, 2.0 Hz, 1H), 7.41 (ddd, *J* = 7.8, 4.8, 0.9 Hz, 1H), 2.89 (s, 4H), 2.55 (s, 3H), 1.72 – 1.64 (m, 4H), 1.46 (p, *J* = 6.2 Hz, 2H) ppm.

^{13}C{^{1}H} NMR (101 MHz, DMSO-d_6) δ 167.98 (s), 150.95 (s), 150.34 (s), 136.44 (s), 123.07 (s), 53.76 (s), 43.40 (s), 23.12 (s), 21.60 (s) ppm.

IR (KBr disc, ν): 3424 m br, 3070 w, 2822 w, 2656 m, 2438 m, 1921 m, 1709 s, 1592 m, 1485 w, 1417 m, 1324 s, 1298 s, 1183 m, 1134 w, 1113 m, 1086 m, 1035 s, 951 w, 809 m, 746 s, 690 m, 639 m cm^{-1}.

N-Ethylpiperidinium Nicotinate (2b)

N-Ethylpiperidinium nicotinate was synthesized by a similar method as N-methylpiperidinium nicotinate and was obtained as a yellowish solid (8.59 g, 36.4 mmol, >99%).

Melting point ~170 ºC dec.

^{1}H NMR (400 MHz, DMSO-d_6) δ 9.03 (s, 1H), 8.60 (dd, *J* = 4.8, 1.6 Hz, 1H), 8.19 (dt, *J* = 7.7, 1.8 Hz, 1H), 7.40 (ddd, *J* = 7.8, 4.8, 0.8 Hz, 1H), 2.85 (dt, *J* = 14.5, 3.8 Hz, 5H), 1.76 – 1.64 (m, 4H), 1.53 – 1.43 (m, 2H), 1.16 (t, *J* = 7.3 Hz, 3H) ppm.

$^{13}C\{^{1}H\}$ NMR (101 MHz, DMSO-d_6) δ 167.91 (s), 150.84 (s), 150.36 (s), 136.40 (s), 131.80 (s), 123.02 (s), 51.53 (s), 50.92 (s), 23.15 (s), 22.28 (s), 9.53 (s) ppm.

FT-IR(KBr disc, ν): 3425 s br, 3054 m, 2952 m, 2670 w, 2538 w, 1604 s, 1562 m, 1477 w, 1454 w, 1381 s, 1325 w, 1297 w, 1147 w, 1111 w, 1028 w, 949 w, 839 w, 811 w, 755 m, 699 m, 637 w cm^{-1}.

HRMS(ESI): m/z calcd for $[C_7H_{16}N]^+$ 114.1282; m/z found 114.1281; m/z calcd for $[C_6H_4NO_2]^-$ 122.0242; m/z found 122.0241.

N-Butylpiperidinium Nictotinate (2c)

N-Butylpiperidinium nicotinate was synthesized by a similar method as N-methylpiperidinium nicotinate and was obtained as a yellowish solid (1.87 g, 7.08 mmol, >99%).

Melting point 76–77 ºC

^{1}H NMR (400 MHz, CD_3OD) δ 9.11 (d, *J* = 1.1 Hz, 1H), 8.63 (dd, *J* = 4.9, 1.6 Hz, 1H), 8.37 (dt, 1H), 7.51 (ddd, *J* = 7.8, 4.9, 0.8 Hz, 1H), 3.78 – 2.73 (m, 4H), 3.07 (dd, *J* = 9.7, 7.0 Hz, 2H), 2.01 – 1.79 (m, 4H), 1.80 – 1.66 (m, 2H), 1.78 – 1.47 (m, 2H), 1.46 – 1.35 (m, 2H), 0.98 (t, *J* = 7.4 Hz, 3H) ppm.

$^{13}C\{^{1}H\}$ NMR (101 MHz, CD_3OD) δ 171.05 (s), 151.91 (s), 151.19 (s), 138.92 (s), 133.20 (s), 124.90 (s), 58.03 (s), 54.12 (s), 27.00 (s), 24.27 (s), 22.86 (s), 21.02 (s), 13.92 (s) ppm.

FT-IR(KBr disc, ν): 3416 m br, 3043 w, 2936 s, 2875 m, 2677 m, 2651 s, 2543 m, 1700 w, 1592 s, 1548 s, 1482 w, 1458 s, 1408 s, 1386 s. 1198 w, 1117 w, 1088 w, 1023 m, 955 w, 841 m, 820 w, 756 s, 704 s, 640 w, 621 w, 575 w, 511 w cm^{-1}.

HRMS(ESI): m/z calcd for $[C_9H_{20}N]^+$ 142.1595; m/z found 142.1592; m/z calcd for $[C_6H_4NO_2]^-$ 122.0247; m/z found 122.0244.

N-Hexylpiperidinium Nicotinate (2d)

N-Hexylpiperidinium nicotinate was synthesized by a similar method as N-methylpiperidinium nicotinate and was obtained as a dark yellow oil (1.78 g, 6.08 mmol, >99%).

^{1}H NMR (400 MHz, CD_3OD) δ 9.05 (s, 1H), 8.55 (dt, *J* = 4.9, 1.6 Hz, 1H), 8.30 (dq, *J* = 8.0, 1.8 Hz, 1H), 7.44 (ddd, *J* = 7.8, 4.9, 0.7 Hz, 1H), 3.48 – 2.85 (m, 4H), 3.07 – 2.95 (m, 2H), 1.83 (dd, *J* = 11.8, 5.9 Hz, 4H), 1.75 – 1.48 (m, 4H), 1.25 (s, 6H), 0.81 (t, *J* = 7.3 Hz, 3H) ppm.

$^{13}C\{^1H\}$ NMR (101 MHz, CD_3OD) δ 171.76 (s), 151.42 (s), 151.16 (s), 138.71 (s), 134.31 (s), 124.71 (s), 58.10 (s), 53.92 (s), 32.28 (s), 27.36 (s), 24.82 (s), 24.16 (s), 23.38 (s), 22.85 (s), 14.26 (s) ppm.

FT-IR(KBr disc, ν): 3411 s br, 3043 m, 2955 s, 2930 s, 2860 s, 2536 w, 1681 w, 1605 s, 1558 w, 1455 w, 1415 w, 1383 s, 1259 w, 1192 s, 1142 w, 1090 w, 1042 m, 1027 m, 953 w, 834 w, 807 w, 757 m, 699 m, 622 w, 535 w cm^{-1}.

HRMS(ESI): m/z calcd for $[C_{11}H_{24}N]^+$ 170.1908; m/z found 170.1906; m/z calcd for $[C_6H_4NO_2]^-$ 122.0242; m/z found 122.0246.

N-Methylpiperidinium Nipecotate (3a)

Nipecotic acid (500 mg, 3.87 mmol) was weighed and placed in a heavy-walled glass pressure tube equipped with a magnetic stir bar (the smallest pressure tube that can contain the total amount of the reagents should be used to minimize the head space). An equimolar amount of N-methylpiperidine (0.47 ml, 384 mg, 3.87 mmol) was added and the pressure tube was sealed and placed in an oil bath (equipped with a magnetic stirrer) that was preheated to 150 ºC. The reaction is complete when the mixture ceases boiling and there is no visible reflux of the N-methylpiperidine in the pressure tube (approximately 15–30 min). The mixture was then allowed to cool to ambient pressure and the cap was removed from the pressure tube and replaced with a rubber septum. The pressure tube was then subjected to high vacuum to remove traces of unreacted N-methylpiperidine. The product N-methylpiperidinium nipecotate (884 mg, 3.87 mmol, >99%) was obtained as a yellowish solid.

Melting point ~225 ºC dec.

^{1}H NMR (400 MHz, D_2O) δ 3.09 (dt, *J* = 12.5, 3.0 Hz, 1H), 2.97 (dt, *J* = 12.8, 3.7 Hz, 1H), 2.79 – 2.63 (m, 3H), 2.39 – 2.30 (m, 2H), 2.28 (s, 3H), 1.91 – 1.80 (m, 1H), 1.73 – 1.61 (m, 2H), 1.60 – 1.19 (m, 9H) ppm.

$^{13}C\{^{1}H\}$ NMR (101 MHz, D_2O) δ 181.52 (s), 55.06 (s), 46.68 (s), 44.35 (s), 42.73 (s), 26.61 (s), 24.11 (s), 22.55 (s), 21.94 (s) ppm.

IR (KBr disc, ν): 3408 w br, 2988 m, 2956 s, 2926 m, 2886 m, 2851 m, 2748 m, 2644 m, 2562 m, 2359 m, 1634 s, 1570 s, 1483 m, 1454 m, 1434 m, 1399 s, 1370 s, 1294 m, 1279 m, 1253 m, 1228 m, 1156 m, 1140 m, 1098 w, 1078 m, 1066 m, 1038 m, 977 m, 947 m, 924 m, 855 m, 807 w, 766 m, 736 s, 561 m cm^{-1}.

HRMS(ESI): m/z calcd for $[C_6H_{14}N]^+$ 100.1126; m/z found 100.1123; m/z calcd for $[C_6H_{10}NO_2]^-$ 128.0711; m/z found 128.0711.

N-Ethylpiperidinium Nipecotate (3b)

N-Ethylpiperidinium nipecotate was synthesized by a similar method as N-methylpiperidinium nipecotate and was obtained as a yellowish solid (938 mg, 3.87 mmol, >99%).

Melting point ~225 dec.

^{1}H NMR (400 MHz, D_2O) δ 3.02 (dd, J = 12.6, 3.1 Hz, 1H), 2.90 (dd, J = 12.6, 3.0 Hz, 1H), 2.68 – 2.52 (m, 7H), 2.31 – 2.22 (m, 1H), 1.87 – 1.77 (m, 1H), 1.66 – 1.58 (m, 2H), 1.52 (d, J = 3.5 Hz, 5H), 1.40 (dd, J = 13.9, 4.7 Hz, 3H), 1.07 – 0.91 (m, 3H) ppm.

$^{13}C\{^{1}H\}$ NMR (101 MHz, D_2O) δ 181.88 (s), 52.71 (s), 51.96 (s), 46.96 (s), 44.46 (s), 43.31 (s), 26.90 (s), 23.84 (s), 23.04 (s), 22.41 (s), 9.56 (s) ppm.

FT-IR(KBr disc, ν): 3413 m br, 3019 s, 2988 s, 2956 s, 2927 s, 2886 s, 2851 s, 2748 s, 2646 s, 2562 s, 2360 s, 1634 s, 1569 s, 1483 s, 1453 s, 1440 s, 1398 s, 1370 s, 1294 s,

1279 s, 1253 s, 1228 s, 1155 m, 1140 m, 1097 w, 1078 m, 1066 s, 1030 m, 971 m, 947 s, 924 m, 854 m, 807 w, 765 m, 735 s, 561 s, 520 s, 455 s cm^{-1}.

HRMS(ESI): m/z calcd for $[C_7H_{16}N]^+$ 114.1288; m/z found 114.1282; m/z calcd for $[C_6H_{10}NO_2]^-$ 128.0717; m/z found 128.0711.

N-Butylpiperidinium Nipecotate (3c)

N-Butylpiperidinium nipecotate was synthesized by a similar method as N-methylpiperidinium nipecotate and was obtained as a yellowish solid (1.05 g, 3.87 mmol, >99%).

Melting point ~225 ºC dec.

^1H NMR (400 MHz, D_2O) δ 3.17 (dd, *J* = 12.6, 2.6 Hz, 1H), 3.05 (t, *J* = 8.1 Hz, 1H), 2.85 (ddd, *J* = 18.5, 14.0, 5.9 Hz, 7H), 2.46 – 2.37 (m, 1H), 1.93 – 1.83 (m, 1H), 1.83 – 1.39 (m, 11H), 1.26 – 1.15 (m, 3H), 0.78 (t, *J* = 7.4 Hz, 3H) ppm.

$^{13}C\{^1H\}$ NMR (101 MHz, D_2O) δ 180.67 (s), 56.90 (s), 53.06 (s), 46.13 (s), 44.10 (s), 41.60 (s), 26.05 (s), 25.68 (s), 23.04 (s), 21.63 (s), 21.54 – 21.44 (m), 19.40 (s), 12.79 (s) ppm.

FT-IR(KBr disc, ν): 3010 s, 2945 s, 2874 s, 2769 s, 2548 m, 2420 m, 1636 s, 1548 s, 1439 s, 1392 s, 1286 m, 1245 m, 1221 m, 1137 w, 1114 w, 1074 w, 1058 m, 1033 m, 964 w, 944 m, 910 m, 769 s, 653 s, 541 s, 507 m, 451 m cm^{-1}.

HRMS(ESI): m/z calcd for $[C_9H_{20}N]^+$ 142.1596; m/z found 142.1594; m/z calcd for $[C_6H_{10}NO_2]^-$ 128.0711; m/z found 128.0711.

N-Hexylpiperidinium Nipecotate (3d)

N-Hexylpiperidinium nipecotate was synthesized by a similar method as N-methylpiperidinium nipecotate and was obtained as a dark yellow oil (1.16 mg, 3.87 mmol, >99%).

^{1}H NMR (400 MHz, D_2O) δ 3.22 (dd, *J* = 12.7, 3.9 Hz, 1H), 3.12 (dt, *J* = 9.6, 4.4 Hz, 1H), 3.03 – 2.85 (m, 2H), 2.54 – 2.43 (m, 1H), 2.43 – 2.25 (m, 4H), 1.99 – 1.84 (m, 1H), 1.84 – 1.70 (m, 1H), 1.70 – 1.48 (m, 4H), 1.47 – 1.33 (m, 4H), 1.28 – 1.11 (m, 4H), 1.10 – 0.93 (m, 6H), 0.74 (t, *J* = 6.6 Hz, 3H) ppm.

^{13}C{^{1}H} NMR (101 MHz, D_2O) δ 180.28 (s), 59.38 (s), 53.01 (s), 45.88 (s), 44.00 (s), 41.04 (s), 32.08 (s), 27.34 (s), 26.26 (s), 25.77 (s), 24.90 (s), 23.34 (s), 22.84 (s), 21.18 (s), 14.01 (s) ppm.

FT-IR(KBr disc, ν): 3389 w br, 2929 s, 2855 s, 2801 m, 2764 m, 1633 w, 1562 w, 1467 m, 1378 m, 1351 w, 1307 w, 1259 w, 1157 m, 1131 m, 1102 m, 1040 w, 861 w, 781 w, 755 w, 726 w cm^{-1}.

N-Methylpiperidinium 3-Pyridinesulfonate (4)

3-Pyridinesulfonic acid (500 mg, 3.14 mmol) was weighed and placed in a heavy-walled glass pressure tube equipped with a magnetic stir bar (the smallest pressure tube that can contain the total amount of the reagents should be used to minimize the head space). An equimolar amount of N-methylpiperidine (382 µl, 312 mg, 3.14 mmol) was

added and the pressure tube was sealed and placed in an oil bath (equipped with a magnetic stirrer) that was preheated to 150 ºC. The reaction is complete when the mixture ceases boiling and there is no visible reflux of the N-methylpiperidine in the pressure tube (approximately 15–30 min). The mixture was then allowed to cool to ambient pressure and the cap was removed from the pressure tube and replaced with a rubber septum. The pressure tube was then subjected to high vacuum to remove traces of unreacted N-methylpiperidine. The product N-methylpiperidinium 3-pyridinesulfonate (812 mg, 3.14 mmol, >99%) was obtained as a beige oil.

^{1}H NMR (400 MHz, DMSO-d_6) δ 8.79 (d, *J* = 2.2 Hz, 1H), 8.54 (dd, *J* = 4.9, 1.6 Hz, 1H), 7.97 (dt, *J* = 7.8, 1.9 Hz, 1H), 7.41 (dd, *J* = 7.9, 4.8 Hz, 1H), 3.36 (d, *J* = 12.7 Hz, 2H), 2.87 (t, *J* = 12.6 Hz, 2H), 2.74 (s, 3H), 1.78 (d, *J* = 14.7 Hz, 2H), 1.70 – 1.51 (m, 3H), 1.38 – 1.26 (m, 1H) ppm.

^{13}C{^{1}H} NMR (101 MHz, DMSO-d_6) δ 149.20 (s), 146.24 (s), 143.56 (s), 133.45 (s), 123.30 (s), 53.74 (s), 42.71 (s), 22.64 (s), 20.72 (s) ppm.

FT-IR(KBr disc, ν): 3454 s br, 3042 s, 2950 s, 2864 s, 2736 s, 2584 s, 1645 m, 1578 s, 1471 s, 1415 s, 1322 w, 1219 s, 1140 s, 1117 s, 1095 s, 972 s, 949 m, 854 w, 813 m, 737 s, 709 s, 635 s, 615 s, 571 s, 554 s, 479 m cm^{-1}.

HRMS(ESI): m/z calcd for $[C_6H_{14}N]^+$ 100.1126; m/z found 100.1129; m/z calcd for $[C_5H_5NO_3S]^-$ 157.9911; m/z found 157.9910.

N-Methylpiperidinium 2-(4'-Pyridyl)ethanesulfonate (5)

2-(4'-Pyridyl)ethanesulfonic acid (500 mg, 4.06 mmol) was weighed and placed in a heavy walled glass pressure tube equipped with a magnetic stir bar (the smallest pressure tube that can contain the total amount of the reagents should be used to minimize the head space). An equimolar amount of N-methylpiperidine (325 µl, 265 mg, 2.67 mmol) was added and the pressure tube was sealed and placed in an oil bath (equipped with a magnetic stirrer) that was preheated to 150 ºC. The reaction is complete when the mixture ceases boiling and there is no visible reflux of the N-methylpiperidine in the pressure tube (approximately 15–30 min). The mixture was then allowed to cool to ambient pressure and the cap was removed from the pressure tube and replaced with a rubber septum. The pressure tube was then subjected to high vacuum to remove traces of unreacted N-methylpiperidine. The product N-methylpiperidinium 2-(4'-pyridyl) ethanesulfonate (765 mg, 2.67 mmol, >99%) was obtained as a beige oil.

^{1}H NMR (400 MHz, D_2O) δ 8.29 (d, *J* = 4.5 Hz, 2H), 7.25 (d, *J* = 4.4 Hz, 2H), 3.31 (d, *J* = 12.0 Hz, 2H), 3.03 (dt, *J* = 14.9, 6.7 Hz, 4H), 2.78 (t, *J* = 12.5 Hz, 2H), 2.68 (s, 3H), 1.78 (d, *J* = 14.2 Hz, 2H), 1.70 – 1.47 (m, 3H), 1.29 (dd, *J* = 25.0, 12.5 Hz, 1H) ppm.

^{13}C{^{1}H} NMR (101 MHz, D_2O) δ 150.63 (s), 148.09 (s), 124.57 (s), 54.87 (s), 50.76 (s), 43.13 (s), 29.82 (s), 22.93 (s), 20.57 (s) ppm.

FT-IR(KBr disc, ν): 3419 s br, 3030 s, 2871 m, 2822 m, 2710 s, 2582 m, 2540 m, 2368 m, 2113 w, 1953 w, 1634 m, 1603 s, 1561 w, 1480 m, 1421 m, 1325 w, 1191 s, 1038 s, 856 w, 807 m cm^{-1}.

HRMS(ESI): m/z calcd for $[C_7H_8NO_3S]^-$ 186.0230; m/z found 186.0222; m/z calcd for $[C_6H_{14}N]^+$ 100.1126; m/z found 100.1124.

Sodium Isonicotinate (6a)

Isonicotinic acid (500 mg, 4.06 mmol) was weighed into a 25 ml single–necked round bottomed flask. Approximately 5 ml of methanol was added to the acid and a magnetic stir bar was added to the mixture and the solution was stirred without heating. A solution of sodium methoxide (0.5 M in methanol, 8.12 ml, 4.06 mmol) was carefully measured and added to the stirred solution; any previously undissolved material entered solution at this point. The magnetic stir bar was removed and rinsed off into the flask with a small amount of methanol and the solution was concentrated *in vacuo* to yield sodium isonicotinate (589 mg, 4.06 mmol, >99%) as a white solid.

Melting point >300 ºC

^{1}H NMR (400 MHz, DMSO-d_6) δ 8.70 (d, *J* = 5.1 Hz, 2H), 7.84 (d, *J* = 5.2 Hz, 2H) ppm.

^{13}C{^{1}H} NMR (101 MHz, DMSO-d_6) δ 167.53 (s), 149.78 (s), 143.49 (s), 123.02 (s) ppm.

FT-IR(KBr disc, ν): 3380 vs br, 3028 m, 2964 m, 2930 m, 2899 m, 1632 s, 1545 m, 1480 s, 1456 s, 1411 s, 1379 s, 1256 w, 1226 w, 1048 s, 975 w, 942 m, 768 m, 711 m, 681 m cm^{-1}.

HRMS(ESI): m/z calcd for $[C_6H_4NO_2]^-$ 122.0242; m/z found 122.0243.

Sodium Nicotinate (7a)

Sodium nicotinate was prepared by the same method as sodium isonicotinate and obtained as a white solid (589 mg, 4.06 mmol, >99%).

Melting point >300 ºC (lit. 234 ºC)[220]

^{1}H NMR (400 MHz, D_2O) δ 8.77 – 8.73 (m, 1H), 8.41 (dd, *J* = 4.9, 0.9 Hz, 1H), 8.06 (dt, *J* = 7.9, 1.4 Hz, 1H), 7.32 (dd, *J* = 7.9, 5.0 Hz, 1H) ppm.

^{13}C{^{1}H} NMR (101 MHz, D_2O) δ 173.16 (s), 150.35 (s), 148.99 (s), 137.55 (s), 132.19 (s), 123.82 (s) ppm.

FT-IR(KBr disc, ν): 3421 s br, 3007 m, 3054 s, 2968 m, 1993 w, 1968 w, 1945 w, 1919 w, 1898 w, 1607 s, 1558 s, 1406 s, 1199 s, 1153 m, 1120 m, 1091 s, 1031 s, 996 w, 974 w, 966 m, 949 m, 847 s, 837 s, 769 s, 755 s, 704 s, 629 m, 621 m, 528 s cm^{-1}.

HRMS(ESI): m/z calcd for $[C_6H_4NO_2]^-$ 122.0242; m/z found 122.0241.

Sodium 2-Furoate (8a)

Sodium 2-furoate was prepared by the same method as sodium isonicotinate and obtained as a white solid (598 mg, 4.46 mmol, >99%).

Melting point >300 ºC

^{1}H NMR (400 MHz, DMSO-d_6) δ 7.72 (dd, *J* = 1.7, 0.9 Hz, 1H), 6.91 (dd, *J* = 3.3, 0.9 Hz, 1H), 6.55 (dd, *J* = 3.3, 1.7 Hz, 1H) ppm.

$^{13}C\{^{1}H\}$ NMR (101 MHz, DMSO-d_6) δ 161.57 (s), 143.80 (s), 113.22 (s), 111.09 (s) ppm.

FT-IR(KBr disc, ν): 3448 w br, 3125 w, 3107 m, 2957 w, 2931 w, 1701 m, 1593 s, 1566 s, 1484 s, 1426 m, 1398 m, 1375 m, 1308 w, 1221 w, 1190 m, 1143 w, 1124 w, 1080 w, 1009 m, 926 m, 884 w, 809 m, 798 m, 725 s, 608 m cm^{-1}.

HRMS(ESI): m/z calcd for $[C_5H_3O_3]^-$ 111.0082; m/z found 111.0079.

Sodium Isonipecotate (6b)

Sodium isonipecotate was prepared by the same method as sodium isonicotinate and obtained as a white solid(585 mg, 3.87 mmol, >99%).

Melting point 252 ºC dec.

^{1}H NMR (400 MHz, D_2O) δ 3.09 (dt, *J* = 12.7, 3.0 Hz, 2H), 2.67 (td, *J* = 12.4, 2.4 Hz, 2H), 2.24 (tt, *J* = 11.5, 3.5 Hz, 1H), 1.83 (dd, *J* = 13.8, 2.0 Hz, 2H), 1.51 (qd, *J* = 12.5, 3.9 Hz, 2H) ppm.

$^{13}C\{^{1}H\}$ NMR (101 MHz, D_2O) δ 183.68 (s), 44.09 (s), 43.04 (s), 27.40 (s) ppm.

FT-IR(KBr disc, ν): 3422 vs br, 2954 m, 2855 m, 2767 m, 2675 m, 2534 w, 1568 s, 1411 s, 1293 m, 1239 m, 1145 w, 1096 w, 1074 w, 1041 w, 939 w, 811 w, 781 w, 741 w, 646 w cm^{-1}.

HRMS(ESI): m/z calcd for $[C_6H_{10}NO_2]^-$ 128.0711; m/z found 128.0709.

Sodium Nipecotate (7b)

Sodium nipecotate was prepared by the same method as sodium isonicotinate and obtained as a white solid (585 mg, 3.87 mmol, >99%).

Melting point 188–190 ºC

^{1}H NMR (400 MHz, D_2O) δ 3.18 – 3.03 (m, 1H), 2.96 (d, *J* = 12.3 Hz, 1H), 2.82 – 2.57 (m, 2H), 2.43 – 2.25 (m, 1H), 1.87 (s, 1H), 1.66 (s, 1H), 1.48 (dd, *J* = 19.9, 10.2 Hz, 2H) ppm.

^{13}C{^{1}H} NMR (101 MHz, D_2O) δ 182.06 (s), 144.59 (s), 46.89 (s), 44.46 (s), 43.21 (s), 26.83 (s), 22.92 (s) ppm.

FT-IR(KBr disc, ν): 3416 s br, 3073 m, 2956 m, 2858 m, 2662 w, 2548 w, 2366 w, 1573 s, 1477 m, 1447 m, 1400 s, 1320 m, 1299 m, 1280 m, 1184 w, 1112 w, 1036 w, 945 w, 903 w, 809 w, 772 m, 746 m, 688 m, 642 m cm^{-1}.

HRMS(ESI): m/z calcd for $[C_6H_{10}NO_2]^-$ 128.0711; m/z found 128.0710.

Sodium 2-Tetrahydrofuroate (8b)

Sodium 2-tetrahydrofuroate was prepared by the same method as sodium isonicotinate and obtained as a white solid(492 mg, 3.56 mmol, >99%).

Melting point 237–238 ºC

^{1}H NMR (400 MHz, D_2O) δ 4.16 (dd, *J* = 8.1, 6.3 Hz, 1H), 3.87 – 3.70 (m, 2H), 2.24 – 2.10 (m, 1H), 1.89 – 1.68 (m, 3H) ppm.

$^{13}C\{^{1}H\}$ NMR (101 MHz, D_2O) δ 181.51 (s), 78.43 (s), 68.84 (s), 30.48 (s), 25.05 (s) ppm.

FT-IR(KBr disc, ν): 3378 m br, 2975 m, 2950 m, 2862 m, 2694 w, 2346 w, 1611 s, 1412 m, 1355 w, 1319 m, 1305 m, 1235 w, 1185 w, 1068 s, 946 m, 925 w, 849 m, 775 m, 698 s, 640 s cm^{-1}.

HRMS(ESI): m/z calcd for $[C_5H_7O_3]$- 115.0395; m/z found 115.0393.

N-Methylpyridinium Trifluoromethylsulfonate (9a)

Pyridine (250 µl, 245 µg, 3.09 mmol) was dissolved in ~10 ml of methylene chloride in a 20 ml glass vial and stoppered with a rubber septum. The vial was then flushed with argon briefly. Methyl trifluoromethanesulfonate (350 µl, 507 mg, 3.09 mmol) was removed from a Schlenk storage flask and slowly added to the solution of the N-heterocycle to minimize boiling. After several min, the solvent was removed *in vacuo* to yield N-methylpyridinium trifluoromethanesulfonate (752 mg, 3.09 mmol, >99%) as a beige semisolid.

The NMR spectra are consistent with that presented in the literature.[221]

^{1}H NMR (400 MHz, D_2O) δ 8.75 (d, J = 6.0 Hz, 2H), 8.50 (t, J = 7.9 Hz, H), 8.02 (t, J = 6.9 Hz, 2H), 4.37 (s, 3H) ppm.

$^{13}C\{^{1}H\}$ NMR (101 MHz, D_2O) δ 145.34 (s), 145.07 (s), 128.04 (s), 119.73 (q, J = 317.4 Hz), 48.16 (s) ppm.

FT-IR(KBr disc, ν): 3140 m, 3072 s, 2943 s, 2867 s, 2379 w, 2294 m, 2253 w, 1738 m, 1638 s, 1591 m, 1548 m, 1494 s, 1454 s, 1406 m, 1381 m, 1254 s, 1160 s, 1115 s, 1031 s, 912 m, 833 m, 767 s, 715 w, 680 s, 639 s, 575 s, 518 s, 448 m cm^{-1}.

HRMS(ESI): m/z calcd for $[C_6H_8N]^+$ 94.0657; m/z found 94.0659; m/z calcd for $[CO_3F_3S]^-$ 148.9520; m/z found 148.9522.

N-Methylpyrazinium Trifluoromethylsulfonate (10a)

N-Methylpyrazinium trifluoromethanesulfonate was prepared by a similar method as N-methylpyridinium trifluoromethanesulfonate and was obtained as a yellowish solid (762 mg, 3.12 mmol, >99%).

Melting point ~125 ºC dec.

^{1}H NMR (400 MHz, DMSO-d_6) δ 9.52 – 9.47 (m, 2H), 9.12 (d, J = 4.3 Hz, 2H), 4.44 (s, 3H) ppm.

$^{13}C\{^1H\}$ NMR (101 MHz, DMSO-d_6) δ 150.25 (s), 138.00 (t, J_{CN} = 8.9 Hz), 120.51 (q, J_{CF} = 321.9 Hz), 48.57 (s) ppm.

FT-IR(KBr disc, ν): 3447 m br, 3062 w, 2943 m, 2861 m, 1637 w, 1482 m, 1451m, 1371 m, 1263 s, 1166 s, 1115 s, 1033 s, 845 w, 757 w, 641 s, 572 m cm^{-1}.

HRMS(ESI): m/z calcd for $[C_5H_7N_2]^+$ 95.0609; m/z found 95.0611; m/z calcd for $[CO_3F_3S]^-$ 148.9520; m/z found 148.9527.

N-Methylpiperidinium Trifluoromethanesulfonate (9b)

N-Methylpiperidine (500 µl, 408 mg, 4.11 mmol) was weighed and dissolved in ~10 ml of methylene chloride in a 20 ml glass vial and stoppered with a rubber septum. The vial was then flushed with argon briefly. Trifluoromethanesulfonic acid (364 µl, 617 mg, 4.11 mmol) was removed from a Schlenk storage flask and slowly added to the solution of the N-heterocycle to minimize boiling. After several min, the solvent was removed *in vacuo* to yield N-methylpiperidinium trifluoromethanesulfonate (1.03 g, 4.11 mmol, >99%) as a yellowish oil.

^{1}H NMR (400 MHz, DMSO-d_6) δ 8.99 (s, 1H), 3.36 (d, *J* = 12.1 Hz, 2H), 2.86 (qd, *J* = 12.2, 2.5 Hz, 1H), 2.73 (d, *J* = 4.9 Hz, 1H), 1.80 (d, *J* = 14.2 Hz, 2H), 1.71 – 1.51 (m, 3H), 1.43 – 1.21 (m, 1H) ppm.

^{13}C{^{1}H} NMR (101 MHz, DMSO-d_6) δ 120.63 (q, *J* = 322.2 Hz), 53.75 (s), 42.62 (s), 22.62 (s), 20.65 (s) ppm.

^{1}H-NMR (400 MHz, MeOH-d_4): δ 3.54 (d, *J* = 50.8 Hz, 2H), 2.94 (t, *J* = 1.3 Hz, 2H), 2.84 (s, 3H), 1.95 (d, *J* = 14.4 Hz, 2H), 1.84 (m, 1H), 1.71 (qt, *J* = 13.6 Hz, *J* = 3.5 Hz, 2H), 1.48 (qt, *J* = 12.4 Hz, *J* = 4.1 Hz, 1H) ppm.

FT-IR(KBr disc, ν): 3079 m, 2965 m, 2248 w, 1694 w, 1514 w, 1461 w, 1286 s, 1249 s, 1228 s, 1172 s, 1026 s, 972 w, 947 w, 803 w, 764 w, 637 s, 579 w, 516 m cm^{-1}.

HRMS(ESI): m/z calcd for $[C_6H_{14}N]^+$ 100.1126; m/z found 100.1129; m/z calcd for $[CO_3F_3S]^-$ 148.9514; m/z found 148.9518.

N-Ethylpiperazinium Trifluoromethanesulfonate (10b)

N-Ethylpiperazinium trifluoromethanesulfonate was prepared by a similar method as N-methylpiperidinium trifluoromethanesulfonate and was obtained as a yellowish solid (1.04 g, 3.94 mmol, >99%).

Melting point 182–183 ºC

^{1}H NMR (400 MHz, D_2O) δ 3.10 (t, *J* = 5.3 Hz, 4H), 2.84 – 2.78 (m, 4H), 2.64 (q, *J* = 7.3 Hz, 2H), 1.05 (t, *J* = 7.3 Hz, 3H) ppm.

^{13}C{^{1}H} NMR (101 MHz, D_2O) δ 119.65 (q, *J* = 317.3 Hz), 51.75 (s), 49.46 (s), 42.68 (s), 9.61 (s) ppm.

FT-IR(KBr disc, ν) 3440 s br, 3064 w, 2962 w, 2851 w, 2760 w, 2527 w, 2364 w, 1637 w, 1560 s, 1471 w, 1449 w, 1411 s, 1288 m, 1260 m, 1238 m, 1167 m, 1035 m, 936 w, 912 w, 852 w, 817 w, 776 w, 762 w, 643 m, 575 m.

HRMS(ESI): m/z calcd for $[C_6H_{15}N_2]^+$ 115.1240; m/z found 115.1236; m/z calcd for $[CO_3F_3S]^-$ 148.9520; m/z found 148.9518.

4-(Ammoniummethyl)pyridine Trifluoromethanesulfonate (11a)

4-(Ammoniummethyl)pyridine trifluoromethanesulfonate was prepared by a similar method as N-methylpiperidinium trifluoromethanesulfonate and was obtained as a yellow solid (1.27 g, 4.92 mmol, >99%).

Melting point 103–104 ºC

^{1}H NMR (400 MHz, D_2O) δ 8.35 (d, *J* = 5.7 Hz, 2H), 7.27 (d, *J* = 5.5 Hz, 2H), 3.92 (s, 2H) ppm.

$^{13}C\{^{1}H\}$ NMR (101 MHz, D_2O) δ 148.92 (s), 147.04 (s), 123.08 (s), 119.61 (q, *J* = 317.4 Hz), 42.52 (s) ppm.

FT-IR(KBr disc, ν): 3426 m br, 3043 m, 2959 s, 2936 s, 2874 m, 2676 s, 2649 s, 2543 m, 1595 s, 1549 s, 1458 m, 1419 s, 1386 m, 1278 s, 1225 s, 1166 s, 1079 w, 1031 s, 1004 m, 963 w, 905 m, 840 w, 794 m, 759 m, 639 s, 575 m, 517 m, 486 m cm^{-1}.

HRMS(ESI): m/z calcd for $[C_6H_9N_2]^+$ 109.0766; m/z found 109.0771; m/z calcd for $[CO_3F_3S]^-$ 148.9520; m/z found 148.9522.

4-(Ammoniummethyl)piperidine Trifluoromethanesulfonate (11b)

4-(Ammoniummethyl)piperidine trifluoromethanesulfonate was prepared by a similar method as N-methylpiperidinium trifluoromethanesulfonate and was obtained as a beige semisolid (1.16 g, 4.38 mmol, >99%).

^{1}H NMR (400 MHz, D_2O) δ 3.24 (s, 1H), 3.15 (d, *J* = 12.6 Hz, 2H), 2.69 (t, *J* = 12.8 Hz, 2H), 2.48 (d, *J* = 6.8 Hz, 2H), 1.76 (d, *J* = 13.1 Hz, 2H), 1.62 – 1.46 (m, 1H), 1.15 (ddd, *J* = 15.7, 13.1, 3.4 Hz, 2H) ppm.

$^{13}C\{^{1}H\}$ NMR (101 MHz, D_2O) δ 119.57 (q, *J* = 305.5 Hz), 45.77 (s), 44.18 (s), 35.89 (s), 27.45 (s) ppm.

FT-IR(KBr disc, ν): 3442 m br, 2943 m, 2861 m, 2798 w, 1630 w, 1455 m, 1371 s, 1286 s, 1167 s, 1082 s, 1030 s, 856 m, 760 m, 639 s, 579 m, 519 m, 476 w, 438 w.

HRMS(ESI): m/z calcd for $[C_6H_{15}N_2]^+$ 115.1235; m/z found 115.1235; m/z calcd for $[CO_3F_3S]^-$ 148.9520; m/z found 148.9519.

Preparation of Tetrabutylphosphonium Salts

Tetrabutylphosphonium salts of organic acids were prepared by the accurate addition of an equimolar amount of tetrabutylphosphonium hydroxide (as a 40 wt% solution in water) to the organic acid. This was followed by ultrasonication in a bath until all the solid material dissolved. The aqueous solutions of the tetrabutylphosphonium salts were then evaporated to dryness at ambient temperature by placing samples in a desiccator filled with anhydrous calcium sulfate and subjecting them to dynamic high vacuum. After 8 h the bulk of the water had been removed, the calcium sulfate was replaced and dynamic high vacuum was continued for an additional 24 h until the materials were shown to be dry gravimetrically. All salts were obtained as liquids in quantitative yield.

Tetrabutylphosphonium Benzoate (12a)

Colorless oil, quantitative yield.

^{1}H NMR (400 MHz, D_2O) δ 7.80 (d, J = 6.9 Hz, 2H), 7.38 (t, J = 7.1 Hz, 1H), 7.32 (t, J = 7.3 Hz, 2H), 1.89 – 1.80 (m, 8H), 1.33 – 1.23 (m, 16H), 0.77 (t, J = 6.9 Hz, 12H) ppm.

$^{13}C\{^{1}H\}$ NMR (101 MHz, D_2O) δ 174.14 (s), 136.30 (s), 131.12 (s), 129.13 (s), 128.20 (s), 23.24 (d, J = 15.2 Hz), 22.66 (d, J = 4.5 Hz), 17.51 (d, J = 48.1 Hz), 12.64 (s) ppm.

^{31}P NMR{H} (162 MHz, D_2O) δ 33.19 (s) ppm.

IR (KBr disc, ν): 3428, 2969, 2915, 2873, 1697, 1594, 1547, 1466, 1402, 1308, 1232, 1104, 1065, 1014, 963, 907, 831, 716, 511 cm^{-1}.

HRMS(ESI): m/z calcd for $[C_{16}H_{36}P]^+$, 259.2555; m/z found 259.2563; m/z calcd for $[C_7H_5O_2]^-$, 121.0289; m/z found 121.0293.

Tetrabutylphosphonium Cyclohexanoate (13a)

Colorless oil, quantitative yield.

^{1}H NMR (400 MHz, D_2O) δ 2.23 – 1.95 (m, 9H), 1.80 – 1.68 (m, 2H), 1.65 (dt, J = 19.1, 12.3 Hz, 2H), 1.58 – 1.30 (m, 17H), 1.31 – 1.06 (m, 5H), 0.85 (t, J = 7.2 Hz, 12H) ppm.

$^{13}C\{^{1}H\}$ NMR (101 MHz, D_2O) δ 186.04 (s), 47.10 (s), 29.99 (s), 25.87 (s), 25.74 (s), 23.34 (d, J = 15.2 Hz), 22.80 (d, J = 4.5 Hz), 17.73 (d, J = 48.2 Hz), 12.68 (s) ppm.

^{31}P NMR{H} (162 MHz, D_2O) δ 33.43 (s) ppm.

IR (KBr disc, ν): 3405, 2959, 2931, 2878, 1555, 1469, 1411, 1287, 1235, 1144, 1101, 1010, 967, 905 cm^{-1}.

HRMS(ESI): m/z calcd for $[C_{16}H_{36}P]^+$, 259.2555; m/z found 259.2554; m/z calcd for $[C_7H_{11}O_2]^-$, 127.0759; m/z found 121.0758.

Tetrabutylphosphonium Isonicotinate (12b)

Colorless oil, quantitative yield.

^{1}H NMR (400 MHz, D_2O) δ 8.46 (d, *J* = 5.5 Hz, 2H), 7.64 (d, *J* = 6.0 Hz, 2H), 2.02 – 1.80 (m, 8H), 1.28 (dd, *J* = 17.0, 10.8 Hz, 16H), 0.75 (t, *J* = 7.1 Hz, 12H) ppm.

^{13}C{^{1}H} NMR (101 MHz, D_2O) δ 172.10 (s), 148.94 (s), 145.63 (s), 123.38 (s), 23.22 (d, *J* = 15.2 Hz), 22.64 (d, *J* = 4.5 Hz), 17.53 (d, *J* = 48.2 Hz), 12.58 (s) ppm.

^{31}P NMR{H} (162 MHz, D_2O) δ 33.28 (s) ppm.

IR (KBr disc, ν): 3428, 2963, 2932, 2817, 1603, 1550, 1469, 1416, 1374, 1320, 1228, 1102, 1067, 1002, 975, 926, 772, 723, 688 cm^{-1}.

HRMS(ESI): m/z calcd for $[C_{16}H_{36}P]^{+}$, 259.2555; m/z found 259.2551; m/z calcd for $[C_6H_4NO_2]^{-}$, 122.0242; m/z found 122.0242.

Tetrabutylphosphonium Isonipecotate (13b)

Colorless oil, quantitative yield.

^{1}H NMR (400 MHz, D_2O) δ 3.13 (dt, *J* = 12.7, 3.4 Hz, 2H), 2.71 (td, *J* = 12.5, 2.9 Hz, 2H), 2.24 (tt, *J* = 11.5, 3.7 Hz, 1H), 2.13 – 1.97 (m, 8H), 1.85 (dd, *J* = 13.9, 2.5 Hz, 2H), 1.56 (td, 2H), 1.50 – 1.25 (m, 16H), 0.82 (t, *J* = 7.2 Hz, 12H) ppm.

^{13}C{^{1}H} NMR (101 MHz, D_2O) δ 183.11 (s), 44.02 (s), 42.80 (s), 27.18 (s), 23.28 (d, *J* = 15.2 Hz), 22.71 (d, *J* = 4.5 Hz), 17.65 (d, *J* = 48.2 Hz), 12.60 (s) ppm.

^{31}P NMR{H} (162 MHz, D_2O) δ 33.42 (s) ppm.

IR (KBr disc, ν): 3396, 2970, 2935, 2871, 1549, 1415, 1292, 1242, 1088, 920, 816, 786, 727 cm^{-1}.

HRMS(ESI): m/z calcd for $[C_{16}H_{36}P]^+$, 259.2555; m/z found 259.2546 m/z calcd for $[C_6H_{10}NO_2]^-$, 128.0711; m/z found 128.0713.

Tetrabutylphosphonium Nicotinate (12c)

Colorless oil, quantitative yield.

^1H NMR (400 MHz, D_2O) δ 8.80 (s, 1H), 8.42 (dd, *J* = 4.8, 1.2 Hz, 1H), 8.11 (dd, *J* = 7.9, 1.6 Hz, 1H), 7.35 (dd, *J* = 7.9, 5.0 Hz, 1H), 2.00 – 1.79 (m, 8H), 1.44 – 1.07 (m, 16H), 0.73 (t, *J* = 7.1 Hz, 12H) ppm.

$^{13}C\{^1H\}$ NMR (101 MHz, D_2O) δ 171.85 (s), 150.04 (s), 149.07 (s), 137.91 (s), 132.80 (s), 124.00 (s), 23.22 (d, *J* = 15.2 Hz), 22.63 (d, *J* = 4.5 Hz), 17.52 (d, *J* = 48.2 Hz), 12.60 (s) ppm.

^{31}P NMR{H} (162 MHz, D_2O) δ 33.28 (s) ppm.

IR (KBr disc, ν): 3408, 3045, 2965, 2929, 2879, 1601, 1554, 1467, 1414, 1387, 1314, 1230, 1190, 1097, 1023, 970, 927, 840, 763, 703, 620, 509 cm^{-1}.

HRMS(ESI): m/z calcd for $[C_{16}H_{36}P]^+$, 259.2555; m/z found 259.2561; m/z calcd for $[C_6H_4NO_2]^-$, 122.0242; m/z found 122.0247.

Tetrabutylphosphonium Nipecotate (13c)

Colorless oil, quantitative yield.

^{1}H NMR (400 MHz, D_2O) δ 2.99 (dd, *J* = 12.4, 3.8 Hz, 1H), 2.84 (dt, *J* = 5.8, 3.2 Hz, 1H), 2.46 (ddd, *J* = 23.1, 14.1, 5.8 Hz, 2H), 2.24 – 2.14 (m, 1H), 2.14 – 1.97 (m, 8H), 1.91 – 1.79 (m, 1H), 1.64 – 1.53 (m, 1H), 1.53 – 1.27 (m, 18H), 0.85 (t, *J* = 7.2 Hz, 12H) ppm.

^{13}C{^{1}H} NMR (101 MHz, D_2O) δ 182.48 (s), 48.07 (s), 45.06 (s), 45.01 (s), 27.90 (s), 24.66 (s), 23.35 (d, *J* = 15.1 Hz), 22.82 (d, *J* = 4.5 Hz), 17.71 (d, *J* = 48.1 Hz), 12.82 (s) ppm.

^{31}P NMR{H} (162 MHz, D_2O) δ 33.47 (s) ppm.

IR (KBr disc, ν): 3357, 2957, 2933, 2865, 1567, 1462, 1404, 1303, 1282, 1248, 1163, 1095, 1004, 970, 908, 817, 779, 725 cm^{-1}.

HRMS(ESI): m/z calcd for $[C_{16}H_{36}P]^{+}$, 259.2555; m/z found 259.2566; m/z calcd for $[C_6H_{10}NO_2]^{-}$, 128.0711; m/z found 128.0710.

Tetrabutylphosphonium Picolinate (12d)

Colorless oil, quantitative yield.

^{1}H NMR (400 MHz, D_2O) δ 8.41 (d, *J* = 5.0 Hz, 1H), 7.80 – 7.75 (m, 2H), 7.36 (dd, *J* = 8.5, 5.2 Hz, 1H), 2.05 – 1.84 (m, 8H), 1.48 – 1.15 (m, 16H), 0.75 (t, *J* = 7.2 Hz, 12H) ppm.

$^{13}C\{^{1}H\}$ NMR (101 MHz, D_2O) δ 172.21 (s), 153.37 (s), 148.15 (s), 138.09 (s), 125.67 (s), 123.83 (s), 23.23 (d, *J* = 15.2 Hz), 22.66 (d, *J* = 4.5 Hz), 17.56 (d, *J* = 48.2 Hz), 12.60 (s) ppm.

^{31}P NMR{H} (162 MHz, D_2O) δ 33.34 (s) ppm.

IR (KBr disc, ν): 3442, 3044, 2968, 2939, 2876, 1615, 1586, 1560, 1469, 1402, 1234, 1096, 1050, 926, 845, 7648, 706, 623 cm^{-1}.

HRMS(ESI): m/z calcd for $[C_{16}H_{36}P]^+$, 259.2555; m/z found 259.2554; m/z calcd for $[C_6H_4NO_2]^-$, 122.0242; m/z found 122.0242.

Tetrabutylphosphonium Pipecolinate (13d)

Colorless oil, quantitative yield.

^{1}H NMR (400 MHz, D_2O) δ 3.07 (dd, *J* = 10.5, 3.3 Hz, 1H), 2.97 (dt, *J* = 7.1, 3.8 Hz, 1H), 2.55 (td, 1H), 2.13 – 2.00 (m, 8H), 1.90 – 1.82 (m, 1H), 1.74 – 1.66 (m, 1H), 1.58 – 1.25 (m, 20H), 0.84 (t, *J* = 7.2 Hz, 12H) ppm.

$^{13}C\{^{1}H\}$ NMR (101 MHz, D_2O) δ 179.95 (s), 60.22 (s), 44.50 (s), 28.93 (s), 24.48 (s), 23.56 (s), 23.31 (d, *J* = 15.2 Hz), 22.75 (d, *J* = 4.5 Hz), 17.68 (d, *J* = 48.2 Hz), 12.66 (s) ppm.

^{31}P NMR{H} (162 MHz, D_2O) δ 33.44 (s) ppm.

IR (KBr disc, ν): 3419, 2954, 2936, 2872, 1587, 1462, 1409, 1309, 1274, 1248, 1092, 918, 714 cm^{-1}.

HRMS(ESI): m/z calcd for $[C_{16}H_{36}P]^+$, 259.2555; m/z found 259.2551; m/z calcd for $[C_6H_{10}NO_2]^-$, 128.0711; m/z found 128.0710.

Tetrabutylphosphonium 2-Furoate (12e)

Colorless oil, quantitative yield.

^{1}H NMR (400 MHz, D_2O) δ 7.50 (d, *J* = 0.8 Hz, 1H), 6.88 (d, *J* = 3.4 Hz, 1H), 6.45 (dd, *J* = 3.4, 1.7 Hz, 1H), 2.13 – 1.84 (m, 8H), 1.59 – 1.20 (m, 16H), 0.81 (t, *J* = 7.1 Hz, 12H) ppm.

^{13}C{^{1}H} NMR (101 MHz, D_2O) δ 166.01 (s), 149.79 (s), 144.71 (s), 114.58 (s), 111.57 (s), 23.27 (d, *J* = 15.1 Hz), 22.71 (d, *J* = 4.5 Hz), 17.61 (d, *J* = 48.2 Hz), 12.64 (s) ppm.

^{31}P NMR{H} (162 MHz, D_2O) δ 33.39 (s) ppm.

IR (KBr disc, ν): 3435, 2963, 2939, 2875, 1607, 1567, 1493, 1458, 1414, 1368, 1233, 1178, 1140, 1094, 1011, 964, 922, 802, 732, 607 cm^{-1}.

HRMS(ESI): m/z calcd for $[C_{16}H_{36}P]^+$, 259.2555; m/z found 259.2549; m/z calcd for $[C_5H_3O_3]^-$, 111.0082; m/z found 111.0084.

Tetrabutylphosphonium 2-Tetrahydrofuroate (13e)

Colorless oil, quantitative yield.

^{1}H NMR (400 MHz, D_2O) δ 4.15 (dd, *J* = 8.2, 6.0 Hz, 1H), 3.88 – 3.79 (m, 1H), 3.79 – 3.71 (m, 1H), 2.22 – 2.13 (m, 1H), 2.13 – 2.00 (m, 8H), 1.88 – 1.69 (m, 3H), 1.56 – 1.27 (m, 16H), 0.84 (t, *J* = 7.2 Hz, 12H) ppm.

^{13}C{^{1}H} NMR (101 MHz, D_2O) δ 181.15 (s), 78.47 (s), 68.81 (s), 30.53 (s), 25.09 (s), 23.30 (d, *J* = 15.2 Hz), 22.72 (d, *J* = 4.5 Hz), 17.65 (d, *J* = 48.2 Hz), 12.61 (s) ppm.

^{31}P NMR{H} (162 MHz, D_2O) δ 33.42 (s) ppm.

IR (KBr disc, ν): 3334, 2964, 2932, 2870, 1673, 1596, 1450, 1416, 1317, 1231, 1072, 1008, 965, 918, 794, 712 cm^{-1}.

HRMS(ESI): m/z calcd for $[C_{16}H_{36}P]^{+}$, 259.2555; m/z found 259.2549; m/z calcd for $[C_5H_7O_3]^{-}$, 115.0395; m/z found 115.0390.

Tetrabutylphosphonium 2-Pyrrolate (12f)

Colorless oil, quantitative yield.

^{1}H NMR (400 MHz, D_2O) δ 6.84 (d, *J* = 1.3 Hz, 1H), 6.67 – 6.58 (m, 1H), 6.14 – 6.08 (m, 1H), 2.01 – 1.83 (m, 8H), 1.44 – 1.23 (m, 16H), 0.82 (t, *J* = 6.4 Hz, 12H) ppm.

^{13}C{^{1}H} NMR (101 MHz, D_2O) δ 168.58 (s), 128.79 (s), 121.11 (s), 112.48 (s), 108.81 (s), 23.28 (d, *J* = 15.1 Hz), 22.72 (d, *J* = 4.5 Hz), 17.58 (d, *J* = 48.1 Hz), 12.70 (s) ppm.

^{31}P NMR{H} (162 MHz, D_2O) δ 33.30 (s) ppm.

IR (KBr disc, ν): 3409, 2969, 2936, 2877, 1557, 1453, 1415, 1371, 1316, 1281, 1234, 1209, 1106, 1031, 924, 906, 883, 794, 731, 576, 526 cm^{-1}.

HRMS(ESI): m/z calcd for $[C_{16}H_{36}P]^+$, 259.2555; m/z found 259.2567; m/z calcd for $[C_5H_7NO_2]^-$, 110.0242; m/z found 110.0245.

Tetrabutylphosphonium Prolinate (13f)

Colorless oil, quantitative yield.

^1H NMR (400 MHz, D_2O) δ 3.64 (dd, *J* = 8.7, 6.0 Hz, 1H), 3.10 (dt, *J* = 11.2, 6.8 Hz, 1H), 2.90 (dt, *J* = 11.2, 6.8 Hz, 1H), 2.16 – 1.96 (m, 9H), 1.82 – 1.65 (m, 3H), 1.56 – 1.26 (m, 16H), 0.83 (t, *J* = 7.2 Hz, 12H) ppm.

$^{13}C\{^1H\}$ NMR (101 MHz, D_2O) δ 178.64 (s), 61.37 (s), 46.06 (s), 30.04 (s), 24.59 (s), 23.29 (d, *J* = 15.2 Hz), 22.73 (d, *J* = 4.5 Hz), 17.66 (d, *J* = 48.2 Hz), 12.64 (s) ppm.

^{31}P NMR{H} (162 MHz, D_2O) δ 33.42 (s) ppm.

IR (KBr disc, ν): 3407, 2964, 2936, 2874, 1587, 1416, 1347, 1314, 1237, 1205, 1099, 1054, 1009, 965, 925, 905, 832, 726, 629 cm^{-1}.

HRMS(ESI): m/z calcd for $[C_{16}H_{36}P]^+$, 259.2555; m/z found 259.2553; m/z calcd for $[C_5H_8NO_2]^-$, 114.0555; m/z found 114.0558.

Tetrabutylphosphonium 3-Pyridinesulfonate (12g)

Colorless oil, quantitative yield.

^{1}H NMR (400 MHz, D_2O) δ 8.82 (d, *J* = 1.8 Hz, 1H), 8.58 (dd, *J* = 4.8, 0.7 Hz, 1H), 8.13 (d, *J* = 8.0 Hz, 1H), 7.52 (dd, *J* = 8.0, 5.0 Hz, 1H), 2.12 – 1.93 (m, 8H), 1.52 – 1.26 (m, 16H), 0.82 (t, *J* = 7.2 Hz, 12H) ppm.

^{13}C{^{1}H} NMR (101 MHz, D_2O) δ 150.97 (s), 145.58 (s), 139.83 (s), 134.71 (s), 124.54 (s), 23.28 (d, *J* = 15.2 Hz), 22.70 (d, *J* = 4.5 Hz), 17.62 (d, *J* = 48.2 Hz), 12.60 (s) ppm.

^{31}P NMR{H} (162 MHz, D_2O) δ 33.39 (s) ppm.

IR (KBr disc, ν): 3471, 2964, 2930, 2866, 1630, 1583, 1463, 1412, 1384, 1233, 1203, 1147, 1095, 1048, 1010, 969, 922, 814, 748, 701, 641, 614, 568 cm^{-1}.

HRMS(ESI): m/z calcd for $[C_{16}H_{36}P]^+$, 259.2555; m/z found 259.2551; m/z calcd for $[C_5H_4NO_3S]^-$, 157.9911; m/z found 157.9910.

Tetrabutylphosphonium 2-(4'-Pyridyl)ethanesulfonate (12h)

Colorless oil, quantitative yield.

^{1}H NMR (400 MHz, D_2O) δ 8.32 (d, *J* = 5.2 Hz, 2H), 7.26 (d, *J* = 5.8 Hz, 2H), 3.12 – 3.04 (m, 2H), 3.03 – 2.95 (m, 2H), 2.13 – 1.90 (m, 8H), 1.53 – 1.22 (m, 16H), 0.82 (t, *J* = 7.2 Hz, 12H) ppm.

^{13}C{^{1}H} NMR (101 MHz, D_2O) δ 150.23 (s), 148.53 (s), 124.50 (s), 50.93 (s), 23.29 (d, *J* = 15.2 Hz), 22.71 (d, *J* = 4.5 Hz), 17.62 (d, *J* = 48.2 Hz), 12.61 (s) ppm.

^{31}P NMR{H} (162 MHz, D_2O) δ 33.37 (s) ppm.

IR (KBr disc, ν): 3454, 2964, 2930, 2870, 1608, 1565, 1471, 1420, 1386, 1211, 1096, 1045, 1002, 972, 917, 785, 729, 631, 537, 512 cm^{-1}.

HRMS(ESI): m/z calcd for $[C_{16}H_{36}P]^+$, 259.2555; m/z found 259.2549; m/z calcd for $[C_7H_8NO_3S]^-$, 186.0224; m/z found 186.0228.

Tris(2-Chloroethyl)Amine Hydrochloride (14)

To a round-bottom equipped with a stir bar was added triethanolamine (2.0 mL, 15.07 mmol), dry THF (20 mL) and thionyl chloride (6.0 mL, 82.26 mmol). Upon addition of thionyl chloride a white precipitate started to form. The round-bottom was equipped with a condenser and the system was placed under a low argon flow for the duration of the experiment. The reaction mixture was heated at 60 °C and magnetically stirred for 20 h. The precipitate was isolated by suction filtration and the solid washed with THF (3 x 10 mL) and dried in-vacuo resulting in a white solid (2.588 g, 10.74 mmol, 70 %).

Melting point: 122.5 – 123.5 °C.

^{1}H NMR (400 MHz, DMSO-d_6) δ 3.99 (t, J = 7.1 Hz, 6H), 3.50 (t, J = 6.8 Hz, 6H) ppm.

^{13}C{^{1}H} NMR (101 MHz, DMSO-d_6) δ 53.84 (s), 38.03 (s) ppm.

FT-IR(KBr disc, ν): 3417 m br, 3024 m, 3012 m, 2991 s, 2972 s, 2937 s, 2886 m, 2830 m, 2775 m, 2664 s, 2596 s, 2547 s, 2415 s, 1637 w, 1448 s, 1413 s, 1395 s, 1379 s, 1310 m, 1282 m, 1268 m, 1210 m, 1197 m, 1174 m, 1104 w, 1079 w, 1068 w, 1036 m, 1023 m,

972 m, 944 m, 920 w, 880 w, 809 w, 790 w, 762 s, 733 s, 686 s, 590 m, 542 m, 471 m cm^{-1}.

HRMS(ESI): m/z calcd for $[C_6H_{13}NCl_3]^+$ 204.0113; m/z found 204.0112.

Tris((2-Carbazolyl)Ethyl)Amine (15)

Within the glovebox, into a round-bottom Schlenk flask equipped with a stir bar was added tris(2-chloroethyl)amine hydrochloride (1.678 g, 6.963 mmol), carbazole (3.494 g, 20.89 mmol) and sodium hydride (0.704 g, 29.3 mmol). Magnetic stirring was initiated and THF (30-40 mL) was slowly added via Pasteur pipette to avoid boiling over. The flask was sealed with a glass stopper and removed from the glovebox. The reaction was magnetically stirred at 60 °C for 4 days during which time a white/grey precipitate formed. The reaction mixture was filtered through a glass frit and the filtrate was dried in-vacuo. The remaining yellowish solid was washed with toluene (3 x 15 mL) resulting in a white solid. (3.214 g, 5.386 mmol, 77 %).

Melting point: 199 – 201 °C.

^{1}H NMR (400 MHz, $CDCl_3$) δ 8.00 (d, *J* = 7.7 Hz, 6H), 7.33 (t, *J* = 7.3 Hz, 6H), 7.14 (t, *J* = 7.4 Hz, 6H), 6.99 (d, *J* = 8.2 Hz, 6H), 3.97 (t, *J* = 6.8 Hz, 6H), 2.83 (t, *J* = 6.8 Hz, 6H) ppm.

^{13}C{^{1}H} NMR (101 MHz, $CDCl_3$) δ 140.20 (s), 125.79 (s), 122.93 (s), 120.51 (s), 119.14 (s), 108.55 (s), 53.96 (s), 42.27 (s) ppm.

^{1}H NMR (400 MHz, DMSO-d_6) δ 8.12 (d, 6H, J_{HH} = 7.6 Hz, 3 Cb-C$_1$*H* & 3 Cb-C$_8$*H*), 7.36 (t, 6H, J_{HH} = 7.6 Hz, 3 Cb-C$_3$*H* & 3 Cb-C$_6$*H*), 7.18-7.13 (m, 12H, J_{HH} = 7.6 Hz, 3 Cb-C$_2$*H* & 3 Cb-C$_7$*H* and 3 Cb-C$_4$*H* & 3 Cb-C$_5$*H*), 4.03 (t, 6H, J_{HH} = 6.8 Hz, 3 CbC*H*$_2$CH$_2$N), 2.81 (t, 6H, J_{HH} = 6.8 Hz, 3 CbCH$_2$C*H*$_2$N) ppm.

^{13}C{^{1}H} NMR (101 MHz DMSO-d_6) δ 139.8 (3 Cb-C$_{9a}$ & 3 Cb-C$_{8a}$), 125.6 (3 Cb-*C*$_3$H & 3 Cb-*C*$_6$H), 122.1 (3 Cb-C$_{4a}$ & 3 Cb-C$_{5a}$), 120.2 (3 Cb-*C*$_1$H & 3 Cb-*C*$_8$H), 118.7 (3 Cb-*C*$_2$H & 3 Cb-*C*$_7$H), 109.2 (3 Cb-*C*$_4$H & 3 Cb-*C*$_5$H), 53.4 (3 CbCH$_2$*C*H$_2$N), 41.8 (3 Cb*C*H$_2$CH$_2$N) ppm.

FT-IR(KBr disc, ν): 3044 w, 2974 w, 2937 w, 2837 w, 1920 w, 1885 w, 1854 w, 1803 w, 1772 w, 1686 w, 1625 w, 1594 m, 1483 s, 1461 s, 1454 s, 1381 w, 1349 m, 1325 s, 1271 w, 1216 w, 1227 m, 1216 m, 1154 m, 1120 m, 1050 w, 1017 w, 997 w, 985 w, 926 w, 906 w, 880 w, 857 w, 841 w, 800 w, 750 s, 723 s, 616 m cm^{-1}.

HRMS(ESI): m/z calcd for $C_{42}H_{36}N_4$ 596.2940; m/z found 596.2947.

Butyldi(2-Chloroethyl)Amine Hydrochloride (16)

Butyldiethanolamine (2.50 ml, 2.47 g, 15.3 mmol) was added dropwise to a great excess of thionyl chloride (10.0 ml, 16.3 g, 137 mmol) with stirring. The reaction was allowed to proceed for 2 h beyond the cessation of gas evolution (hydrogen chloride and sulfur dioxide) from the reaction mixture. The thionyl chloride was removed *in vacuo* and traces of thionyl chloride were removed after several hours under high vacuum. The

desired product, butyldi(2-chloroethyl)amine hydrochloride (3.57 g, 15.2 mmol, >99%), was obtained as a white solid.

Melting point 95–96 ºC

^{1}H NMR (400 MHz, DMSO-d_6) δ 11.68 (s, 1H), 4.07 (t, *J* = 6.6 Hz, 4H), 3.60 – 3.44 (m, 4H), 3.23 – 3.08 (m, 2H), 1.75 – 1.62 (m, 2H), 1.44 – 1.20 (m, 1H), 0.91 (t, *J* = 7.3 Hz, 3H) ppm.

^{13}C{^{1}H} NMR (101 MHz, DMSO-d_6) δ 52.92 (s), 52.45 (s), 37.13 (s), 24.68 (s), 19.33 (s), 13.46 (s) ppm.

FT-IR(KBr disc, ν): 3334 s br, 3145 w, 3056 m, 3023 m, 2964 s, 2875 m, 2682 m, 2603 m, 1635 s, 1488 s, 1465 m, 1384 w, 1316 w, 1286 w, 1217 w, 1175 s, 1050 m, 974 w, 926 w, 778 m, 742 w, 680 s, 587 m, 446 w cm^{-1}.

HRMS(ESI): m/z calcd for $[C_8H_{18}NCl_2]^+$ 198.0816; m/z found 198.0821.

Butyldi(2-(Carbazol-9-yl)Ethyl)Amine (17)

Butyldi(2-(carbazol-9-yl)ethyl)amine was prepared by a method similar to tris((2-carbazolyl)ethyl)amine and was obtained as a white solid. (3.214 g, 5.386 mmol, 77 %).

Melting point 101–102 ºC

^{1}H NMR (400 MHz, $CDCl_3$) δ 8.03 (t, *J* = 10.9 Hz, 4H), 7.46 – 7.33 (m, 4H), 7.25 – 7.09 (m, 8H), 4.08 (t, *J* = 7.1 Hz, 4H), 2.79 (t, *J* = 7.2 Hz, 4H), 2.53 (dd, *J* = 15.1, 7.6 Hz, 2H), 1.45 – 1.28 (m, 2H), 1.22 (dt, *J* = 15.4, 7.2 Hz, 2H), 0.86 (t, *J* = 7.3 Hz, 3H) ppm.

$^{13}C\{^{1}H\}$ NMR (101 MHz, $CDCl_3$) δ 140.19 (s), 125.60 (s), 122.81 (s), 120.26 (s), 119.13 (s), 118.89 (s), 108.52 (s), 55.05 (s), 53.24 (s), 41.94 (s), 29.69 (s), 20.42 (s), 14.03 (s) ppm.

FT-IR(KBr disc, ν): 3048 m, 2931 m, 2868 w, 2802 m, 2360 w, 2342 w, 1922 w, 1885 w, 1852 w, 1802 w, 1772 w, 1627 m, 1596 m, 1484 s, 1462 s, 1451 s, 1387 w, 1374 w, 1351 m, 1334 m, 1326 m, 1297 w, 1268 w, 1252 w, 1227 m, 1180 w, 1163 w, 1151 m, 1120 w, 1061 w, 924 w, 747 s, 719 s, 616 w cm^{-1}.

HRMS(ESI): m/z calcd for $C_{32}H_{33}N_3$ 459.2674; m/z found 459.2679.

Tetra(2-Ethanol)Ammonium Chloride (18)

Triethanolamine (2.50 ml, 2.81 g, 18.8 mmol) was weighed and placed in a heavy walled glass pressure tube equipped with a magnetic stir bar (the smallest pressure tube that can contain the total amount of the reagents should be used to minimize the head space). An equimolar amount of 2-chloroethanol (1.26 ml, 1.52 g, 18.8 mmol) was added and the pressure tube was sealed and placed in an oil bath (equipped with a magnetic stirrer) that was preheated to 150 ºC. The reaction is complete when the mixture ceases boiling and there is no visible reflux of the 2-chloroethanol in the pressure tube (approximately 15–30 min). The mixture was then allowed to cool to ambient pressure and the cap was removed from the pressure tube and replaced with a rubber septum. The pressure tube was then subjected to high vacuum to remove traces of unreacted 2-

chloroethanol. The product tetra(2-ethanol)ammonium chloride (4.31 g, 18.7 mmol, >99%) was obtained as a white solid.

Melting point 133–134 ºC

The NMR spectra are consistent with that presented in the literature.[222]

^{1}H NMR (400 MHz, DMSO-d_6) δ 5.38 (t, J = 5.2 Hz, 4H), 3.82 (q, J = 5.3 Hz, 8H), 3.60 – 3.55 (m, 8H) ppm.

^{13}C{^{1}H} NMR (101 MHz, DMSO-d_6) δ 61.74 (s), 54.63 (s) ppm.

FT-IR(KBr disc, ν): 3387 s br, 2969 s, 1637 m, 1484 s, 1372 s, 1246 m, 1048 s, 975 m, 943 s, 777 w, 592 m cm^{-1}.

HRMS(ESI): m/z calcd for $[C_8H_{20}NO_4]^+$ 194.1394; m/z found 194.1390.

Tetra(2-Chloroethyl)Ammonium Chloride (19)

Tetra(2-ethanol)ammonium chloride (2.00 g, 8.71 mmol) was dissolved in a great excess of thionyl chloride (10 ml, 16.3 g, 137 mmol) with stirring. The reaction was allowed to proceed for 2 h beyond the cessation of gas evolution (hydrogen chloride and sulfur dioxide) from the reaction mixture. The thionyl chloride was removed *in vacuo* and traces of thionyl chloride were removed after several hours under high vacuum. The desired product, tetra(2-chloroethyl)ammonium chloride (2.63 g, 8.66 mmol, >99%), as a white solid.

Melting point 185–186 ºC dec.

^{1}H NMR (400 MHz, DMSO-d_6) δ 4.16 (t, J = 6.3 Hz, 4H), 4.06 (t, J = 6.6 Hz, 4H) ppm.

$^{13}C\{^{1}H\}$ NMR (101 MHz, DMSO-d_6) δ 59.11 (s), 35.80 (s) ppm.

FT-IR(KBr disc, ν): 3422 m br, 3006 s, 2988 s, 2971 s, 2963 s, 2865 s, 2754 w, 2719 w, 2580 w, 2502 w, 1636 w, 1488 s, 1458 s, 1440 s, 1421 m, 1382 m, 1348 m, 1294 m, 1284 m, 1224 w, 1208 w, 1173 w, 1090 m, 1043 m, 1006 w, 946 w, 923 w, 862 m, 815 m, 766 s, 699 w, 675 m, 659 m, 641 w, 542 w cm^{-1}.

HRMS(ESI): m/z calcd for $[C_8H_{16}NCl_4]^+$ 266.0036; m/z found 266.0035.

N-Allylcarbazole (20)

Carbazole (recrystallized from toluene, 2.00 g, 12.0 mmol) was measured into a 250 ml single–necked round bottom flask equipped with a stirrer and a rubber septum. Approximately 100 ml of dry tetrahydrofuran was added and a colorless solution formed. To this was added an equimolar amount of potassium tert-butoxide solution (1.0M in THF, 12.0 ml, 12.0 mmol). The solution turned dark yellow. After stirring at ambient temperature for 30 min, allyl chloride (1.07 ml, 1.01 g, 13.2 mmol) was added. A white precipitate of potassium chloride started to form immediately. The solution was allowed to stir for 2 h before the rubber septum was removed and a reflux condenser was attached. The solution was heated to reflux for an additional hour. After cooling the potassium chloride was removed by filtration and the filtrate was concentrated *in vacuo* to yield N-allylcarbazole (2.38 g, 11.5 mmol, 96%) as a yellow solid.

Melting point 55 ºC (lit. 54–55 ºC)[223]

The NMR spectra are consistent with that presented in the literature.[223]

^{1}H NMR (400 MHz, DMSO-d_6) δ 8.17 (d, *J* = 7.8 Hz, 2H), 7.55 (d, *J* = 8.2 Hz, 2H), 7.45 (t, *J* = 7.7 Hz, 2H), 7.22 (t, *J* = 7.4 Hz, 2H), 5.97 (ddt, *J* = 21.9, 10.2, 5.1 Hz, 1H), 5.09 (d, *J* = 10.3 Hz, 1H), 5.00 (d, *J* = 4.9 Hz, 2H), 4.96 (d, *J* = 17.2 Hz, 1H) ppm.

^{13}C{^{1}H} NMR (101 MHz, DMSO-d_6) δ 139.97 (s), 133.05 (s), 125.67 (s), 122.18 (s), 120.24 (s), 118.86 (s), 116.30 (s), 109.32 (s), 44.52 (s) ppm.

HRMS(ESI): m/z calcd for $C_{15}H_{13}N$ 207.1048; m/z found 207.1053.

Tetraallylammonium Chloride (21)

Triallylamine (2.50 ml, 1.98 g, 14.4 mmol) was placed in a heavy walled glass pressure tube equipped with a magnetic stir bar (the smallest pressure tube that can contain the total amount of the reagents should be used to minimize the head space). An excess amount of allyl chloride (1.29 ml, 1.21 g, 15.8 mmol) was added and the pressure tube was sealed and placed in an oil bath (equipped with a magnetic stirrer) that was preheated to 150 ºC. The reaction is complete when the mixture ceases boiling and there is no visible reflux of the allyl chloride in the pressure tube (approximately 15–30 min). The mixture was then allowed to cool to ambient pressure and the cap was removed from the pressure tube and replaced with a rubber septum. The pressure tube was then subjected to high vacuum to remove traces of unreacted allyl chloride. The product tetraallylammonium chloride (3.01 g, 14.1 mmol, 98%) was obtained as a white solid.

Melting point 104–105 ºC

^{1}H NMR (400 MHz, DMSO-d_6) δ 6.16 (ddt, *J* = 17.3, 10.3, 7.1 Hz, 4H), 5.70 (dd, *J* = 16.9, 1.4 Hz, 4H), 5.58 (dd, *J* = 10.2, 1.7 Hz, 4H), 4.01 (d, *J* = 7.3 Hz, 8H) ppm.

^{13}C{^{1}H} NMR (101 MHz, DMSO-d_6) δ 127.06 (s), 125.91 (s), 60.65 (s) ppm.

FT-IR(KBr disc, ν): 3438 m br, 3082 m, 3016 w, 2968 m, 2884 w, 1902 w, 1639 m, 1463 s, 1422 s, 1364 m, 1312 w, 1274 m, 1178 w, 1157 w, 1033 s, 1005 s, 991 s, 941 s, 896 m, 841 m, 788 w cm^{-1}.

9-(3'-Chloropropyl)Carbazole (22)

Carbazole (recrystallized from toluene, 5.00 g, 29.9 mmol) was measured into a 250 ml single–necked round bottom flask equipped with a stirrer and a rubber septum. Approximately 100 ml of dry tetrahydrofuran was added and a colorless solution formed. To this was added an equimolar amount of potassium tert-butoxide solution (1.0 M in THF, 29.9 ml, 29.9 mmol). The solution turned dark yellow. After stirring at ambient temperature for 30 min, 1.1 equivalents of 1-bromo-3-chloropropane (3.25 ml, 5.18 g, 32.9 mmol) was added. A white precipitate of potassium bromide started to form immediately. The solution was allowed to stir for 2 h before the rubber septum was removed and a reflux condenser was attached. The solution was heated to reflux for an additional hour. After cooling the potassium bromide was removed by filtration and the filtrate was concentrated *in vacuo*. The resulting mixture can be purified via silica gel column chromatography eluting with hexanes. However, the desired product has low solubility in hexanes and a great deal of solvent is required. A short plug of silica gel

provides sufficient separation with only a moderate amount of hexanes used. Chloropropylcarbazole (4.74 g, 19.4 mmol, 65%) was obtained as a viscous yellowish oil.

Melting point (lit. 32-33ºC)[224]

The NMR spectra are consistent with that presented in the literature.[192]

^{1}H NMR (400 MHz, $CDCl_3$) δ 8.44 (d, *J* = 7.8 Hz, 2H), 7.80 (t, *J* = 7.3 Hz, 2H), 7.68 (d, *J* = 8.3 Hz, 2H), 7.62 (t, *J* = 7.4 Hz, 2H), 4.57 (t, *J* = 6.5 Hz, 2H), 3.61 (t, *J* = 6.1 Hz, 2H), 2.45 – 2.37 (m, 2H) ppm.

^{13}C{^{1}H} NMR (101 MHz, $CDCl_3$) δ 140.72 (s), 126.28 (s), 123.33 (s), 120.82 (s), 119.59 (s), 109.01 (s), 42.67 (s), 39.91 (s), 32.03 (s) ppm.

FT-IR(NaCl thin film, ν): 3051 s, 3021 s, 2950 s, 2881 m, 2833 w, 2816 w, 1927 w, 1889 w, 1772 w, 1626 s, 1597 s, 1576 m, 1484 s, 1452 s, 1424 m, 1382 m, 1347 s, 1325 s, 1297 m, 1281 m, 1242 s, 1212 m, 1193 s, 1152 s, 1121 s, 1078 w, 1062 m, 1048 w, 1019 m, 1001 m, 963 w, 926 w, 845 m, 802 m, 749 s, 723 s, 663 m, 616 m, 558 m.

HRMS(ESI): m/z calcd for $C_{15}H_{14}ClN$, 243.0815; m/z found 243.0809.

1-(3'-(Carbazol-9''-yl)Propyl)-3-Methylimidazolium Bistriflimide (23)

9-(3'-Chloropropyl)carbazole (2.00 g, 8.21 mmol) was weighed and placed in a heavy walled glass pressure tube equipped with a magnetic stir bar (the smallest pressure tube that can contain the total amount of the reagents should be used to minimize the head space). An equimolar amount of 1-methylimidazole (654 µl, 674 mg, 8.21 mmol)

was added and the pressure tube was sealed and placed in an oil bath (equipped with a magnetic stirrer) that was preheated to 150 ºC. The reaction was allowed to proceed for 2 h as both starting materials are well below their boiling points (and the end of the reaction could not be easily observed). The mixture was then allowed to cool to ambient pressure and the cap was removed from the pressure tube and the intermediate product, 1-(3'-(carbazol-9''-yl)propyl)-3-methylimidazolium chloride, was dissolved in methylene chloride. An equimolar amount of an aqueous solution of lithium bis(trifluoromethane) sulfonimide (2.36 g, 8.21 mmol) in 10 ml of water was mixed with the methylene chloride solution in a separatory funnel. Ion exchange occurred with shaking. The methylene chloride layer was isolated and concentrated *in vacuo*. 1-(3'-(Carbazol-9''-yl) propyl)-3-methylimidazolium bistriflimide (4.59 g, 8.04 mmol, 98%) was obtained as a yellow oil.

^{1}H NMR (400 MHz, $CDCl_3$) δ 8.02 (d, J = 7.8 Hz, 2H), 7.51 – 7.44 (m, 4H), 7.27 (s, 1H), 7.26 – 7.18 (m, 2H), 7.04 (s, 1H), 6.88 (s, 1H), 4.56 (t, J = 6.5 Hz, 2H), 4.43 (t, J = 6.7 Hz, 2H), 3.75 (s, 3H), 2.69 – 2.56 (m, 2H).

^{13}C{^{1}H} NMR (101 MHz, $CDCl_3$) δ 140.4 (s), 132.4 (s), 125.8 (s), 123.1 (s), 123.0 (s), 120.5 (s), 120.3 (s), 119.8 (q, J = 320 Hz), 119.2 (s), 108.6 (s), 42.4 (s), 40.6 (s), 39.8 (s), 31.7 (s) ppm.

FT-IR(KBr disc, ν): 3153 w, 3118 w, 3097 w, 3054 w, 2959 w, 1626 w, 1596 m, 1573 w, 1485 s, 1463 s, 1327 s, 1228 s, 1138 s, 1056 s, 1001 w, 831 w, 789 m, 755 s, 727 s, 654 m, 617 s, 601 m, 570 m, 513 m cm^{-1}.

HRMS(ESI): m/z calcd for $[C_{19}H_{20}N_3]^+$, 290.1657; m/z found 290.1662; m/z calcd for $[C_2NO_4F_6S_2]^-$, 279.9173; m/z found 279.9170.

A.2 Unsuccessful Syntheses

Attempted Alkylation of Tri(2-(Carbazolyl)Ethyl)Amine with Butyl Iodide

Tri(2-(carbazolyl)ethyl)amine (500 mg, 0.84 mmol) was weighed and placed in a heavy walled glass pressure tube equipped with a magnetic stir bar (the smallest pressure tube that can contain the total amount of the reagents should be used to minimize the head space). An excess amount of butyl iodide (1 ml, 1.62 g, 8.8 mmol) was added and the pressure tube was sealed and placed in an oil bath (equipped with a magnetic stirrer) that was preheated to 150 ºC. The reaction was allowed to proceed for 1 h. The mixture was then allowed to cool to ambient pressure and the cap was removed from the pressure tube and replaced with a rubber septum. The pressure tube was then subjected to high vacuum to remove traces of unreacted butyl iodide. The product was dissolved in DMSO-d_6 and analyzed by ^{1}H NMR spectroscopy but only tri(2-(carbazolyl)ethyl)amine was recovered.

Attempted Alkylation of Tri(2-(Carbazolyl)Ethyl)Amine with Butyl Tosylate

This reaction was performed by the same method as attempted alkylation of tri(2-(carbazolyl)ethyl)amine with butyl iodide with the exception that butyl tosylate was used as the electrophile.

Attempted Alkylation of Tri(2-(Carbazolyl)Ethyl)Amine with Butyl Tosylate Catalyzed by Sodium Iodide

This reaction was performed by the same method as attempted alkylation of tri(2-(carbazolyl)ethyl)amine with butyl iodide with the exception that butyl tosylate was used as the electrophile and sodium iodide (5 mol%) was added as a catalyst.

Attempted Alkylation of Butyldi(2-(Carbazolyl)Ethyl)Amine with Butyl Iodide

This reaction was performed by the same method as attempted alkylation of tri(2-(carbazolyl)ethyl)amine with butyl iodide but using butyldi(2-carbazolyl)ethyl)amine as the nucleophile.

Metathesis of Tetraallylammonium Chloride with N-AllylCarbazole

To a 25 ml single–necked round bottomed flask were added tetraallylammonium chloride (129 mg, 0.6 mmol) and N-allylcarbazole (500 mg, 2.41 mmol). To this were added 10 ml of isopropanol and a magnetic stir bar. The mixture was stirred until it was homogeneous. At this point 2 mol% equivalent of the catalyst, tricyclohexylphosphine [1,3-bis(2,4,6-trimethylphenyl)-4,5-dihydroimidazol-2-ylidene][(phenylthio)methylene] ruthenium(II) dichloride (10.6 mg, 12 μmol), was added and the solution was allowed to stir for 4 h. The ruthenium catalyst was then removed by filtering the solution through a short column of silica gel. The solution was then concentrated *in vacuo* and redissolved in DMSO-d_6. ^{1}H NMR spectroscopy showed very low conversion to undetermined products with no easily identifiable peaks associated with the desired products.

A.3 Reactions of Ionic Compounds

Hydrogenation of N-Methylpyridinium Nicotinate

N-Methylpyridinium nicotinate (1 g, 4.6 mmol) was measured into a 31 ml stainless steel autoclave. To this was added 1 mol% equivalent of Pd/C (10 wt%) (49.2 mg Pd/C, 4.9 mg Pd, 46.2 μmol) powder and a magnetic stir bar. The autoclave was sealed and placed in an electric heating apparatus above a magnetic stirrer. Stirring was initiated and the autoclave was pressurized to approximately 10 bar of hydrogen for one

minute then slowly depressurized. This pressurization/depressurization cycle was performed three times to flush the autoclave and gas lines of air and insure an atmosphere of hydrogen. The flushed autoclave was resealed at ambient pressure and heated to 100 ºC. The temperature inside the autoclave was allowed to equilibrate for 30 min. The autoclave was then pressurized with 100 bar of hydrogen, sealed and the contents were left to react for a period of 18 h. The autoclave was then removed from the electric heater and immersed in an ice water bath for 15 min to rapidly cool the apparatus. The gas pressure was then slowly vented in a fumehood. The autoclave was opened and the contents were diluted with methanol and filtered through diatomaceous earth to remove the catalyst. The solution was concentrated *in vacuo* to remove the methanol. The product mixture was dissolved in DMSO-d_6 and analyzed by ^{1}H NMR spectroscopy. Results were presented in **Section 1.2.1.3**.

Thermal Decomposition of N-Methylpiperidinium Nipecotate

Approximately 5 ml of N-methylpiperidinium nipecotate was dispensed into a 10 ml single–necked round bottom flask equipped with a magnetic stir bar and a reflux condenser. The contents of the flask were heated to 200 ºC for 1 h. At this point, a small ring of condensation formed on the inside of the reflux condenser. After the apparatus was allowed to cool, the reflux condenser was carefully removed so as to not disturb the droplets of condensate and was rinsed with DMSO-d_6 into a clean flask. The solution of

condensate was analyzed by ^{1}H NMR spectroscopy. Results were presented in **Section 1.2.1.5**.

Dehydrogenation of N-Methylpiperidinium Nipecotate

N-Methylpiperidinium nipecotate (100 mg, 0.44 mmol) in 2 ml of ethylene glycol and catalyst (approximately 1 mol% loading as noted in **Table 1.2**) were stirred at 600 rpm with a magnetic stir bar and heated to 150 ºC for 3 h in a test tube in air. Samples were diluted with 5 ml of methanol, filtered through diatomaceous earth and the solvents were removed under high vacuum. The remaining solid was dissolved in D_2O and analyzed by ^{1}H NMR spectroscopy for conversion to aromatic products. Results presented in **Table 1.2**.

Dehydrogenation of N-Hexylpiperidinium Nicotinate

This experiment was performed by a method similar to the dehydrogenation of N-methylpiperidinium nipecotate with the exeception that N-Hexylpiperidinium nicotinate was the substrate, there was no solvent used during the reaction, and only the Ru/C catalyst was used. Results presented in Section **1.2.1.4**.

Hydrogenation of N-Methylpiperidinium 3-Pyridinesulfonate

These experiments were performed by a method similar to the hydrogenation of N-methylpyridinium nicotinate with the exception that N-Methylpiperidinium 3-pyridinesulfonate was the substrate, the reactions were carried out at 100 ºC or 200 ºC, and the reaction times were reduced to 6 h. Results presented in **Section 1.2.2.2**.

Hydrogenation of N-Methylpiperidinium 2-(4'-Pyridyl)ethanesulfonate

N-Methylpiperidine (315 µl, 265 mg, 2.7 mmol) and 2-(4'-pyridyl)ethanesulfonic acid (500 mg, 2.7 mmol) were measured into a 31 ml stainless steel autoclave. To this were added 1 mol% equivalent of Pd/C (10 wt%) (28.4 mg Pd/C, 2.8 mg Pd, 26.7 µmol) powder and a magnetic stir bar. The autoclave was sealed and placed in an electric heating apparatus above a magnetic stirrer. Stirring was initiated and the autoclave was pressurized to approximately 10 bar of hydrogen for one minute then slowly depressurized. This pressurization was repeated twice more to flush the autoclave and gas lines of air and insure an atmosphere of hydrogen. The flushed autoclave was resealed at ambient pressure and was heated to 200 ºC. The temperature inside the autoclave was allowed to equilibrate for 30 min. The autoclave was then pressurized with 100 bar of hydrogen and sealed and was left to react for a period of 6 h. The autoclave was then removed from the electric heater and immersed in an ice water bath for 15 min to rapidly cool the apparatus. The gas pressure was then slowly vented in a fumehood. The

autoclave was opened and the contents were diluted with methanol and filtered through diatomaceous Earth to remove the catalyst. The solution was concentrated *in vacuo* to remove the methanol. The product mixture was dissolved in DMSO-d_6 and analyzed by ^{1}H NMR spectroscopy. Results presented in **Section 1.2.3.2**.

Hydrogenation of Sodium Carboxylates

Solutions of sodium carboxylates (10 ml, 20 mM in ethanol) were added to a 160 ml stainless steel autoclave. To the autoclave were added a magnetic stir bar and 10 mol% equivalent of Pd in the form of Pd/C (10 wt%) (21.3 mg Pd/C, 2.1 mg Pd, 20 μmol). The autoclave was sealed then flushed three times with 10 bar of hydrogen to remove any air inside. The autoclave was then heated to a prescribed temperature (80, 100, 125 or 200 ºC) using an electric heater and stirred using a magnetic stirrer. After reaching thermal equilibrium after a period of 30 min the autoclave was pressurized to 100 bar of hydrogen and sealed. The reaction was allowed to proceed for 18 h before the autoclave was removed from the electric heater and submerged in ice water for 15 min. The autoclave was then slowly vented to ambient pressure in a fume hood and was then opened. The contents of the autoclave were then filtered through a small plug of diatomaceous earth before being concentrated *in vacuo*. The residue was dissolved in deuterium oxide, which was spiked with a known quantity of 1,4-dioxane as an internal standard, and analyzed by ^{1}H NMR spectroscopy. Results presented in **Table 1.3**.

Dehydrogenation of Sodium Carboxylates Neat and in Ethylene Glycol

The saturated sodium carboxylates were dehydrogenated by stirring in a test tube which was open to the atmosphere at 200 ˚C, using 1 mol% Pd/C (10 wt%) over 3 h. Sodium isonipecotate (mp 182-185 ºC) could be dehydrogenated without the use of a solvent. Sodium nipecotate and sodium furoate were dehydrogenated in ethylene glycol solution at reflux (195 °C). If necessary, the product solution was dissolved in methanol before being filtered through diatomaceous earth to remove the catalyst. The solvent was removed *in vacuo* (in the case of ethylene glycol by distillation under high vacuum) and the resulting mixtures were dissolved in deuterium oxide and analyzed by ^{1}H NMR spectroscopy using dioxane as an internal standard. Results presented in Section 1.3.3.

Dehydrogenation of Sodium Carboxylates in Formamide

These reactions were carried out using a method similar to the dehydrogenation of sodium carboxylates neat and the ethylene glycol with the exception that the solent used was formamide. Results presented in Table 1.5.

Hydrogenation of N-Heterocyclic Trifluoromethanesulfonates

Solutions of N-heterocyclic trifluoromethanesulfonates (2 ml, 0.5 M in D_2O) were added to a 160 ml stainless steel autoclave. To the autoclave were added a magnetic stir bar and 10 mol% equivalent of Pd in the form of Pd/C (10 wt%) (106 mg Pd/C, 10.6 mg Pd, 0.1 mmol). The autoclave was sealed then flushed three times with 10 bar of hydrogen to remove any air inside. The autoclave was then heated to 50 ºC using an electric heater and stirred using a magnetic stirrer. After reaching thermal equilibrium after a period of 30 min, the autoclave was pressurized to 50 bar of hydrogen and sealed. The reaction was allowed to proceed for either 1 or 21 h before the autoclave was removed from the electric heater and submerged in ice water for 15 min. The autoclave was then slowly vented to ambient pressure in a fume hood and was then opened. The contents of the autoclave were then filtered through a small plug of diatomaceous earth and was spiked with a known quantity of 1,4-dioxane as an internal standard, and analyzed by ^{1}H NMR spectroscopy. Results presented in **Table 1.4**.

Dehydrogenation of N-Heterocyclic Trifluoromethanesulfonates

The saturated N-heterocyclic cations were dehydrogenated without solvent. They were dehydrogenated by stirring in a test tube open to the atmosphere at either 100, 150, or 200 ºC, with 1 mol% Pd/C for 3 h. The samples were then dissolved in methanol and filtered through diatomaceous earth to remove the heterogeneous catalyst and then

concentrated *in vacuo*. The resulting mixtures were dissolved in D_2O and analysed by ^1H NMR spectroscopy using dioxane as an internal standard. Results presented in Table 1.6.

Hydrogenation of Unsaturated Anionic Heterocycles

Samples of tetrabutylphosphonium salts of anionic heterocycles (~100 mg) were diluted with 0.5 ml of isopropyl alcohol and placed in 0.8 ml autosampler vials over palladium on silica (5 wt% Pd/SiO_2, 1 mol% equivalent with respect to Pd) ppm. The autosampler vials were evenly spaced in a 36-well sample holder and sealed in a 160 ml stainless steel autoclave. The autoclave was flushed three times with hydrogen and then sealed and heated to 75 ºC in an electric heater for a period of 1 h to reach thermal equilibrium. At this point the autoclave was pressurized using 70 bar of hydrogen gas and resealed. After 20 h the autoclave was removed from the electric heater and placed in an ice bath for fifteen min to rapidly cool the apparatus and then the hydrogen was vented to atmospheric pressure over a period of fifteen min to prevent spattering of the contents of the autosampler vials. The autoclave was opened and the vials, which were still venting hydrogen, were removed and allowed to slowly evaporate at ambient temperature and pressure for two days to remove the isopropyl alcohol. Each autosampler vial was charged with 0.5 ml of deuterium oxide and mixed well to suspend the catalyst particles. The suspensions were filtered through a small plug of diatomaceous earth in a pasteur pipette into dry NMR tubes and were analyzed by ^1H-NMR spectroscopy. The results are summarized in **Table 1.7**.

Dehydrogenation of Saturated Anionic Heterocycles

Samples of tetrabutylphosphonium salts of saturated anionic heterocycles (~100 mg) were quantitatively transferred into 10 mm test tubes over palladium on silica (5 wt% Pd/SiO_2, 1 mol% equivalent with respect to Pd) ppm. Each tube was sealed with a new rubber septum and was flushed with argon at a flow rate of approximately 10 ml per minute for 15 min. At this point, while argon flow was continued, the test tubes were submerged in an oil bath preheated to 175 ºC for one hour. The test tubes were then rapidly cooled in an ice bath for fifteen min. Each test tube was then charged with 0.5 ml of deuterium oxide and the solutions were thoroughly mixed to suspend the catalyst particles. The suspensions were then filtered through a small plug of diatomaceous earth in a pasteur pipette into dry NMR tubes. The solutions were analyzed by ^{1}H-NMR spectroscopy. The results are summarized in **Table 1.8**.

Hydrogenation of 1-(3'-(Carbazol-9''-yl)Propyl)-3-Methylimidazolium Bistriflimide

1-(3'-(Carbazol-9''-yl)propyl)-3-methylimidazolium bistriflimide (285 mg, 0.50 mmol) was carefully weighed into a beaker and then transferred quantitatively into a 31 ml stainless steel autoclave by diluting it in a small amount of methylene chloride, rinsing the beaker several times, and adding the rinses to the autoclave. The methylene chloride was allowed to evaporate for several hours until none remained. To the autoclave

were added a magnetic stir bar and 1 mol% equivalent of Pd in the form of Pd/C (10 wt %) (5.3 mg Pd/C, 0.53 mg Pd, 5 μmol). The autoclave was sealed and flushed three times with 10 bar of hydrogen to remove any air inside. The autoclave was then heated to 70 ºC using an electric heater and stirred using a magnetic stirrer. After reaching thermal equilibrium after a period of 30 min the autoclave was pressurized to 50 bar of hydrogen and sealed. The reaction was allowed to proceed for 24 h before the autoclave was removed from the electric heater and submerged in ice water for 15 min. The autoclave was then slowly vented to ambient pressure in a fume hood and was then opened. The contents of the autoclave were diluted with methylene chloride and then filtered through a small plug of diatomaceous earth before being concentrated *in vacuo*. The residue was dissolved in CD_2Cl_2 and analyzed by ^1H NMR spectroscopy showing only starting material. Results presented in **Section 1.5.2.2**.

Hydrogenation of 1-(3'-(Carbazol-9''-yl)Propyl)-3-Methylimidazolium Bistriflimide in Methylene Chloride

This reaction was carried out by a method similar to the hydrogenation of 1-(3'-(carbazol-9''-yl)propyl)-3-methylimidazolium bistriflimide with the exception that it was diluted to a 50% w/w solution in methylene chloride before hydrogenation. Results presented in **Section 1.5.2.2**.

A.4 Thermally Regenerative Fuel Cell Experiments

Hydrogenation at Ambient Pressure

The apparatus for these experiments consisted of a 25 ml two–necked pear shaped flask, the vertical neck of which was attached to a Dimroth condenser. The top of the condenser and the second neck on the flask were fitted with rubber septa. Before the reaction was initiated, the flask was charged with 5 ml of the organic liquid, a measured amount (0.1 mol% equivalent of Pd) of 10 wt% palladium on carbon, and a magnetic stir bar. The apparatus was clamped in place above an oil bath that had been preheated to 100 ºC. A needle attached to by a hose to a bubbler, was placed through the septa at the top of the condenser. Another needle, attached to a hydrogen gas cylinder, was placed through the septum at the side of the flask so that the tip was below the liquid level. The regulator on the hydrogen cylinder was adjusted to provide a steady slow flow of hydrogen gas through the reaction mixture at a rate of about 10 ml min^{-1}. The reaction mixture was sparged for ten minutes to purge the system of oxygen and then the apparatus was lowered into the oil bath so that the liquid levels of the oil bath and the fluid in the flask were at the same height. A timer was started at this point and the reaction was allowed to run for six hours. After this time elapsed, the flask was raised out of the oil bath. A syringe was used to withdraw a sample of about 50 µl of the reaction mixture. That sample and 0.5 ml of deuterated chloroform were mixed in a small vial and then added and the solution was filtered through a Kimwipe™ plug into an NMR tube.

The composition of the product mixture was determined by NMR spectroscopy. Results are presented in **Table 2.3**.

Dehydrogenation Under Argon

These experiments were performed as detailed for hydrogenation at ambient pressure with the exception that the flask was sparged with argon and the reaction temperature was increased to 200 ºC. Results are presented in **Table 2.4**.

Kinetics of Dehydrogenation of 1-Phenyl-1-Propanol over Pd/C

This reaction was performed as detailed for hydrogenation at ambient pressure with the exception that the reaction temperature was increased to 200 ºC and at regular intervals a syringe was used to withdraw about 50 µl of the reaction mixture. Those samples were mixed with 0.5 ml of deuterated chloroform in a small vial and then filtered through a Kimwipe™ plug into NMR tubes. The composition of the product mixture as a function of time was determined by NMR spectroscopy. Results are presented in **Figure 2.1**.

Dehydrogenation of 1-Phenyl-1-Propanol under Hydrogen

These reactions were performed as detailed in hydrogenation at ambient pressure with the exception that the reaction temperature was increased to 200 ºC and a measured amount (0.1 mol% equivalent of Pd) of either 10 wt% palladium on carbon, 5 wt% palladium on alumina, or 5 wt% palladium on silica were used. The reaction time was also reduced to 4 h. Results are presented in **Table 2.5**.

Kinetics of Dehydrogenation of 1-Phenyl-1-Propanol over Pd/SiO2

This reaction was performed as detailed for kinetics of dehydrogenation of 1-phenyl-1-propanol over Pd/C with the exception that the catalyst was changed to Pd/ SiO_2. Results are presented in **Figure 2.2**.

Kinetics of Dehydrogenation of Benzylic Alcohols over Pd/SiO2

These reactions were performed using the method detailed in kinetics of dehydrogenation of 1-phenyl-1-propanol over Pd/SiO_2 with the exception of using 1-phenyl-1-propanol, 1-phenyl-1-ethanol, or benzyl alcohol as the organic fluid. Results are presented in **Figure 2.3**.

Determining Selectivity through Gas Chromatography

Gas chromatography method development consisted of making a solution of 1-phenyl-1-propanol, propiophenone, propylbenzene, and hexadecane in approximately equal amounts in methanol. The temperature program of the gas chromatogram was adjusted until all four components were adequately resolved (this was only challenging for the alcohol and ketone because they have similar boiling points). The column used was a DB-5 column purchased from Aglient. The column dimensions were 30 m long, with an inner diameter of 0.250 mm, with a wall coating 0.25 μm thick. The temperature program used was as follows: the initial temperature was 70 ºC and was increased to 90 ºC (at 15 ºC/min) where it was held for 1 min, the temperature was then increased to 120 ºC (at 10 ºC/min) where it was held for 2 min, finally the temperature was increased to 230 ºC (at 10 ºC/min) where it was held for 1 min. Under these conditions the analytes elute from the column at 3.40 min (propylbenzene), 6.10 min (1-phenyl-1-propanol), and 6.40 min (propiophenone). Potential side products elute from the column at 3.15 min (propylcyclohexane), 5.70 min (1-cyclohexyl-1-propanone), and 6.00 min (1-cyclohexyl-1-propanol). Four calibration solutions were prepared for each of the analytes consisting of both the analyte and hexadecane accurately measured gravimetrically in different proportions and then diluted with methanol. These were analyzed using the chosen temperature program and the ratio of peak areas was plotted against the mole ratio of the analyte to the internal standard to determine the response factor for each analyte.

The apparatus for the catalyst screening experiments consisted of a 16x150 mm test tube containing a magnetic stir bar, sealed with a rubber septum, and clamped above an oil bath preheated to 200 ºC. The test tube was filled with 1 ml of 1-phenyl-1-propanol, and a measured amount (0.1 mol% equivalent of Pd or Pt or 1.0 mol% equivalent of Ni) of either 56 wt% nickel on kieselguhr, 5 wt% platinum on carbon, 10 wt % palladium on carbon, and 5 wt% palladium on alumina or silica. The septum at the top of the test tube was pierced by two needles, one connected to hydrogen gas flow, and the other to a bubbler. The reaction mixture was stirred vigorously while the headspace of the test tube was flushed with hydrogen gas at a rate of 10 ml per minute for ten minutes. At this point, the test tube was lowered into the preheated oil bath until the liquid levels of the reaction mixture and the oil bath were equal. Hydrogen evolution began almost immediately as could be observed in the test tube and the bubbler. However, the slow flow of hydrogen from the gas cylinder was continued because the rate of dehydrogenation decreases as the reaction proceeds. After four hours, the test tube was removed from the oil bath, injected with 0.5 ml of hexadecane (the internal standard), and cooled in a prepared ice water bath. About 50 µl of the reaction mixture was then dispensed into a vial and was heavily diluted with methanol. This solution was analyzed by gas chromatography under the conditions above. Results are presented in **Table 2.6**.

Catalyst Screening for Dehydrogenation of 1-Phenyl-1-Propanol

These reactions were performed by Vanessa Little. These reactions were performed in test tubes as detailed in determining selectivity through gas chromatography but were analyzed by ^{1}H NMR spectroscopy as detailed in dehydrogenation of 1-phenyl-1-propanol under hydrogen and various commercially available heterogeneous catalysts were used. Results are presented in **Table 2.7**.

Dehydrogenation of Conjugated Carbon–Carbon Single Bonds

These reactions were performed in test tubes as detailed in determining selectivity through gas chromatography but were analyzed by ^{1}H NMR spectroscopy as detailed in dehydrogenation of 1-phenyl-1-propanol under hydrogen and various commercially available heterogeneous catalysts were used. Various carbon-carbon bond containing organic substrates were investigated with the following catalyst loadings: 1.0 mol% equivalent of Pd, Pt, Rh or Ru, or 10 mol% equivalent of Ni.

Phase Behaviour and the Dehydrogenation of Diols

A carousel reactor was used for these experiments. Each of the carousel reactor tubes was fitted with a magnetic stir bar and was filled with 1 ml of ethylene glycol, 1,2-propanediol, 2,3-butanediol, 1,3-propanediol, 1,3-butandiol, or 2,4-pentanediol; and a

measured amount (0.1 mol% of catalytic metal) of 5 wt% palladium on silica or 5 wt% ruthenium on alumina. The flow of hydrogen was initiated ten minutes before the heater on the carousel reactor was turned on. The reaction was allowed to run for one hour, after which the reactor tubes were cooled and about 0.1 ml of the reaction mixture from each was removed and placed in separate vials. These samples were diluted with 0.5 ml of deuterium oxide and the suspended catalyst particles were allowed to settle overnight. The solutions were then decanted into NMR tubes and analyzed. The composition of the product mixture was determined by NMR spectroscopy. Results are presented in **Table 2.8** and **Table 2.9**.

Dehydrogenation of Benzylic Amines

These reactions were performed as detailed in phase behaviour and the dehydrogenation of diols. Results are presented in **Table 2.10** and **Table 2.11**.

Determination of Equilibrium Constant

These reactions were performed as detailed in kinetics of dehydrogenation of 1-phenyl-1-propanol over Pd/SiO_2 with the exception that each experiment either started with 1-phenyl-1-propanol or propiophenone, and each was carried out at different temperatures at regular intervals between 100 ºC and 200 ºC. Reactions at temperatures

other than 200 ºC were performed by John Vandersleen. Results are presented in **Table A. 1**.

Table A.1. Equilibrium constant for the dehydrogenation of 1-phenyl-1-propanol as a function of temperature

T (K)	K
373	0.023±0.002
393	0.056±0.006
413	0.13±0.02
433	0.23±0.01
453	0.45±0.04
473	1.15±0.1

Equilibrium constants were measured by separately heating 1-phenyl-1-propanol and propiophenone at constant temperature over Pd/SiO_2 catalyst under a hydrogen atmosphere and measuring the composition of the reaction contents periodically (using ^1H NMR) until the composition of both flasks was identical within experimental error.

Kinetics of Dehydrogenation of 1-Phenyl-1-Propanol over Pd on Mesoporous Silica

This experiment was performed as detailed in kinetics of dehydrogenation od 1-phenyl-1-propanol over Pd/SiO2 with the exception that pieces of palladium reduced onto a mesoporous silica monolith that were obtained from Jenny Du were used as the catalyst. Results are presented in **Figure 2.8**.

Impregnation of Silica with Palladium

Five grams of amorphous silica (99.5+%) pellets (provided by Saint-Gobain NorPro, 3 mm diameter, 250 m^2/g surface area, 12 nm median pore diameter, 1.0 cm^3/g total pore volume, and a 350 kg/m^3 packing density were placed in a 50 ml Erlenmeyer flask and were covered by methanol. 555 mg of palladium (II) acetate (enough to make a 5 wt% catalyst) was added to the pellets with vigorous stirring. The mixture was allowed to stir overnight after which it had lost most of its orange color, the sides of the flask and pellets were grey, and visible grey particulates were suspended in the methanol. The pellets were filtered and then placed in a round bottomed flask which was sparged with hydrogen gas and heated to 200 ºC for four hours. The resulting pellets were black with reduced palladium metal.

Dehydrogenation of 1-Phenyl-1-Propanol over Silica Impregnated with Pd

The impregnated silica pellets contained an unknown amount of palladium metal due to the reduction of palladium on the sides of the flask and in the bulk solvent. However, the loading was known to be less than 5 wt%. Kinetics would be meaningless because the catalyst loading was unknown, but the selectivity of the impregnated catalyst could be determined. 5 ml of 1-phenyl-1-propanol and about 500 mg of pellets were placed in a pear shaped flask and sparged with hydrogen. They were then submerged in

an oil bath preheated to 200 ºC for four hours. A sample of the reaction mixture was removed, diluted with deuterated chloroform and analyzed by NMR spectroscopy.

Appendix B

X-Ray Diffraction Data

B.1 N,N-Bis(2-(9'-carbazolyl)ethyl)butylamine

A crystal of the compound (colorless, block-shaped, size 0.33 x 0.30 x 0.25 mm) was mounted on a glass fiber with grease and cooled to -93 °C in a stream of nitrogen gas controlled with Cryostream Controller 700. Data collection was performed on a Bruker SMART APEX II X-ray diffractometer with graphite-monochromated Mo K_α radiation (λ = 0.71073 Å), operating at 50 kV and 30 mA over 2θ ranges of 2.88 ~ 52.00º. No significant decay was observed during the data collection.

Data were processed on a PC using the Bruker AXS Crystal Structure Analysis Package: [1] Data collection: APEX2 (Bruker, 2006); cell refinement: SAINT (Bruker, 2005); data reduction: SAINT (Bruker, 2005); structure solution: XPREP (Bruker, 2005) and SHELXTL (Bruker, 2000); structure refinement: SHELXTL; molecular graphics: SHELXTL; publication materials: SHELXTL. Neutral atom scattering factors were taken from Cromer and Waber.[2] The crystal is triclinic space group P-1, based on the systematic absences, E statistics and successful refinement of the structure. The structure was solved by direct methods. Full-matrix least-square refinements minimizing the

function $\sum w (F_o^2 - F_c^2)^2$ were applied to the compound. All non-hydrogen atoms were refined anisotropically. Only the H atoms on one carbon atoms (C31) were located from difference Fourier map and refined with Uiso(H)=1.2 Ueq(C). All other H atoms were placed in geometrically calculated positions, with C-H = 0.95 (aromatic), 0.98 (CH_3) and 0.99 (CH_2) Å with Uiso(H) = 1.5 UeqC(methyl), or 1.2 Ueq(other C). In addition, the methyl groups were refined with AFIX 137, which allowed the rotation of the methyl groups whilst keeping the C-H distances and X-C-H angles fixed. One of the methyl groups is disordered and was split into two positions (C32a and C32b) and refined without any restriction.

Convergence to final R_1 = 0.0648 and wR_2 = 0.1653 for 6398 ($I>2\sigma(I)$) independent reflections, and R_1 = 0.0993 and wR_2 = 0.1880 for all 9980 (R(int) = 0.0540) independent reflections, with 650 parameters and 0 restraints, were achieved.[3] The largest residual peak and hole to be 0.308 and – 0.259 e/Å^3, respectively. Crystallographic data, atomic coordinates and equivalent isotropic displacement parameters, bond lengths and angles, anisotropic displacement parameters, hydrogen coordinates and isotropic displacement parameters, and torsion angles are given in **Tables B.1 to B.6**. The molecular structure and the cell packing are shown in **Figures B.1 and B.2**.

---

[1] Bruker AXS Crystal Structure Analysis Package:

Bruker (2000). SHELXTL. Version 6.14. Bruker AXS Inc., Madison, Wisconsin, USA.

Bruker (2005). XPREP. Version 2005/2. Bruker AXS Inc., Madison, Wisconsin, USA.

Bruker (2005). SAINT. Version 7.23A. Bruker AXS Inc., Madison,Wisconsin, USA.

Bruker (2006). APEX2. Version 2.0-2. Bruker AXS Inc., Madison, Wisconsin, USA.

[2] Cromer, D. T.; Waber, J. T. International Tables for X-ray Crystallography; Kynoch Press: Birmingham, UK, 1974; Vol. 4, Table 2.2 A.

[3] $R_1 = \sum | |Fo| - |Fc| | / \sum |Fo|$

$wR_2 = \{\sum [w (Fo^2 – Fc^2)^2] / \sum [w(Fo^2)^2]\}^{1/2}$

$(w = 1 / [\sigma^2(Fo^2) + (0.0760P)^2 + 1.0168P]$, where $P = [Max (Fo^2, 0) + 2Fc^2] / 3)$

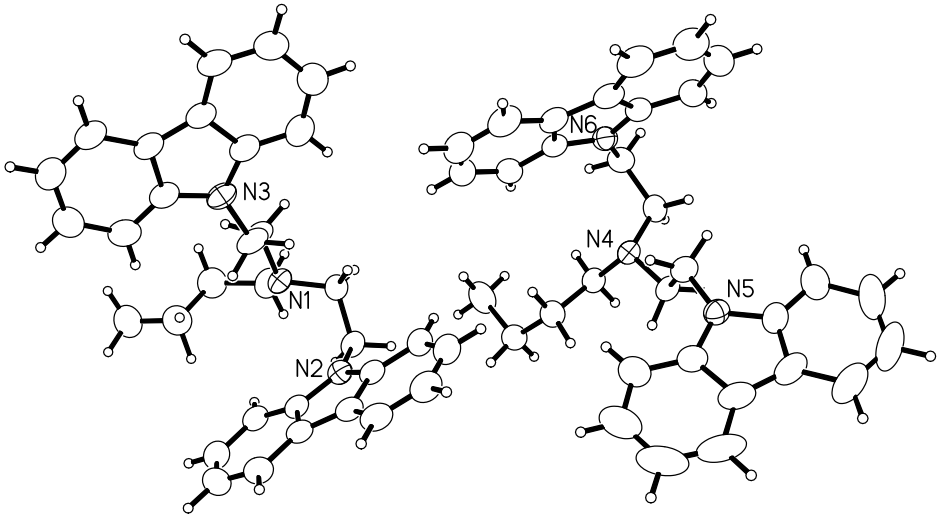

Figure B.1. Molecular Structure N,N-Bis(2-(9'-carbazolyl)ethyl)butylamine (There are two molecules in the asymmetric unit. Displacement ellipsoids for non-H atoms are shown at the 50% probability level and H atoms are represented by circles of arbitrary size.)

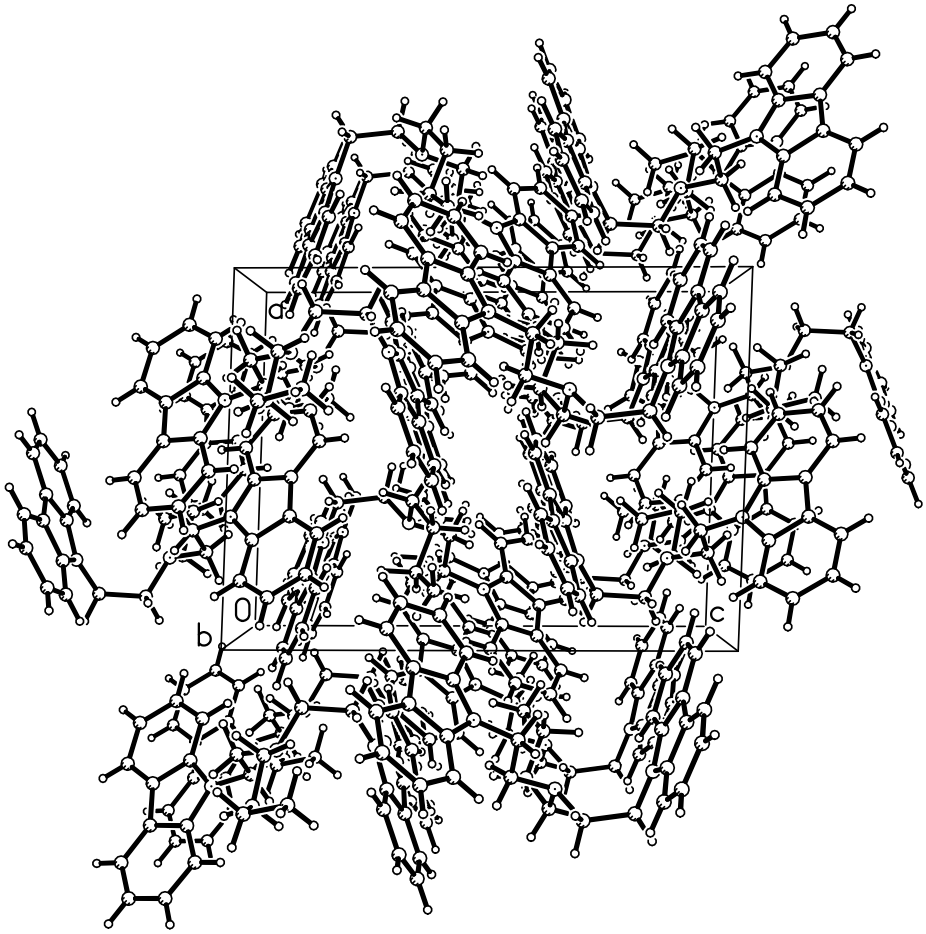

Figure B.2. Unit cell packing of N,N-Bis(2-(9'-carbazolyl)ethyl)butylamine

Table B.1 Crystal data and structure refinement for N,N-Bis(2-(9'-carbazolyl)ethyl) butylamine

Empirical formula	C32 H33 N3	
Formula weight	459.61	
Temperature	180(2) K	
Wavelength	0.71073 Å	
Crystal system	Triclinic	
Space group	P-1	
Unit cell dimensions	a = 11.587(3) Å	α= 87.805(3)°.
	b = 14.175(4) Å	β= 87.895(3)°.
	c = 15.621(4) Å	γ = 89.068(3)°.
Volume	2561.8(11) $Å^3$	
Z	4	
Density (calculated)	1.192 Mg/m^3	
Absorption coefficient	0.070 mm^{-1}	
F(000)	984	
Crystal size	0.33 x 0.30 x 0.25 mm^3	
Theta range for data collection	1.44 to 26.00°.	
Index ranges	-14<=h<=14, -17<=k<=17, -19<=l<=19	
Reflections collected	25186	
Independent reflections	9980 [R(int) = 0.0540]	
Completeness to theta = 26.00°	99.0%	

Table B.1 Crystal data and structure refinement for N,N-Bis(2-(9'-carbazolyl)ethyl) butylamine

Absorption correction	Multi-scan
Max. and min. transmission	0.9827 and 0.9773
Refinement method	Full-matrix least-squares on F^2
Data / restraints / parameters	9980 / 0 / 650
Goodness-of-fit on F^2	1.035
Final R indices [I>2sigma (I)]	R1 = 0.0648, wR2 = 0.1653
R indices (all data)	R1 = 0.0993, wR2 = 0.1880
Extinction coefficient	0.0046(9)
Largest diff. peak and hole	0.308 and -0.259 e.$Å^{-3}$

Table B.2. Atomic coordinates ($x10^4$) and equivalent isotropic displacement parameters ($Å^2x10^3$) for N,N-Bis(2-(9'-carbazolyl)ethyl)butylamine. U(eq) is defined as one third of the trace of the orthogonalized U^{ij} tensor.

	x	y	z	U(eq)
N(1)	3262(2)	7256(1)	3496(1)	36(1)
N(2)	2711(2)	6442(1)	1737(1)	37(1)
N(3)	1394(2)	5844(2)	5050(1)	45(1)
N(4)	7679(2)	2642(1)	1297(1)	35(1)
N(5)	6525(2)	776(1)	-39(1)	39(1)

Table B.2. Atomic coordinates ($x10^4$) and equivalent isotropic displacement parameters ($Å^2x10^3$) for N,N-Bis(2-(9'-carbazolyl)ethyl)butylamine. U(eq) is defined as one third of the trace of the orthogonalized U^{ij} tensor.

	x	y	z	U(eq)
N(6)	7714(2)	1933(2)	3105(1)	40(1)
C(1)	3964(2)	6613(2)	2974(2)	38(1)
C(2)	3808(2)	6783(2)	2021(2)	38(1)
C(3)	1727(2)	6977(2)	1577(1)	36(1)
C(4)	1518(2)	7932(2)	1696(2)	44(1)
C(5)	454(3)	8296(2)	1473(2)	54(1)
C(6)	-387(2)	7736(2)	1139(2)	55(1)
C(7)	-177(2)	6789(2)	1023(2)	48(1)
C(8)	885(2)	6393(2)	1244(1)	38(1)
C(9)	1392(2)	5455(2)	1214(1)	38(1)
C(10)	1006(2)	4586(2)	962(2)	47(1)
C(11)	1721(3)	3807(2)	1030(2)	50(1)
C(12)	2824(3)	3872(2)	1351(2)	50(1)
C(13)	3236(2)	4724(2)	1607(2)	43(1)
C(14)	2513(2)	5516(2)	1529(1)	37(1)
C(15)	2914(2)	6822(2)	4327(2)	40(1)
C(16)	1915(2)	6160(2)	4226(2)	47(1)
C(17)	1701(2)	5030(2)	5516(2)	43(1)
C(18)	2619(3)	4409(2)	5376(2)	52(1)
C(19)	2722(3)	3642(2)	5946(2)	58(1)
C(20)	1933(3)	3492(2)	6629(2)	58(1)
C(21)	1030(3)	4117(2)	6777(2)	50(1)
C(22)	910(2)	4906(2)	6221(2)	41(1)

Table B.2. Atomic coordinates ($x10^4$) and equivalent isotropic displacement parameters ($Å^2x10^3$) for N,N-Bis(2-(9'-carbazolyl)ethyl)butylamine. U(eq) is defined as one third of the trace of the orthogonalized U^{ij} tensor.

	x	y	z	U(eq)
C(23)	105(2)	5694(2)	6179(2)	41(1)
C(24)	-837(2)	5974(2)	6694(2)	47(1)
C(25)	-1423(2)	6793(2)	6478(2)	54(1)
C(26)	-1083(3)	7339(2)	5752(2)	56(1)
C(27)	-156(2)	7081(2)	5230(2)	51(1)
C(28)	440(2)	6256(2)	5451(2)	41(1)
C(29)	3871(2)	8146(2)	3573(2)	49(1)
C(30)	3186(3)	8913(2)	4017(2)	55(1)
C(31)	2002(3)	9137(2)	3713(2)	64(1)
C(32A)	1578(15)	10015(15)	4087(10)	80(4)
C(32B)	1238(16)	9750(14)	4359(10)	86(5)
C(33)	7510(2)	2126(2)	523(2)	37(1)
C(34)	6894(2)	1200(2)	734(2)	41(1)
C(35)	5537(2)	1057(2)	-459(2)	41(1)
C(36)	4696(2)	1722(2)	-229(2)	51(1)
C(37)	3790(3)	1865(3)	-759(2)	70(1)
C(38)	3703(3)	1381(3)	-1497(3)	81(1)
C(39)	4521(4)	715(3)	-1732(2)	73(1)
C(40)	5474(3)	547(2)	-1212(2)	52(1)
C(41)	6488(3)	-61(2)	-1245(2)	56(1)
C(42)	6923(5)	-730(3)	-1814(2)	83(1)
C(43)	7962(5)	-1184(3)	-1644(3)	102(2)
C(44)	8568(4)	-997(2)	-919(3)	86(1)

Table B.2. Atomic coordinates ($x10^4$) and equivalent isotropic displacement parameters ($Å^2x10^3$) for N,N-Bis(2-(9'-carbazolyl)ethyl)butylamine. U(eq) is defined as one third of the trace of the orthogonalized U^{ij} tensor.

	x	y	z	U(eq)
C(45)	8167(3)	-345(2)	-343(2)	60(1)
C(46)	7118(2)	112(2)	-516(2)	46(1)
C(47)	8723(2)	2322(2)	1721(2)	40(1)
C(48)	8656(2)	2450(2)	2682(2)	42(1)
C(49)	7703(2)	968(2)	3260(2)	40(1)
C(50)	8566(3)	297(2)	3098(2)	51(1)
C(51)	8339(3)	-633(2)	3349(2)	65(1)
C(52)	7297(4)	-885(2)	3753(2)	69(1)
C(53)	6443(3)	-227(2)	3903(2)	58(1)
C(54)	6624(2)	718(2)	3645(2)	45(1)
C(55)	5950(2)	1579(2)	3711(2)	45(1)
C(56)	4838(3)	1787(3)	4028(2)	63(1)
C(57)	4466(3)	2717(3)	4005(2)	73(1)
C(58)	5179(3)	3437(3)	3666(2)	72(1)
C(59)	6281(3)	3253(2)	3349(2)	56(1)
C(60)	6657(2)	2311(2)	3370(2)	42(1)
C(61)	7661(2)	3669(2)	1126(2)	38(1)
C(62)	6455(2)	4058(2)	971(2)	44(1)
C(63)	6408(2)	5133(2)	880(2)	48(1)
C(64)	6689(3)	5604(2)	1696(2)	61(1)

Table B.3 Bond lengths [Å] and angles [°] for N,N-Bis(2-(9'-carbazolyl)ethyl)butylamine.

N(1)-C(15)	1.460(3)
N(1)-C(1)	1.464(3)
N(1)-C(29)	1.465(3)
N(2)-C(3)	1.384(3)
N(2)-C(14)	1.387(3)
N(2)-C(2)	1.458(3)
N(3)-C(28)	1.382(3)
N(3)-C(17)	1.389(3)
N(3)-C(16)	1.459(3)
N(4)-C(33)	1.458(3)
N(4)-C(47)	1.458(3)
N(4)-C(61)	1.469(3)
N(5)-C(46)	1.381(3)
N(5)-C(35)	1.385(3)
N(5)-C(34)	1.451(3)
N(6)-C(49)	1.380(3)
N(6)-C(60)	1.384(3)
N(6)-C(48)	1.450(3)
C(1)-C(2)	1.516(3)
C(1)-H(1A)	0.9900
C(1)-H(1B)	0.9900
C(2)-H(2A)	0.9900

Table B.3 Bond lengths [Å] and angles [°] for N,N-Bis(2-(9'-carbazolyl)ethyl)butylamine.

C(2)-H(2B)	0.9900
C(3)-C(4)	1.390(4)
C(3)-C(8)	1.415(3)
C(4)-C(5)	1.380(4)
C(4)-H(4A)	0.9500
C(5)-C(6)	1.395(4)
C(5)-H(5A)	0.9500
C(6)-C(7)	1.377(4)
C(6)-H(6A)	0.9500
C(7)-C(8)	1.393(4)
C(7)-H(7A)	0.9500
C(8)-C(9)	1.447(4)
C(9)-C(10)	1.394(4)
C(9)-C(14)	1.411(3)
C(10)-C(11)	1.372(4)
C(10)-H(10A)	0.9500
C(11)-C(12)	1.395(4)
C(11)-H(11A)	0.9500
C(12)-C(13)	1.385(4)
C(12)-H(12A)	0.9500
C(13)-C(14)	1.395(4)
C(13)-H(13A)	0.9500
C(15)-C(16)	1.520(3)
C(15)-H(15A)	0.9900

Table B.3 Bond lengths [Å] and angles [°] for N,N-Bis(2-(9'-carbazolyl)ethyl)butylamine.

C(15)-H(15B)	0.9900
C(16)-H(16A)	0.9900
C(16)-H(16B)	0.9900
C(17)-C(18)	1.386(4)
C(17)-C(22)	1.414(3)
C(18)-C(19)	1.386(4)
C(18)-H(18A)	0.9500
C(19)-C(20)	1.392(4)
C(19)-H(19A)	0.9500
C(20)-C(21)	1.378(4)
C(20)-H(20A)	0.9500
C(21)-C(22)	1.398(4)
C(21)-H(21A)	0.9500
C(22)-C(23)	1.444(4)
C(23)-C(24)	1.394(4)
C(23)-C(28)	1.410(3)
C(24)-C(25)	1.372(4)
C(24)-H(24A)	0.9500
C(25)-C(26)	1.397(4)
C(25)-H(25A)	0.9500
C(26)-C(27)	1.378(4)
C(26)-H(26A)	0.9500
C(27)-C(28)	1.387(4)
C(27)-H(27A)	0.9500

Table B.3 Bond lengths [Å] and angles [°] for N,N-Bis(2-(9'-carbazolyl)ethyl)butylamine.

C(29)-C(30)	1.510(4)
C(29)-H(29A)	0.9900
C(29)-H(29B)	0.9900
C(30)-C(31)	1.493(5)
C(30)-H(30A)	0.9900
C(30)-H(30B)	0.9900
C(31)-C(32A)	1.47(2)
C(31)-C(32B)	1.592(18)
C(31)-H(31A)	0.98(4)
C(31)-H(31B)	1.09(3)
C(32A)-H(32A)	0.9800
C(32A)-H(32B)	0.9800
C(32A)-H(32C)	0.9800
C(32B)-H(32D)	0.9800
C(32B)-H(32E)	0.9800
C(32B)-H(32F)	0.9800
C(33)-C(34)	1.523(3)
C(33)-H(33A)	0.9900
C(33)-H(33B)	0.9900
C(34)-H(34A)	0.9900
C(34)-H(34B)	0.9900
C(35)-C(36)	1.392(4)
C(35)-C(40)	1.409(4)
C(36)-C(37)	1.369(4)

Table B.3 Bond lengths [Å] and angles [°] for N,N-Bis(2-(9'-carbazolyl)ethyl)butylamine.

C(36)-H(36A)	0.9500
C(37)-C(38)	1.371(5)
C(37)-H(37A)	0.9500
C(38)-C(39)	1.378(5)
C(38)-H(38A)	0.9500
C(39)-C(40)	1.406(5)
C(39)-H(39A)	0.9500
C(40)-C(41)	1.446(4)
C(41)-C(42)	1.400(5)
C(41)-C(46)	1.407(4)
C(42)-C(43)	1.385(6)
C(42)-H(42A)	0.9500
C(43)-C(44)	1.390(6)
C(43)-H(43A)	0.9500
C(44)-C(45)	1.379(5)
C(44)-H(44A)	0.9500
C(45)-C(46)	1.398(4)
C(45)-H(45A)	0.9500
C(47)-C(48)	1.517(3)
C(47)-H(47A)	0.9900
C(47)-H(47B)	0.9900
C(48)-H(48A)	0.9900
C(48)-H(48B)	0.9900
C(49)-C(50)	1.393(4)

Table B.3 Bond lengths [Å] and angles [°] for N,N-Bis(2-(9'-carbazolyl)ethyl)butylamine.

C(49)-C(54)	1.412(4)
C(50)-C(51)	1.388(4)
C(50)-H(50A)	0.9500
C(51)-C(52)	1.387(5)
C(51)-H(51A)	0.9500
C(52)-C(53)	1.369(5)
C(52)-H(52A)	0.9500
C(53)-C(54)	1.400(4)
C(53)-H(53A)	0.9500
C(54)-C(55)	1.443(4)
C(55)-C(56)	1.394(4)
C(55)-C(60)	1.408(4)
C(56)-C(57)	1.380(5)
C(56)-H(56A)	0.9500
C(57)-C(58)	1.399(5)
C(57)-H(57A)	0.9500
C(58)-C(59)	1.377(4)
C(58)-H(58A)	0.9500
C(59)-C(60)	1.398(4)
C(59)-H(59A)	0.9500
C(61)-C(62)	1.519(3)
C(61)-H(61A)	0.9900
C(61)-H(61B)	0.9900
C(62)-C(63)	1.525(4)

Table B.3 Bond lengths [Å] and angles [°] for N,N-Bis(2-(9'-carbazolyl)ethyl)butylamine.

C(62)-H(62A)	0.9900
C(62)-H(62B)	0.9900
C(63)-C(64)	1.509(4)
C(63)-H(63A)	0.9900
C(63)-H(63B)	0.9900
C(64)-H(64A)	0.9800
C(64)-H(64B)	0.9800
C(64)-H(64C)	0.9800
C(15)-N(1)-C(1)	112.0(2)
C(15)-N(1)-C(29)	112.76(19)
C(1)-N(1)-C(29)	109.90(19)
C(3)-N(2)-C(14)	108.59(19)
C(3)-N(2)-C(2)	126.8(2)
C(14)-N(2)-C(2)	124.5(2)
C(28)-N(3)-C(17)	108.8(2)
C(28)-N(3)-C(16)	125.3(2)
C(17)-N(3)-C(16)	125.5(2)
C(33)-N(4)-C(47)	111.39(19)
C(33)-N(4)-C(61)	111.94(18)
C(47)-N(4)-C(61)	112.08(19)
C(46)-N(5)-C(35)	109.1(2)
C(46)-N(5)-C(34)	127.2(2)
C(35)-N(5)-C(34)	123.5(2)
C(49)-N(6)-C(60)	108.8(2)

Table B.3 Bond lengths [Å] and angles [°] for N,N-Bis(2-(9'-carbazolyl)ethyl)butylamine.

C(49)-N(6)-C(48)	125.1(2)
C(60)-N(6)-C(48)	126.0(2)
N(1)-C(1)-C(2)	112.8(2)
N(1)-C(1)-H(1A)	109.0
C(2)-C(1)-H(1A)	109.0
N(1)-C(1)-H(1B)	109.0
C(2)-C(1)-H(1B)	109.0
H(1A)-C(1)-H(1B)	107.8
N(2)-C(2)-C(1)	113.05(18)
N(2)-C(2)-H(2A)	109.0
C(1)-C(2)-H(2A)	109.0
N(2)-C(2)-H(2B)	109.0
C(1)-C(2)-H(2B)	109.0
H(2A)-C(2)-H(2B)	107.8
N(2)-C(3)-C(4)	129.2(2)
N(2)-C(3)-C(8)	109.1(2)
C(4)-C(3)-C(8)	121.7(2)
C(5)-C(4)-C(3)	117.3(3)
C(5)-C(4)-H(4A)	121.3
C(3)-C(4)-H(4A)	121.3
C(4)-C(5)-C(6)	122.0(3)
C(4)-C(5)-H(5A)	119.0
C(6)-C(5)-H(5A)	119.0
C(7)-C(6)-C(5)	120.5(3)

Table B.3 Bond lengths [Å] and angles [°] for N,N-Bis(2-(9'-carbazolyl)ethyl)butylamine.

C(7)-C(6)-H(6A)	119.8
C(5)-C(6)-H(6A)	119.8
C(6)-C(7)-C(8)	119.4(3)
C(6)-C(7)-H(7A)	120.3
C(8)-C(7)-H(7A)	120.3
C(7)-C(8)-C(3)	119.1(3)
C(7)-C(8)-C(9)	134.4(2)
C(3)-C(8)-C(9)	106.5(2)
C(10)-C(9)-C(14)	119.2(2)
C(10)-C(9)-C(8)	134.2(2)
C(14)-C(9)-C(8)	106.5(2)
C(11)-C(10)-C(9)	119.3(3)
C(11)-C(10)-H(10A)	120.3
C(9)-C(10)-H(10A)	120.3
C(10)-C(11)-C(12)	121.1(3)
C(10)-C(11)-H(11A)	119.4
C(12)-C(11)-H(11A)	119.4
C(13)-C(12)-C(11)	121.2(3)
C(13)-C(12)-H(12A)	119.4
C(11)-C(12)-H(12A)	119.4
C(12)-C(13)-C(14)	117.7(2)
C(12)-C(13)-H(13A)	121.2
C(14)-C(13)-H(13A)	121.2
N(2)-C(14)-C(13)	129.3(2)

Table B.3 Bond lengths [Å] and angles [°] for N,N-Bis(2-(9'-carbazolyl)ethyl)butylamine.

N(2)-C(14)-C(9)	109.2(2)
C(13)-C(14)-C(9)	121.5(2)
N(1)-C(15)-C(16)	110.11(19)
N(1)-C(15)-H(15A)	109.6
C(16)-C(15)-H(15A)	109.6
N(1)-C(15)-H(15B)	109.6
C(16)-C(15)-H(15B)	109.6
H(15A)-C(15)-H(15B)	108.2
N(3)-C(16)-C(15)	112.2(2)
N(3)-C(16)-H(16A)	109.2
C(15)-C(16)-H(16A)	109.2
N(3)-C(16)-H(16B)	109.2
C(15)-C(16)-H(16B)	109.2
H(16A)-C(16)-H(16B)	107.9
C(18)-C(17)-N(3)	129.3(2)
C(18)-C(17)-C(22)	121.9(3)
N(3)-C(17)-C(22)	108.7(2)
C(19)-C(18)-C(17)	117.3(3)
C(19)-C(18)-H(18A)	121.3
C(17)-C(18)-H(18A)	121.3
C(18)-C(19)-C(20)	121.6(3)
C(18)-C(19)-H(19A)	119.2
C(20)-C(19)-H(19A)	119.2
C(21)-C(20)-C(19)	121.1(3)

Table B.3 Bond lengths [Å] and angles [°] for N,N-Bis(2-(9'-carbazolyl)ethyl)butylamine.

C(21)-C(20)-H(20A)	119.4
C(19)-C(20)-H(20A)	119.4
C(20)-C(21)-C(22)	118.8(3)
C(20)-C(21)-H(21A)	120.6
C(22)-C(21)-H(21A)	120.6
C(21)-C(22)-C(17)	119.2(3)
C(21)-C(22)-C(23)	134.2(2)
C(17)-C(22)-C(23)	106.6(2)
C(24)-C(23)-C(28)	119.6(3)
C(24)-C(23)-C(22)	133.7(2)
C(28)-C(23)-C(22)	106.7(2)
C(25)-C(24)-C(23)	119.1(3)
C(25)-C(24)-H(24A)	120.4
C(23)-C(24)-H(24A)	120.4
C(24)-C(25)-C(26)	120.6(3)
C(24)-C(25)-H(25A)	119.7
C(26)-C(25)-H(25A)	119.7
C(27)-C(26)-C(25)	121.7(3)
C(27)-C(26)-H(26A)	119.1
C(25)-C(26)-H(26A)	119.1
C(26)-C(27)-C(28)	117.7(3)
C(26)-C(27)-H(27A)	121.2
C(28)-C(27)-H(27A)	121.2
N(3)-C(28)-C(27)	129.6(2)

Table B.3 Bond lengths [Å] and angles [°] for N,N-Bis(2-(9'-carbazolyl)ethyl)butylamine.

N(3)-C(28)-C(23)	109.1(2)
C(27)-C(28)-C(23)	121.3(2)
N(1)-C(29)-C(30)	115.2(2)
N(1)-C(29)-H(29A)	108.5
C(30)-C(29)-H(29A)	108.5
N(1)-C(29)-H(29B)	108.5
C(30)-C(29)-H(29B)	108.5
H(29A)-C(29)-H(29B)	107.5
C(31)-C(30)-C(29)	117.6(2)
C(31)-C(30)-H(30A)	107.9
C(29)-C(30)-H(30A)	107.9
C(31)-C(30)-H(30B)	107.9
C(29)-C(30)-H(30B)	107.9
H(30A)-C(30)-H(30B)	107.2
C(32A)-C(31)-C(30)	109.4(8)
C(32A)-C(31)-C(32B)	25.1(9)
C(30)-C(31)-C(32B)	113.5(8)
C(32A)-C(31)-H(31A)	123(2)
C(30)-C(31)-H(31A)	110(2)
C(32B)-C(31)-H(31A)	100(2)
C(32A)-C(31)-H(31B)	100.6(18)
C(30)-C(31)-H(31B)	109.0(17)
C(32B)-C(31)-H(31B)	119.4(18)
H(31A)-C(31)-H(31B)	103(3)

Table B.3 Bond lengths [Å] and angles [°] for N,N-Bis(2-(9'-carbazolyl)ethyl)butylamine.

C(31)-C(32A)-H(32A)	109.5
C(31)-C(32A)-H(32B)	109.5
C(31)-C(32A)-H(32C)	109.5
C(31)-C(32B)-H(32D)	109.5
C(31)-C(32B)-H(32E)	109.5
H(32D)-C(32B)-H(32E)	109.5
C(31)-C(32B)-H(32F)	109.5
H(32D)-C(32B)-H(32F)	109.5
H(32E)-C(32B)-H(32F)	109.5
N(4)-C(33)-C(34)	111.00(19)
N(4)-C(33)-H(33A)	109.4
C(34)-C(33)-H(33A)	109.4
N(4)-C(33)-H(33B)	109.4
C(34)-C(33)-H(33B)	109.4
H(33A)-C(33)-H(33B)	108.0
N(5)-C(34)-C(33)	110.97(19)
N(5)-C(34)-H(34A)	109.4
C(33)-C(34)-H(34A)	109.4
N(5)-C(34)-H(34B)	109.4
C(33)-C(34)-H(34B)	109.4
H(34A)-C(34)-H(34B)	108.0
N(5)-C(35)-C(36)	129.3(2)
N(5)-C(35)-C(40)	108.9(2)
C(36)-C(35)-C(40)	121.8(3)

Table B.3 Bond lengths [Å] and angles [°] for N,N-Bis(2-(9'-carbazolyl)ethyl)butylamine.

C(37)-C(36)-C(35)	117.7(3)
C(37)-C(36)-H(36A)	121.2
C(35)-C(36)-H(36A)	121.1
C(36)-C(37)-C(38)	121.9(4)
C(36)-C(37)-H(37A)	119.0
C(38)-C(37)-H(37A)	119.0
C(37)-C(38)-C(39)	121.3(3)
C(37)-C(38)-H(38A)	119.4
C(39)-C(38)-H(38A)	119.4
C(38)-C(39)-C(40)	119.0(3)
C(38)-C(39)-H(39A)	120.5
C(40)-C(39)-H(39A)	120.5
C(39)-C(40)-C(35)	118.3(3)
C(39)-C(40)-C(41)	135.4(3)
C(35)-C(40)-C(41)	106.3(2)
C(42)-C(41)-C(46)	118.4(4)
C(42)-C(41)-C(40)	134.6(3)
C(46)-C(41)-C(40)	106.9(2)
C(43)-C(42)-C(41)	118.9(4)
C(43)-C(42)-H(42A)	120.6
C(41)-C(42)-H(42A)	120.6
C(42)-C(43)-C(44)	121.5(4)
C(42)-C(43)-H(43A)	119.3
C(44)-C(43)-H(43A)	119.3

Table B.3 Bond lengths [Å] and angles [°] for N,N-Bis(2-(9'-carbazolyl)ethyl)butylamine.

C(45)-C(44)-C(43)	121.4(4)
C(45)-C(44)-H(44A)	119.3
C(43)-C(44)-H(44A)	119.3
C(44)-C(45)-C(46)	117.0(4)
C(44)-C(45)-H(45A)	121.5
C(46)-C(45)-H(45A)	121.5
N(5)-C(46)-C(45)	128.4(3)
N(5)-C(46)-C(41)	108.7(3)
C(45)-C(46)-C(41)	122.8(3)
N(4)-C(47)-C(48)	113.0(2)
N(4)-C(47)-H(47A)	109.0
C(48)-C(47)-H(47A)	109.0
N(4)-C(47)-H(47B)	109.0
C(48)-C(47)-H(47B)	109.0
H(47A)-C(47)-H(47B)	107.8
N(6)-C(48)-C(47)	112.53(19)
N(6)-C(48)-H(48A)	109.1
C(47)-C(48)-H(48A)	109.1
N(6)-C(48)-H(48B)	109.1
C(47)-C(48)-H(48B)	109.1
H(48A)-C(48)-H(48B)	107.8
N(6)-C(49)-C(50)	129.3(2)
N(6)-C(49)-C(54)	108.8(2)
C(50)-C(49)-C(54)	121.8(3)

Table B.3 Bond lengths [Å] and angles [°] for N,N-Bis(2-(9'-carbazolyl)ethyl)butylamine.

C(51)-C(50)-C(49)	117.4(3)
C(51)-C(50)-H(50A)	121.3
C(49)-C(50)-H(50A)	121.3
C(52)-C(51)-C(50)	121.4(3)
C(52)-C(51)-H(51A)	119.3
C(50)-C(51)-H(51A)	119.3
C(53)-C(52)-C(51)	121.2(3)
C(53)-C(52)-H(52A)	119.4
C(51)-C(52)-H(52A)	119.4
C(52)-C(53)-C(54)	119.5(3)
C(52)-C(53)-H(53A)	120.3
C(54)-C(53)-H(53A)	120.3
C(53)-C(54)-C(49)	118.7(3)
C(53)-C(54)-C(55)	134.5(3)
C(49)-C(54)-C(55)	106.8(2)
C(56)-C(55)-C(60)	119.9(3)
C(56)-C(55)-C(54)	133.8(3)
C(60)-C(55)-C(54)	106.4(2)
C(57)-C(56)-C(55)	118.4(3)
C(57)-C(56)-H(56A)	120.8
C(55)-C(56)-H(56A)	120.8
C(56)-C(57)-C(58)	121.1(3)
C(56)-C(57)-H(57A)	119.4
C(58)-C(57)-H(57A)	119.4

Table B.3 Bond lengths [Å] and angles [°] for N,N-Bis(2-(9'-carbazolyl)ethyl)butylamine.

C(59)-C(58)-C(57)	121.8(3)
C(59)-C(58)-H(58A)	119.1
C(57)-C(58)-H(58A)	119.1
C(58)-C(59)-C(60)	117.1(3)
C(58)-C(59)-H(59A)	121.5
C(60)-C(59)-H(59A)	121.5
N(6)-C(60)-C(59)	129.1(3)
N(6)-C(60)-C(55)	109.2(2)
C(59)-C(60)-C(55)	121.7(3)
N(4)-C(61)-C(62)	112.6(2)
N(4)-C(61)-H(61A)	109.1
C(62)-C(61)-H(61A)	109.1
N(4)-C(61)-H(61B)	109.1
C(62)-C(61)-H(61B)	109.1
H(61A)-C(61)-H(61B)	107.8
C(61)-C(62)-C(63)	113.0(2)
C(61)-C(62)-H(62A)	109.0
C(63)-C(62)-H(62A)	109.0
C(61)-C(62)-H(62B)	109.0
C(63)-C(62)-H(62B)	109.0
H(62A)-C(62)-H(62B)	107.8
C(64)-C(63)-C(62)	112.8(2)
C(64)-C(63)-H(63A)	109.0
C(62)-C(63)-H(63A)	109.0

Table B.3 Bond lengths [Å] and angles [°] for N,N-Bis(2-(9'-carbazolyl)ethyl)butylamine.

C(64)-C(63)-H(63B)	109.0
C(62)-C(63)-H(63B)	109.0
H(63A)-C(63)-H(63B)	107.8
C(63)-C(64)-H(64A)	109.5
C(63)-C(64)-H(64B)	109.5
H(64A)-C(64)-H(64B)	109.5
C(63)-C(64)-H(64C)	109.5
H(64A)-C(64)-H(64C)	109.5
H(64B)-C(64)-H(64C)	109.5

Symmetry transformations used to generate equivalent atoms:

Table B.4 Anisotropic displacement parameters ($Å^2 x\ 10^3$) for N,N-Bis(2-(9'-carbazolyl)ethyl)butylamine. The anisotropic displacement factor exponent takes the form: $-2\pi^2[\ h^2\ a^{*2}U^{11} + ...\ + 2\ h\ k\ a^*\ b^*\ U^{12}\ ]$

	U^{11}	U^{22}	U^{33}	U^{23}	U^{13}	U^{12}
N(1)	37(1)	37(1)	34(1)	-4(1)	5(1)	-11(1)
N(2)	33(1)	41(1)	35(1)	-2(1)	0(1)	-6(1)
N(3)	52(1)	49(1)	35(1)	2(1)	6(1)	-14(1)
N(4)	35(1)	36(1)	32(1)	-4(1)	1(1)	-3(1)
N(5)	45(1)	36(1)	37(1)	-4(1)	-3(1)	-5(1)
N(6)	39(1)	43(1)	37(1)	0(1)	-2(1)	0(1)
C(1)	30(1)	42(2)	43(1)	-6(1)	0(1)	-4(1)
C(2)	30(1)	44(2)	39(1)	-6(1)	5(1)	-11(1)
C(3)	38(1)	41(1)	28(1)	2(1)	6(1)	-5(1)
C(4)	51(2)	46(2)	35(1)	-2(1)	4(1)	-3(1)
C(5)	63(2)	52(2)	46(2)	3(1)	9(1)	8(2)
C(6)	43(2)	69(2)	52(2)	8(2)	0(1)	6(1)
C(7)	41(2)	62(2)	42(2)	4(1)	1(1)	-7(1)
C(8)	37(1)	50(2)	28(1)	2(1)	2(1)	-7(1)
C(9)	39(1)	46(2)	30(1)	3(1)	4(1)	-10(1)
C(10)	47(2)	54(2)	40(1)	1(1)	0(1)	-18(1)
C(11)	61(2)	43(2)	47(2)	-3(1)	5(1)	-16(1)
C(12)	57(2)	44(2)	48(2)	0(1)	10(1)	-1(1)
C(13)	41(1)	47(2)	42(1)	-3(1)	5(1)	-2(1)
C(14)	38(1)	42(2)	30(1)	-1(1)	5(1)	-8(1)
C(15)	43(1)	48(2)	30(1)	-3(1)	1(1)	-11(1)
C(16)	55(2)	56(2)	31(1)	-1(1)	5(1)	-20(1)
C(17)	51(2)	42(2)	36(1)	-4(1)	-1(1)	-16(1)

Table B.4 Anisotropic displacement parameters ($Å^2 x\ 10^3$) for N,N-Bis(2-(9'-carbazolyl)ethyl)butylamine. The anisotropic displacement factor exponent takes the form: $-2\pi^2[\ h^2\ a^{*2}U^{11} + ...\ + 2\ h\ k\ a^*\ b^*\ U^{12}\ ]$

	U^{11}	U^{22}	U^{33}	U^{23}	U^{13}	U^{12}
C(18)	55(2)	50(2)	51(2)	-12(1)	4(1)	-11(1)
C(19)	65(2)	52(2)	59(2)	-11(2)	-7(2)	0(2)
C(20)	77(2)	47(2)	49(2)	-1(1)	-9(2)	-7(2)
C(21)	63(2)	51(2)	37(1)	1(1)	-4(1)	-16(2)
C(22)	48(2)	43(2)	32(1)	-4(1)	-2(1)	-15(1)
C(23)	42(1)	48(2)	33(1)	-5(1)	0(1)	-18(1)
C(24)	49(2)	56(2)	37(1)	-5(1)	0(1)	-19(1)
C(25)	45(2)	66(2)	51(2)	-12(1)	-1(1)	-12(2)
C(26)	51(2)	54(2)	62(2)	-4(1)	-12(1)	-4(1)
C(27)	53(2)	54(2)	46(2)	5(1)	-7(1)	-15(1)
C(28)	45(2)	45(2)	36(1)	-2(1)	-2(1)	-16(1)
C(29)	47(2)	46(2)	56(2)	-8(1)	7(1)	-18(1)
C(30)	62(2)	39(2)	66(2)	-11(1)	-6(2)	-12(1)
C(31)	81(2)	49(2)	63(2)	-16(2)	-14(2)	9(2)
C(32A)	70(9)	96(11)	77(10)	-30(7)	-21(7)	24(6)
C(32B)	93(12)	94(12)	75(9)	-40(7)	-14(7)	37(9)
C(33)	41(1)	38(1)	32(1)	-4(1)	5(1)	-7(1)
C(34)	47(2)	40(2)	38(1)	-1(1)	0(1)	-8(1)
C(35)	46(2)	37(1)	41(1)	6(1)	-1(1)	-15(1)
C(36)	42(2)	52(2)	59(2)	12(1)	3(1)	-8(1)
C(37)	44(2)	82(2)	82(2)	36(2)	-3(2)	-11(2)
C(38)	57(2)	104(3)	81(3)	46(2)	-24(2)	-34(2)
C(39)	97(3)	78(2)	44(2)	20(2)	-20(2)	-55(2)

Table B.4 Anisotropic displacement parameters ($Å^2 x\ 10^3$) for N,N-Bis(2-(9'-carbazolyl)ethyl)butylamine. The anisotropic displacement factor exponent takes the form: $-2\pi^2[\ h^2\ a^{*2}U^{11} + ...\ + 2\ h\ k\ a^*\ b^*\ U^{12}\ ]$

	U^{11}	U^{22}	U^{33}	U^{23}	U^{13}	U^{12}
C(40)	72(2)	46(2)	39(2)	10(1)	-5(1)	-29(2)
C(41)	92(2)	37(2)	39(2)	-3(1)	11(2)	-26(2)
C(42)	152(4)	45(2)	52(2)	-9(2)	25(2)	-30(2)
C(43)	180(5)	43(2)	80(3)	-13(2)	65(3)	-5(3)
C(44)	109(3)	43(2)	101(3)	2(2)	48(3)	12(2)
C(45)	66(2)	40(2)	72(2)	4(1)	16(2)	-1(2)
C(46)	60(2)	29(1)	47(2)	-1(1)	11(1)	-8(1)
C(47)	30(1)	40(2)	50(2)	-3(1)	3(1)	-4(1)
C(48)	35(1)	45(2)	46(2)	-2(1)	-9(1)	-7(1)
C(49)	44(1)	42(2)	34(1)	-4(1)	-7(1)	-3(1)
C(50)	55(2)	50(2)	47(2)	-2(1)	-5(1)	3(1)
C(51)	88(2)	47(2)	60(2)	-8(2)	-12(2)	7(2)
C(52)	105(3)	44(2)	58(2)	-4(2)	-8(2)	-15(2)
C(53)	72(2)	56(2)	47(2)	-7(1)	-5(1)	-28(2)
C(54)	51(2)	53(2)	32(1)	-4(1)	-7(1)	-13(1)
C(55)	41(1)	64(2)	31(1)	-8(1)	-5(1)	-4(1)
C(56)	46(2)	99(3)	45(2)	-9(2)	-2(1)	-5(2)
C(57)	50(2)	119(3)	50(2)	-8(2)	0(2)	23(2)
C(58)	79(2)	91(3)	46(2)	-3(2)	0(2)	38(2)
C(59)	65(2)	61(2)	42(2)	1(1)	-2(1)	18(2)
C(60)	41(1)	56(2)	29(1)	-3(1)	-4(1)	4(1)
C(61)	39(1)	35(1)	40(1)	-4(1)	0(1)	-4(1)
C(62)	39(1)	45(2)	48(2)	-8(1)	-5(1)	-1(1)

Table B.4 Anisotropic displacement parameters ($Å^2 x\ 10^3$) for N,N-Bis(2-(9'-carbazolyl)ethyl)butylamine. The anisotropic displacement factor exponent takes the form: $-2\pi^2[\ h^2\ a^{*2}U^{11} + ...\ + 2\ h\ k\ a^*\ b^*\ U^{12}\ ]$

	U^{11}	U^{22}	U^{33}	U^{23}	U^{13}	U^{12}
C(63)	50(2)	49(2)	45(2)	4(1)	3(1)	4(1)
C(64)	60(2)	42(2)	83(2)	-13(2)	-15(2)	6(1)

Table B.5 Hydrogen coordinates ($x\ 10^4$) and isotropic displacement parameters ($Å^2 x\ 10^3$) for N,N-Bis(2-(9'-carbazolyl)ethyl)butylamine.

	x	y	z	U(eq)
H(1A)	3753	5954	3136	46
H(1B)	4788	6689	3098	46
H(2A)	3857	7469	1881	45
H(2B)	4447	6464	1702	45
H(4A)	2086	8320	1923	53
H(5A)	289	8946	1548	65
H(6A)	-1110	8009	990	66
H(7A)	-750	6410	794	58
H(10A)	255	4532	745	56
H(11A)	1461	3215	855	60
H(12A)	3300	3321	1394	60
H(13A)	3985	4767	1828	52
H(15A)	2678	7320	4728	49
H(15B)	3575	6466	4569	49
H(16A)	1319	6487	3880	57

Table B.5 Hydrogen coordinates (x 10^4) and isotropic displacement parameters (Å^{2}x 10^3) for N,N-Bis(2-(9'-carbazolyl)ethyl)butylamine.

	x	y	z	U(eq)
H(16B)	2195	5602	3912	57
H(18A)	3156	4506	4908	62
H(19A)	3346	3207	5868	70
H(20A)	2018	2951	7000	69
H(21A)	499	4013	7247	60
H(24A)	-1071	5603	7188	56
H(25A)	-2066	6990	6826	65
H(26A)	-1502	7903	5615	67
H(27A)	67	7455	4736	61
H(29A)	4109	8386	2991	59
H(29B)	4582	8014	3892	59
H(30A)	3117	8732	4635	66
H(30B)	3640	9499	3962	66
H(31A)	1540(30)	8560(30)	3720(20)	77
H(31B)	2060(30)	9350(20)	3040(20)	77
H(32A)	2190	10485	4044	120
H(32B)	1352	9893	4692	120
H(32C)	908	10255	3776	120
H(32D)	1018	9359	4868	129
H(32E)	541	9981	4077	129
H(32F)	1685	10288	4531	129
H(33A)	8268	1993	237	45

Table B.5 Hydrogen coordinates (x 10^4) and isotropic displacement parameters ($Å^2$x 10^3) for N,N-Bis(2-(9'-carbazolyl)ethyl)butylamine.

	x	y	z	U(eq)
H(33B)	7046	2519	122	45
H(34A)	7421	757	1040	50
H(34B)	6213	1319	1119	50
H(36A)	4750	2065	279	61
H(37A)	3203	2312	-611	84
H(38A)	3068	1509	-1852	97
H(39A)	4443	374	-2238	87
H(42A)	6514	-870	-2308	100
H(43A)	8267	-1632	-2031	123
H(44A)	9274	-1327	-818	103
H(45A)	8584	-211	150	72
H(47A)	9390	2677	1469	48
H(47B)	8860	1645	1612	48
H(48A)	9393	2233	2929	50
H(48B)	8554	3130	2792	50
H(50A)	9283	470	2826	61
H(51A)	8909	-1107	3243	78
H(52A)	7174	-1525	3929	82
H(53A)	5733	-410	4179	70
H(56A)	4348	1300	4254	76
H(57A)	3714	2872	4224	88
H(58A)	4895	4070	3653	87

Table B.5 Hydrogen coordinates (x 10^4) and isotropic displacement parameters ($Å^2$x 10^3) for N,N-Bis(2-(9'-carbazolyl)ethyl)butylamine.

	x	y	z	U(eq)
H(59A)	6764	3746	3125	68
H(61A)	8167	3821	617	45
H(61B)	7977	3982	1621	45
H(62A)	5931	3850	1455	53
H(62B)	6170	3791	443	53
H(63A)	6962	5343	417	58
H(63B)	5625	5337	711	58
H(64A)	6590	6289	1616	91
H(64B)	7491	5455	1837	91
H(64C)	6170	5373	2164	91

Table B.6 Torsion angles [°] for N,N-Bis(2-(9'-carbazolyl) ethyl)butylamine.

C(15)-N(1)-C(1)-C(2)	149.18(19)
C(29)-N(1)-C(1)-C(2)	-84.6(2)
C(3)-N(2)-C(2)-C(1)	100.4(3)
C(14)-N(2)-C(2)-C(1)	-83.9(3)
N(1)-C(1)-C(2)-N(2)	-74.5(3)
C(14)-N(2)-C(3)-C(4)	179.3(2)
C(2)-N(2)-C(3)-C(4)	-4.5(4)
C(14)-N(2)-C(3)-C(8)	-1.2(2)

Table B.6 Torsion angles [°] for N,N-Bis(2-(9'-carbazolyl) ethyl)butylamine.

C(2)-N(2)-C(3)-C(8)	175.1(2)
N(2)-C(3)-C(4)-C(5)	179.2(2)
C(8)-C(3)-C(4)-C(5)	-0.3(3)
C(3)-C(4)-C(5)-C(6)	-0.1(4)
C(4)-C(5)-C(6)-C(7)	0.2(4)
C(5)-C(6)-C(7)-C(8)	0.1(4)
C(6)-C(7)-C(8)-C(3)	-0.5(4)
C(6)-C(7)-C(8)-C(9)	179.8(2)
N(2)-C(3)-C(8)-C(7)	-179.0(2)
C(4)-C(3)-C(8)-C(7)	0.6(3)
N(2)-C(3)-C(8)-C(9)	0.8(2)
C(4)-C(3)-C(8)-C(9)	-179.6(2)
C(7)-C(8)-C(9)-C(10)	-0.9(5)
C(3)-C(8)-C(9)-C(10)	179.4(3)
C(7)-C(8)-C(9)-C(14)	179.6(3)
C(3)-C(8)-C(9)-C(14)	-0.1(2)
C(14)-C(9)-C(10)-C(11)	0.4(3)
C(8)-C(9)-C(10)-C(11)	-179.0(2)
C(9)-C(10)-C(11)-C(12)	0.3(4)
C(10)-C(11)-C(12)-C(13)	-0.4(4)
C(11)-C(12)-C(13)-C(14)	-0.3(4)
C(3)-N(2)-C(14)-C(13)	-177.8(2)
C(2)-N(2)-C(14)-C(13)	5.8(4)
C(3)-N(2)-C(14)-C(9)	1.1(2)

Table B.6 Torsion angles [°] for N,N-Bis(2-(9'-carbazolyl) ethyl)butylamine.

C(2)-N(2)-C(14)-C(9)	-175.21(19)
C(12)-C(13)-C(14)-N(2)	179.9(2)
C(12)-C(13)-C(14)-C(9)	1.1(3)
C(10)-C(9)-C(14)-N(2)	179.8(2)
C(8)-C(9)-C(14)-N(2)	-0.6(2)
C(10)-C(9)-C(14)-C(13)	-1.2(3)
C(8)-C(9)-C(14)-C(13)	178.4(2)
C(1)-N(1)-C(15)-C(16)	-78.0(3)
C(29)-N(1)-C(15)-C(16)	157.3(2)
C(28)-N(3)-C(16)-C(15)	94.8(3)
C(17)-N(3)-C(16)-C(15)	-92.1(3)
N(1)-C(15)-C(16)-N(3)	-169.3(2)
C(28)-N(3)-C(17)-C(18)	-177.6(2)
C(16)-N(3)-C(17)-C(18)	8.4(4)
C(28)-N(3)-C(17)-C(22)	1.3(3)
C(16)-N(3)-C(17)-C(22)	-172.8(2)
N(3)-C(17)-C(18)-C(19)	-179.8(3)
C(22)-C(17)-C(18)-C(19)	1.5(4)
C(17)-C(18)-C(19)-C(20)	0.4(4)
C(18)-C(19)-C(20)-C(21)	-1.5(5)
C(19)-C(20)-C(21)-C(22)	0.5(4)
C(20)-C(21)-C(22)-C(17)	1.4(4)
C(20)-C(21)-C(22)-C(23)	-179.2(3)
C(18)-C(17)-C(22)-C(21)	-2.4(4)

Table B.6 Torsion angles [°] for N,N-Bis(2-(9'-carbazolyl) ethyl)butylamine.

N(3)-C(17)-C(22)-C(21)	178.6(2)
C(18)-C(17)-C(22)-C(23)	178.0(2)
N(3)-C(17)-C(22)-C(23)	-0.9(3)
C(21)-C(22)-C(23)-C(24)	2.1(5)
C(17)-C(22)-C(23)-C(24)	-178.4(3)
C(21)-C(22)-C(23)-C(28)	-179.2(3)
C(17)-C(22)-C(23)-C(28)	0.2(3)
C(28)-C(23)-C(24)-C(25)	0.2(4)
C(22)-C(23)-C(24)-C(25)	178.7(3)
C(23)-C(24)-C(25)-C(26)	0.1(4)
C(24)-C(25)-C(26)-C(27)	-0.1(4)
C(25)-C(26)-C(27)-C(28)	-0.3(4)
C(17)-N(3)-C(28)-C(27)	178.8(3)
C(16)-N(3)-C(28)-C(27)	-7.1(4)
C(17)-N(3)-C(28)-C(23)	-1.1(3)
C(16)-N(3)-C(28)-C(23)	172.9(2)
C(26)-C(27)-C(28)-N(3)	-179.3(2)
C(26)-C(27)-C(28)-C(23)	0.6(4)
C(24)-C(23)-C(28)-N(3)	179.4(2)
C(22)-C(23)-C(28)-N(3)	0.5(3)
C(24)-C(23)-C(28)-C(27)	-0.5(4)
C(22)-C(23)-C(28)-C(27)	-179.4(2)
C(15)-N(1)-C(29)-C(30)	-60.6(3)
C(1)-N(1)-C(29)-C(30)	173.7(2)

Table B.6 Torsion angles [°] for N,N-Bis(2-(9'-carbazolyl) ethyl)butylamine.

N(1)-C(29)-C(30)-C(31)	-50.3(4)
C(29)-C(30)-C(31)-C(32A)	-168.2(6)
C(29)-C(30)-C(31)-C(32B)	165.2(7)
C(47)-N(4)-C(33)-C(34)	84.7(2)
C(61)-N(4)-C(33)-C(34)	-149.0(2)
C(46)-N(5)-C(34)-C(33)	93.4(3)
C(35)-N(5)-C(34)-C(33)	-80.2(3)
N(4)-C(33)-C(34)-N(5)	168.9(2)
C(46)-N(5)-C(35)-C(36)	-178.5(2)
C(34)-N(5)-C(35)-C(36)	-3.9(4)
C(46)-N(5)-C(35)-C(40)	1.6(3)
C(34)-N(5)-C(35)-C(40)	176.2(2)
N(5)-C(35)-C(36)-C(37)	-179.5(2)
C(40)-C(35)-C(36)-C(37)	0.4(4)
C(35)-C(36)-C(37)-C(38)	-0.5(4)
C(36)-C(37)-C(38)-C(39)	1.1(5)
C(37)-C(38)-C(39)-C(40)	-1.4(5)
C(38)-C(39)-C(40)-C(35)	1.3(4)
C(38)-C(39)-C(40)-C(41)	-178.8(3)
N(5)-C(35)-C(40)-C(39)	179.1(2)
C(36)-C(35)-C(40)-C(39)	-0.8(4)
N(5)-C(35)-C(40)-C(41)	-0.8(3)
C(36)-C(35)-C(40)-C(41)	179.3(2)
C(39)-C(40)-C(41)-C(42)	-0.2(5)

Table B.6 Torsion angles [°] for N,N-Bis(2-(9'-carbazolyl) ethyl)butylamine.

C(35)-C(40)-C(41)-C(42)	179.7(3)
C(39)-C(40)-C(41)-C(46)	179.9(3)
C(35)-C(40)-C(41)-C(46)	-0.2(3)
C(46)-C(41)-C(42)-C(43)	-0.9(4)
C(40)-C(41)-C(42)-C(43)	179.2(3)
C(41)-C(42)-C(43)-C(44)	0.8(5)
C(42)-C(43)-C(44)-C(45)	-0.7(6)
C(43)-C(44)-C(45)-C(46)	0.7(5)
C(35)-N(5)-C(46)-C(45)	178.6(2)
C(34)-N(5)-C(46)-C(45)	4.2(4)
C(35)-N(5)-C(46)-C(41)	-1.7(3)
C(34)-N(5)-C(46)-C(41)	-176.1(2)
C(44)-C(45)-C(46)-N(5)	178.8(3)
C(44)-C(45)-C(46)-C(41)	-0.9(4)
C(42)-C(41)-C(46)-N(5)	-178.7(2)
C(40)-C(41)-C(46)-N(5)	1.2(3)
C(42)-C(41)-C(46)-C(45)	1.0(4)
C(40)-C(41)-C(46)-C(45)	-179.1(2)
C(33)-N(4)-C(47)-C(48)	-152.0(2)
C(61)-N(4)-C(47)-C(48)	81.7(2)
C(49)-N(6)-C(48)-C(47)	74.5(3)
C(60)-N(6)-C(48)-C(47)	-101.1(3)
N(4)-C(47)-C(48)-N(6)	60.0(3)
C(60)-N(6)-C(49)-C(50)	179.8(2)

Table B.6 Torsion angles [°] for N,N-Bis(2-(9'-carbazolyl) ethyl)butylamine.

C(48)-N(6)-C(49)-C(50)	3.5(4)
C(60)-N(6)-C(49)-C(54)	-0.9(3)
C(48)-N(6)-C(49)-C(54)	-177.2(2)
N(6)-C(49)-C(50)-C(51)	177.7(3)
C(54)-C(49)-C(50)-C(51)	-1.6(4)
C(49)-C(50)-C(51)-C(52)	-0.5(4)
C(50)-C(51)-C(52)-C(53)	1.4(5)
C(51)-C(52)-C(53)-C(54)	-0.1(5)
C(52)-C(53)-C(54)-C(49)	-1.9(4)
C(52)-C(53)-C(54)-C(55)	-178.4(3)
N(6)-C(49)-C(54)-C(53)	-176.6(2)
C(50)-C(49)-C(54)-C(53)	2.8(4)
N(6)-C(49)-C(54)-C(55)	0.9(3)
C(50)-C(49)-C(54)-C(55)	-179.8(2)
C(53)-C(54)-C(55)-C(56)	-3.2(5)
C(49)-C(54)-C(55)-C(56)	180.0(3)
C(53)-C(54)-C(55)-C(60)	176.3(3)
C(49)-C(54)-C(55)-C(60)	-0.5(3)
C(60)-C(55)-C(56)-C(57)	-0.7(4)
C(54)-C(55)-C(56)-C(57)	178.7(3)
C(55)-C(56)-C(57)-C(58)	0.7(5)
C(56)-C(57)-C(58)-C(59)	-0.7(5)
C(57)-C(58)-C(59)-C(60)	0.8(5)
C(49)-N(6)-C(60)-C(59)	179.2(2)

Table B.6 Torsion angles [°] for N,N-Bis(2-(9'-carbazolyl) ethyl)butylamine.

C(48)-N(6)-C(60)-C(59)	-4.6(4)
C(49)-N(6)-C(60)-C(55)	0.6(3)
C(48)-N(6)-C(60)-C(55)	176.8(2)
C(58)-C(59)-C(60)-N(6)	-179.3(3)
C(58)-C(59)-C(60)-C(55)	-0.9(4)
C(56)-C(55)-C(60)-N(6)	179.6(2)
C(54)-C(55)-C(60)-N(6)	0.0(3)
C(56)-C(55)-C(60)-C(59)	0.9(4)
C(54)-C(55)-C(60)-C(59)	-178.7(2)
C(33)-N(4)-C(61)-C(62)	73.4(2)
C(47)-N(4)-C(61)-C(62)	-160.6(2)
N(4)-C(61)-C(62)-C(63)	174.4(2)
C(61)-C(62)-C(63)-C(64)	-65.6(3)

Symmetry transformations used to generate equivalent atoms:

B.2 Tris(2-(9'-carbazolyl)ethyl)amine

A crystal of the compound (colorless, block-shaped, size 0.35 x 0.25 x 0.25 mm) was mounted on a glass fiber with grease and cooled to -93 °C in a stream of nitrogen gas controlled with Cryostream Controller 700. Data collection was performed on a Bruker SMART APEX II X-ray diffractometer with graphite-monochromated Mo K_α radiation (λ = 0.71073 Å), operating at 50 kV and 30 mA over 2θ ranges of 4.10 ~ 52.00º. No significant decay was observed during the data collection.

Data were processed on a PC using the Bruker AXS Crystal Structure Analysis Package: [1] Data collection: APEX2 (Bruker, 2006); cell refinement: SAINT (Bruker, 2005); data reduction: SAINT (Bruker, 2005); structure solution: XPREP (Bruker, 2005) and SHELXTL (Bruker, 2000); structure refinement: SHELXTL; molecular graphics: SHELXTL; publication materials: SHELXTL. Neutral atom scattering factors were taken from Cromer and Waber.[2] The crystal is monoclinic space group $P2_1/c$, based on the systematic absences, E statistics and successful refinement of the structure. The structure was solved by direct methods. Full-matrix least-square refinements minimizing the function $\sum w (F_o^2 - F_c^2)^2$ were applied to the compound. All non-hydrogen atoms were refined anisotropically. All H atoms were placed in geometrically calculated positions, with C-H = 0.95 (aromatic), 0.99 (CH_2) and 0.98 Å (CH_3), and refined as riding atoms, with Uiso(H) = 1.2 Ueq(C).

Convergence to final R_1 = 0.0358 and wR_2 = 0.0851 for 5095 ($I>2\sigma(I)$) independent reflections, and R_1 = 0.0459 and wR_2 = 0.0928 for all 6148 (R(int) = 0.0225) independent reflections, with 415 parameters and 0 restraints, were achieved.[3] The largest residual peak and hole to be 0.139 and – 0.216 e/Å^3, respectively. Crystallographic data, atomic coordinates and equivalent isotropic displacement parameters, bond lengths and angles, anisotropic displacement parameters, hydrogen coordinates and isotropic displacement parameters, and torsion angles are given in **Tables B.7 to B.12**. The molecular structure and the cell packing are shown in **Figures B.3 and B.4**.

---

[1] Bruker AXS Crystal Structure Analysis Package:

Bruker (2000). SHELXTL. Version 6.14. Bruker AXS Inc., Madison, Wisconsin, USA.

Bruker (2005). XPREP. Version 2005/2. Bruker AXS Inc., Madison, Wisconsin, USA.

Bruker (2005). SAINT. Version 7.23A. Bruker AXS Inc., Madison,Wisconsin, USA.

Bruker (2006). APEX2. Version 2.0-2. Bruker AXS Inc., Madison, Wisconsin, USA.

[2] Cromer, D. T.; Waber, J. T. International Tables for X-ray Crystallography; Kynoch Press: Birmingham, UK, 1974; Vol. 4, Table 2.2 A.

[3] $R_1 = \sum | |Fo| - |Fc| | / \sum |Fo|$

$wR_2 = \{\sum [w (Fo^2 – Fc^2)^2] / \sum [w(Fo^2)^2]\}^{1/2}$

($w = 1 / [\sigma^2(Fo^2) + (0.0453P)^2 + 0.65P]$, where $P = [Max (Fo^2, 0) + 2Fc^2] / 3$)

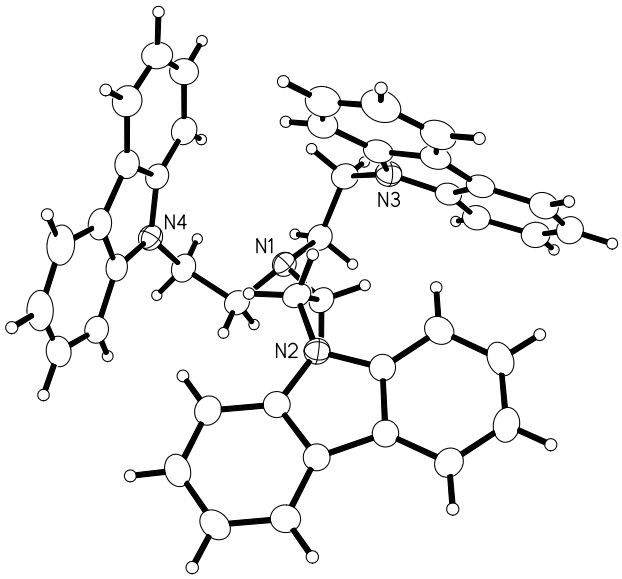

Figure B.3. Molecular Structure Tris(2-(9'-carbazolyl)ethyl)amine (Displacement ellipsoids for non-H atoms are shown at the 50% probability level and H atoms are represented by circles of arbitrary size.)

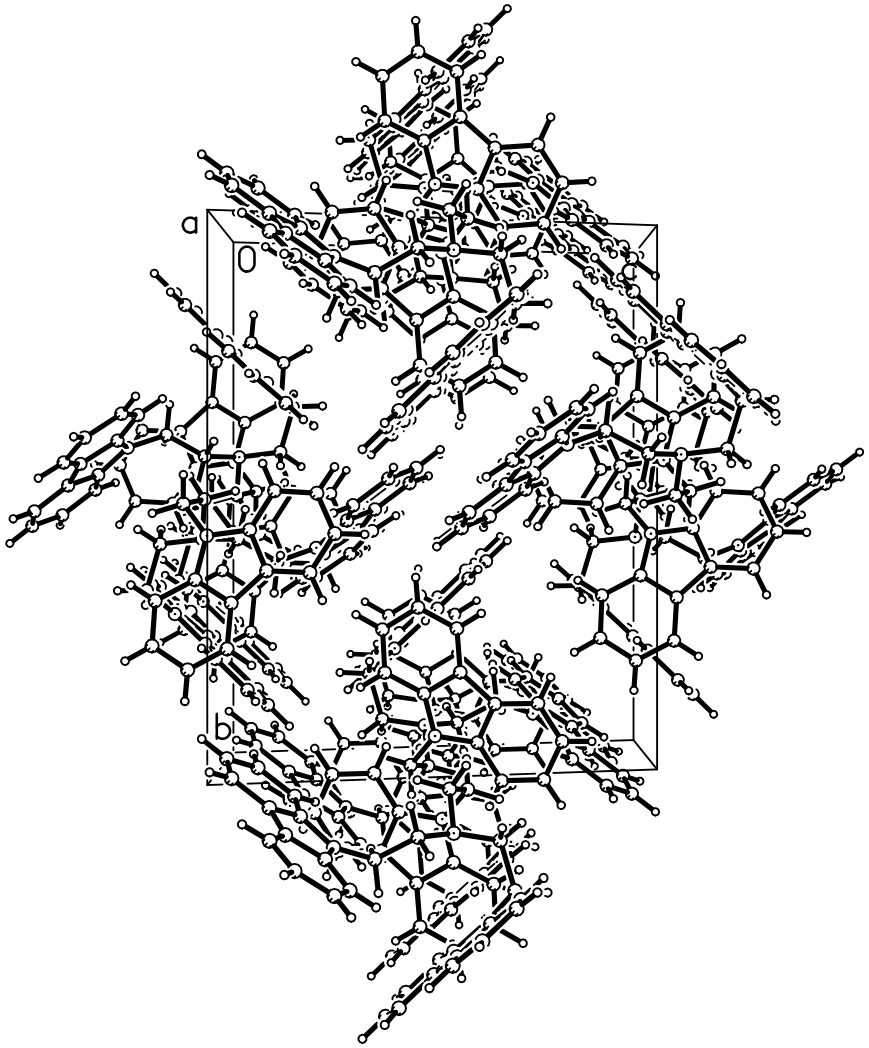

Figure B.4. Unit cell packing of Tris(2-(9'-carbazolyl)ethyl)amine

Table B.7. Crystal data and structure refinement for tris(2-(9'-carbazolyl)ethyl)amine

Empirical formula	C42 H36 N4	
Formula weight	596.75	
Temperature	180(2) K	
Wavelength	0.71073 Å	
Crystal system	Monoclinic	
Space group	P2(1)/c	
Unit cell dimensions	a = 13.2472(2) Å	α= 90°.
	b = 17.1444(2) Å	β= 113.4200(10)°.
	c = 15.0082(2) Å	γ = 90°.
Volume	3127.78(7) $Å^3$	
Z	4	
Density (calculated)	1.267 Mg/m^3	
Absorption coefficient	0.075 mm^{-1}	
F(000)	1264	
Crystal size	0.30 x 0.25 x 0.25 mm^3	
Theta range for data collection	2.05 to 26.00°.	
Index ranges	-16<=h<=13, -21<=k<=18, -18<=l<=18	
Reflections collected	21029	
Independent reflections	6148 [R(int) = 0.0225]	
Completeness to theta = 26.00°	100.0%	

Table B.7. Crystal data and structure refinement for tris(2-(9'-carbazolyl)ethyl)amine

Absorption correction	Multi-scan
Max. and min. transmission	0.9816 and 0.9779
Refinement method	Full-matrix least-squares on F^2
Data / restraints / parameters	6148 / 0 / 415
Goodness-of-fit on F^2	1.013
Final R indices [I>2sigma (I)]	R1 = 0.0358, wR2 = 0.0851
R indices (all data)	R1 = 0.0459, wR2 = 0.0928
Largest diff. peak and hole	0.139 and -0.216 e.$Å^{-3}$

Table B.8 Atomic coordinates ($x10^4$) and equivalent isotropic displacement parameters ($Å^2x10^3$) for tris(2-(9'-carbazolyl)ethyl)amine. U(eq) is defined as one third of the trace of the orthogonalized U^{ij} tensor.

	x	y	z	U(eq)
N(1)	3483(1)	4244(1)	10326(1)	28(1)
N(2)	3316(1)	4074(1)	7791(1)	29(1)
N(3)	5032(1)	2853(1)	11032(1)	33(1)
N(4)	1124(1)	4324(1)	10081(1)	30(1)
C(1)	3923(1)	4234(1)	9568(1)	30(1)
C(2)	3134(1)	3830(1)	8647(1)	31(1)
C(3)	2647(1)	4579(1)	7078(1)	27(1)
C(4)	1602(1)	4856(1)	6920(1)	33(1)
C(5)	1094(1)	5336(1)	6126(1)	38(1)
C(6)	1602(1)	5537(1)	5503(1)	41(1)
C(7)	2638(1)	5261(1)	5661(1)	36(1)
C(8)	3177(1)	4778(1)	6458(1)	28(1)
C(9)	4225(1)	4387(1)	6830(1)	27(1)
C(10)	5113(1)	4367(1)	6554(1)	32(1)
C(11)	6023(1)	3927(1)	7088(1)	36(1)
C(12)	6052(1)	3491(1)	7886(1)	37(1)
C(13)	5184(1)	3495(1)	8172(1)	34(1)
C(14)	4276(1)	3955(1)	7646(1)	27(1)
C(15)	4337(1)	4151(1)	11308(1)	31(1)
C(16)	4596(1)	3303(1)	11619(1)	35(1)
C(17)	4454(1)	2315(1)	10322(1)	33(1)
C(18)	3366(1)	2072(1)	10024(1)	39(1)

Table B.8 Atomic coordinates (x10^4) and equivalent isotropic displacement parameters (Å^{2}x10^3) for tris(2-(9'-carbazolyl)ethyl)amine. U(eq) is defined as one third of the trace of the orthogonalized U^{ij} tensor.

	x	y	z	U(eq)
C(19)	2996(1)	1511(1)	9306(1)	46(1)
C(20)	3678(1)	1200(1)	8886(1)	47(1)
C(21)	4753(1)	1448(1)	9178(1)	41(1)
C(22)	5158(1)	2014(1)	9905(1)	34(1)
C(23)	6210(1)	2395(1)	10385(1)	34(1)
C(24)	7213(1)	2363(1)	10288(1)	41(1)
C(25)	8075(1)	2819(1)	10882(1)	45(1)
C(26)	7953(1)	3306(1)	11581(1)	43(1)
C(27)	6969(1)	3359(1)	11691(1)	38(1)
C(28)	6097(1)	2902(1)	11082(1)	32(1)
C(29)	2847(1)	4964(1)	10238(1)	34(1)
C(30)	1960(1)	4886(1)	10635(1)	35(1)
C(31)	1084(1)	3550(1)	10325(1)	31(1)
C(32)	1623(1)	3176(1)	11211(1)	39(1)
C(33)	1418(1)	2389(1)	11260(1)	51(1)
C(34)	699(1)	1981(1)	10458(1)	55(1)
C(35)	145(1)	2355(1)	9590(1)	47(1)
C(36)	329(1)	3149(1)	9514(1)	34(1)
C(37)	-108(1)	3715(1)	8741(1)	34(1)
C(38)	-885(1)	3689(1)	7785(1)	48(1)
C(39)	-1133(1)	4370(1)	7247(1)	55(1)
C(40)	-629(1)	5073(1)	7644(1)	52(1)
C(41)	147(1)	5116(1)	8582(1)	41(1)

Table B.8 Atomic coordinates ($x10^4$) and equivalent isotropic displacement parameters ($Å^2x10^3$) for tris(2-(9'-carbazolyl)ethyl)amine. U(eq) is defined as one third of the trace of the orthogonalized U^{ij} tensor.

	x	y	z	U(eq)
C(42)	407(1)	4429(1)	9126(1)	31(1)

Table B.9. Bond lengths [Å] and angles [°] for tris(2-(9'-carbazolyl)ethyl)amine.

N(1)-C(15)	1.4678(15)
N(1)-C(1)	1.4698(14)
N(1)-C(29)	1.4704(15)
N(2)-C(3)	1.3866(14)
N(2)-C(14)	1.3886(15)
N(2)-C(2)	1.4590(14)
N(3)-C(28)	1.3858(16)
N(3)-C(17)	1.3870(15)
N(3)-C(16)	1.4517(15)
N(4)-C(42)	1.3816(15)
N(4)-C(31)	1.3842(15)
N(4)-C(30)	1.4539(15)
C(1)-C(2)	1.5280(16)
C(1)-H(1A)	0.9900
C(1)-H(1B)	0.9900
C(2)-H(2A)	0.9900
C(2)-H(2B)	0.9900
C(3)-C(4)	1.3916(17)

Table B.9. Bond lengths [Å] and angles [°] for tris(2-(9'-carbazolyl)ethyl)amine.

C(3)-C(8)	1.4120(16)
C(4)-C(5)	1.3833(17)
C(4)-H(4A)	0.9500
C(5)-C(6)	1.3950(18)
C(5)-H(5A)	0.9500
C(6)-C(7)	1.3799(18)
C(6)-H(6A)	0.9500
C(7)-C(8)	1.3949(16)
C(7)-H(7A)	0.9500
C(8)-C(9)	1.4409(16)
C(9)-C(10)	1.3933(16)
C(9)-C(14)	1.4099(15)
C(10)-C(11)	1.3777(17)
C(10)-H(10A)	0.9500
C(11)-C(12)	1.3988(18)
C(11)-H(11A)	0.9500
C(12)-C(13)	1.3792(18)
C(12)-H(12A)	0.9500
C(13)-C(14)	1.3915(16)
C(13)-H(13A)	0.9500
C(15)-C(16)	1.5224(17)
C(15)-H(15A)	0.9900
C(15)-H(15B)	0.9900
C(16)-H(16A)	0.9900

Table B.9. Bond lengths [Å] and angles [°] for tris(2-(9'-carbazolyl)ethyl)amine.

C(16)-H(16B)	0.9900
C(17)-C(18)	1.3924(18)
C(17)-C(22)	1.4120(17)
C(18)-C(19)	1.3810(19)
C(18)-H(18A)	0.9500
C(19)-C(20)	1.395(2)
C(19)-H(19A)	0.9500
C(20)-C(21)	1.380(2)
C(20)-H(20A)	0.9500
C(21)-C(22)	1.3977(17)
C(21)-H(21A)	0.9500
C(22)-C(23)	1.4456(18)
C(23)-C(24)	1.3943(18)
C(23)-C(28)	1.4134(17)
C(24)-C(25)	1.379(2)
C(24)-H(24A)	0.9500
C(25)-C(26)	1.399(2)
C(25)-H(25A)	0.9500
C(26)-C(27)	1.3809(19)
C(26)-H(26A)	0.9500
C(27)-C(28)	1.3936(18)
C(27)-H(27A)	0.9500
C(29)-C(30)	1.5195(17)
C(29)-H(29A)	0.9900

Table B.9. Bond lengths [Å] and angles [°] for tris(2-(9'-carbazolyl)ethyl)amine.

C(29)-H(29B)	0.9900
C(30)-H(30A)	0.9900
C(30)-H(30B)	0.9900
C(31)-C(32)	1.3903(17)
C(31)-C(36)	1.4087(17)
C(32)-C(33)	1.3846(19)
C(32)-H(32A)	0.9500
C(33)-C(34)	1.391(2)
C(33)-H(33A)	0.9500
C(34)-C(35)	1.373(2)
C(34)-H(34A)	0.9500
C(35)-C(36)	1.3957(18)
C(35)-H(35A)	0.9500
C(36)-C(37)	1.4455(17)
C(37)-C(38)	1.3956(18)
C(37)-C(42)	1.4078(17)
C(38)-C(39)	1.382(2)
C(38)-H(38A)	0.9500
C(39)-C(40)	1.393(2)
C(39)-H(39A)	0.9500
C(40)-C(41)	1.377(2)
C(40)-H(40A)	0.9500
C(41)-C(42)	1.3958(17)
C(41)-H(41A)	0.9500

Table B.9. Bond lengths [Å] and angles [°] for tris(2-(9'-carbazolyl)ethyl)amine.

C(15)-N(1)-C(1)	113.06(9)
C(15)-N(1)-C(29)	111.50(9)
C(1)-N(1)-C(29)	109.20(9)
C(3)-N(2)-C(14)	108.39(9)
C(3)-N(2)-C(2)	125.42(10)
C(14)-N(2)-C(2)	125.27(10)
C(28)-N(3)-C(17)	108.68(10)
C(28)-N(3)-C(16)	125.22(10)
C(17)-N(3)-C(16)	126.08(10)
C(42)-N(4)-C(31)	108.45(10)
C(42)-N(4)-C(30)	124.11(10)
C(31)-N(4)-C(30)	125.82(10)
N(1)-C(1)-C(2)	111.49(9)
N(1)-C(1)-H(1A)	109.3
C(2)-C(1)-H(1A)	109.3
N(1)-C(1)-H(1B)	109.3
C(2)-C(1)-H(1B)	109.3
H(1A)-C(1)-H(1B)	108.0
N(2)-C(2)-C(1)	111.95(9)
N(2)-C(2)-H(2A)	109.2
C(1)-C(2)-H(2A)	109.2
N(2)-C(2)-H(2B)	109.2
C(1)-C(2)-H(2B)	109.2

Table B.9. Bond lengths [Å] and angles [°] for tris(2-(9'-carbazolyl)ethyl)amine.

H(2A)-C(2)-H(2B)	107.9
N(2)-C(3)-C(4)	129.18(10)
N(2)-C(3)-C(8)	109.10(10)
C(4)-C(3)-C(8)	121.69(11)
C(5)-C(4)-C(3)	117.45(11)
C(5)-C(4)-H(4A)	121.3
C(3)-C(4)-H(4A)	121.3
C(4)-C(5)-C(6)	121.66(12)
C(4)-C(5)-H(5A)	119.2
C(6)-C(5)-H(5A)	119.2
C(7)-C(6)-C(5)	120.79(12)
C(7)-C(6)-H(6A)	119.6
C(5)-C(6)-H(6A)	119.6
C(6)-C(7)-C(8)	119.04(11)
C(6)-C(7)-H(7A)	120.5
C(8)-C(7)-H(7A)	120.5
C(7)-C(8)-C(3)	119.37(11)
C(7)-C(8)-C(9)	133.94(11)
C(3)-C(8)-C(9)	106.68(10)
C(10)-C(9)-C(14)	119.40(10)
C(10)-C(9)-C(8)	133.94(11)
C(14)-C(9)-C(8)	106.67(10)
C(11)-C(10)-C(9)	119.14(11)
C(11)-C(10)-H(10A)	120.4

Table B.9. Bond lengths [Å] and angles [°] for tris(2-(9'-carbazolyl)ethyl)amine.

C(9)-C(10)-H(10A)	120.4
C(10)-C(11)-C(12)	120.71(12)
C(10)-C(11)-H(11A)	119.6
C(12)-C(11)-H(11A)	119.6
C(13)-C(12)-C(11)	121.46(11)
C(13)-C(12)-H(12A)	119.3
C(11)-C(12)-H(12A)	119.3
C(12)-C(13)-C(14)	117.70(11)
C(12)-C(13)-H(13A)	121.2
C(14)-C(13)-H(13A)	121.2
N(2)-C(14)-C(13)	129.28(11)
N(2)-C(14)-C(9)	109.16(10)
C(13)-C(14)-C(9)	121.56(11)
N(1)-C(15)-C(16)	113.66(10)
N(1)-C(15)-H(15A)	108.8
C(16)-C(15)-H(15A)	108.8
N(1)-C(15)-H(15B)	108.8
C(16)-C(15)-H(15B)	108.8
H(15A)-C(15)-H(15B)	107.7
N(3)-C(16)-C(15)	114.63(9)
N(3)-C(16)-H(16A)	108.6
C(15)-C(16)-H(16A)	108.6
N(3)-C(16)-H(16B)	108.6
C(15)-C(16)-H(16B)	108.6

Table B.9. Bond lengths [Å] and angles [°] for tris(2-(9'-carbazolyl)ethyl)amine.

H(16A)-C(16)-H(16B)	107.6
N(3)-C(17)-C(18)	129.08(12)
N(3)-C(17)-C(22)	108.96(11)
C(18)-C(17)-C(22)	121.96(11)
C(19)-C(18)-C(17)	117.42(13)
C(19)-C(18)-H(18A)	121.3
C(17)-C(18)-H(18A)	121.3
C(18)-C(19)-C(20)	121.68(13)
C(18)-C(19)-H(19A)	119.2
C(20)-C(19)-H(19A)	119.2
C(21)-C(20)-C(19)	120.76(13)
C(21)-C(20)-H(20A)	119.6
C(19)-C(20)-H(20A)	119.6
C(20)-C(21)-C(22)	119.20(13)
C(20)-C(21)-H(21A)	120.4
C(22)-C(21)-H(21A)	120.4
C(21)-C(22)-C(17)	118.98(12)
C(21)-C(22)-C(23)	134.25(12)
C(17)-C(22)-C(23)	106.77(10)
C(24)-C(23)-C(28)	119.18(12)
C(24)-C(23)-C(22)	134.38(12)
C(28)-C(23)-C(22)	106.44(11)
C(25)-C(24)-C(23)	119.25(12)
C(25)-C(24)-H(24A)	120.4

Table B.9. Bond lengths [Å] and angles [°] for tris(2-(9'-carbazolyl)ethyl)amine.

C(23)-C(24)-H(24A)	120.4
C(24)-C(25)-C(26)	120.69(13)
C(24)-C(25)-H(25A)	119.7
C(26)-C(25)-H(25A)	119.7
C(27)-C(26)-C(25)	121.65(13)
C(27)-C(26)-H(26A)	119.2
C(25)-C(26)-H(26A)	119.2
C(26)-C(27)-C(28)	117.43(12)
C(26)-C(27)-H(27A)	121.3
C(28)-C(27)-H(27A)	121.3
N(3)-C(28)-C(27)	129.08(11)
N(3)-C(28)-C(23)	109.14(11)
C(27)-C(28)-C(23)	121.78(12)
N(1)-C(29)-C(30)	113.33(10)
N(1)-C(29)-H(29A)	108.9
C(30)-C(29)-H(29A)	108.9
N(1)-C(29)-H(29B)	108.9
C(30)-C(29)-H(29B)	108.9
H(29A)-C(29)-H(29B)	107.7
N(4)-C(30)-C(29)	111.45(10)
N(4)-C(30)-H(30A)	109.3
C(29)-C(30)-H(30A)	109.3
N(4)-C(30)-H(30B)	109.3
C(29)-C(30)-H(30B)	109.3

Table B.9. Bond lengths [Å] and angles [°] for tris(2-(9'-carbazolyl)ethyl)amine.

H(30A)-C(30)-H(30B)	108.0
N(4)-C(31)-C(32)	129.47(11)
N(4)-C(31)-C(36)	109.12(10)
C(32)-C(31)-C(36)	121.36(11)
C(33)-C(32)-C(31)	117.58(13)
C(33)-C(32)-H(32A)	121.2
C(31)-C(32)-H(32A)	121.2
C(32)-C(33)-C(34)	121.64(13)
C(32)-C(33)-H(33A)	119.2
C(34)-C(33)-H(33A)	119.2
C(35)-C(34)-C(33)	120.70(13)
C(35)-C(34)-H(34A)	119.6
C(33)-C(34)-H(34A)	119.6
C(34)-C(35)-C(36)	119.23(13)
C(34)-C(35)-H(35A)	120.4
C(36)-C(35)-H(35A)	120.4
C(35)-C(36)-C(31)	119.44(12)
C(35)-C(36)-C(37)	133.90(12)
C(31)-C(36)-C(37)	106.66(10)
C(38)-C(37)-C(42)	119.26(12)
C(38)-C(37)-C(36)	134.45(12)
C(42)-C(37)-C(36)	106.27(10)
C(39)-C(38)-C(37)	118.73(14)
C(39)-C(38)-H(38A)	120.6

Table B.9. Bond lengths [Å] and angles [°] for tris(2-(9'-carbazolyl)ethyl)amine.

C(37)-C(38)-H(38A)	120.6
C(38)-C(39)-C(40)	121.24(14)
C(38)-C(39)-H(39A)	119.4
C(40)-C(39)-H(39A)	119.4
C(41)-C(40)-C(39)	121.37(14)
C(41)-C(40)-H(40A)	119.3
C(39)-C(40)-H(40A)	119.3
C(40)-C(41)-C(42)	117.56(14)
C(40)-C(41)-H(41A)	121.2
C(42)-C(41)-H(41A)	121.2
N(4)-C(42)-C(41)	128.63(12)
N(4)-C(42)-C(37)	109.50(10)
C(41)-C(42)-C(37)	121.82(12)

Symmetry transformations used to generate equivalent atoms:

Table B.10. Anisotropic displacement parameters ($Å^2 x\ 10^3$) for tris(2-(9'-carbazolyl) ethyl)amine. The anisotropic displacement factor exponent takes the form: $-2\pi^2[\ h^2 a^{*2} U^{11} + ...\ + 2\ h\ k\ a^*\ b^*\ U^{12}\ ]$

	U^{11}	U^{22}	U^{33}	U^{23}	U^{13}	U^{12}
N(1)	30(1)	30(1)	27(1)	-2(1)	14(1)	0(1)
N(2)	29(1)	34(1)	25(1)	2(1)	11(1)	1(1)
N(3)	36(1)	30(1)	33(1)	-1(1)	14(1)	0(1)
N(4)	29(1)	30(1)	32(1)	-3(1)	13(1)	-3(1)
C(1)	29(1)	34(1)	28(1)	-1(1)	13(1)	-4(1)
C(2)	34(1)	34(1)	27(1)	1(1)	14(1)	-6(1)
C(3)	29(1)	26(1)	25(1)	-4(1)	9(1)	-3(1)
C(4)	31(1)	34(1)	35(1)	-4(1)	15(1)	-2(1)
C(5)	30(1)	38(1)	43(1)	1(1)	12(1)	6(1)
C(6)	39(1)	41(1)	38(1)	10(1)	11(1)	9(1)
C(7)	37(1)	39(1)	31(1)	5(1)	14(1)	2(1)
C(8)	29(1)	28(1)	26(1)	-3(1)	10(1)	-2(1)
C(9)	28(1)	27(1)	24(1)	-4(1)	9(1)	-2(1)
C(10)	34(1)	34(1)	30(1)	-5(1)	14(1)	-3(1)
C(11)	30(1)	41(1)	38(1)	-10(1)	15(1)	-2(1)
C(12)	31(1)	38(1)	35(1)	-5(1)	6(1)	7(1)
C(13)	36(1)	33(1)	29(1)	1(1)	9(1)	3(1)
C(14)	28(1)	27(1)	25(1)	-4(1)	9(1)	-2(1)
C(15)	34(1)	34(1)	27(1)	-6(1)	14(1)	-3(1)
C(16)	39(1)	39(1)	28(1)	1(1)	16(1)	0(1)
C(17)	40(1)	27(1)	29(1)	5(1)	10(1)	1(1)

Table B.10. Anisotropic displacement parameters ($Å^2 x\ 10^3$) for tris(2-(9'-carbazolyl) ethyl)amine. The anisotropic displacement factor exponent takes the form: $-2\pi^2[\ h^2 a^{*2} U^{11} + ...\ + 2\ h\ k\ a^*\ b^*\ U^{12}\ ]$

	U^{11}	U^{22}	U^{33}	U^{23}	U^{13}	U^{12}
C(18)	41(1)	36(1)	38(1)	5(1)	12(1)	0(1)
C(19)	45(1)	40(1)	42(1)	2(1)	6(1)	-5(1)
C(20)	59(1)	38(1)	33(1)	-3(1)	7(1)	0(1)
C(21)	56(1)	36(1)	30(1)	3(1)	15(1)	6(1)
C(22)	45(1)	29(1)	28(1)	7(1)	14(1)	4(1)
C(23)	42(1)	29(1)	31(1)	8(1)	16(1)	5(1)
C(24)	50(1)	38(1)	42(1)	10(1)	25(1)	10(1)
C(25)	41(1)	46(1)	54(1)	13(1)	24(1)	6(1)
C(26)	39(1)	41(1)	48(1)	9(1)	15(1)	-2(1)
C(27)	41(1)	33(1)	39(1)	3(1)	15(1)	0(1)
C(28)	36(1)	29(1)	32(1)	7(1)	14(1)	3(1)
C(29)	33(1)	26(1)	43(1)	-2(1)	17(1)	-4(1)
C(30)	32(1)	32(1)	43(1)	-11(1)	18(1)	-4(1)
C(31)	27(1)	32(1)	36(1)	-1(1)	15(1)	-1(1)
C(32)	31(1)	47(1)	37(1)	5(1)	12(1)	-2(1)
C(33)	41(1)	50(1)	59(1)	22(1)	17(1)	3(1)
C(34)	42(1)	35(1)	81(1)	11(1)	18(1)	-5(1)
C(35)	37(1)	35(1)	64(1)	-6(1)	14(1)	-7(1)
C(36)	27(1)	34(1)	40(1)	-4(1)	12(1)	-2(1)
C(37)	25(1)	43(1)	34(1)	-4(1)	12(1)	0(1)
C(38)	31(1)	69(1)	38(1)	-8(1)	10(1)	-1(1)
C(39)	30(1)	98(1)	35(1)	13(1)	12(1)	10(1)
C(40)	34(1)	75(1)	55(1)	30(1)	25(1)	18(1)

Table B.10. Anisotropic displacement parameters ($Å^2 x\ 10^3$) for tris(2-(9'-carbazolyl) ethyl)amine. The anisotropic displacement factor exponent takes the form: $-2\pi^2[\ h^2 a^{*2} U^{11} + ...\ + 2\ h\ k\ a^*\ b^*\ U^{12}\ ]$

	U^{11}	U^{22}	U^{33}	U^{23}	U^{13}	U^{12}
C(41)	32(1)	45(1)	54(1)	13(1)	26(1)	8(1)
C(42)	25(1)	38(1)	35(1)	2(1)	16(1)	4(1)

Table B.11. Hydrogen coordinates (x 10^4) and isotropic displacement parameters ($Å^2$x 10^3) for tris(2-(9'-carbazolyl)ethyl)amine.

	x	y	z	U(eq)
H(1A)	4639	3959	9815	36
H(1B)	4050	4777	9411	36
H(2A)	3234	3258	8726	37
H(2B)	2367	3952	8550	37
H(4A)	1252	4721	7341	39
H(5A)	381	5535	6002	46
H(6A)	1231	5867	4963	49
H(7A)	2979	5397	5233	43
H(10A)	5090	4654	6004	38
H(11A)	6638	3920	6913	43
H(12A)	6684	3186	8238	44
H(13A)	5204	3193	8710	41
H(15A)	4096	4419	11774	37
H(15B)	5019	4409	11339	37
H(16A)	5136	3291	12302	42
H(16B)	3915	3048	11595	42
H(18A)	2897	2284	10303	47
H(19A)	2259	1332	9092	55
H(20A)	3399	814	8395	57
H(21A)	5213	1236	8887	49
H(24A)	7301	2030	9817	49

Table B.11. Hydrogen coordinates (x 10^4) and isotropic displacement parameters ($Å^2$x 10^3) for tris(2-(9'-carbazolyl)ethyl)amine.

	x	y	z	U(eq)
H(25A)	8759	2802	10816	54
H(26A)	8563	3607	11989	52
H(27A)	6889	3693	12163	46
H(29A)	2498	5114	9545	40
H(29B)	3357	5388	10590	40
H(30A)	2301	4718	11322	42
H(30B)	1611	5401	10612	42
H(32A)	2115	3451	11762	47
H(33A)	1777	2121	11858	61
H(34A)	590	1438	10510	66
H(35A)	-357	2077	9048	56
H(38A)	-1237	3213	7509	57
H(39A)	-1658	4357	6594	66
H(40A)	-825	5533	7259	63
H(41A)	493	5596	8850	49

Table B.12. Torsion angles [°] for tris(2-(9'-carbazolyl)ethyl) amine.

C(15)-N(1)-C(1)-C(2)	144.05(10)
C(29)-N(1)-C(1)-C(2)	-91.19(11)
C(3)-N(2)-C(2)-C(1)	-104.99(12)
C(14)-N(2)-C(2)-C(1)	62.71(14)
N(1)-C(1)-C(2)-N(2)	157.29(10)
C(14)-N(2)-C(3)-C(4)	178.87(11)
C(2)-N(2)-C(3)-C(4)	-11.69(18)
C(14)-N(2)-C(3)-C(8)	0.85(12)
C(2)-N(2)-C(3)-C(8)	170.29(10)
N(2)-C(3)-C(4)-C(5)	-177.62(11)
C(8)-C(3)-C(4)-C(5)	0.19(17)
C(3)-C(4)-C(5)-C(6)	0.14(18)
C(4)-C(5)-C(6)-C(7)	-0.1(2)
C(5)-C(6)-C(7)-C(8)	-0.3(2)
C(6)-C(7)-C(8)-C(3)	0.59(17)
C(6)-C(7)-C(8)-C(9)	179.08(12)
N(2)-C(3)-C(8)-C(7)	177.64(10)
C(4)-C(3)-C(8)-C(7)	-0.56(17)
N(2)-C(3)-C(8)-C(9)	-1.23(12)
C(4)-C(3)-C(8)-C(9)	-179.43(10)
C(7)-C(8)-C(9)-C(10)	3.0(2)
C(3)-C(8)-C(9)-C(10)	-178.36(12)
C(7)-C(8)-C(9)-C(14)	-177.49(12)
C(3)-C(8)-C(9)-C(14)	1.13(12)

Table B.12. Torsion angles [°] for tris(2-(9'-carbazolyl)ethyl) amine.

C(14)-C(9)-C(10)-C(11)	-0.21(16)
C(8)-C(9)-C(10)-C(11)	179.23(12)
C(9)-C(10)-C(11)-C(12)	1.39(17)
C(10)-C(11)-C(12)-C(13)	-0.97(18)
C(11)-C(12)-C(13)-C(14)	-0.66(18)
C(3)-N(2)-C(14)-C(13)	-179.68(11)
C(2)-N(2)-C(14)-C(13)	10.86(18)
C(3)-N(2)-C(14)-C(9)	-0.11(12)
C(2)-N(2)-C(14)-C(9)	-169.57(10)
C(12)-C(13)-C(14)-N(2)	-178.61(11)
C(12)-C(13)-C(14)-C(9)	1.86(17)
C(10)-C(9)-C(14)-N(2)	178.93(10)
C(8)-C(9)-C(14)-N(2)	-0.64(12)
C(10)-C(9)-C(14)-C(13)	-1.46(16)
C(8)-C(9)-C(14)-C(13)	178.97(10)
C(1)-N(1)-C(15)-C(16)	-87.25(12)
C(29)-N(1)-C(15)-C(16)	149.25(10)
C(28)-N(3)-C(16)-C(15)	75.86(15)
C(17)-N(3)-C(16)-C(15)	-102.99(13)
N(1)-C(15)-C(16)-N(3)	62.44(14)
C(28)-N(3)-C(17)-C(18)	179.48(12)
C(16)-N(3)-C(17)-C(18)	-1.52(19)
C(28)-N(3)-C(17)-C(22)	-0.13(13)
C(16)-N(3)-C(17)-C(22)	178.87(10)
N(3)-C(17)-C(18)-C(19)	-178.71(11)

Table B.12. Torsion angles [°] for tris(2-(9'-carbazolyl)ethyl) amine.

C(22)-C(17)-C(18)-C(19)	0.86(18)
C(17)-C(18)-C(19)-C(20)	-0.47(19)
C(18)-C(19)-C(20)-C(21)	-0.1(2)
C(19)-C(20)-C(21)-C(22)	0.29(19)
C(20)-C(21)-C(22)-C(17)	0.08(17)
C(20)-C(21)-C(22)-C(23)	179.30(12)
N(3)-C(17)-C(22)-C(21)	178.97(10)
C(18)-C(17)-C(22)-C(21)	-0.68(17)
N(3)-C(17)-C(22)-C(23)	-0.44(12)
C(18)-C(17)-C(22)-C(23)	179.91(11)
C(21)-C(22)-C(23)-C(24)	2.3(2)
C(17)-C(22)-C(23)-C(24)	-178.37(13)
C(21)-C(22)-C(23)-C(28)	-178.45(13)
C(17)-C(22)-C(23)-C(28)	0.83(12)
C(28)-C(23)-C(24)-C(25)	0.85(17)
C(22)-C(23)-C(24)-C(25)	179.98(12)
C(23)-C(24)-C(25)-C(26)	0.41(19)
C(24)-C(25)-C(26)-C(27)	-1.1(2)
C(25)-C(26)-C(27)-C(28)	0.48(18)
C(17)-N(3)-C(28)-C(27)	-179.42(11)
C(16)-N(3)-C(28)-C(27)	1.56(19)
C(17)-N(3)-C(28)-C(23)	0.68(13)
C(16)-N(3)-C(28)-C(23)	-178.34(10)
C(26)-C(27)-C(28)-N(3)	-179.07(12)
C(26)-C(27)-C(28)-C(23)	0.82(17)

Table B.12. Torsion angles [°] for tris(2-(9'-carbazolyl)ethyl) amine.

C(24)-C(23)-C(28)-N(3)	178.41(10)
C(22)-C(23)-C(28)-N(3)	-0.93(12)
C(24)-C(23)-C(28)-C(27)	-1.50(17)
C(22)-C(23)-C(28)-C(27)	179.16(10)
C(15)-N(1)-C(29)-C(30)	-80.50(12)
C(1)-N(1)-C(29)-C(30)	153.83(10)
C(42)-N(4)-C(30)-C(29)	-66.80(14)
C(31)-N(4)-C(30)-C(29)	96.95(13)
N(1)-C(29)-C(30)-N(4)	-64.28(14)
C(42)-N(4)-C(31)-C(32)	-177.21(12)
C(30)-N(4)-C(31)-C(32)	16.92(19)
C(42)-N(4)-C(31)-C(36)	0.07(13)
C(30)-N(4)-C(31)-C(36)	-165.80(10)
N(4)-C(31)-C(32)-C(33)	178.87(12)
C(36)-C(31)-C(32)-C(33)	1.89(19)
C(31)-C(32)-C(33)-C(34)	0.0(2)
C(32)-C(33)-C(34)-C(35)	-1.7(2)
C(33)-C(34)-C(35)-C(36)	1.4(2)
C(34)-C(35)-C(36)-C(31)	0.4(2)
C(34)-C(35)-C(36)-C(37)	-179.03(14)
N(4)-C(31)-C(36)-C(35)	-179.65(11)
C(32)-C(31)-C(36)-C(35)	-2.11(18)
N(4)-C(31)-C(36)-C(37)	-0.07(13)
C(32)-C(31)-C(36)-C(37)	177.47(11)
C(35)-C(36)-C(37)-C(38)	1.0(3)

Table B.12. Torsion angles [°] for tris(2-(9'-carbazolyl)ethyl) amine.

C(31)-C(36)-C(37)-C(38)	-178.50(13)
C(35)-C(36)-C(37)-C(42)	179.54(14)
C(31)-C(36)-C(37)-C(42)	0.05(13)
C(42)-C(37)-C(38)-C(39)	-0.59(19)
C(36)-C(37)-C(38)-C(39)	177.81(13)
C(37)-C(38)-C(39)-C(40)	-0.4(2)
C(38)-C(39)-C(40)-C(41)	0.9(2)
C(39)-C(40)-C(41)-C(42)	-0.37(19)
C(31)-N(4)-C(42)-C(41)	177.38(12)
C(30)-N(4)-C(42)-C(41)	-16.46(18)
C(31)-N(4)-C(42)-C(37)	-0.04(13)
C(30)-N(4)-C(42)-C(37)	166.13(10)
C(40)-C(41)-C(42)-N(4)	-177.82(12)
C(40)-C(41)-C(42)-C(37)	-0.69(18)
C(38)-C(37)-C(42)-N(4)	178.80(11)
C(36)-C(37)-C(42)-N(4)	-0.01(13)
C(38)-C(37)-C(42)-C(41)	1.18(18)
C(36)-C(37)-C(42)-C(41)	-177.63(11)

Symmetry transformations used to generate equivalent atoms: